Optimisation of nanovibrational stimulation to control the mechanical properties and differentiation of adult stem cells

Olivia Johnson-Love, MSc, BSc

University of Strathclyde Glasgow

Thesis submitted in partial fulfilment of the requirements of the University of Strathclyde for the award of Doctor of Philosophy

Department of Biomedical Engineering, University of Strathclyde

4th September 2024

Declaration

I hereby declare that the work presented here is my own and has not been submitted in part or whole, for any other degree at this or any other University or Institution. Where other sources of information have been used, they have been acknowledged appropriately.

Olivia Johnson-Love

4th September 2024

Contents

Contents iii
List of figures ix
List of tables xiv
List of abbreviations xv
Acknowledgements xxi
Preface xxiv
Summary xxvi
Chapter 1: 1
Introduction – Rationale for Mechanical Cell Stimulation 1
1.1 Cell Therapies for Clinical Use 1
1.2 Mesenchymal Stem Cell Differentiation 4
1.3 Mechanotransduction 9
1.3.1 *In vivo* Mechanical Forces 9
1.3.2 Extracellular Stiffness and Topography 11
1.3.3 Mechanosensing 14
1.3.4 Cytoskeleton 18
1.3.5 Tensegrity 20
1.3.6 Nuclear Mechanotransduction 21
1.4 Physical Control of Stem Cell Differentiation 23
1.4.1 Electrical Stimulation 23
1.4.2 Compression 25
1.4.3 Tension 26
1.4.4 Shear stress/perfusion 27
1.5 Vibrational Stimulation of Stem Cells 28
1.5.1 Impact on Proliferation 28
1.5.2 Vibration Directionality 29
1.5.3 Impact of Seeding Density 32
1.5.4 Intermittent Vibration 32
1.5.5 Phenotypes reported following vibration 34
1.5.5.1 Osteogenesis 34
1.5.5.2 Adipogenesis 36

1.5.5.3 Chondrogenesis 38
1.5.5.4 Myogenesis 38
1.5.5.5 Neurogenesis 40
1.5.6 Vibration only studies 41
1.6 Nanovibrational Stimulation 41
1.7 Aims and Objectives 43
Chapter 2: 46
Device Redesign 46
2.1 Introduction 46
2.2 Investigating different piezo actuator arrays 47
2.2.1 Laser interferometry 47
2.2.2 Testing different piezo actuator arrays 48
2.2.3 FEA modelling of the piezo actuator arrays 50
2.4 Testing limitations of vertical device at higher frequencies 52
2.4.1 Laser interferometry measurements 52
2.4.2 Modifying the top plate in ANSYS 53
2.5 Redesigning a variable frequency and amplitude power supply unit (PSU) 55
2.5.1 Designing an adjustable frequency power supply 55
2.5.2 Designing an adjustable amplitude power supply 56
2.6 Development of a horizontal nanovibration device 61
2.6.1 Motivation 61
2.6.2 Modelling MSCs in ANSYS 61
2.6.2.1 Designing cell models 61
2.6.2.2 Measuring the stress on cell models 63
2.6.2.3 Measuring strain hardening of cell models 66
2.6.2.4 Discussion/hypotheses from cell models 67
2.6.3 Designing a horizontal device 68
2.6.3.1 Prototype 1 68
2.6.3.2 Prototype 2 69
2.6.3.3 Prototype 3 70
2.6.3.3 Prototype 4 72
2.6.3.4 Prototype 5 74
2.7 Calibration of Devices 76

2.7.1 Interferometry calibration 76
2.7.2 Vibration analysis within incubator 76
2.7.3 Laser doppler vibrometer measurements 78
2.8 Discussion 79
Chapter 3: 80
Nanovibrational Stimulation of NIH 3T3 Murine Cells 80
3.1 Introduction 80
3.2 Methodology 82
3.2.1 Cell Culture Protocol 82
3.2.2 Nanovibrational stimulation protocol 82
3.2.3 Immunofluorescence Staining 83
3.2.4 Microscopy 86
3.2.5 Image Analysis 87
3.2.6 Atomic Force Microscopy 89
3.2.7 Statistics 90
3.3 Results 92
3.3.1 Nanovibrational stimulation increases cell proliferation 92
3.3.2 Initial seeding density affects cell response to nanovibrational stimulation 93
3.3.3 Adhesion time prior to stimulation affects cell response to nanovibrational stimulation 97
3.3.4 Morphological changes occur at different timescales for nanovibrated cells 102
3.3.5 Cells stiffen in response to nanovibrational stimulation 105
3.3.5.1 Initial investigations into stiffening response of nanovibrated cells 105
3.3.5.2 Cell stiffness is time dependent in nanovibrated cells 107
3.3.5.3 Changes in morphology correspond with changes in stiffness in nanovibrated cells 111
3.3.5.4 Inhibiting actin prevents stiffening response of cells to nanovibrational stimulation 113
3.3.5.5 Fixed nanovibrated cells show no changes in stiffness 115
3.4 Discussion 116
Chapter 4: 119
Optimising osteogenic response using MG63 cells 119

4.1 Introduction 119
4.2 Methodology 120
4.2.1 Cell culture 120
4.2.2 Application of nanovibrational stimulation 120
4.2.3 Immunofluorescent Staining 123
4.2.4 Gene expression analysis 123
4.2.5 Real-time deformability cytometry 126
4.2.6 Alizarin Red Staining 127
4.2.7 Cell/Nuclear Alignment Analysis 128
4.2.8 Atomic Force Microscopy 128
4.3 Results 129
4.3.1 Nanovibrational stimulation does not increase proliferation in MG63 cells 129
4.3.2 Initial seeding density affects MG63 morphological response to nanovibrational stimulation 130
4.3.3 Adhesion time affects MG63 cells response to nanovibrational stimulation 132
4.3.4 Time course of gene expression for 1 kHz, 30 nm vibration 135
4.3.4.1 Nuclear and osteogenic gene expression changes during nanovibrational stimulation 135
4.3.4.2 Investigating the relationship between LINC and osteogenesis 137
4.3.5 Frequency may not influence osteogenic cell response 139
4.3.5.1 Initial cell response to multiple frequencies 139
4.3.5.2 Long-term osteogenic response to multiple frequencies 143
4.3.6 Comparing the effects of intermittent and continuous vibration on cell response 148
4.3.7 Comparing horizontal and vertical vibration 150
4.3.7.1 Short-term cell response to horizontal vibration 151
4.3.7.1.1 Morphology is not a reliable marker of cell response in MG63 cells 151
4.3.7.1.2 MG63 cells do not align in the direction of horizontal vibration 154
4.3.7.1.3 Lack of osteogenic response in cells at early timepoints 156
4.3.7.2 Long-term cell response to horizontal vibration 158

4.3.8 The cytoplasm of MG63 cells stiffens within the first 3 hours of stimulation 161
4.3.9 MG63 cell deformability 163
4.4 Discussion 166
Chapter 5: 171
Vibration of Mesenchymal Stem Cells (MSCs) 171
5.1 Introduction 171
5.2 Methodology 172
5.2.1 MSC Donors 172
5.3 Comparing the effects of intermittent and continuous vibration on MSCs 173
5.4 Applying optimal vibration conditions to induce osteogenesis in MSCs 175
5.4.1 Morphological changes in MSCs in response to optimal vibration conditions 176
5.4.2 Mechanical response to stiffness across donors 180
5.4.3 Immunofluorescence data in response to optimised vibration conditions 182
5.4.4 Gene expression in MSCs exposed to optimal vibration conditions 184
5.4.5 Mineralisation in MSC samples 189
5.5 Discussion 191
Chapter 6: 194
Discussion 194
6.1 Introduction 194
6.2 Device Development 197
6.3 The impact of nanovibrational stimulation on cells 199
6.3.1 Relationship between morphological and mechanical changes in cells 201
6.3.2 Identifying key vibration conditions for osteogenic differentiation 204
6.3.3 Impact of donor variability on mechanobiology studies 207
6.4 Future Work 209
6.4.1 Future nanovibrational stimulation devices 209
6.4.2 Development of cell therapies 209
6.4.3 Developing wearable technology 211
6.4.4 Nanovibrational stimulation outside of bone research 211

6.5 Conclusion 212
Appendices: 214
Appendix A 214
Appendix B 229
B.1 Introduction 229
B.2 Methods 230
B.2.1 Cell Culture Protocol 230
B.2.2 Immunofluorescence Staining 230
B.2.3 Gene expression analysis 230
B.2.4 MTT Assay 231
B.3 Results 231
B.3.1 Optimising vibration conditions to induce a neural response in SH-SY5Y cells 231
B.3.1.1 Changes over time 232
B.3.1.2 Horizontal vs Vertical Response 233
B.3.1.3 qPCR and MTT assay results 235
B.3.2 Seeding Density Experiment 236
B.3.3 Investigating a neural lineage commitment in MSCs 239
B.4 Discussion 241
Appendix C 244
C.1 Published journal articles 244
C.2 Unpublished journal articles 244
References 246

List of Figures

Figure 1: Trilineage potential of MSCs 2
Figure 2: Signalling pathways regulating osteogenesis in MSCs. 7
Figure 3: Frost's Mechanostat Theory 10
Figure 4: Substrate stiffness directs stem cell lineage commitment. 13
Figure 5: Calcium ion channels activation 15
Figure 6: Integrin activation 16
Figure 7: Interplay between focal adhesion kinase (FAK) and cell lineage commitment in MSCs. 17
Figure 8: Actin-myosin contractility 19
Figure 9: Tensegrity model of a cell also with nuclear tensegrity. 21
Figure 10: LINC complex. 23
Figure 11: Micro cell chip designed to apply pneumatic pressure to MSCs. 25
Figure 12: Flexcell mechanism for applying strain to cell cultures 26
Figure 13: Setup used by Uzer *et al* when testing a range of vibration conditions on human ASCs 30
Figure 14: Vibration device used by Halonen *et al* to compare horizontal and vertical vibration] 31
Figure 15: Setup used by Ambattu *et al* to apply surface-reflected bulk waves (SRBW) to cells. 33
Figure 16: Setup used by Judex et al 35
Figure 17: Setup used by Baskan *et al*. 37
Figure 18: Custom built vocal fold device built by Tong *et al* 39
Figure 19: Setup used by Choi *et al* and Cho *et al* when using vibration to direct MSCs toward a neural lineage. 40
Figure 20: Cell mechanisms induced by nanovibrational stimulation 43
Figure 21: Nanovibrational stimulation system 46
Figure 22: Laser interferometer. 48
Figure 23: Arrangement of piezo actuators 49

Figure 24: Interferometry measurements at multiple frequencies for five different combinations of piezo actuators. 50
Figure 25: Interferometry measurements of device top plate 52
Figure 26: Modal analysis of device top plate. 55
Figure 27: Electronic circuit design 56
Figure 28: Voltages required to produce average displacements in devices. 57
Figure 29: Class AB amplifier design 59
Figure 30: ANSYS models of a cell at different stages of adherence 62
Figure 31: Maximum normal stress experienced by the cell 64
Figure 32: Comparing different Young's Modulus for the cytoplasm 65
Figure 33: Predicted Young's modulus for the cell. 66
Figure 34: Initial horizontal setup (Prototype 1) 68
Figure 35: Second horizontal setup (Prototype 2) 70
Figure 36: Third horizontal set up (Prototype 3) 71
Figure 37: Fourth horizontal set up (Prototype 4) 73
Figure 38: Final horizontal device designed (Prototype 5) 75
Figure 39: Accelerometer data for several devices within incubator. 77
Figure 40: Laser Doppler Vibrometry data for devices. 78
Figure 41: Immunofluorescent staining of NIH 3T3 cells 84
Figure 42: Testing different secondary antibodies 85
Figure 43: DAPI images 87
Figure 44: Actin and vinculin images 88
Figure 45: Statistical tests flowchart. 91
Figure 46: Proliferation of NIH 3T3 cells 92
Figure 47: Nuclear and cell area data for NIH 3T3 seeding density experiment 94
Figure 48: Actin data for NIH 3T3 seeding density experiment 96
Figure 49: Nuclear area data for NIH 3T3 adherence experiment. 98
Figure 50: Actin data for NIH 3T3 adherence experiment. 100
Figure 51: Vinculin data for NIH 3T3 adherence experiment 101
Figure 52: Nuclear and cell area data for NIH 3T3 cells stimulated for 5 days 103
Figure 53: Actin and vinculin data for cells stimulated for 5 days 104

Figure 54: AFM measurements of the cell following 72 hours of stimulation .106
Figure 55: AFM measurements of NIH 3T3 cells 108
Figure 56: AFM measurements of NIH 3T3 cells at multiple timepoints on JPK AFM 109
Figure 57: AFM measurements of NIH 3T3 cells at multiple timepoints on Asylum AFM.....110
Figure 58: Morphology data for corresponding timepoints in AFM data 112
Figure 59: AFM actin inhibition of NIH 3T3 cells.....114
Figure 60: Fixed Asylum AFM measurements of NIH 3T3 cells.. 115
Figure 61: Deformability Cytometer.....127
Figure 62: Proliferation data for MG63 cells 129
Figure 63: Morphology data for MG63 seeding density experiment 131
Figure 64: Nuclear and cell area for MG63 adherence experiment. 133
Figure 65: Actin and vinculin data for MG63 adherence experiment.....134
Figure 66: Gene expression results of MG63 cells over 7 days.....136
Figure 67: Relationship between osteocalcin and Sun1 138
Figure 68: Morphology results showing initial cell response to multiple frequencies.....141
Figure 69: Gene expression results showing MG63 cell response to multiple frequencies.....142
Figure 70: Morphology data of MG63 cell response to multiple frequencies at later timepoints of Day 3 and Day 7 144
Figure 71: Gene expression results showing MG63 cell response to multiple freqencies at later timepoints of Day 3 and Day 7. 146
Figure 72: Alizarin red absorbance on Day 7. 147
Figure 73: Gene expression response for cells vibrated at two amplitudes, continuously or intermittently.....149
Figure 74: Nuclear area data for initial horizontal experiments following 72 hours of stimulation 152
Figure 75: Actin intensity data for initial horizontal experiments 153
Figure 76: Vinculin intensity and YAP translocation data for initial horizontal studies.....154

Figure 77: Investigating alignment in stimulated cells following vibration. 155
Figure 78: Investigating alignment in stimulated cells at two amplitudes either vertically or horizontally. 156
Figure 79: Gene expression data for multiple amplitude, multiple directional experiment 157
Figure 80: Morphology results after 7 days of stimulation both horizontally and vertically at two amplitudes 158
Figure 81: Gene expression data for multiple amplitude, multiple direcional experiment following 7 days of vibraiton 159
Figure 82: Alizarin red data fr multiple direction, multiple amplitude experiment 160
Figure 83: AFM measurements of MG63 cells 162
Figure 84: Deformability cytometry data showing proof of concept 164
Figure 85: Deformation against area graphs of MG63 cells as measured by deformability cytometry. 165
Figure 86: Area and deformation of MG63 cells as measured by deformability cytometry at two flow rates 166
Figure 87: Gene expression results for MSCs vibrated at two amplitudes, continuously or intermittently 174
Figure 88: Morphology data for three MSC donors 177
Figure 89: Whole well images for each MSC donor at each condition showing actin staining. 178
Figure 90: Whole well images of each MSC donor 180
Figure 91: AFM results for three MSC donors 181
Figure 92: Intensity data for three MSC donors 183
Figure 93: Gene expression data for three MSC donors. 185
Figure 94: Time course analysis for OPN and OCN gene expression data for three MSC donors. 186
Figure 95: Comparing gene expression between MSC donors 187
Figure 96: Comparing gene expression between MSC donors for OPN and OCN 188
Figure 97: Alizarin red analysis results for three MSC donors. 190

Figure 98: Two final horizontal devices used for directionality experiments..198
Figure 99: Summary of aims/hypotheses and the findings of this study. 201
Figure 100: Different culture systems used in the expansion of stem cells 210
Figure 101: Neural stem cell differentiation. 229
Figure 102: Morphology results of SH-SY5Y cells following 1, 3 and 7 days of vertical vibration.....232
Figure 103: Morphology results for SH-SY5Y cells vibrated either horizontally or vertically at 30 or 50 nm amplitudes 234
Figure 104: Gene expression results and MTT assay following 7 days of horizontal vibration.....235
Figure 105: Morphology analysis for SH-SY5Y cells seeded at either 1000 or 10,000 cells/cm2 237
Figure 106: Gene expression data analysis for SH-SY5Y cells seeded at either 1000 or 10,000 cells/cm2 and vibrated horizontally.....238
Figure 107: MTT assay. 239
Figure 108: Neural gene expression analysis of MSCs.....241

List of Tables

Table 1: Growth factors stimulating and signalling pathways involved in stem cell lineage differentiation. 5
Table 2: Chemical factors used to induce differentiation into specific cell lines ..8
Table 3: ANSYS amplitudes. 51
Table 4: ANSYS top plate materials 54
Table 5: Young's Modulus and Poisson Ratios for cell models 62
Table 6: Dimensions of cell at different stages of adherence 63
Table 7: Interferometry measurements of horizontal devices 74
Table 8: Interferometry measurements of various devices used for in vitro experiments. 76
Table 9: Summary of nanovibrational stimulation conditions for each experiment described in Chapter 3 83
Table 10: Primary antibodies used for immunofluorescent staining 86
Table 11: Summary of nanovibrational stimulation conditions for each experiment described in Chapter 4 121
Table 12: Device calibration for multiple frequency experiments. 122
Table 13: Target genes used during qPCR experiments 124
Table 14: Spectrophotometer results. 125
Table 15: MSC donor information 173
Table 16: Summary of optimal vibration conditions 176
Table 17: Comparison of responses to nanovibrational stimulation between cell types investigated in this study 200
Table 18: Summary of dual chemical-vibration studies applied on a range of cell types investigating cell response. 214
Table 19: Summary of vibration only studies 223
Table 20: arget genes used during qPCR experiments on both SH-SY5Y cells and MSCs 231

List of Abbreviations

2D	Two dimensional
3D	Three dimensional
g	Unit of acceleration = 9.81 m/s^2
AC	Alternating current
ADP	Adenosine diphosphate
AFM	Atomic force microscopy
ALP	Alkaline phosphatase
ANOVA	Analysis of variance
Arp2/3	Actin related protein 2/3
ASCs	Adipose-derived stem cells
ATP	Adenosine triphosphate
BM	Basal media
BMP2	Bone morphogenetic protein 2
BSA	Bovine serum albumin
CAD	Computer assisted design
cDNA	Complimentary deoxyribonucleic acid
Col1	Collagen type 1
CL	Control sample
CT	Cycle threshold
CTCF	Corrected total cell fluorescence
DAPI	4', 6-diamidino-2-phenlindole

DC	Direct current
DDS	Direct digital synthesis
DMEM	Dulbecco's modified essential medium
DNA	Deoxyribonucleic acid
ECM	Extracellular Matric
EGF	Epidermal growth factor
ERK	Extracellular related kinase
FA	Focal adhesion
FACs	Focal adhesion complexes
F-actin	Filament of actin
FAK	Focal adhesion kinase
FBS	Foetal bovine serum
FEA	Finite element analysis
FFT	Fast Fourier transform
FITC	Fluorescein isothiocynate
g	Gram
G-actin	Single globular actin
GAPDH	Glyceraldehyde 3-phosphate dehydrogenase
GFAP	Glial fibrillary acidic protein
hESCs	Human embryonic stem cells
hDPSCs	Human dental pulp stem cells
hiPSCs	Human induced pluripotent stem cells
hVFF	Human vocal fold fibroblasts

H	Hour
Hz	Hertz
L	Litre
LINC	Linker of nucleoskeleton and cytoskeleton
M	Mole
m	Metre
MAP2	Microtubule-associated protein 2
MBP	Myelin basic protein
MC	Microcontroller
MEM NEAA	Minimum essential medium non-essential amino acid solution
MTT	3-(4, 5-dimethylthiazolyl-2)-2, 5-diphenyltetrazolium bromide
mRNA	Messenger ribonucleic acid
MSCs	Mesenchymal stem cells
NeuD	Neurogenic differentiation 1
NeuN	Neuronal nuclei
NK	Nanovibrated sample
NPCs	Nuclear pore complexes
NPN	Negative positive negative
nRT	No reverse transcriptase control
nT	No template control
OCN	Osteocalcin
ON	Osteonectin
OM	Osteogenic media

OPN	Osteopontin
Pa	Pascal
PBS	Phosphate-buffered saline
PCB	Printed circuit board
PCR	Polymerase chain reaction
PGE2	Prostaglandin E2
pk-pk	Peak-to-peak
PNP	Positive negative positive
PPARγ	Peroxisome proliferator-activated receptor gamma
PSU	Power supply unit
qPCR	Quantitative polymerase chain reaction
RhoA	Ras homolg gene family, member A
RNA	Ribonucleic acid
ROCK	Rho-associated protein kinase
ROIs	Regions of interest
RT	Reverse transcription
RT-DC	Real-time deformability cytometry
RUNX2	Runt-related transcription factor 2
s	Second
SMCs	Smooth muscle cells
SFs	Stress fibres
TFT	Thin film transistor
TGF-β1	Transforming growth factor β 1

TRITC	Tetramethylrhodamine
TXRD	Texas Red
UC-MSCs	Umbilical-cord-derived Mesenchymal Stem Cells
V	Volt
v/v	volume by volume
WAS	Wiskott-Aldrich syndrome
Wnt	Wingless type
w/v	weight by volume
YAP	Yes-associated protein
°C	Degrees Celsius

"Four things do not come back: the spoken word, the sped arrow, the past life, and the neglected opportunity"

Ted Chiang, The Merchant and the Alchemist's Gate

"Every cell is a triumph of natural selection, and we're made of trillions of cells. Within us, is a little universe"

Carl Sagan

Acknowledgements

I started my journey in academia as a physicist, before becoming an engineer, and finally a hybrid physicist-engineer-cell-biologist that can only be fittingly titled as ‘scientist’. As such, the first, and arguably most instrumental person to thank, is my supervisor and mentor: Peter Geoffrey Childs. As someone with a similar background to myself, he allowed me to ask as many stupid biology questions as I needed to (and there have been quite a few). He is possibly the most patient person I have ever met, giving me endless support, not only in my project, but also in my career. He has been one of the main influences that have driven me to become the confident, independent researcher I am now. Without him, this PhD would not have been nearly as fun or as inspiring, and for that I cannot thank him enough for taking a chance on a fellow hybrid scientist.

I would also like to thank Stuart Reid for initially introducing me to ‘nanokicking’, by taking time out of his (very) busy schedule to show me around his labs whilst I was still a physics student. He encouraged and inspired me to step into the world of cell biology, which I think now I am here, I will probably never leave.

I also have to thank the other ‘nanokicking’ researchers I have worked alongside: Jonathan Williams, Paul Campsie and Rui Pedro Pereira Sousa. Jonathan has been a big support throughout my PhD, offering advice on experiments and device development, assisting with laser doppler vibrometery and accelerometery measurements, and sharing his enthusiasm for bone research. Paul gave me a lot of electronics guidance, which I was extremely grateful for as I am someone who still finds electricity to be mind boggling. And finally Rui, who joined me as a fellow PhD student when I was at the half-way point, and has assisted in many of my later experiments. He shares my enthusiasm for all things science and it has been fantastic to have such a kind-hearted and passionate colleague to work with.

As well as my own research group, I’d like to thank the various lab technicians: Catherine Henderson, Stuart O’Farrell and Stephen Murray, who do fantastic work in keeping the department running. Katie has been exceptionally helpful in

training and assisting me in various aspects of cell work and microscopy, whilst Stephen had endless patience with me during the design of my horizontal device.

I would also like to thank the funders of my project: EPSRC, and various other funding bodies who have been involved in 'nanokicking' projects. Their support makes this work possible.

During my PhD I had the opportunity to live and work for 2 months in Spain at the Material Science Institute of Madrid in Professor Ricardo Garcia's ForceTool Lab. Here, Dr Francisco Espinosa shared his knowledge and experience in using AFM, skills I brought back to the University of Strathclyde, and which have vastly enriched my own knowledge. I would like to thank Fran, Ricardo and the rest of the group for being such fantastic hosts and sharing their knowledge. I would also like to thank the funders of the Saltire scheme and Scottish Universities Physics Alliance (SUPA) for making the trip possible.

Although I began my PhD journey during the COVID-19 pandemic, once we had access to offices and labs, and could return to some semblance of normality, I quickly discovered a wonderful group of people working alongside me in the PhD offices. It is to them that I want to extend unending thanks for keeping me sane, always ensuring we had something social to do during the week, from knit nights to pub quizzes. Thank you for being the finest collection of human beings in the world, I am lucky to have found such wonderful friendships in you all. I would like to especially thank Ben Hicks, who proved to me that I would walk away with far more than a PhD from this experience: I would gain a best friend and partner too. Thank you for all of the love and laughter, for grounding me when times are tough, and lifting me higher when life is good. And for always being there to cheer me on.

Finally, I would like to thank my parents: George William Love and Sharon Johnson-Love. Throughout my life, they have always told me I could be whatever I wanted to be, no matter what challenges were in the way. Their belief and pride in me, alongside their love, and unwavering support have shaped me into who I am today. Someone who even I am proud of.

It is to you both, George and Sharon, who I dedicate this thesis to.

Preface

Chapter One introduces mechanotransduction in cells and describes various methods for controlling stem cell differentiation. Studies using vibrational stimulation are thoroughly described, and the concept of nanovibrational stimulation is introduced.

In Chapter Two, modifications to the current nanovibrational stimulation device are explored, including exploring potential future alterations to the current power supply unit. For the electrical work, Dr Paul Campsie (University of Strathclyde) and Dr Kieran Craig (University of Strathclyde) helped immensely when troubleshooting and exploring design ideas. This chapter also includes the development of a horizontal vibration device used in further experiments. Mr Stephen Murray (University of Strathclyde) built the cradle used in the final horizontal prototype (Prototype 5) from my design drawings. Dr Jonathan Williams (University of Strathclyde) assisted with accelerometer and laser doppler vibrometer measurements.

Chapter Three applied nanovibrational stimulation to murine fibroblast cells (NIH 3T3s) investigating cell response. As well as exploring morphological changes within the cell, mechanical changes were also explored using atomic force microscopy (AFM). Initial training was given by Mr Alexander Macdonald (University of Strathclyde), whilst all the work done using the JPK AFM system was done in Madrid, Spain, alongside Prof Ricardo Garcia (Materials Science Institute of Madrid) and Dr Francisco Espinosa (Materials Science Institute of Madrid). Power law analysis was carried out by Mr Jaime Tejedor (Materials Science Institute of Madrid).

Chapter Four moved onto human osteosarcoma cell lines, investigating, alongside both morphological and mechanical changes within the cells, an osteogenic response to nanovibrational stimulation. Here, optimal vibration conditions were identified to produce the highest response in cells. Initial morphological experiments investigating the effect of horizontal vibration on cell response

(including cell alignment measurements) were done by Mr Alexander Caskie (BSc student, University of Strathclyde). Subsequent rose plots were made in MATLAB by Mr Ben Hicks (University of Strathclyde). Deformability cytometry measurements were done under the guidance of Ms Jessie Howell (University of Glasgow) and further analysis by Mr Rui Pereira Sousa (University of Strathclyde).

Chapter Five applied optimal vibration conditions identified in Chapter Four to mesenchymal stem cells (MSCs). Cells donors were initially cultured by Mr Rui Pereira Sousa (University of Strathclyde), who also seeded subsequent AFM experiments using MSCs.

Chapter Six summarises the results from previous chapters discussing their relevance and contribution to the field and also presenting some discussion of future work to be conducted.

Appendix A contains summary tables of vibration studies found within the literature.

Appendix B explores a small study conducted into the effects of nanovibrational stimulation on human neuroblastoma cells (SH-SY5Y) and MSCs. The majority of the SH-SY5Y data was obtained by Mr Jonathan Griffin (MSc student, University of Strathclyde) and further analysed by this author.

Appendix C details publications and future publications this author has written and has been involved in producing.

Summary

Interdisciplinary science has become more common in recent years, with fields such as mechanobiology exploring the interconnection between biology and engineering to focus on how mechanical forces influence cell behaviour and tissue function. Understanding how cells sense and respond to their environment is key to understand a range of diseases such as cancer, cardiovascular disorders, and musculoskeletal conditions. In stem cells, understanding their mechanobiology and controlling their differentiation is essential when designing cell therapies.

Mechanical stimulation has been widely used to induce a response in cells, using techniques such as cyclic stretch, compression, and fluid shear stress. Vibrational stimulation is another method and has the potential to be used to engineer cells for therapeutic use *in vitro*, or to be used directly on patients through wearable devices. However, studies have vastly differed on the optimal vibration conditions to induce specific cell responses. This has made it challenging to understand precisely which parameters optimise a desired response.

Nanovibrational stimulation, a technique previously conceptualised by Prof. Adam Curtis applies nanoamplitude vibrations to cells in an attempt to induce a response by targeting motion at the protein length scale. It has previously successfully induced osteogenic responses in stem cells, as well as being used in other applications such as reducing biofilm formation in *Pseudomonas aeruginosa* biofilms. However, a full study into the optimisation of nanovibrational stimulation has never been done.

This thesis aimed to explore the effect of different vibration conditions on cells in an attempt to enhance cell response to mechanical stimulation. Four vibration parameters were explored: frequency and amplitude of vibration, duration of stimulation and the direction of the applied force. Four cell types were also investigated: murine fibroblasts cells (NIH 3T3s), human osteosarcoma cells (MG63s), human neuroblastoma cells (SH-SY5Y) and human mesenchymal stem cells (MSCs).

We present data investigating the relationship between the mechanical, morphological and gene expression response in cells, identifying an initial increase in the stiffness of cells following the application of vibration. In fibroblasts, this corresponded with an increased nuclear area and increased actin intensity, demonstrating for the first time, the relationship between mechanical and morphological changes in cells exposed to nanovibrational stimulation.

Here, we also developed a new nanovibration device capable of applying horizontal vibration to cells at a frequency of 1 kHz and up to 100 nm in amplitude. Experiments conducted on MG63 cells, with horizontal vibration at a higher amplitude resulted in an increased response in cells. When applied to MSCs, some cell responses were indeed increased compared to cells vibrated vertically at 1 kHz, 30 nm.

Finally, we also present data using three mesenchymal stem cell (MSC) donors testing the donor response to vibrational stimulation. The varied response across all three donors highlights the need to optimise vibration parameters for different donor ages, genders, and potentially ethnicities, which must be explored further before nanovibrational stimulation may be used for cell therapies or as wearable devices.

Chapter 1:

Introduction – Rationale for Mechanical Cell Stimulation

1.1 Cell Therapies for Clinical Use

Regenerative medicine is quickly becoming a growing field in the treatment of both injury and disease. As part of this, cell based therapies are under development to treat a range of conditions, from skeletal diseases such as osteoporosis, to cardiovascular and even neurodegenerative diseases including multiple sclerosis, Parkinson's and Alzheimer's [1]. The use of immune-modulatory cells in therapy may also have the prospective to treat autoimmune diseases and to reduce the rejection of allogenic cells/tissue [2]. Meanwhile stem cells hold promising potential to treat diseases currently lacking an effective standard therapy, such as spinal cord injury [3]. There are two main approaches in using stem cells for cell therapy: either by stimulating cells to repair damaged tissue through the release of paracrine factors, or by engrafting stem cells to become new tissue [4].

Stem cells are a promising option for therapy due to their ability to self-renew and differentiate into a range of other cell types. Mesenchymal stem cells (MSCs) are perhaps the most commonly used in clinical studies, due to their availability within a range of tissue sources [4]. To assist standardisation, MSCs are characterised through guidelines issued by the International Society of Cellular Therapy [5]. The cells must adhere to plastic, have trilineage potential (Figure 1) to differentiate in to osteoblasts, adipocytes and chondrocytes *in vitro*, and also express surface antigens CD73, CD90, and CD105, whilst not expressing CD11b,

CD14, CD19, CD34, CD45, CD79a, and HLA-DR [5]. Having such guidelines in place, ensures MSCs are standardised, enabling stricter quality control. This is particularly useful when isolating MSCs from a wide range of tissue sources. However, many studies and many clinical products do not follow the ISCT definition of MSCs, labelling cells as mesenchymal stromal cells or labelling based on the tissue they are isolated from. This makes comparing studies particularly challenging, as cells may have a more heterogenous population.

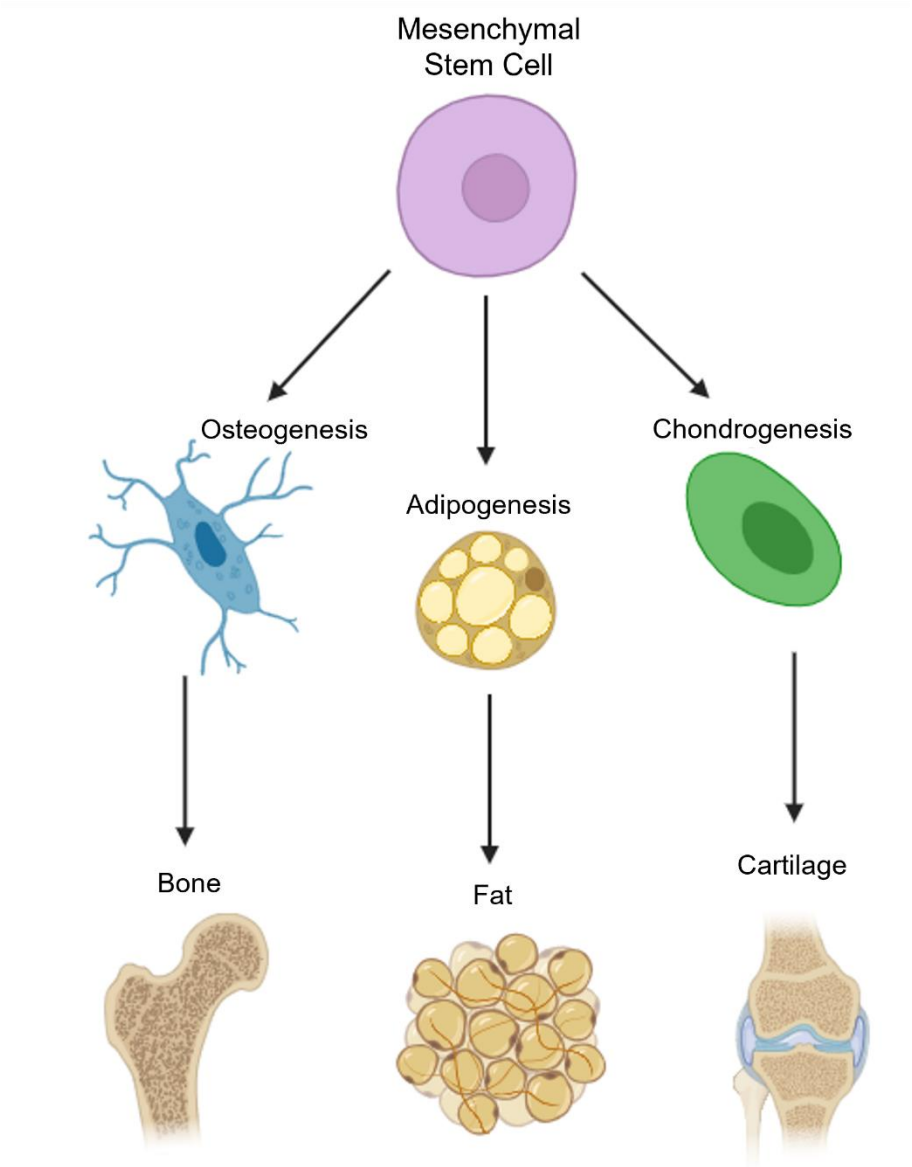

Figure 1: Trilineage potential of mesenchymal stem cells (MSCs) with the ability to differentiate into osteogenic, adipogenic and chondrogenic cell types. Image created in BioRender.

Since the first clinical trials on MSCs in 1995, the past 20 years have seen the number of clinical trials involving MSCs increase rapidly [4]. However despite the vast amount of research conducted in stem-cell based therapies, as of 2019, there are only 31 products containing MSCs or mesenchymal progenitor cells, such as osteoblasts and chondrocytes that are available commercially [6]. Few products contain carriers/scaffolds for cells, and most do not use differentiated MSCs, despite the vast amount of research being conducted in MSC phenotypic control [4]. Alongside research being conducted into developing cell therapies, there have also been the emergence of industrial cell manufacturing. Agencies such as The Cell and Gene Therapy Catapult aim to support development of novel cell therapies for clinical use [7].

Whilst primarily harvested from bone tissue, MSCs have been found in nearly all adult tissue, including adipose, umbilical cord, dental pulp, dermis, spleen, pancreas, lung and heart tissue, and within fluids such as amniotic fluid and peripheral blood [8]. Umbilical cord-derived MSCs (UC-MSCs) are particularly of note as they have been shown to express neurogenic markers, although no study has derived functioning neuronal cells from UC-MSCs [9]. MSCs are particularly advantageous as they are easily accessible from a patient's own allogenic tissue, allowing for the potential treatment of patients using their own cells. However, older patients may have ongoing conditions which reduce the number of healthy viable stem cells, and older stem cells may also have a decreased proliferation and differentiation potential, impacting efficacy as a cell therapy [10, 11]. Due to this, allogeneic stem cell therapies are being explored using donor cells for implantation into patients [12]. Whilst organ transplantation have been shown to illicit an immune reaction within a patient, MSCs have been shown to have the ability to avoid triggering an immune response, making them an attractive option in cell therapies [12].

It is also challenging to culture MSCs in large enough numbers to allow for the treatment of certain diseases – for use in cell therapies trillions of cells may be required, whilst culturing MSCs in a standard cultureware flask (T75 – T125) only warrants numbers up to the scale of millions [13]. Different technologies have

been developed that allow for the *in vitro* scale-up of MSCs such as multi-layer cell stacks, hollowfibre bioreactors and spinner flasks [4, 13]. These technologies are still in the early stages of development, with multiple studies using them to assess their full potential in scaling up MSCs for clinical use [14-17].

The clinical administration of MSCs is also a challenge that must be overcome, with implanted cells often having a low efficacy. Injecting stem cells intravenously has been found to result in a very low target efficacy and may not be effective in growing new tissue. Instead, using stem cells in combination with biomaterial scaffolds or hydrogels allows for implantation at target sites, whilst also providing cells with a more *in vivo* representative environment. Using carrier materials to encapsulate MSCs has been shown to increase the retention of MSCs up to 50-60% compared to 10% of saline delivered MSCs [18, 19]. The use of scaffolds, both synthetic and natural, enables MSCs to also receive topographic, chemical and mechanical cues to direct their differentiation. MSCs grown on softer materials tend to differentiate toward an adipogenic lineage, whilst those grown on harder surfaces favour an osteogenic lineage [20]. Very soft substrates typically mimic the stiffness of brain tissues, resulting in neurogenic lineage differentiation, whilst slightly stiffer substrates mimic muscle, resulting in myogenic differentiation, and even stiffer substrates direct differentiation into osteoblasts [21-24].

1.2 Mesenchymal Stem Cell Differentiation

Whilst MSCs have the potential to differentiate into multiple different cell types, during cell therapy, cells of a specific function are required. Therefore, MSCs are required to commit to a specific lineage prior to implantation. Studies have successfully identified certain molecules, pathways, and genes involved in regulating the commitment of MSCs (see Table 1) to specific lineages based on markers expressed. Early markers indicate initial commitments to specific lineages, whilst late markers suggest cells have reached later stages of lineage differentiation. However, molecules, signalling pathways and genes often overlap

across lineages, making it challenging to ensure MSC differentiation and lineage commitment.

Table 1: Growth factors stimulating and signalling pathways involved in stem cell lineage differentiation. Also included are early and late-stage markers of differentiation.

Lineage	**Growth Factors**	**Signalling Pathways**	**Early markers**		**Late markers**
Osteogenesis [8, 25-34]	TGFβ, BMP2, BMP4, BMP6, Runx2, FGF-2, IGF1 and 2, VEGF, β-catenin, ERK1 and 2, FOXO1, Zinc finger protein, OMD, PPARγ2, Fibronectin	BMP/TGFβ, ROCK, Wnt, Hedgehog, Notch, IGF, ERK1/2, MAPK, FGF, NELL-1	Runx2, ALP, OPN, BSP, BMP2		Osterix, OCN, Col1
Adipogenesis [8, 25, 34-37]	PPARγ1 and 2, C/EBPα, BMP2, 4 and 7, Wnt4 and 5a, Notch1 and 4, Twist-1, Dermo-1, Sox2 and 9, Oct4, EBF-1	BMP, Wnt, Notch, IGF, PKC-CamKII	PPARγ, C/EBPα, FABP4		Adiponectin, LEP, FAS, GPDH, ACC, Malic enzyme, Glu4, Insulin receptor, aP2
Chondrogenesis [8, 26, 35, 38, 39]	TGFβ1,2 and 3, FGF2, 4 and 6, BMP2, 4 and 7, Sox9, Hif1α, Shh, sFRP1, Dkk1, HOXD9, 10, 11 and 13, ZNF145, OXO3A, STAT3, Wnt11, IGFI	BMP/TGFβ, IGFR, MAPK, Hedgehog, Wnt	Sox9, Col2a1, Aggrecan, Ihh, Pth1r		Col10a1, VEGFA, MMP13, OPN
Neurogenesis [40-42]	EGF, FGF, NGFβ, NRP1, RA, Shh, Wnt7a and Wnt5a, BMP 4, Smad	Wnt, JNK, Notch, Hedgehog	**Neuron**	**Astro-cyte**	**Oligoden-drocyte**
			NeuroD 1, NF-L	S100, GFAP	NKx2.2, MBP, Olig 1 and 2

Signalling pathways are highly complex and convoluted; one pathway might be promoted, whilst another is inhibited. For example, the growth factor bone morphogenic protein 4 (BMP4) promotes adipogenic lineage commitment whilst also inhibiting myogenic lineage commitment [43]. Multiple signalling pathways can regulate a single transcription factor and there have been hundreds of genes that have been identified as being involved in directing stem cell fate [25]. Pathways such as the wingless type (Wnt) signalling pathway has been reported to promote both osteogenesis and myogenesis whilst also inhibiting adipogenesis [44, 45]. There are also many cues which may be involved in multiple cell lineages, such as the crosstalk between chondrogenic and adipogenic signalling pathways [35]. Table 1 summarizes some of the main transcription factors and signalling pathways involved in osteogenesis, chondrogenesis, adipogenesis and neurogenesis.

Osteogenesis is regulated primarily by Wnt, Hedgehog and Notch signalling, working individually or in harmony with other signalling molecules, activating specific transcription factors for osteogenesis (Figure 2) [46]. The Wnt pathway is involved in regulating cell proliferation, differentiation, and migration [41]. Wnt ligands are comprised of nineteen secreted signalling glycolipoproteins which can bind to more than 15 different Wnt receptors and co-receptors, with different combinations influencing both the signalling cascade and response from the cell [47]. These receptors include frizzled (FZD) and low density lipoprotein receptor-related protein (LRP) receptor complexes on the cell membrane which activate signalling cascades leading to changes in the cytoskeleton [41]. There are at least three signalling pathways activated by Wnt ligands: Wnt/β-catenin (canonical, β-catenin dependent), Wnt/Ca2+ (noncanonical, not dependent on β-catenin), and Wnt/planar polarity [41]. The canonical pathway has been found to be vital in the formation of bone, as blocking of β-catenin has been shown to lead to chondrogenesis [48]. The Wnt/Ca2+ pathway leads to the release of calcium from the endoplasmic reticulum and is also thought to be vital in the formation of bone whilst the Wnt/planar polarity pathway has been identified in the regulation of

osteoblast-specific gene expression and the modulation of the cytoskeleton [27, 41].

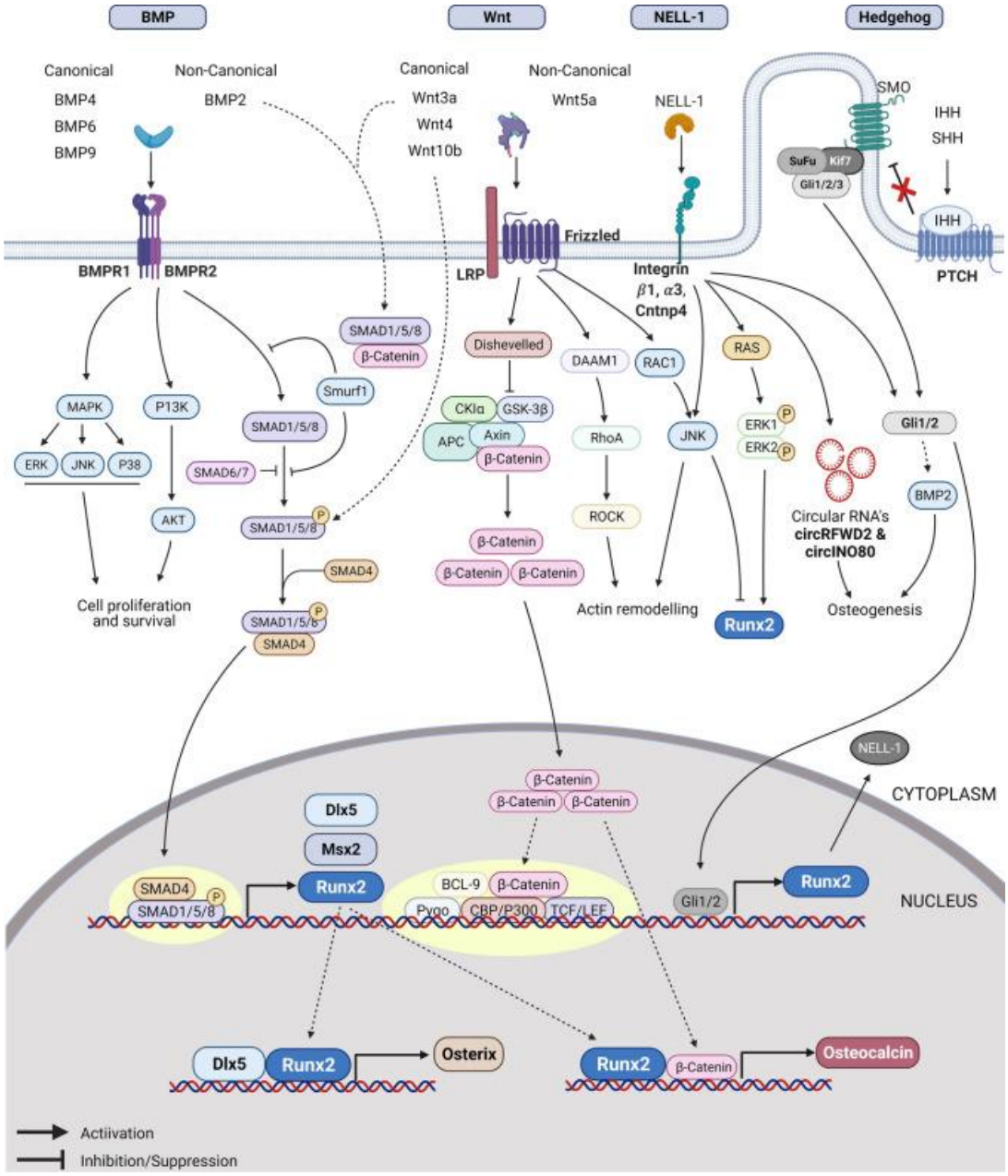

Figure 2: Signalling pathways regulating osteogenesis in MSCs. Pathways are highly complex and convoluted often involved in crosstalk and are often not specific to only osteogenesis. Figure reproduced with permission from [46].

The Notch signalling pathway has been found to both induce and inhibit MSC osteoblastic differentiation depending on the timing of Notch activation and the stage of cellular differentiation [32]. Meanwhile, the Hedgehog signalling

pathway has been found to play a role in bone formation, enhancing osteogenic differentiation whilst also promoting osteoblast activity [49, 50]. Stimulation of this pathway may assist in bone repair in regenerative medicine [51].

One of the main osteogenic transcription factors is Runt-related transcription factor 2 (Runx2), which has been shown to play an important role in directing bone-marrow-derived MSCs (BM-MSCs) toward osteogenesis and in activating several osteogenic genes including osteocalcin (OCN), collagen 1 (Col1), osteopontin (OPN), bone sialoprotein (BSP) and osterix [52]. Whilst important in inducing osteogenesis, the expression of Runx2 decreases in mature osteoblasts [53]. Runx2 is also involved in several signalling pathways such as bone morphogenetic protein (BMP), Notch, and Wnt [54].

Table 2: Chemical factors used to induce differentiation into specific cell lines

Cell line	Medium Supplementation
Osteogenesis [8]	β-glycerophosphate, dexamethasone, ascorbic acid-2-phosphate, TGF-β, BMPs, Vitamin D3
Adipogenesis [8]	3-isobutyl-methyl-xanthine, insulin, indomethacin, triiodothyronine, Asc-2-P, basic FGF, dexamethasone
Chondrogenesis [8]	ascorbic acid phosphate, dexamethasone, linoleic acid, selenous acid, proline, L-gutamine, TGF-β1, transferrin
Neurogenesis [55, 56]	butylted hydroxyanisole, KCl, valproic acid, forskolin, hydrocortisone, insulin

It is possible to control the differentiation of MSCs by using chemical factors, a summary of which is provided in Table 2. The effects may be controlled by adjusting both the concentration and the combination of chemicals [57]. However such methods are limited, with some osteogenic factors also inducing off-target differentiation, e.g. adipogenesis, in MSCs, which would be undesirable for cell based therapies targeting bone repair for example [58]. Also, in moving toward a

clinical application, such a technique will not be ideal for transplantation into the body and may it may prove difficult to ensure all drugs are removed from the final product [57]. The use of chemical induction therefore is not ideal when designing a cell therapy and the addition of growth factors to induce cell differentiation ought to be avoided. In recent years, new physical differentiation techniques have been explored, including mechanical and electrical stimulation [59, 60]. Such techniques target the mechanosensitive properties of cells, exploiting this to direct stem cell fate.

1.3 Mechanotransduction

1.3.1 *In vivo* Mechanical Forces

During early development, mechanical cues are highly important, with forces and strains being responsible for the differentiation and control of certain cell lineages, production of important extracellular matrix (ECM) proteins, and ensuring the accurate development of some tissues [61-63]. In embryonic development, mechanical forces are crucial to direct stem cell differentiation and organogenesis [64]. Mechanical signals can be generated and transmitted faster than chemical signals, which require diffusible messengers restricting their timescale of action, whilst mechanical signals can be transmitted rapidly through fibres already in tension [65]. The duration mechanical signals are applied for is also vital in regulating their effect. The application of mechanical stimulation for longer than 225 s can permanently change a cell's protein structure [63]. However, shorter durations of stimulation only results in temporary, reversible changes [63].

Mechanical forces and stresses are commonplace within the body, produced when in locomotion, from shear stress due to blood circulation, and from acoustic waves [66]. They are often periodic and produced at low frequencies, and these small, repetitive stimulations have influences upon cells, resulting in cell signalling and gene transcription being altered [67]. Some of the mechanical forces experience by cells *in vivo* include compression, tension, shear force, hydrostatic pressure, and force due to gravity, all of which have influences

on cellular function and development [68-71]. However, high magnitude forces can be damaging to cells. Forces of 300 – 600 nanonewtons can break actin fibre bundles in the cell, and studies also suggest that individual actin fibres can be broken by forces of the order of hundreds of piconewtons [72, 73]. Mechanical force transmission stops once these bonds are broken [74].

Mechanical stimulation is vital for the maintenance of healthy cells and tissues. A key example has been found in astronauts, whose bone density decreases in microgravity and weightlessness, losing 1-1.5% of their bone mineral density every month, even with current countermeasures in place such as medication and in-space exercise [75-77]. Moderate exercise loads the bone and has been shown to increase MSC proliferation and differentiation [69, 78-80]. However, for astronauts in microgravity, it is difficult to load bones. In gravity, bone experiences strains of between 10 – 1000 $\mu\varepsilon$ daily [81, 82]. When loaded to 2000 – 3000 $\mu\varepsilon$, there results an increase in bone formation [81, 82]. This is an example of Frost's Mechanostat Theory (Figure 3), where a decrease in applied mechanical forces to bone leads to a decrease in bone health, as astronauts experience, as well as patients on bed rest and the elderly who are less active [83]. Bone responds to mechanical stimuli, with osteocytes acting as mechanosensors, initiating the formation of new bone [84].

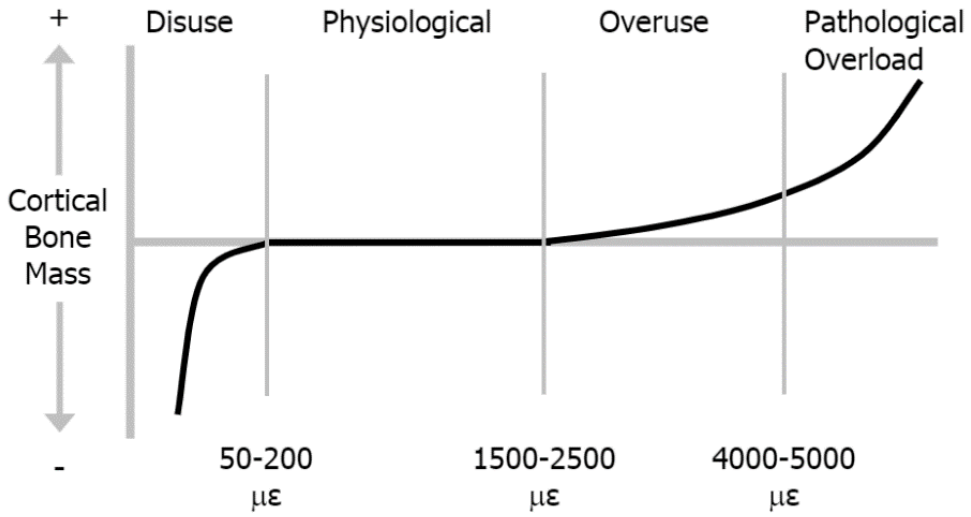

Figure 3: Frost's Mechanostat Theory, showing lower applied strains and disuse leading to a decrease in bone density as experienced by astronauts [85].

In tissue, cells sense multiple inputs simultaneously. Bone experiences tension, compression, and fluid-induced shear, all of which have an effect on MSCs [86, 87]. Vascular endothelial cells or smooth muscle cells might bind to mitogen whilst also forming adhesions to other ECM molecules and cells, and as a result will experience hemodynamic forces or contractions from other cells [88].

1.3.2 Extracellular Stiffness and Topography

Within the body, cells are surrounded by the ECM, acting as a support structure for cells and is in regulating many cellular processes. Mechanical properties of the ECM and forces transmitted through the ECM signal to cells leading to a multitude of responses. Cells can respond to signals by changing morphology, stiffness, proliferation, migration, or by differentiating [89]. Mechanical interactions with the ECM are made through adhesions, receptors and ion channels on the cell's surface, and signals are conveyed through mechanotransductive pathways [74].

As well as the ECM having variable mechanical properties, such as stiffness and viscosity which can influence cell response, the ECM also consists of proteins such as laminin, collagen and fibronectin all of which have cell adhesion motifs signalling molecules to bind to separate surface receptors, primarily integrins, on the surface of cells causing signalling and changes within the cell [90]. Both the protein content of the microenvironment and the stiffness of the ECM are two of the key determinants involved in controlling the fate of cells *in vivo*.

Cellular properties can be modified based on mechanical properties of the ECM. The stiffness of the ECM can be affected by the density of cells and by the response of the cells exerting traction forces. The mechanisms by which cells detect mechanical cues, such as stiffness, are likely related to actin-myosin contraction, which can deform the ECM [89]. Models such as the 'molecular clutch' have been used to describe the link between the ECM and cytoskeleton, regulating both cell movement and the transmission of forces [91, 92]. The membrane of cells can be placed under tension, thus activating stretch-sensitive ion channels embedded within the membrane [93].

In vitro, it is possible to mimic the physiological stiffness of a tissue to control stem cell differentiation using hydrogels or other biomaterials (Figure 4) [24, 94]. This culturing of cells on substrates with similar physiological stiffness to the tissue they belong, has resulted in cells developing phenotypes that would be expected *in vivo* [94]. Soft substrates of 0.1-1 kPa typically mimic brain tissues, directing neurogenic lineage differentiation [24, 95]. Stiffer substrates of 8-17 kPa mimic muscle, result in myogenic differentiation, and even stiffer substrates of 25-40 kPa direct differentiation into osteoblasts [24, 95]. Other studies have found that soft substrates reduce the amount that MSCs spread, resulting in a higher chondrogenic and adipogenic potential, whilst stiffer substrates increase the amount MSCs spread, resulting in higher myogenic potential [96]. MSCs also respond to stiffness gradients on surfaces by migrating toward stiffer areas in a process termed durotaxis [97]. The stiffness of the substrate regulates integrin binding, which is thought to be essential for MSC differentiation, as without bond formation, osteogenesis decreases [98]. The stiffness of the substrate also seems to regulate the shape of cells, possibly due to integrin binding changes caused by the mechanical properties of the substrate consequently affecting adhesion strength, cell stiffness and contractility [96, 99-101].

Cell shape is regulated by the cytoskeleton, and can be modified by micropatterned substrates, certain materials/gels, and ECM composition and mechanical properties through interactions with the ECM and other cells [35]. [102]. The study conducted by McBeath *et al* demonstrated that cell morphology also determines cell lineage commitment in stem cells, with rounded cells undergoing adipogenesis, and cells able to flatten and spread undergoing osteogenesis [103]. Cell shape was also found to regulate Rho and Rho associated protein kinase (ROCK) activity, both of which are involved in contractility and are key to osteogenesis, thus demonstrating that cellular contractility controls MSC lineage commitment toward either osteogenesis or adipogenesis [103]. Another similar study conducted by Gao *et al* confirmed that cell shape also affects MSC lineage commitment into chondrogenic and smooth muscle cells (SMCs) [104].

These two studies confirmed that any structural changes made to the cytoskeleton influences the determination of MSC lineage commitment [103, 104]. This said however, it is still not fully understood the full role both the cytoskeleton and Rho have on MSC response to stiffness.

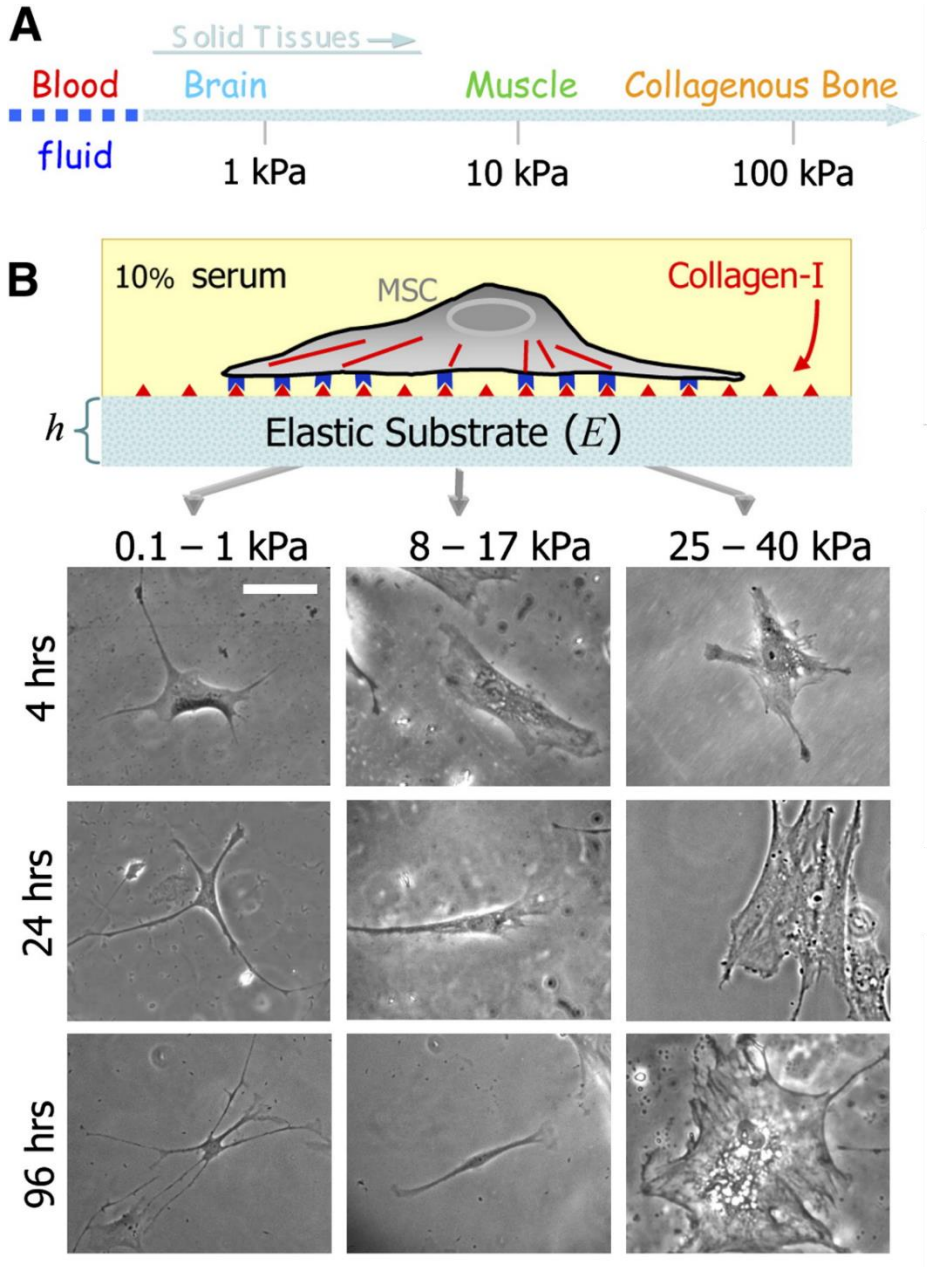

Figure 4: Substrate stiffness directs stem cell lineage commitment. A) Within the body, tissues have different stiffnesses, with blood and the brain being considerably softer than bone. B) A study conducted by Engler *et al* utilised an *in vitro* gel system to test the effect different substrate stiffnesses had on the lineage commitment of MSCs. Figure reproduced with permission from [24].

In vitro, studies have demonstrated that stem cells sense the different mechanical and topographical environments such as stiffness, pattern and size and tend to grow faster within an environment similar to their *in vivo* niche [105, 106]. Topographical cues received on the nanoscale, are capable of causing cells to undergo changes in their adhesion, migration, morphology and gene expression [67]. Recent research has found that nanotopography can successfully stimulate osteogenesis in MSCs, with features that are around 20 nm high being found to induce an osteogenic response [67, 107, 108]. Studies conducted by Dalby *et al* have found that high levels of randomness in nanotopographies can be used to direct osteoblastic differentiation of MSCs with EGF and FGF pathways being stimulated by this technique [106].

1.3.3 Mechanosensing

The process by which cells convert mechanical signals from their surrounding environment into biological signals is termed mechanotransduction [74]. This process is not limited to eukaryotic cells, a response to mechanical stress has also been identified in bacterial cells [109]. However, there have been a limited number of studies conducted on mechanotransduction in bacteria and the process is less understood compared to eukaryotic cells. This is due to chemical signals often dominating in bacteria; however, they do still experience a diverse range of mechanical forces through cell-to-cell interactions, cell-to-surface interactions, and shear flow.

Mechanical and chemical signals are sensed through mechanosensitive molecules embedded in the cell membrane such as mechanically-gated ion channels, integrins, G protein coupled-receptors, and cadherins [94]. These then propagate signals through the cell to the nucleus by activating different signalling pathways within the cell [94]. Ion channels involve ions passing in and out of the cell and can be activated or deactivated through mechanical stimuli [110-113]. Mechanosensitive ion channels, such as calcium ion (Ca2+) channels (Figure 5) and piezo1 can be activated when mechanical stimulation is applied [114, 115]. However, not all mechanical stimuli require ion channel activation to transmit

signals, instead other membrane proteins are involved in mechanosensing, principally integrins [94].

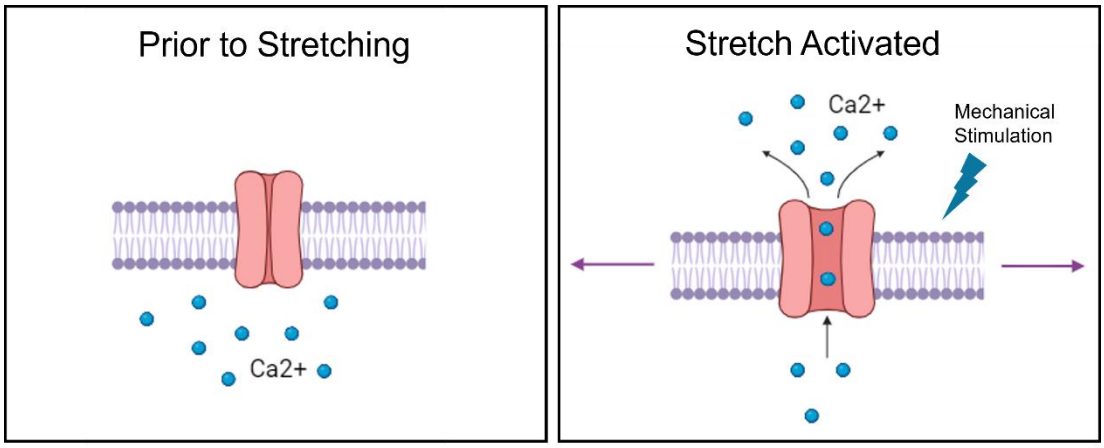

Figure 5: Calcium ion channels activated following application of mechanical stimulation. Image created using BioRender.

Integrins are heterodimeric glycoproteins composed of two transmembrane glycoprotein α- and β- subunits on the cell membrane with links to the ECM and to focal adhesion proteins within the cell [94, 102]. In the human body, 9 β subunits and 24 α subunits have been identified, resulting in a variety of α-β integrin receptor combinations on the cell surface [116]. Different combinations of α and β subunits determines how integrins bind and how cells adhere across different cell types, as well as working with different ECM proteins [117]. Molecules known as ligands, such as laminin, osteopontin, and fibronectin can bind to integrin receptors [117]. This binding causes the integrins to separate by 70 Angstrom which triggers signalling cascades within the cell, transmitting the signal to the cytoskeleton [118, 119].

These signals are transmitted through integrins interacting with cytoplasmic structural proteins which form focal adhesion complexes (FACs), providing a link between the ECM and the cytoskeleton (see Figure 6). This allows signalling cascades to be transmitted to the nucleus, whilst also stabilizing integrin binding and controlling cell shape and tension [102, 120-122]. These focal adhesions (FAs) form two layers: a transmembrane and an intracellular layer, the latter containing signalling proteins, some of which are mechano-responsive [94].

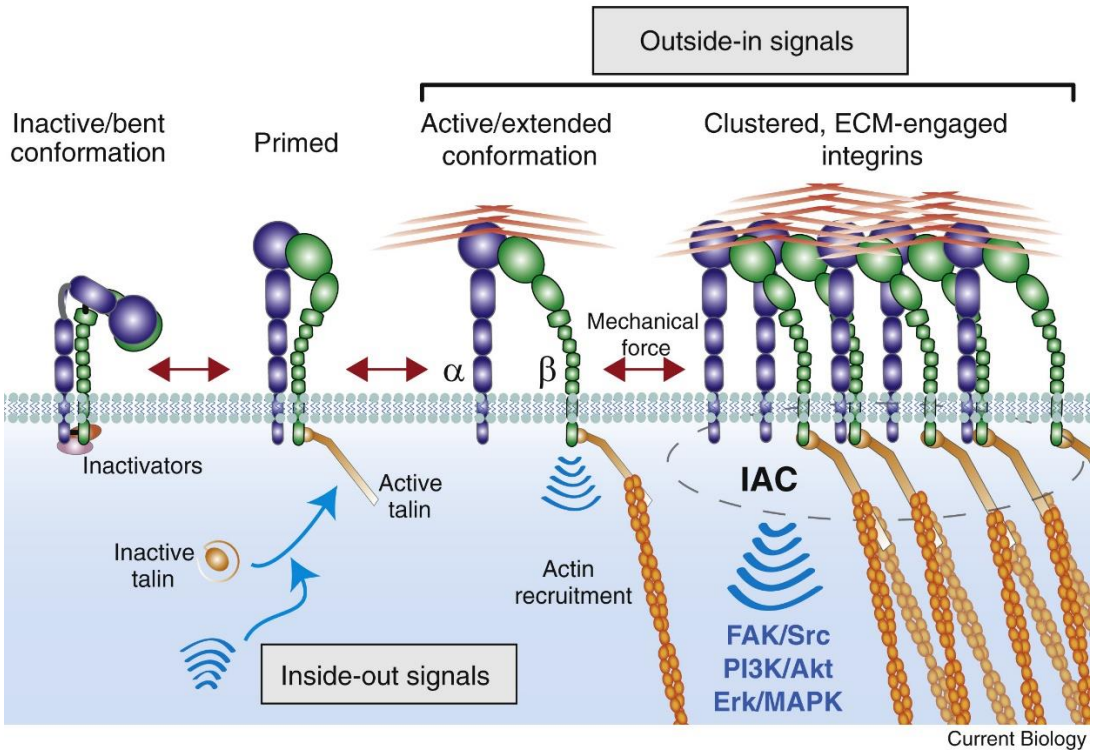

Figure 6: Integrin activation following interaction with signals outside of the cell. These signals activate α and β integrin receptors which subsequently recruit actin, leading to signal cascades inside the cell. Figure reproduced with permissions from [123].

One of the first mechanoresponsive proteins triggered in FA during the response to a mechanical cue is focal adhesion kinase (FAK) [94]. The activation of FAK triggers phosphorylation, the transfer of a phosphate to an amino acid within a protein, which is the mechanism used by proteins to transmit chemical signals [94]. Only three amino acids in the mammalian body can be phosphorylated: tyrosine, serine, and threonine [124]. When a protein is phosphorylated, the phosphate attached to the amino acid attracts other proteins to bind on top of the phosphate allowing signals to be transmitted in the cell. Kinases are proteins able to remove phosphates from adenosine triphosphate (ATP) and reattach them to amino acids [124]. FAK is a tyrosine kinase which can attach to focal adhesions and is involved in the process of integrin cell spreading by controlling the shape of the actin cytoskeleton. Tension and force transmission to the nucleus are also controlled by the interaction between FAK and the cytoskeleton [125]. As a result, high levels of adhesion, and therefore high levels of FAK have been shown to direct

MSCs toward osteogenesis, whilst low levels of adhesion and low levels of FAK result in adipogenic expression (Figure 7) [103, 106, 126, 127].

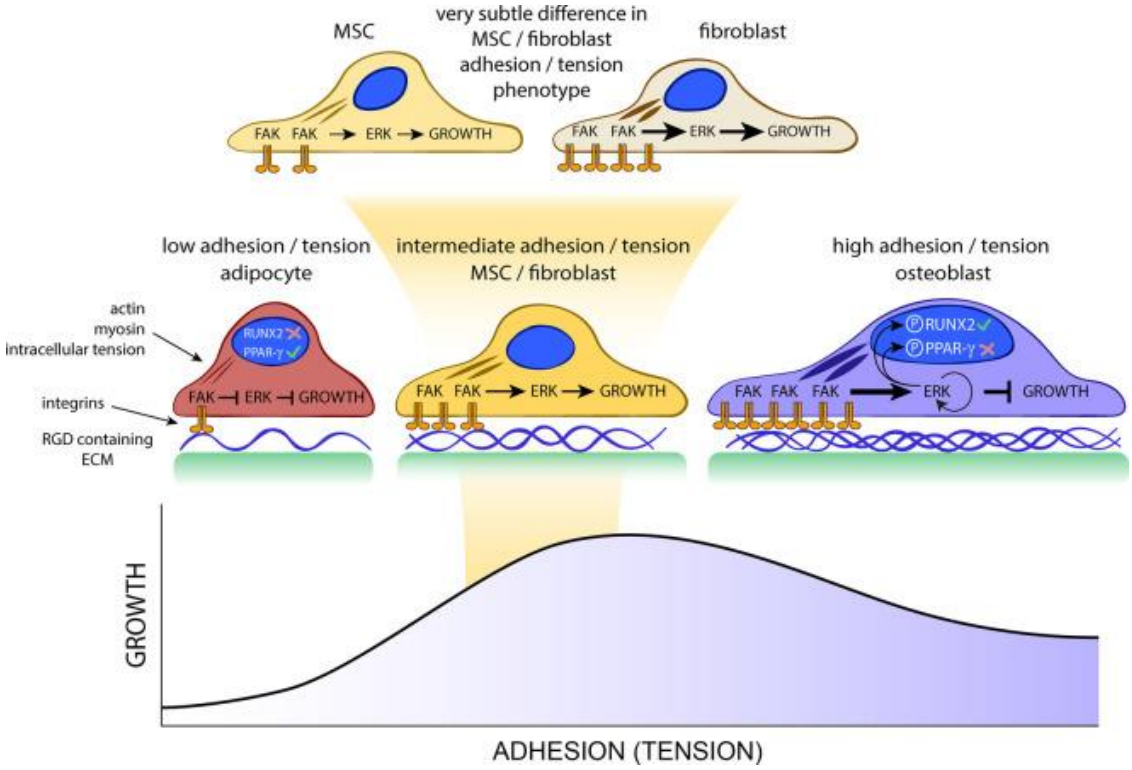

Figure 7: Diagram showing the interplay between focal adhesion kinase (FAK) and cell lineage commitment in MSCs [4]. Low levels of adhesion in MSCs results in adipogenic expression whilst higher levels of adhesion direct MSCs towards osteogenic lineages [103, 106, 126, 127]. Figure reproduced under creative commons licence from [4].

The next protein involved in force transmission is talin, which has a binding site for integrin, two sites for actin and several sites for the protein vinculin. When no force is present, talin rods are fully structured and no sites for vinculin are present. However, the more force applied, the more vinculin molecules are activated. This process is called talin-vinculin mechanosensitivity and successive binding is thought to be vital for transmission of mechanical signals as cells lacking vinculin have been found to have a reduced contractility [94, 128]. The now exposed vinculin binding sites allow for the recruitment of actin related protein 2/3 (Arp2/3) which leads to the promotion of actin polymerization [121]. Once vinculin is bound to talin on a focal adhesion site, conformational changes

occur within the structure [94]. Another protein with the ability to bind to activated vinculin is paxillin, which is localized at the FA intracellular layer [94]. Like vinculin, paxillin can only be recruited by FA sites when extracellular tension is applied [94]. Another mechanoresponsive protein is zyxin which has the ability to promote actin filament assembly, and thus provides a crucial role in mechanosensitivity [129]. Finally, actinins are responsible for crosslinking filamentous actin fibres and are essential in the organisation of the actin filament cytoskeletal network [94].

1.3.4 Cytoskeleton

FAs provide anchorage to the cytoskeleton which is composed of filaments and crosslinking proteins and extends throughout the cell, consisting of microtubules, microfilaments, and intermediate filaments. It provides mechanical support to a cell and helps it maintain its shape. Intermediate filaments are highly flexible, interacting with multiple signalling pathways and are mainly responsible for providing structure to cells [94]. Microtubules, formed by polymerised tubulin dimers, are the stiffest of all the cytoskeletal components and are involved in vital processes including the movement of molecules, formation of mitotic spindles and polarising the cell [94, 130, 131]. Microtubules have also been found to respond to mechanical stress, as one study found that forces could be used to control the positions of mitotic spindles [132].

Microfilaments are strong under tension, but weak under compression and are composed of globular multi-functional proteins known as actin [133]. Single globular actin (G-actin) bind together in a process known as polymerisation, leading to a lengthened filament of actin (F-actin) which forms a helical structure and regulates cell stiffness [133]. G-actin has a barbed end and a pointed end to its monomer and is constantly undergoing actin polymerisation, the hydrolysis of ATP into adenosine diphosphate (ADP), making the structure dynamic and ever changing, which is essential to allow the cell to interact with the ECM [133]. The F-actin filament can also have secondary branching, facilitated by the protein Arp2/3. Other proteins such as profilin and tropomodulin cause actin lengthening, whilst capsazepine (CapZ) leads to actin shortening. Another

protein, tropomyosin binds to the side of actin, stabilising the filament. The actin cytoskeleton is also stabilised by cofilin whose activation leads to the severing of F-actin fibres, allowing the protein to be depolymerised to G-actin, reducing cell tension [134, 135]. Mechanical stimulation leads to constant phosphorylation of cofilin [94].

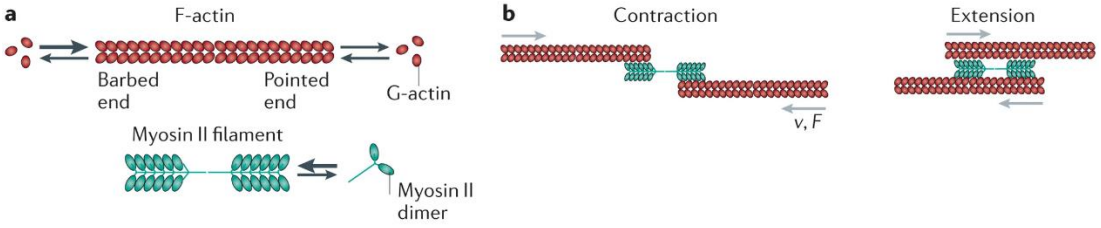

Figure 8: Actin-myosin contractility [136]. Single globular (G-actin) bind together in a process known as polymerisation, leading to a lengthened filament of actin (F-actin) involved in regulating cell stiffness. Cell motility and cytoskeletal contraction occurs due to the interplay between actin filaments and the protein myosin, particularly F-actin interaction with myosin II [102]. These actin-myosin complexes extend to the nucleus, forming a connection between FAs and the nuclear envelope and are also involved in cell division, controlling cell shape, and producing cytoskeletal tension [94, 133, 137]. Figure reproduced with permission from [136].

Actin filaments have multiple roles, aside from their involvement in muscle contraction, including cell adhesion and cell motility. Cell motility and cytoskeletal contraction occurs due to the interplay between actin filaments and the protein myosin, particularly F-actin interaction with myosin II (Figure 8) [102]. Myosin converts ATP to mechanical energy, thus generating force and movement driving cell motility. Actin-myosin complexes extends to the nucleus, forming a connection between FAs and the nuclear envelope [137]. As well as cell motility, actin-myosin interactions are involved in cell division, controlling cell shape, and producing cytoskeletal tension [94, 133]. The size of FAs along with the number of proteins contained, is believed to be associated with the amount of tension it generates, with a larger FA leading to a highly contracted cytoskeleton [67, 138]. This tension is vital for both the transmission of mechanical signals and for the adherence and migration of cells [94]. Through integrin binding, MSCs can sense the stiffness of their surrounding environment, with the cytoskeleton responding to stiffness by adjusting its tension [102]. These adhesion and tension

changes have an impact on osteoblast differentiation [127, 139]. Osteoblasts require larger adhesions and have increased spreading, necessitating a highly contracted cytoskeleton for support, higher tension and thus larger focal adhesions [67].

F-actin and myosin II also form stress fibres (SFs), held together by crosslinking proteins [133]. Three types of stress fibres are formed after mechanosensing: dorsal stress fibres, transverse arcs, and ventral stress fibres [133]. SFs transmit forces between the ECM and nucleus whenever FAs are pulled [94]. Throughout mechanotransduction these SFs and FAs communicate and stabilise each other [94]. SFs have been found to be directly linked with microtubules [140]. Depletions in myosin II levels can lead to problems with contractility, fewer FAs and the reorganization of SFs [141-143].

1.3.5 Tensegrity

The actual structure of the cytoskeleton within the cell is highly complex, heterogeneous and has proven difficult to model. However, a simplified concept, first devised in the 1960's, has since been used to explain the structure of the cell. The architect R. Buckminster Fuller first used tensegrity to explain how structures use tension to achieve stability, before the idea became thoroughly explored in the field of cell modelling, most predominantly by Donald Ingber [144-147]. Both compression and tension are key elements to tensegrity, as compressive and tensile components interact to achieve stability. Compressive elements are commonly referred to as 'struts', whilst tensile elements are known as 'cables'. Compression is applied by cables 'pulling' on the ends of struts whilst struts apply tension by 'pushing' out [144]. This pre-tenses cables, resulting in a tensile pre-stress within the structure [144]. The same design concept may be used with springs [144]. A diagram of the concept is shown in Figure 9.

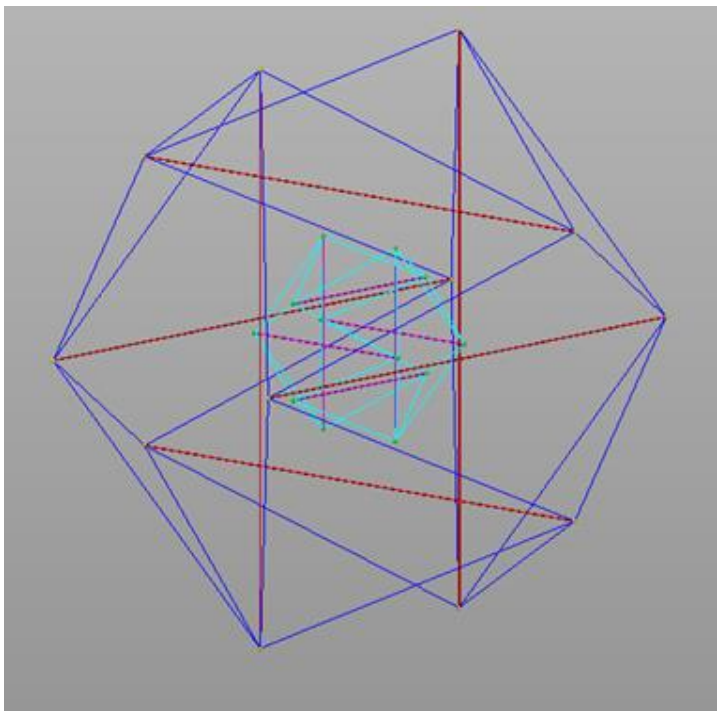

Figure 9: Tensegrity model of a cell also with nuclear tensegrity. Red and magenta lines represent microtubules (struts), whilst the blue and cyan lines represent actin (cables). Model designed in AutoCAD.

Multiple studies have modelled a tensegrity structure within the cell and used this to predict cellular responses [148-153]. In these models, the contractile actin cytoskeleton (cables) exerts tension whilst the microtubules (struts) resist the applied compression [154]. A pre-stress is created within the cell, providing stability to the cell which then responds to changes in structure or the matrix [121, 144]. Tensegrity suggests that a complex relationship exists between actin filaments and microtubules, allowing cells to sense and respond to applied mechanical signals [121]. These forces are then transmitted to the nucleus in a process termed nuclear mechanotransduction [121].

1.3.6 Nuclear Mechanotransduction

That the nucleus has its own mechanosensitive apparatus has only recently been suggested [155, 156]. The nucleus interacts with both actin and microtubules through binding proteins present on the surface of the nuclear membrane [157, 158]. Collectively, these proteins are known as the linker of nucleus and cytoskeleton (LINC) complex [157, 158]. On the nuclear membrane, nuclear pore

complexes (NPCs) create channels, allowing proteins to transfer to the nucleus [159]. Proteins such as yes associated protein (YAP), which play an important role in controlling cell proliferation, have been found to translocate to the nucleus in response to mechanical signals including the rigidity of the ECM, strain, shear stress and adhesive area [160-167]. The LINC complex is also involved in YAP translocation, as the inhibition of the complex decreases nuclear YAP concentration [168]. ECM stiffness and tension in the actin cytoskeleton have both been found to influence YAP concentration in the nucleus [164].

The LINC complex is also essential in force transmission to the nucleus, which leads to a biological response as it connects the nucleoskeleton (the cytoskeleton within the nucleus), nuclear envelope and the cytoskeleton together (see Figure 10) [94]. The forces transmitted to the nucleus control interactions between the nucleus and centrosomes, the architecture of the nucleus, DNA repair and chromosome migration [169]. Research has also found that connections through LINC are essential for the remodelling of the actin cytoskeleton [170]. The main components of the LINC complex are SUN and nesprin proteins as well as lamin within the nuclear lamina. Nesprin are embedded on the outer membrane of the nucleus and extend through the membrane to connect to SUN proteins on the inner membrane [94]. These SUN proteins are then linked to the nuclear lamina and to the intermediate filament lamin A [94, 102]. As such, Sun1 has been shown to be essential for force generation within the cytoskeleton [171]. Meanwhile lamin is involved in transmitting signals within the cell to the nucleus and thus plays a vital role in mechanosensitivity. Any depletion or detachment of lamin A from the nucleoskeleton has been linked to a defective and fragile nucleus [172]. Lamin A/C protein levels are low in stem cells, and have been shown to increase during differentiation [173].

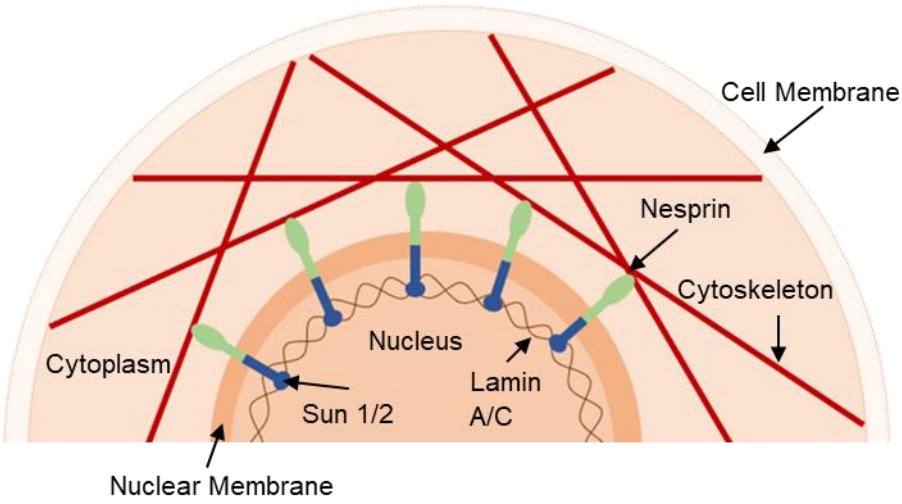

Figure 10: Diagram of the LINC complex within the cell with nuclear membrane proteins and other components labelled.

The nucleus is under constant tension, however the application of stress can lead to increased translocation of proteins such as YAP via nuclear pore complexes, which are then able to regulate gene expression [164]. Increased tension can also lead to chromosome reorganisation leading to the activation of specific transcription factors [174]. Different configurations of chromosome arrangements have been shown to activate different lineages in MSCs [126]. As such, chromosome organisation and nuclear dynamics are essential for gene expression regulation, with different levels of applied forces resulting in different responses from cells [121].

1.4 Physical Control of Stem Cell Differentiation

In recent years, there have been many studies targeting the mechanosensitive properties of cells, applying mechanical stimulation to induce stem cell differentiation *in vitro*. Techniques such as electrical stimulation, compression, tension, shear stress, and vibration have proven to be promising methods to induce cell lineage commitment.

1.4.1 Electrical Stimulation

Electrical stimulation has predominantly been used to direct neural differentiation in neural stem cells [175, 176]. Such a technique can be applied in

a variety of ways, using electrodes within cell media, applying electrical stimulation to materials upon which cells are grown, or by exposing cells to electric fields or electromagnetic fields. Whilst the majority of studies have investigated neural differentiation in neural stem cells, there have been studies inducing neural markers in MSCs. One study found that MSCs show increased neurogenic markers following the application of 8 mV/mm DC for 20 hours/day for 9 days [177]. The application of pulsed electrical stimulation for 21 days has been found to lead to MSCs expressing neural markers [178].

Electrical stimulation has also been used to induce osteogenic differentiation in MSCs. There have been clinical trials applying electrical stimulation to bone, finding positive outcomes when treating fractures [179], osteoporosis [180] and osteonecrosis [181]. *In vitro*, electrical stimulation has been combined with chemical stimulation to induce osteogenesis in MSCs [182]. Some studies used pulsed electrical stimulation to induce osteogenesis [183, 184]. Electrical stimulation has also been used in combination with various materials to induce osteogenesis, such as titanium and O_2 plasma-treated indium tin oxide glass [185, 186]. There have been very few studies which have successfully induced osteogenesis in MSCs using electrical stimulation without using chemical factors [187].

As well as neural and osteogenic differentiation, electrical stimulation has also been found to induce cardiac differentiation in human cardiac progenitor cells [188], human induced pluripotent stem cells [189] and human cardiosphere derived cells [190]. Electrical stimulation has even been found to direct BM-MSCs to differentiate into cardiomyocyte-like cells [191]. Chondrogenic differentiation has also been induced by electrically stimulating MSCs encapsulated within hyaluronic acid gelatine substrates [192]. The morphology of the cells within these hydrogels were found to be rounder than the control and expressing higher levels of chondrogenic markers [192].

1.4.2 Compression

Compression studies are heavily focused on cells and tissues which experience compressive loads *in vivo*, such as cartilage and bone. These tissues are constantly experiencing hydrostatic pressure, and so studies which have applied this pressure *in vitro* to MSCs have found that this results in an upregulation in chondrogenic gene expression [102, 105, 193-198]. By applying hydrostatic pressure within the physiological range of 7-10 MPa, studies have successfully induced chondrogenesis in both MSCs and chondrocytes [193-196]. Some studies have found applying a lower pressure of 5.03 MPa using a cyclic load of 1 Hz for 4 hours/day was sufficient to induce chondrogenesis [197]. Cyclic compressive strain has also been found to induce endothelial progenitor cells to differentiate into vascular networks [199].

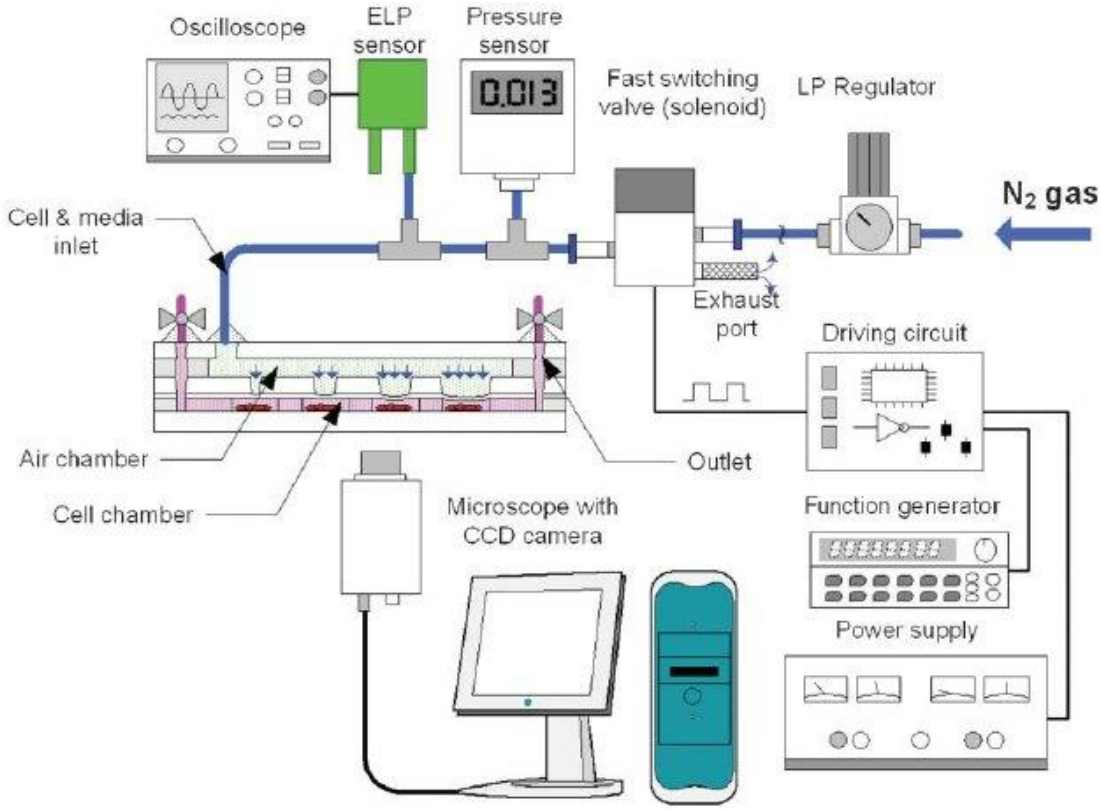

Figure 11: Diagram of experimental set up of micro cell chip designed to apply pneumatic pressure to MSCs to induce osteogenesis. Figure reproduced with permissions from [200].

Pressure can also be applied pneumatically. Such a technique has been used in microchip studies, where cells are cultured within the device and exposed to

pneumatic pressure (see Figure 11). One such study found that the application of such pressure increases osteogenic differentiation in MSCs [200].

1.4.3 Tension

The study of tensile strain on stem cell differentiation involves the use of specific bioreactors (e.g. Uniflex and Bioflex from Flexcell), which apply uniaxial or biaxial strain to cell cultures by using pneumatic pressure changes along a flexible membrane (see Figure 12) [63]. A study by Ouyang *et al* used the BioFlex tensile plates to culture rabbit chondrocytes before applying cyclic sinusoidal tension which resulted in improved proliferation of chondrocytes [201]. Studies into the effects of tensile strain have found lower strains of 0-6% to effectively increase ligamentous/fibrogenic gene expressions [202, 203], whilst strains of 10% increase chondrogenic gene expressions [204, 205]. However, an increase in osteogenic gene expression has been observed across a range of strains between 2.5-12% [206-211].

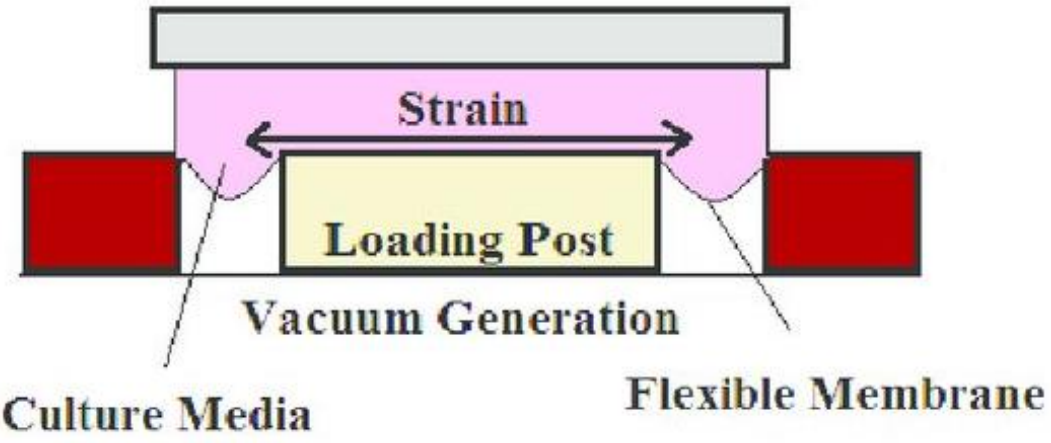

Figure 12: Flexcell mechanism for applying strain to cell cultures. Figure reproduced under open access licence from [63].

Cyclic strain has also been found to increase osteogenic gene expression and calcium deposition [206, 208, 209, 211, 212]. Generally, studies have found that the application of lower strains for longer timescales increases osteogenesis in MSCs [210, 213-216]. One study using a Flexcell Tension System applied a 10% continuous cyclic strain of 0.5 Hz to cells over a period of 14 days resulting in an

increase in osteogenic marker expression [214]. Uniaxial strain has also been investigated as it is experienced by both skeletal muscle and tendons and ligaments *in vivo* [105]. Studies have successfully demonstrated that the application of uniaxial strain with or without chemical induction leads to higher expression of myogenic factors from MSCs [217, 218].

Tensile strain is believed to impact the TGF-β pathway [63, 219, 220]. Studies have shown that this may lead to increased expression cytoskeleton markers [219, 221]. In human embryonic stem cells (hESCs) and human induced pluripotent stem cells (hiPSCs), tensile strain has also been shown to promote cell renewal and cell growth [220, 222]. Tensile strain has also been shown to inhibit cell lineages and direct differentiation in stem cells [63]. However, many tensile studies used both mechanical stimulation and chemical factors to induce osteogenesis. It is likely that this is very representative of the *in vivo* condition within the body that experiences both chemical and mechanical stimulation, however it fails to demonstrate the effectiveness of tensile strain when used in isolation.

1.4.4 Shear stress/perfusion

Shear stress can be defined as the frictional force generated by the movement of a fluid tangential to the solid boundary of its container. This form of mechanical stimulation on stem cells has primarily been investigated for endothelial cells that line blood vessels as well as cardiomyocytes which constantly experience shear stress within their microenvironment [223-225]. Other studies have demonstrated that pulsating shear forces may be used to direct canine MSCs towards an endothelial lineage [226]. Bone cell also experiences shear stress during mechanical loading, due to fluid flow within the canalicular-lacunar and trabecular spaces [121]. *In vivo*, steady laminar fluid shear flow of 12 dynes/cm^2 has been shown to stimulate osteoblast differentiation [227]. *In vitro*, the application of fluid shear stress on MSCs leads to an increase in alkaline phosphatase (ALP), OPN and mineralization, indicating osteogenic differentiation [227-231]. Studies have also shown that shear stress suppresses apoptosis in BM-

MSCs [232]. 3D studies have also successfully demonstrated that perfusion systems effectively promote osteogenesis in MSCs [230, 233].

1.5 Vibrational Stimulation of Stem Cells

One of the simplest forms of mechanical stimulation to apply *in vitro* is vibration. There have been multiple studies investigating the *in vitro* effects of vibration on cells, particularly on stem cell differentiation. The use of vibrational stimulation to induce osteogenesis in both stem cells and bone-like cells have been the most commonly reported, however a vast range of cell types have been vibrated and their responses studied including: human BM-MSCs, adipose-derived stem cells (ASCs), UC-MSCs, SAOS-2, human dental pulp stem cells (hDPSCs), myocytes, neuroblastoma cell lines, metastatic breast cancer cells, human vocal fold epithelial cell line (hVFF), murine osteocyte-like cell line (MLO-Y4), HeLa, HaCaT, rat BM-MSCs, mouse D1-ORL-UVA, MC3T3-E1, BALB/c, C2C12, L929, pig chondrocytes, and rabbit MSCs [234-252]. In addition to stimulating cell lineage commitment, vibrational stimulation has also been shown to promote wound healing [244, 250, 253]. With such an array of responses being induced in a range of cell types, the use of vibration on cell therapy holds vast potential. However, a huge range of vibration conditions have been used, with little consistency between studies, thus making it challenging to compare responses.

1.5.1 Impact on Proliferation

Proliferation rate of cells in response to vibration varies across studies. Multiple studies have found that vibration increases proliferation rate, even restoring proliferation levels of cells grown in simulated microgravity [239, 242, 254-261]. However there have been a number of studies that have found proliferation rate to decrease in vibrated cells [234, 235, 238, 247, 262-265], or observed no change at all [245, 266]. This decrease in proliferation may be an indication of increased differentiation in cells, particularly in stem cells, as cells commit to specific cell lineages. However, these studies use a range of vibration conditions, making it challenging to determine precise conditions under which proliferation rate changes. Some studies have compared proliferation rates at a range of

frequencies, such as Rosenberg *et al* who tested multiple frequencies (20-60 Hz) and found the lower frequency of 20 Hz to be optimal for increasing the proliferation rate of osteoblasts from older patients (55-77 years) [267]. This increased proliferation in cells from older patients agreed with another study by Maredziak *et al* who found proliferation to increase in ASCs from patients with an average age of 69 years following vibration of 25 Hz [257]. Another study comparing proliferation rate at different frequencies found a low frequency of 1 Hz increased proliferation in human keratinocytes, whilst 80 Hz decreased proliferation [244]. These studies suggest that proliferation rate may be frequency dependent, however it is still unclear the precise vibration conditions which influence proliferation rate.

1.5.2 Vibration Directionality

Whilst most vibration studies have applied a vertical vibration (27 studies), fewer have applied vibrations horizontally (9 studies), and fewer still have compared the effects of the two. Applying horizontal vibration to cells (parallel to the cell monolayer) has been found to lead to interesting effects, such as inducing fibroblast cells to collectively migrate in the direction of vibration [250]. However, one of the concerns with using horizontal vibrations is that fluid shear stress may be produced due to media sloshing within the well, pulling into question whether effects observed are solely due to vibration. The majority of the research into this has been conducted by one group who quantified fluid shear stress due to vibration, finding it to be two orders of magnitude greater during horizontal vibration than vertical vibration [170, 268]. Therefore, any responses observed following horizontal vibration may have been influenced by fluid shear stress. In an attempt to eliminate the effects of fluid shear stress, some studies would completely fill and seal cultureware during horizontal vibration [266, 269]. However, to further understand how much of an influence fluid shear stress has during horizontal vibration, Uzer *et al* applied a range of vibration conditions to human ASCs and analysed the effects and quantifying fluid shear stress using both particle velocimetry and finite element modelling (Figure 13) [270]. They found that the vibrations resulting in the lowest fluid shear (100 Hz) showed more

mineralization (3-fold) than cells vibrated at a higher fluid shear. For the highest fluid shear (30 Hz), a larger acceleration magnitude was required to achieve the same level of mineralization as the lowest fluid shear conditions (100 Hz). Therefore, the group concluded that fluid shear stress does not have a significant effect on cells during horizontal vibration. Another paper by the same group, Pongkitwitoon *et al* again found the vibration condition combination that produced the lowest fluid shear stress resulted in the highest osteogenic response [271]. Another study independently assessed the motion of fluid during horizontal vibration and found there to be little motion between the fluid and dish, concluding that cells would be primarily responding to stimulation from vibration and not fluid shear stress [272]. Bacabac *et al* postulates that fluid shear stress may only be significant at low frequencies (<10 Hz) as fluid flow may be attenuated at higher frequencies (>10 Hz) [269]. These models have aimed to isolate vibration as the influencer of cell response, however this is not representative of the *in vivo* conditions of fluid shear stress within the body, and as such shear flow may be of added benefit [273].

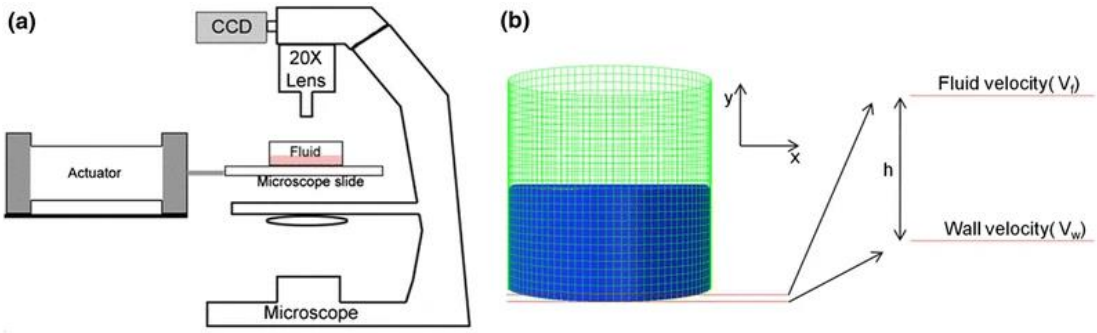

Figure 13: Setup used by Uzer *et al* when testing a range of vibration conditions on human ASCs and quantifying the levels of fluid shear stress. A) Authors used Particle Image Velocimetry (PIV) to quantify fluid shear stress. B) Results were compared to FEMs of wells to predict levels of fluid shear stress during vibration. Figure reproduced with permission from [268].

Studies comparing the effects of horizontal and vertical vibration on cells have found horizontal vibration to have an increased osteogenic effect on cells [271, 274]. Pongkitwitoon *et al* found that the higher horizontal vibration of 100 Hz applied to BM-MSCs produced the optimal response [271]. Horizontal vibration was found to lead to the realignment of the cell cytoskeleton which in turn

increased cell stiffness as measured by atomic force microscopy, an effect not seen in vertical vibration. ALP activity and mineralisation were also increased more than vertical vibration. Similarly, Halonen *et al* found that horizontal vibration in combination with osteogenic media resulted in cell alignment (device used shown in Figure 14) [274]. Horizontal vibration was found to increase ALP activity whilst vertical vibration decreased it. In contrast to Pongkitwitoon *et al,* Halonen *et al* found mineralisation was not increased in horizontally vibrated samples. Despite this, the few studies comparing horizontal and vertical vibration have found a higher response to horizontal vibration, suggesting that response may be directionally dependent, and that this optimal response may likely be primarily due to vibration, but the effects of fluid shear cannot be fully disregarded.

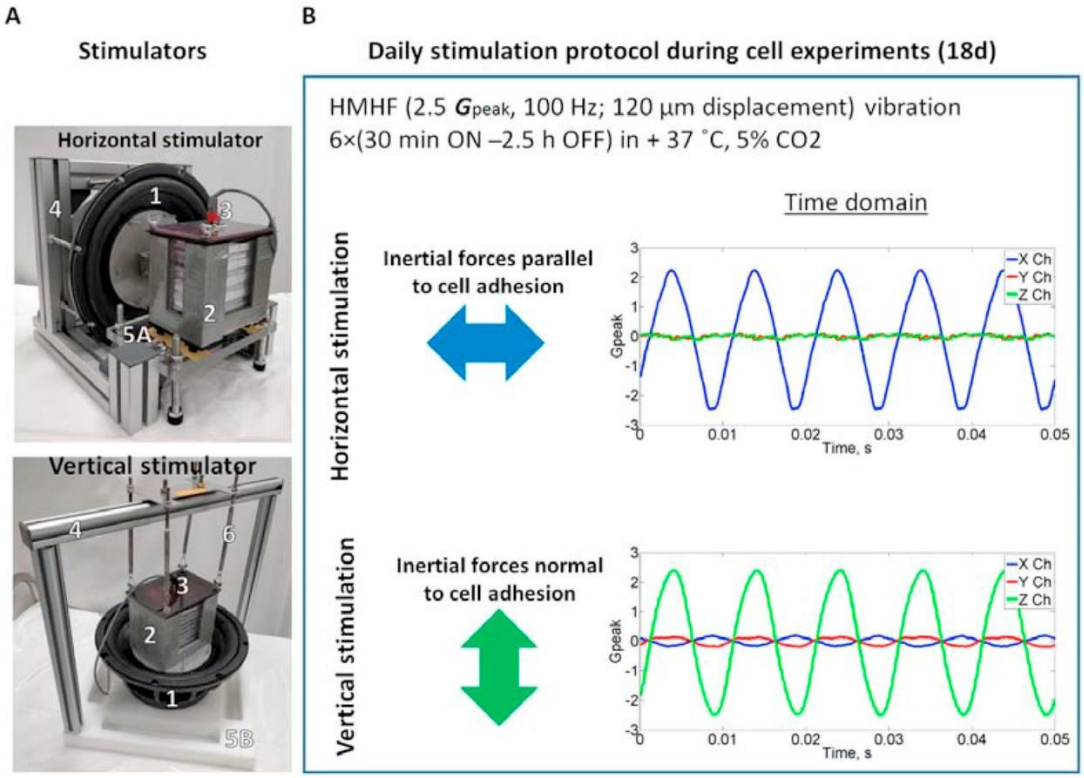

Figure 14: Vibration device used by Halonen *et al* to compare horizontal and vertical vibration. A) Authors used commercial subwoofers to apply vibration to cells held within 3D printed holders. B) Accelerometers characterised vibration in three directions. Figure reproduced under creative commons licence from [274].

1.5.3 Impact of Seeding Density

Culture conditions vary widely across studies, including seeding density. Seeding density is particularly important when working in 3D and seeding scaffolds. Higher seeding densities involve more cell-to-cell interaction, which may affect cell response. However, too high an initial seeding density, and cells may die, or their metabolism and viability may be affected. Inversely, a lower seeding density, means a higher intercellular distance, which results in lower cellular sensitivity of the substrate and too low a seeding density may not provide the required cell-to-cell contact when culturing in 3D [275].

Initial seeding density also has an effect on phenotypic changes. BM-MSCs and MG63s seeded in 3D scaffolds at high cell densities (10^6-10^7) have been found to exhibit higher mRNA expressions of osteogenic markers [276, 277]. Similarly, chondrocytes seeded at higher seeding densities have also been found to lead to an increase in chondrogenic genes compared to lower seeding densities [278, 279]. However, there is a limit to this increase, with higher seeding densities showing a plateau effect as there are no more increases in some gene expression [280]. Seeding densities of the order of 10^5 for ASCs have also been found to lead to an increased production of angiogenic factors [281]. Studies have also found seeding density to affect mechanical properties of cells, such as tensile strength and Young's Modulus where a higher seeding density can lead to a reduction in mechanical properties [282, 283]. This dependency on seeding density for cell response suggests that seeding density is a vital factor, with little investigations being conducted into its effect on cell response during vibration. There may therefore be a need to standardise seeding densities used across studies to ensure that responses observed are due to vibrational effects and are not being influenced by cell-to-cell interactions caused by various seeding densities.

1.5.4 Intermittent Vibration

Vibration duration varies across studies, some applying vibration for only a few minutes, others vibrating continuously, and others using an intermittent vibration, such as Halonen *et al*, who applied vibrations for 30 minutes at a time

with a 2.5 hour break in between, repeating this 6 times [274]. Gene expression changes in response to vibration have been seen after only 10 minutes of vibration by both Ota *et al* and Ambattu *et al* [284, 285]. Ota *et al* saw an increase in three osteogenic genes measured 24 hours after the application of only 10 minutes of vibration, postulating whether a short length of applied vibration would be sufficient to induce an osteogenic response [284]. The group however did not investigate whether this upregulation in osteogenic genes continued at later timepoints, making it unclear whether the observed increase was temporary or permanent. Another study by Ambattu *et al* again observed osteogenic results after only 10 minutes of stimulation, however they continued to apply vibration for 10 mins/day for 4 days (device used shown in Figure 15) [285].

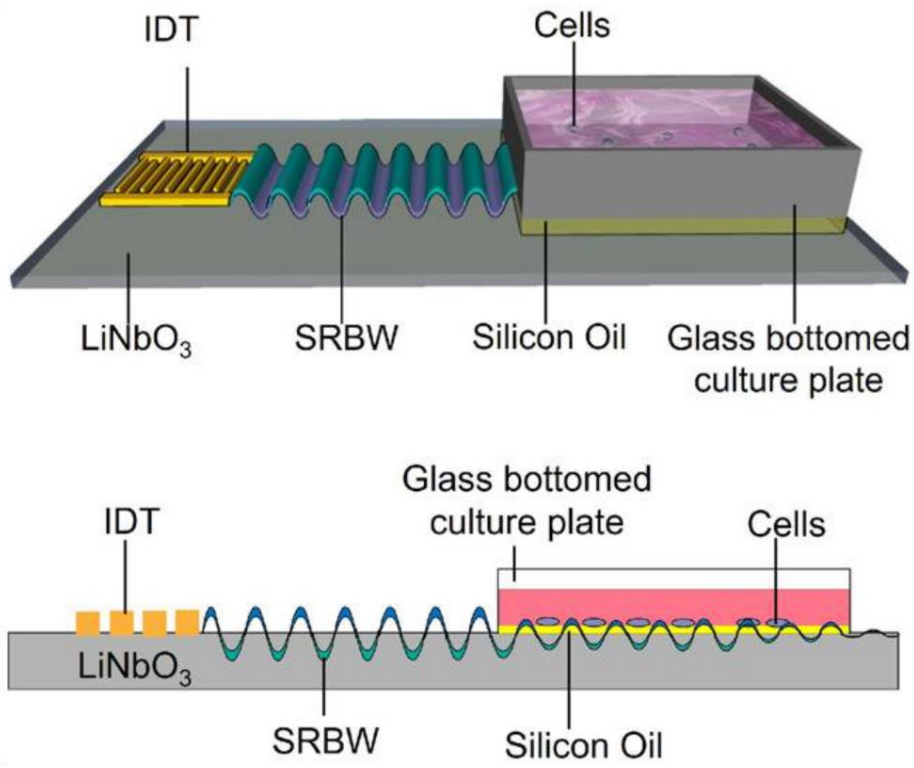

Figure 15: Setup used by Ambattu *et al* to apply surface-reflected bulk waves (SRBW) to cells [285]. Study found that cells expressed osteogenic genes following stimulation for 10 mins/day for 4 days. Figure reproduced with permission from [285].

In contrast to these shorter periods of vibration, a study conducted by Pre *et al* tested several durations to apply vibration and found that longer times (45 and 60 mins per day) are required for an optimal osteogenic response [235]. It may

be that cells do have an initial response to vibration with only a short duration of stimulation required, but to ensure an enhanced response, longer periods of vibration may be required. Some studies continuously stimulate cells with no break in vibration, however few have compared continuous and periodic vibration. One study conducted by Tong *et al* tested continuous and an on/off regime of vibration and found that periodic vibration of BM-MSCs was more effective in producing essential matrix components [286]. The use of continuous vibration may therefore have a detrimental effect on cells, as continuously stimulating cells may result in cells acclimatising to vibration and becoming less responsive. The lack of consistency in how long stimulation is applied to cells highlights a need for further investigations into whether cells do acclimatise to stimulation and whether there is an optimal time for stimulating cells.

1.5.5 Phenotypes reported following vibration

1.5.5.1 Osteogenesis

Osteogenesis has been the most commonly investigated response to vibration with studies investigating a wide range of vibration conditions to induce an osteogenic response in multiple cell types. Pre *et al* conducted several studies testing a range of vibration conditions on BM-MSC, SAOS-2 and ASC cells and found that a frequency of 30 Hz, 11 mm applied for 45-60 mins/day for up to 40 days was sufficient to induce osteogenesis [234-236]. Higher frequencies have also been used to successfully induce osteogenesis. Lee *et al* found vibrations of 100 Hz to result in higher numbers of calcified nodes [238]. Studies conducted by Nikukar *et al,* Kennedy *et al* and Orapiriyakul *et al* used even higher frequencies of 1 kHz to induce osteogenesis in MSCs [67, 287, 288]. These studies also use much lower amplitudes on the nanometre scale, with a recent study finding that osteogenesis increases at higher amplitudes of 90 nm compared to 30 nm [287]. Ultrasound has also been used to induce osteoblast differentiation, successfully increasing mineralisation and osteoblastic gene expression [289].

Few papers have reported a negative osteogenic response to vibration, however Lau *et al* did not find vibrations of 60 Hz, 0.3 G to result in osteogenic differentiation or to change proliferation rate [266]. Instead, vibration was found

to decrease matrix mineralisation and inhibit osterix gene expression [266]. Lorusso *et al* also did not find vibration to increase Ca2+ but did find it to desensitise the response of calcium to exogenous ATP [272]. With such a wide range of vibration conditions used to induce osteogenesis, and some conditions even inhibiting, it is challenging to determine the precise range to optimise osteogenic responses in cells. There have been several studies which have attempted to compare vibration conditions to induce osteogenesis. Judex *et al* compared two vibration devices, the AcceleDent producing 30Hz, 0.24G for 20mins/d and the VPro5 producing 120 Hz, 0.41 G for 5 mins/day (Figure 16) [254]. The VPro5 was found to increase proliferation and gene expression far more effectively than the AcceleDent. Early studies by Pre *et al* tested multiple frequencies and durations of vibration to optimise an osteogenic response [235]. Similarly, other studies have tested multiple frequencies, directions and amplitudes to identify optimal vibration conditions for osteogenesis, however this optimisation has often been limited to a single parameter, with only a few values being tested [238, 270, 271, 287, 290].

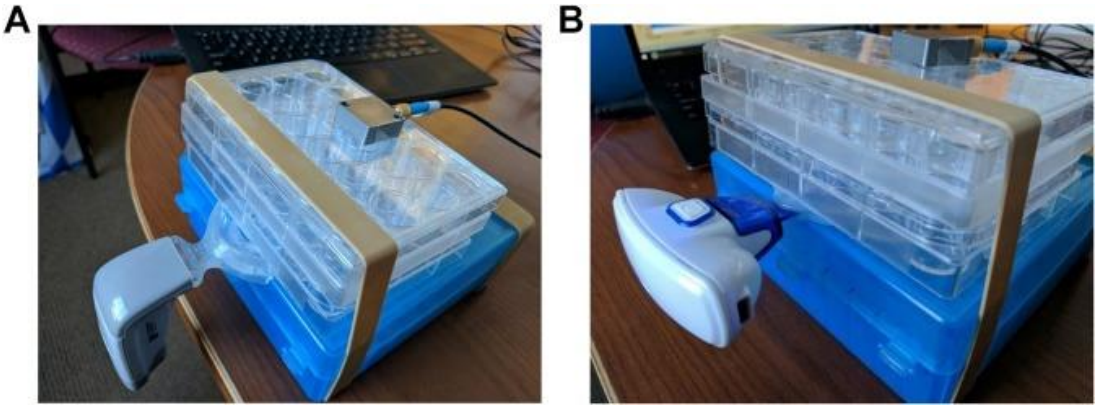

Figure 16: Setup used by Judex *et al* [254]. A) AcceleDent set up providing 30 Hz, 0.24G for 20 mins/day to cells and B) VPro5 setup providing 120 Hz, 0.41 G for 5 mins/day to cells. Figure reproduced under creative commons licence from [254].

Some studies have investigated the effects of vibration on multiple bone-like cells. Pravitharangul *et al* investigated the effects of vibration on two types of osteoblasts: iliac and mandible [290]. They found that the more mature iliac osteoblasts had a more 'potent anti-resorptive response to vibration'. García-López *et al* successfully used vibration to inhibit osteoclasts whilst promoting

apoptosis and activating osteoblasts [248]. Gao *et al* used vibration to increase osteogenic gene expression whilst suppressing sclerostin expression [260]. These studies demonstrate that even between different bone cell types, the response to vibration can be significantly different.

The clinical relevance for most of the studies applying vibration to induce osteogenesis is focused on increasing bone density and osteogenic response for older patients. Yet there have been few papers specifically investigating the effects of vibration on osteogenic response on cells from older patients. Maredziak *et al* used MSCs from older patients (average age of 69) to confirm osteogenesis could still be stimulated [257]. Vibration successfully increased osteogenic differentiation, increasing calcium and phosphorus, and also creating hydroxyapatite-like structures. Rosenberg *et al* also used older osteoblasts from patients aged 55-77 years of age and successfully induced osteogenesis, this time using vibration alone with no osteogenic media [267]. The results of these studies are reassuring, showing that vibration can successfully induce osteogenesis in older cells, however, there still exists a lack of research into comparing the effects of vibration on young and old cells.

1.5.5.2 Adipogenesis

Although there is some overlap in vibration conditions, studies generally agree that low-level vibrations promote adipogenesis, whilst higher vibrations (higher accelerations and frequencies) inhibit [263]. However, there is still some disagreement here, Zhao *et al* and Zhou *et al* found that the same vibration conditions resulted in both adipogenesis and osteogenesis respectively [262, 291]. Zhao *et al* saw increased lipid droplet formation following vibration of BM-MSCs at 40 Hz, 0.3G for 15mins/day for 14 days [291]. Zhou *et al* meanwhile saw increased osteogenesis in BM-MSCs following vibrational stimulation of 40 Hz, 0.3G for 30 mins/day for 26 days [262]. Higher vibration conditions do tend to result in a reduction in adipogenesis. Chen *et al* found adipogenesis to be promoted at 30 Hz, 0.3G for 30 mins/day for 21 days but suppressed at a higher frequency of 800 Hz [259]. This study however used adipogenic media for cells stimulated at the lower frequency of 30 Hz and osteogenic media for cells

stimulated at the higher frequency of 800 Hz. A similar study also found adipogenesis to be promoted at a lower frequency of 25 Hz, 0.3 G for 15 mins/day for 14 days, with the addition of adipogenic media, and was suppressed at 35 Hz, 0.2 G for 15 mins/day for 14 days whilst chondrogenesis increased, with the addition of chondrogenic media [263]. Lineage specific media may therefore be largely contributing to the observed responses in these studies rather than the vibration conditions. A more insightful study was conducted by Baskan *et al* who successfully decreased adipogenesis in vibrated cells grown in adipogenic media whilst stimulating cells at 90 Hz, 0.1 G for 15 mins/day for 7 days (Figure 17) [246].

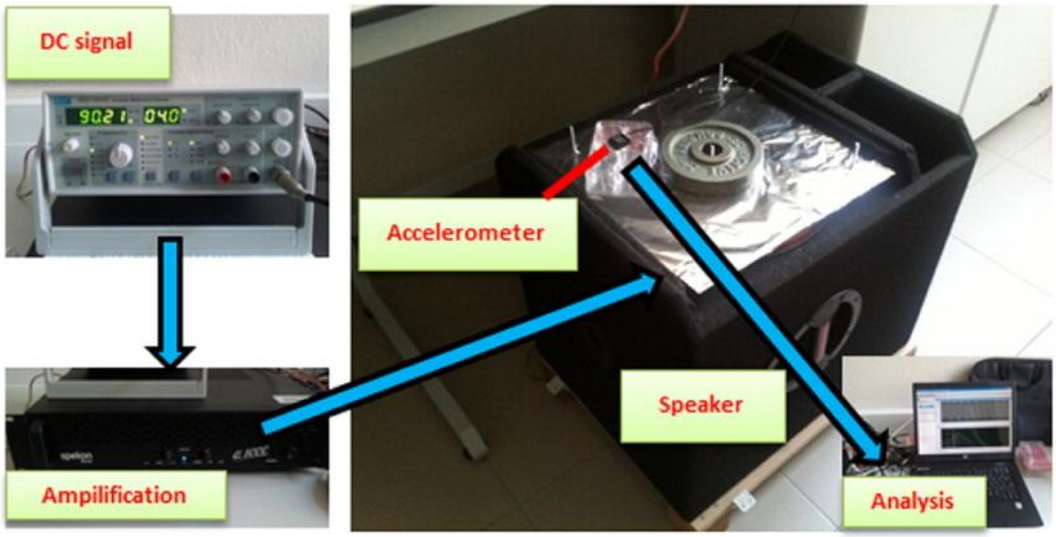

Figure 17: Setup used by Baskan *et al* [246]. Vibrations of 90 Hz, 0.1 G applied for 15 mins/day for 7 days successfully decreased adipogenesis in cells cultured in adipogenic media. Figure reproduced with permission from [246].

There is also some level of disagreement between studies on the precise threshold by which adipogenesis may be promoted and when it may be suppressed. This is particularly crucial, as some studies achieving an osteogenic response use similar vibration conditions to those promoting adipogenesis shown here. Suppressing adipogenesis is vital when designing cell-based therapies used to promote osteogenesis and other responses.

1.5.5.3 Chondrogenesis

Chondrogenesis is less well studied than osteogenesis and most studies have required the use of chondrogenic media. Safavi *et al* applied 300 Hz, 10 μm vibrations to rabbit MSCs for 45 mins/day for 14 days without the use of lineage specific media [251]. They saw a significant increase in osteogenic response, whilst no changes in chondrogenic markers were observed. This lack of response may suggest that chondrogenesis cannot be achieved by vibration alone and that chemical stimulation in the form of chondrogenic media may be required. Another study by Chu *et al* did successfully induce chondrogenesis in MSCs without the need for chondrogenic media, however they found that the effect is enhanced when media and vibrational stimulation were used in combination [292]. A similar study conducted by Takeuchi *et al* vibrated cells in 3D both with and without the addition of hyaluronic acid [252]. They found that using vibration in combination with hyaluronic acid resulted in higher proteoglycan production. The results from these studies may suggest that chondrogenic media is required to achieve a significant chondrogenic response to vibration, although vibration alone may be sufficient to induce chondrogenesis.

1.5.5.4 Myogenesis

Vibration has been shown to successfully increase myotube formation [293, 294]. Wang *et al* found vibrations of 8-10 Hz, 0.4 mm applied to C2C12 cells resulted in increased expression of myogenic regulatory factors and myotube formation [293]. In another study by the same group, they applied 10 Hz, 0.4 mm for 10mins/day for 3 days and found vibration successfully increased myotube formation and expression of cytoskeletal proteins and myogenic regulatory factors [294]. Higher frequencies have also been applied by Tong *et al*, who built a bioreactor to mimic the vocal fold and applied periodic vibrations at human phonation frequencies of 200 Hz (Figure 18) [286]. The group found vibrations resulted in a higher production of matrix components without the need of differentiation media.

The effects of vibration on myocytes taken from both young and old patients have also been investigated. Sancilio *et al* used mechanoacoustic waves to vibrate the

air around cells at 300 Hz [239]. They stimulated both young (23 years) and old (72 years) myocytes in differentiation media and successfully reduced apoptosis whilst increasing cell area and alignment. The mitotic index of cells was also found to increase during stimulation. The two age groups of cells also responded differently to vibration, with younger cells tending to proliferate whilst older cells differentiated in response to vibration. These studies show that myogenesis can successfully be induced in both young and old myocytes using vibrational stimulation.

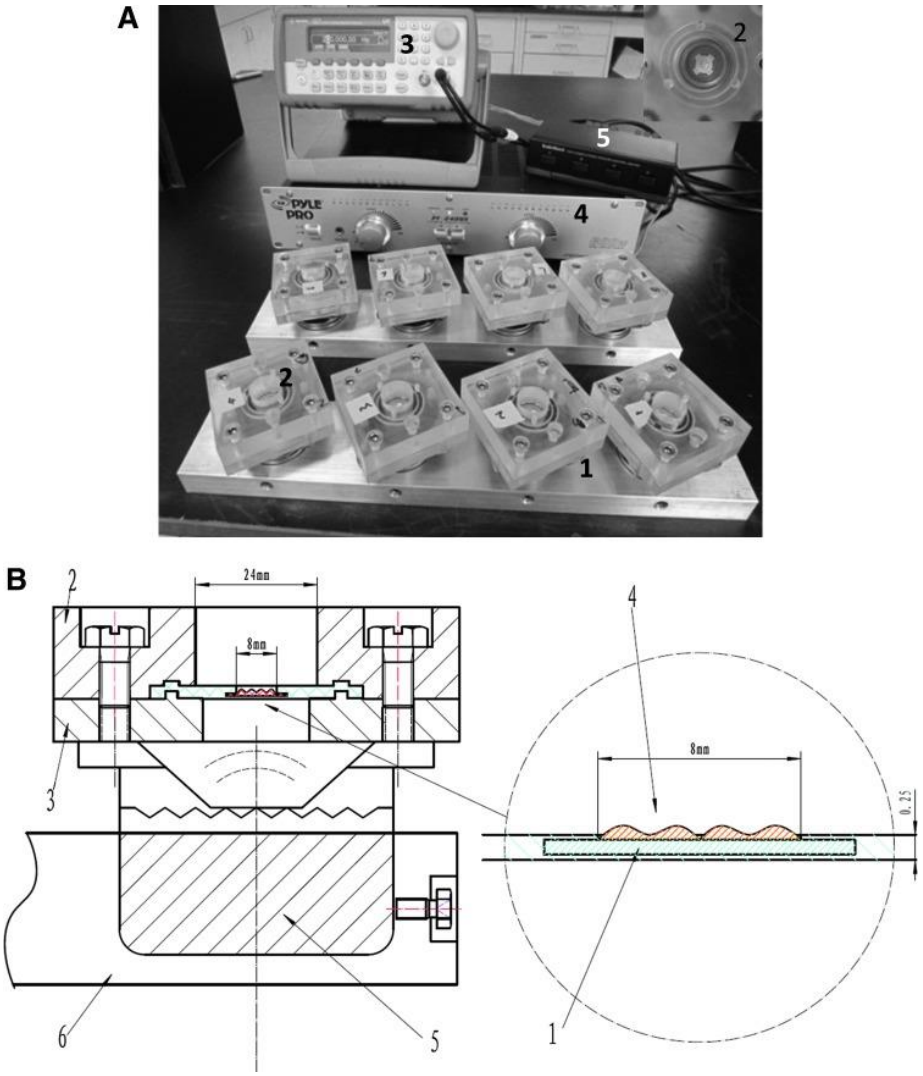

Figure 18: Custom built vocal fold device built by Tong *et al* to investigate the effect of human phonation frequencies of 200 Hz on MSCs [286]. A) Image showing setup. B) Cross-sectional diagram of vibration device. When applied to cells, the group found vibrations to result in a higher production of matrix components without the requirement of differentiation media. Figure reproduced with permission from [286].

1.5.5.5 Neurogenesis

Using vibration to induce a neural response has not been as well studied as inducing an osteogenic response. One study by Grosman-Dziewiszek *et al* applied vibration of 40 Hz, 20-30 nm to a neuroblastoma cell line and successfully increased neurite length with the highest response being on cells grown on a collagen surface using a differentiation medium [258]. There have also been studies applying vibration to stem cells to induce a neurogenic response. Choi *et al* successfully induced a neurogenic response by vibrating human ASCs at 30 Hz, 1.376 G continuously for 4 days in the absence of differentiation media (Figure 19) [42]. Vibration enhanced neural markers whilst inhibiting adipogenesis and vibrated cells achieved elongated and spindle-shaped morphologies. The same group applied vibrations of 40 Hz, 0.938 G continuously for 5 days to human UC-MSCs and again successfully induced a neurogenic response [264]. Although neurogenic markers increased in response to vibration and cells exhibited a more neuronal morphology, the functionality of these cells to be neural-like is still not known and further investigation is required.

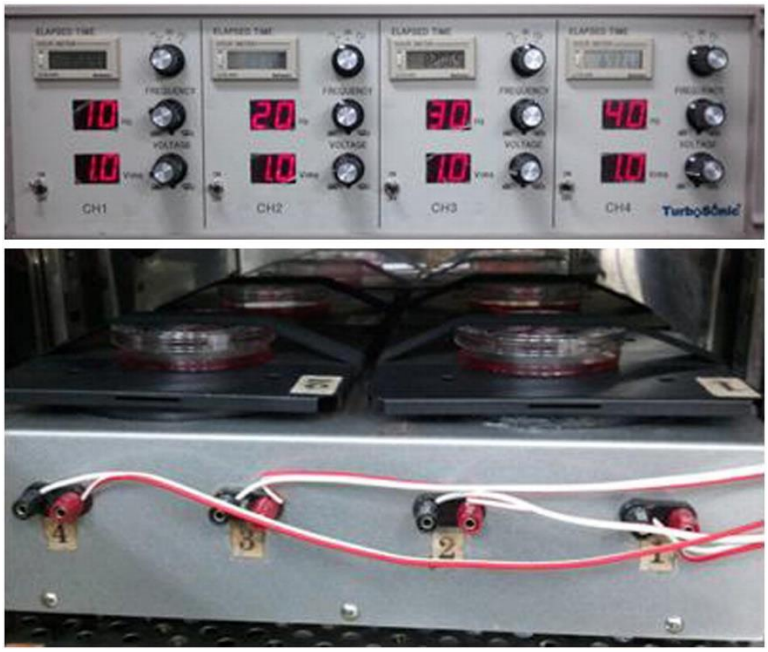

Figure 19: Setup used by Choi *et al* and Cho *et al* when using vibration to direct MSCs toward a neural lineage [42, 264]. Figure reproduced with permission from [42].

1.5.6 Vibration only studies

Many studies use vibrational stimulation in combination with lineage specific media making it difficult to quantify the effect vibration alone is having on cells. Whilst some studies find that vibration alone is not sufficient to promote a response in cells [234], there have been numerous studies which have directed stem cell differentiation using vibration alone (see Appendix A). A relatively recent method of mechanical stimulation using vibration alone is nanovibrational stimulation, also termed 'nanokicking'.

1.6 Nanovibrational Stimulation

Several vibration devices used in previous studies may be considered rudimentary, using loudspeakers to apply stimulation or rubber bands to hold cultureware in place [246, 254]. Another technique, nanovibrational stimulation, developed a the Universities of Strathclyde and Glasgow applies nanoamplitude vibration to cells grown *in vitro* using a custom built device (see Figure 21). The membrane of cells undulates at the nanoscale as they form adhesions, assisting in migration, whilst integrin proteins on the surface are nanometres in size and are involved in interactions with the surrounding environment [67, 295, 296]. Nanovibrational stimulation applies nanometre amplitude vibrations to cultureware, transmitting nanonewton forces to cells grown within in an attempt to trigger a cell response [297]. Based on initial scoping studies, nanovibrational stimulation has been applied to MSCs at a frequency of 1 kHz and amplitude of 30 nm, successfully demonstrating the induction of osteogenesis [67, 139, 287, 298]. Although 1 kHz may be considered to be biologically high, a study measuring the resonance frequencies of temporal bone through patients with skin penetrating titanium implants identified the lowest resonance frequencies to be between 972 – 1164 Hz [299]. In nanovibrational stimulation, a frequency of 1 kHz has previously been deemed to be the optimal frequency for osteogenesis [298]. Whilst previous applied amplitudes of 30 nm have been used, recent studies have suggested that 90 nm produce a more optimal response, suggesting that the

optimal vibration conditions for nanovibrational stimulation have yet to be found [287].

The peak acceleration cells experience during nanovibrational stimulation may be estimated, based on the mass of the fluid on the cell, using Equation 1:

$$a_{\text{peak}} = A_0(2\pi f)^2 \quad (1)$$

where A_0 is the sine wave amplitude and f is the frequency, both produced by nanovibration. Here, both amplitude and frequency are directly related to acceleration experienced by the cell, resulting in higher amplitudes and frequencies leading to an increased peak acceleration experienced by the cell. For osteogenesis, it may be that higher accelerations lead to a higher bone response in MSCs [287].

The majority of nanovibrational stimulation studies has been conducted on 2D monolayer cultures. It has been challenging to apply nanovibrational stimulation in 3D due to the challenges regarding transmitting the vibrations into 3D structures. Tsimbouri *et al* have however successfully demonstrated the 3D culture of osteoblasts from MSCs in hydrogels using the nanovibrational stimulation technique [139]. Mechanoreceptor ion channels piezo, TRP and KCNK were identified as being activated during nanovibrational stimulation, further confirming that nanovibrational stimulation is targeting the mechanotransductive processes within the cell [139]. Studies have successfully mapped several key mechanisms within the cell in response to applied nanovibration (Figure 20) [287]. Recently, nanovibrational stimulation has also been applied to co-cultures of primary human osteoprogenitor and osteoclast progenitor cells, successfully inhibiting osteoclastogenesis whilst enhancing osteogenesis [288].

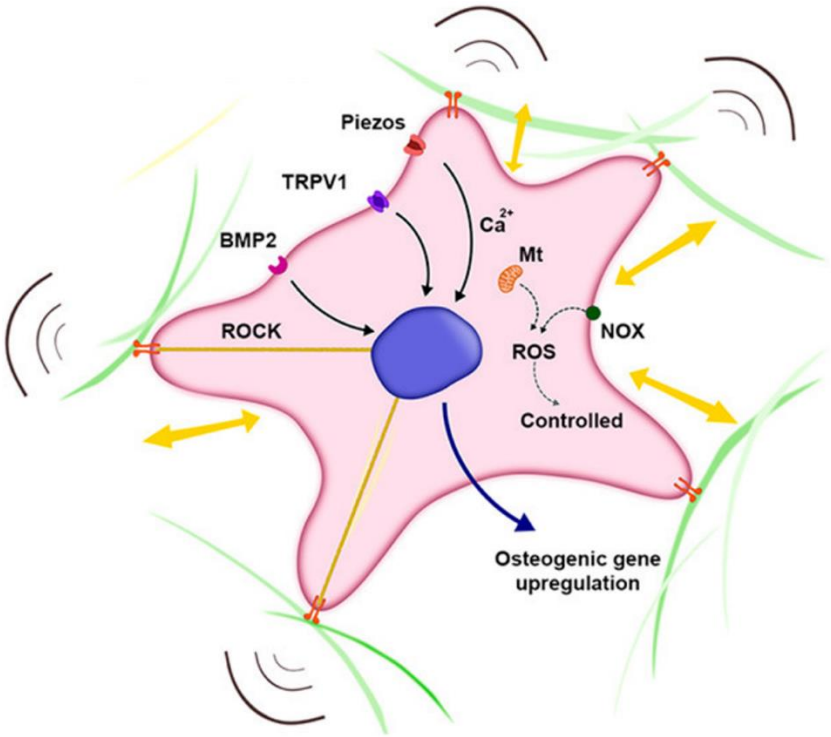

Figure 20: A diagram of cell mechanisms induced by nanovibrational stimulation of MSCs. Nanovibrational stimulation has been shown to activate several key osteogenic pathways including Wnt and BMP. Several mechanosensitive ion channels have also been shown to be activated following nanovibrational stimulation, including Piezo1. Figure reproduced under creative commons licence from [287].

Whilst nanovibrational stimulation has mainly focused on osteogenesis, there have been a small number of studies which have investigated other responses and uses of the technique [300]. Robertson *et al* applied nanovibration to *Pseudomonas aeruginosa* biofilms, successfully reducing their formation [300]. Nanovibrational stimulation has also been applied in the field of immunology to macrophages, influencing the expression of mechanosensors within the cells [301]. With these recent studies into the wider effects of nanovibration, it suggests the technique may not be limited to inducing osteogenesis but may have applications in other areas and may influence other cell types.

1.7 Aims and Objectives

Studies investigating vibration-induced responses often disagree on the optimal vibration parameters. For nanovibrational stimulation, 1 kHz at 30 nm amplitude

has been shown to induce osteogenesis in MSCs. However, recent studies suggest that higher amplitudes may elicit a higher osteogenic effect, potentially due to the increased force exerted on the cells, as force is directly proportional to amplitude (Equation 1) [287]. Furthermore, since force is proportional to the square of frequency, higher frequencies may exert a greater influence on osteogenesis than amplitude alone. Based on these principles, it was hypothesised that increasing frequency and amplitude in nanovibrational stimulation will enhance the osteogenic response in MSCs and bone-like cells, with frequency potentially having a greater effect than amplitude.

As well as applying a wide range of frequencies and amplitudes, vibration studies also apply stimulation in different directions, with few studies comparing the effect of direction on cell response. Studies which have compared horizontal and vertical vibration have found horizontal vibration to result in a higher osteogenic response and increased cell stiffness [271, 274]. Vibrating cells in parallel to the cell monolayer may result in increased tension on actin fibres, resulting in increased cell stiffness. Given the lack of investigation into comparing horizontal and vertical nanovibrational stimulation, it was hypothesised that horizontal vibration will significantly enhance osteogenic differentiation, likely due to increased tension and cellular mechanotransduction.

Nanovibrational stimulation has always been applied continuously to cell samples. However, other vibration studies have shown that shorter, intermittent vibrations are sufficient enough to increase osteogenic response [235]. Despite this, little investigation has been made into whether cells acclimatise to a constant vibration and whether shorter intermittent applications could elicit a similar or even higher osteogenic response. Applying shorter bursts of stimulation would also be more clinically applicable, as patients could wear vibration devices for shorter durations rather than continuously during treatment. Based on this, it was hypothesised that shorter, intermittent nanovibrational stimulation would result in a comparable or higher osteogenic response in cells compared to continuous stimulation, potentially due to reduced cellular acclimatisation.

Changes in adhesion and the actin cytoskeleton have previously been observed following the application of nanovibration, indicating that stimulation leads to changes in the mechanical properties of the cell [67, 302]. However, these changes have not yet been correlated with direct mechanical measurements, such as stiffness, and it is unknown whether the morphological changes are permanent. It was therefore hypothesised that vibration would result in a higher stiffness in the cell as a result from changes in adhesion and the actin cytoskeleton. The LINC complex, which plays a key role in transmitting forces to the nucleus and in remodelling the actin cytoskeleton, is theorised to be a key mediator of these effects. Hence, it was hypothesised that nanovibrational stimulation induces alterations in the LINC complex, contributing to cytoskeletal remodelling and changes in cell mechanical properties, which in turn promote an osteogenic response.

Previous work on nanovibrational stimulation has focused on obtaining an osteogenic response from MSCs, with little research into other potential cellular responses. Most studies applying vibration to stem cells only investigate a single lineage, typically osteogenesis. Nanovibration has not thoroughly explored the potential commitment of cells to other lineages, or other cell responses following stimulation. However, recent findings using nanovibrational stimulation on biofilms, suggests the technique may not be limited to inducing osteogenesis in MSCs and other bone-like cells. It was hypothesised that the modulation of vibration parameters can direct MSC differentiation toward non-osteogenic lineages or influence the differentiation of other non-osteogenic cell types.

This thesis aims to explore a range of vibration parameters to assess their effects on cellular responses, including mechanical and morphological changes as well as alterations in gene expression.

Chapter 2:

Device Redesign

2.1 Introduction

Nanovibrational stimulation is applied to cells using a device previously designed by researchers based at the Universities of Glasgow and Strathclyde (Figure 21) [297]. The device consists of a 13 piezo actuator array attached to a steel top plate. Piezo actuators expand and contract when an oscillating voltage is applied via a power supply unit (PSU). Actuators are clamped in a housing unit which is then bolted to the top plate, translating movement to the steel plate and resulting in vibrational motion. Motion is transferred to cells cultured within cultureware that is magnetically attached to the device top plate.

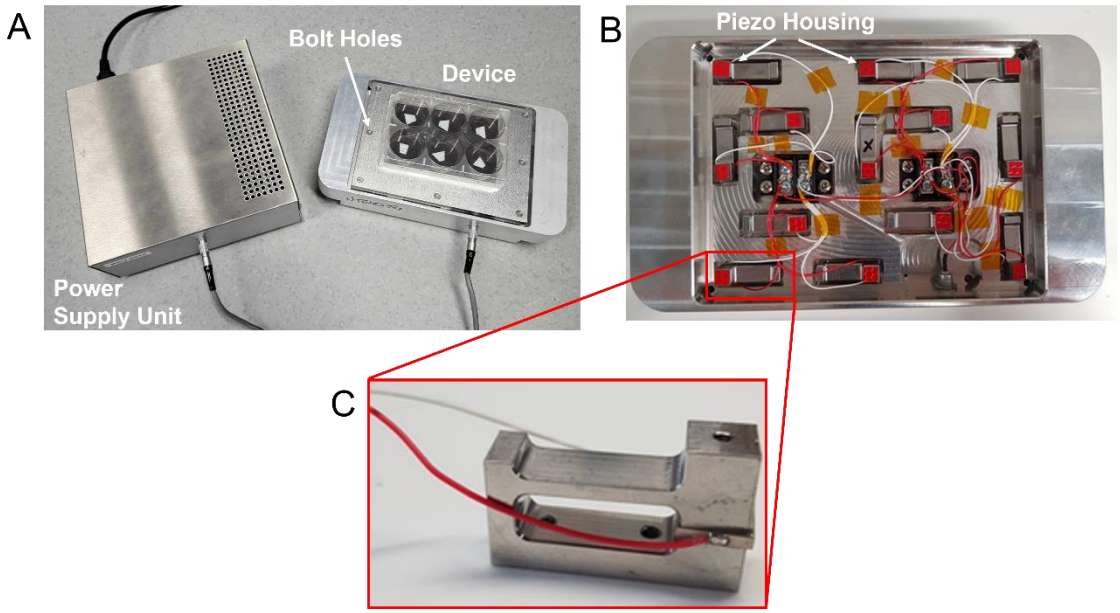

Figure 21: Images of the nanovibrational stimulation system. A) Vibrational platform attached to power supply with cultureware magnetically attached. B) 13-piezo actuator array which is then bolted to the steel top plate providing vibrational motion. C: Piezo actuator housing/clamp.

Currently, the PSU is limited to an output of a single frequency (1 kHz) and single amplitude (30 nm). Although the amplitude can be adjusted to a maximum of

approximately 90 nm, the frequency is limited to a single value. As recent nanovibration studies have suggested, it may be desirable to have a working device capable of reaching higher amplitudes [287]. The effects of different frequencies on cell response have not been investigated extensively on the new device design, and so a PSU capable of producing a range of frequencies may be desirable. It is also essential to test a range of frequencies and amplitudes the current device is capable of in order to determine the limitations of the device. Whilst a variable PSU will allow for easier adjustment of the vibrational conditions for the user, identifying which parameters that are most influential on cell response will enable better future design of the PSU.

2.2 Investigating different piezo actuator arrays

2.2.1 Laser interferometry

Laser interferometry (SP-S SIOS Meβtechnik GmbH) was used to measure vibration amplitude variations across the top plate of the device, capable of accuracy at the sub-nm level at the frequencies of interest (Figure 22). Retro-reflective tape, attached to a moveable magnet, was used to reflect back the laser from the vibrometer to measure the motion. The interferometer functions by splitting a laser beam and recombining them to create an interference pattern. Before being recombined, one beam is reflected from the measurement target (i.e. the reflective tape situated on the device). Any motion of the device will lead to corresponding changes in the interference pattern detected by the device. Time-based data of surface motion (bottom of cultureware) is produced, and the software performs a Fast Fourier Transform to reveal the output motion at specific frequencies. In further measurements, cultureware and Petri dishes lined with reflective tape were attached to the top plate via magnets and were used to measure amplitudes using interferometry.

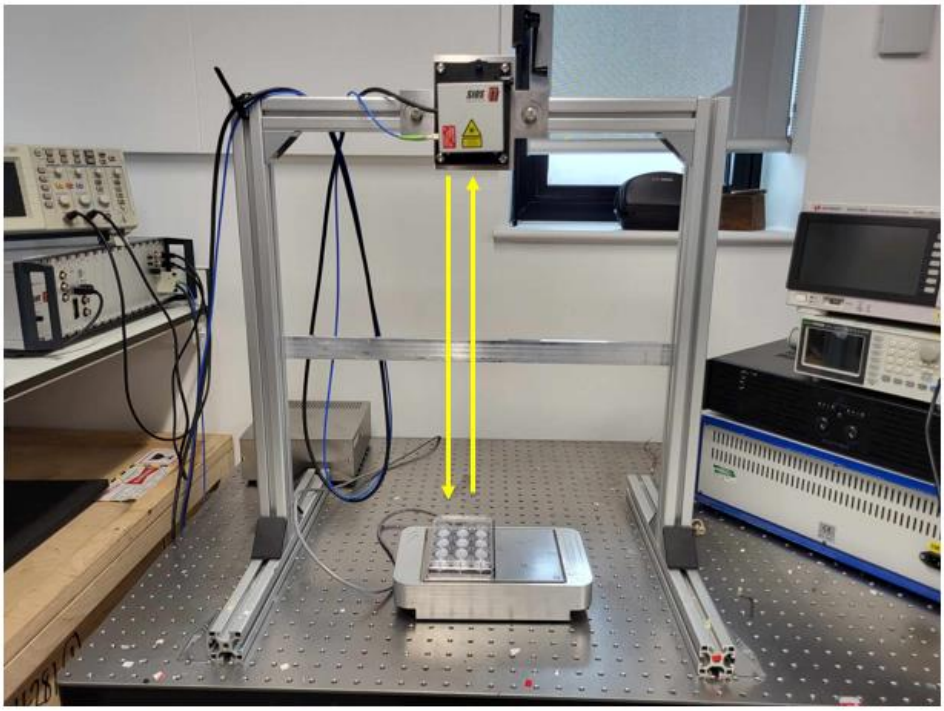

Figure 22: Laser interferometry used to measure the displacement of the top plate. Arrows indicate direction of laser at it reflects on the measurement tape and recombines within the interferometer.

2.2.2 Testing different piezo actuator arrays

The current device design has an array of 13 piezo actuators (Noliac NAC2022), each housed within a metal clamp and applying a pre-loading to the actuator (Figure 21C). These piezo clamps are bolted to a top where the expansion and contraction of the piezo actuators transmit precise motion to the plate, allowing vibrations to be transmitted to cultureware magnetically attached. Due to the high cost of a device with 13 piezo actuators, it was investigated whether the number could be reduced without reducing the consistency of vibration across the top plate.

Five different arrays of piezo actuators were tested, with 5, 7, 9, 11 and the original 13 piezo actuators. These were arranged within the device and connected to an external signal generator (GWInstek AFG-2005) with a commercial audio amplifier (Behringer KM750). The top plate was then bolted to the top of the piezo actuator clamps. Any screw holes not being used due to missing piezo

actuators were bolted using a nut and bolt to minimize distortion across the top plate.

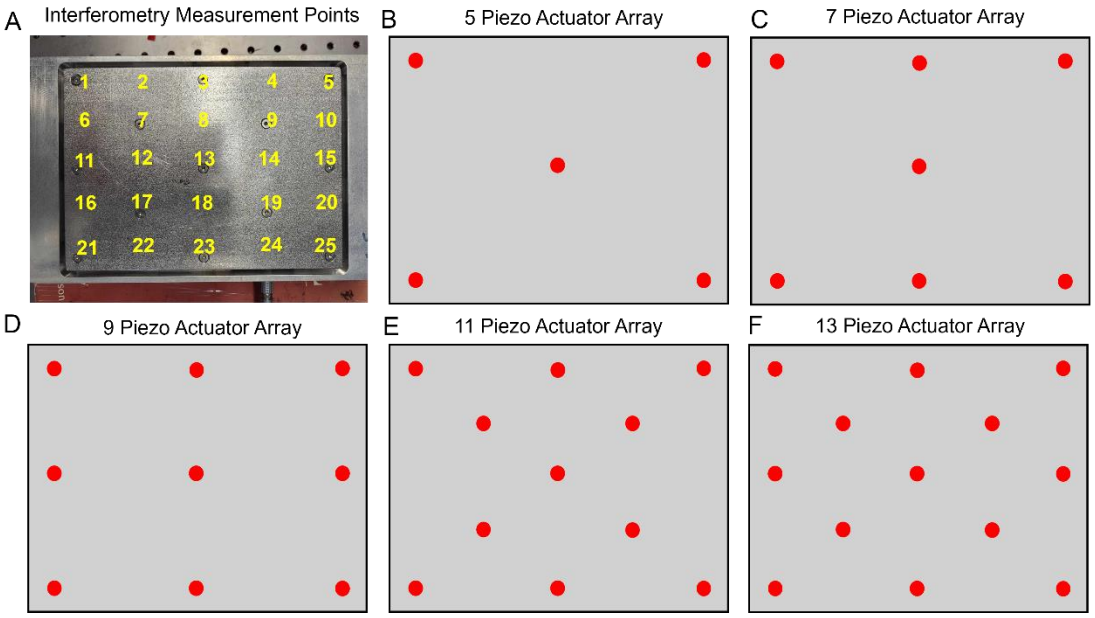

Figure 23: Arrangement of piezo actuators. A) Schematic showing the positions at which interferometry was performed on the device top plate. B) 5 piezo array arrangement. C) 7 piezo array arrangement. D) 9 piezo array arrangement. E) 11 piezo array arrangement. F) 13 piezo array arrangement.

The signal generator produced a voltage of 0.13 V which was amplified to 5.8 $V_{pk\text{-}pk}$ (peak-to-peak electrical potential). Frequencies of 100 Hz, 500 Hz, 1 kHz, 2 kHz, 3 kHz, 4 kHz, and 5 kHz were applied to the device at each of the piezo actuator combinations. To determine the performance of the device with each of the piezo actuator arrays, interferometry was performed on the top plate. This measured the amplitude of vibration across the top plate for each combination of actuators. Twenty-five measurements in total were taken across the top plate, with an average of five measurements taken at each position. The average across the twenty-five top plate points were then averaged and the standard deviation determined. A schematic detailing the positioning of the actuators are shown in Figure 23. The average displacement across the device was then recorded and the standard deviation determined. A summary of the results with the average across the device at each frequency for each of the arrays is shown in Figure 24.

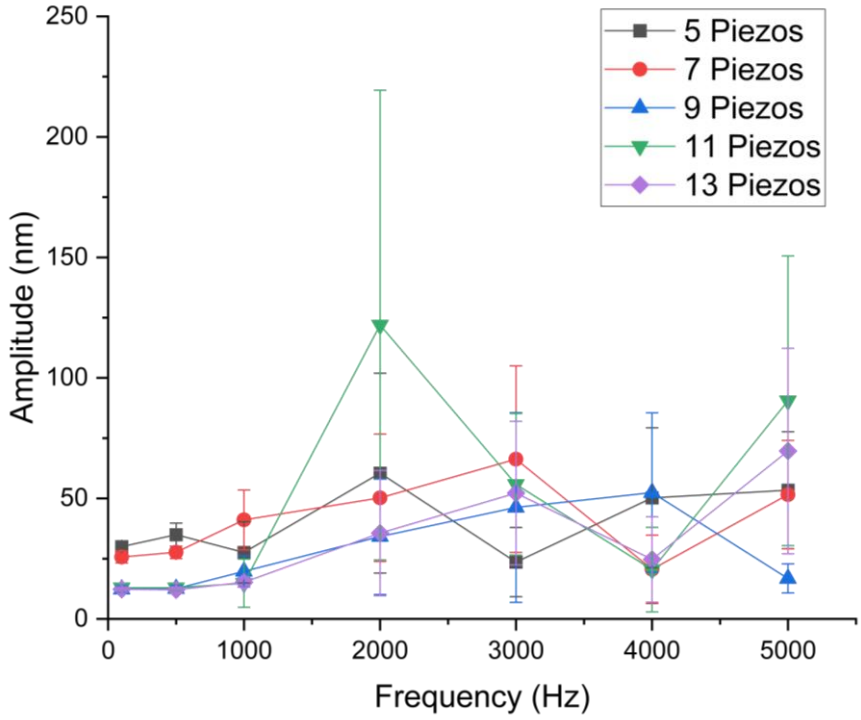

Figure 24: Interferometry measurements at multiple frequencies for five different combinations of piezo actuators. N = 25 where each replicate is a measurement at different points across the top plate surface.

Below 100 Hz, all combinations of piezo actuator arrays resulted in even vibrations across the top plate, however 9 piezo actuators and above resulted in a considerable drop in the average amplitude achieved across the top plate. For 1 kHz, the 9 and 13 piezo array combinations showed the lowest levels of amplitude variation, however above this frequency all piezo arrays resulted in significant variations across the top plate.

2.2.3 FEA modelling of the piezo actuator arrays

To further understand the effects of vibration on the top plate with each piezo actuator combination, finite element analysis (FEA) was performed using ANSYS (version 15.0). This was carried out using device models previously designed by the group within computer assisted design (CAD) software, and using the ANSYS harmonic response analysis package, which shows the deformation within the structure in response to input variation. Fixed supports were defined at the base of the piezo clamps and displacements were defined where they are applied by

the piezo actuators. ANSYS models were run through harmonic response analysis, with analysis settings set to the frequency being tested. The displacement was set to the average amplitude measured by interferometry at 100 Hz for each of the piezo arrays as shown in Table 3.

Table 3: The amplitudes set for each piezo actuator array in ANSYS, corresponding to the average amplitude measured by interferometry at 100 Hz.

Piezo Array	Amplitude (nm)
5	30
7	27
9	12
11	13
13	12

In ANSYS, all of the arrays provided an approximately constant amplitude across the top plate when 100 Hz was applied. However, when the frequency was raised to 500 Hz, there was a small amount of variation in amplitude for the 5 piezo array, whilst all others were again approximately constant. This corresponded to that seen from interferometry.

From interferometry, only the 13 piezo actuator array had an approximately constant amplitude at 1 kHz, however the 9 piezo array only had relatively small variations in amplitude across the top plate. ANSYS models also confirmed this, however models also predicted that the 11 piezo array would also have only a small amount of variation across the top plate at 1 kHz, whilst interferometry found that there were significant variations. That the 11 piezo array shows more amplitude variation than the 9 piezo array may simply be due to the arrangement of piezo actuators, with the 9 piezo array being more evenly spread across the plate. Beyond 1 kHz, ANSYS models and interferometry tended to disagree on the precise variations experienced across the top plate. Some frequencies produce greater variations than higher frequencies in other arrays, with discrepancies between modelled and actual values. It is likely that these discrepancies are most likely due to the mechanical coupling between interfaces and materials being

challenging to model using FEA, thus providing inconsistent results between model and reality.

Despite the differences, both model and actual agree that above 2 kHz, variations across the top plate are significant. Therefore, in conclusion, the 13 piezo array provides the most consistent amplitude across the plate, however the 9 piezo array may be investigated further in the future. It was determined that the 13 piezo actuator array would provide the most reliable results and the effect of different frequencies on the variations across the top plate ought to be investigated.

2.4 Testing limitations of vertical device at higher frequencies

2.4.1 Laser interferometry measurements

The limitations of the current device were explored using a signal generator and Behringer audio amplifier which applied various frequencies and voltages to the device, with the resulting amplitude being measured by the interferometer. The average amplitude across the top plate at each frequency and voltage are shown in Figure 25.

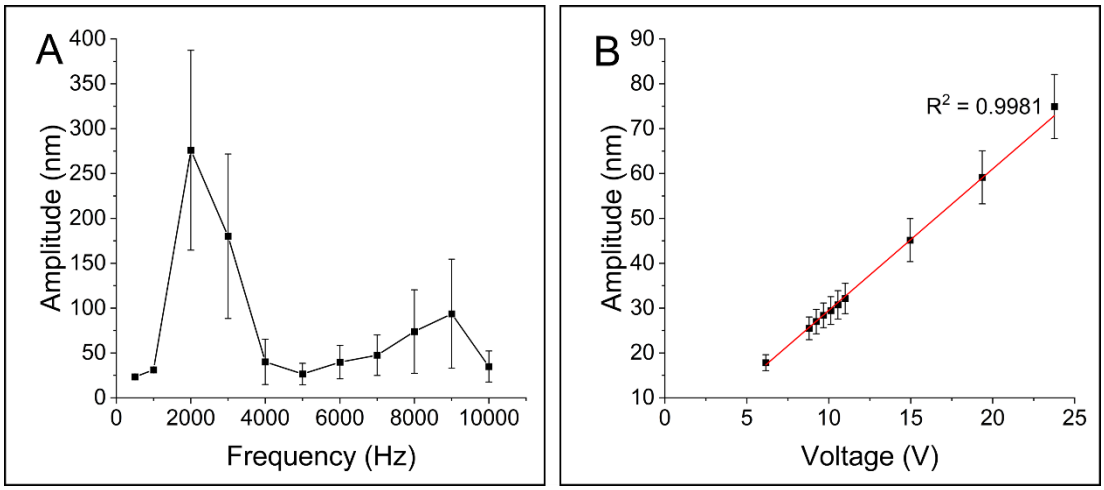

Figure 25: Interferometry measurements of average amplitude across the top plate whilst changing A) Frequency and B) Voltage, keeping frequency consistent at 1 kHz. N = 12, where each replicate is measured at different points across the top plate.

The current device was found to produce a very varied amplitude across the top plate between 2 – 4 kHz. Variations appeared to be much lower between 5 – 6 kHz and again at 10 kHz, however the most consistent amplitudes were observed at the lower frequencies of 1 kHz and below. Amplitude increased linearly with increased voltage as expected [297]. Although the current design could be used at certain frequencies, it was decided that some investigation should go into whether minor changes could be made to the device to make amplitudes across the top plate at frequencies above 1 kHz, more consistent.

2.4.2 Modifying the top plate in ANSYS

To begin, modifications of the top plate were modelled in ANSYS to investigate whether such changes may allow for more consistent vibrations at frequencies higher than 1 kHz. The top plate consists of two layers: an aluminium plate in contact with piezo clamps and a stainless steel plate providing a magnetic surface for cultureware to be attached using magnets. For the aluminium layer, different materials were investigated to see if they would result in fewer variations on the surface of the stainless steel top plate. Modal analysis enables the determination of natural frequencies (resonances) within the model. The number of modes reflects the variation in how the top plate can naturally vibrate at specific frequencies. A material resulting in a high number of modes indicates that there are a large number of ways the system may naturally vibrate – which may result in more variation in amplitude when vibrating at a specific frequency. Here, modal analysis was used to investigate which materials produced the lowest resonant frequency. Motion below the first resonant frequency is pistonic and in-phase and therefore ought to produce consistent vibration. The materials investigated are shown below in Table 4 alongside the mechanical properties used in ANSYS and the first resonant frequency measured.

Table 4: Materials with various Young's Modulus used in modal analysis in ANSYS and the first resonant frequency measured.

Material	Young's Modulus (GPa)	Density (kg/m^3)	No. Modes up to 5 kHz	1st Resonant Frequency (Hz)
Acrylic	3	1190	15	565
Glass	50	2400	11	581
Aluminium	68	2700	10	572
Copper	117	8960	11	423
Steel	200	7850	10	445
Beryllium	287	1850	8	618
Tungsten	400	19300	11	323
Iridium	517	22500	11	303

All materials investigated had first resonant frequencies lower than 1 kHz. Therefore, at higher frequencies motion may become more varied across the top-plate. As is shown in Figure 26, aluminium has a relatively low number of modes up to 5 kHz. Beryllium, although resulting in a lower number of modes than aluminium, is a more expensive and less accessible material. Therefore, aluminium was determined to be a relatively good material for the top plate to ensure minimum variations in amplitude. The thickness of the top plate was also investigated; however, this did not have any effect on reducing variations in amplitude on the top plate (Data not shown).

Interferometry found that frequencies above 1 kHz resulted in large variations across the top plate. Further ANSYS modelling did not find any simple changes that could be made to the current device to reduce these vibrations and allow for more consistent amplitudes across the top plate. Therefore, it was determined that frequencies resulting in the lowest top plate variation would be used for *in vitro* cell culture experiments.

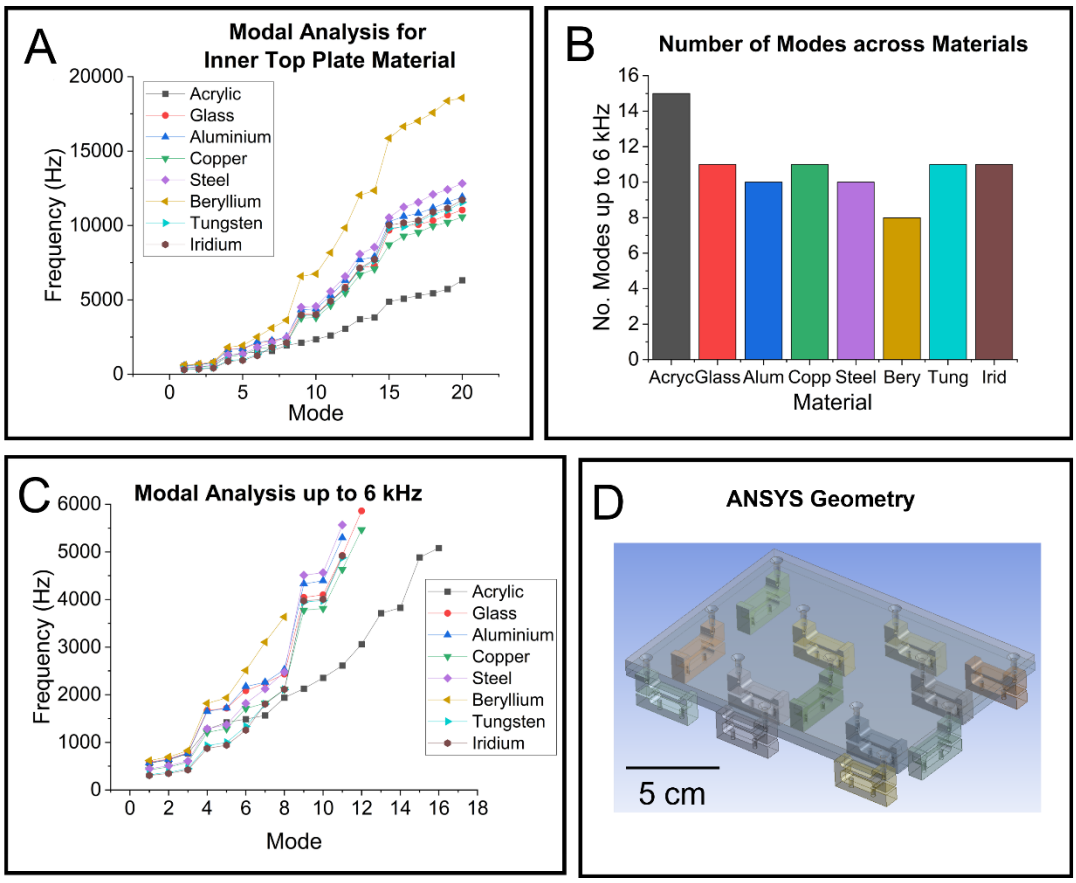

Figure 26: A) Modal analysis for the first 20 modes performed on the top plate with different materials. The Young's Modulus, density and number of modes up to 6 kHz for each material is shown in Table 4. (B) Bar chart detailing number of modes for each material (up to 6 kHz). C) Modal analysis for various top plate materials up to 6 kHz. D) ANSYS geometry of top plate with piezo clamps.

2.5 Redesigning a variable frequency and amplitude power supply unit (PSU)

2.5.1 Designing an adjustable frequency power supply

In order to design an adjustable frequency power supply, a printed circuit board (PCB) was designed containing only a signal generator (direct digital synthesis (DDS)) and a filter. This was done using KiCAD and then printed onto a PCB (JLC PCB) with the components soldered on. A breadboard was utilized to assemble the full variable frequency power supply. An Arduino microcontroller (MC) was used, along with two rotary encoders and a thin film transistor (TFT) LCD display. The MC was connected to a laptop with control software written in the Arduino

IDE package. The rotary encoders were used to increase or decrease the frequency via the MC which then sent the signal to the program, subsequently causing the DDS chip to change in frequency. The TFT display was used to display this change in frequency, to offer a more user-friendly design by attaching it to the front of the power supply, allowing the user to change the frequency by turning the rotary encoders and visually showing that change in frequency on the screen (Figure 27).

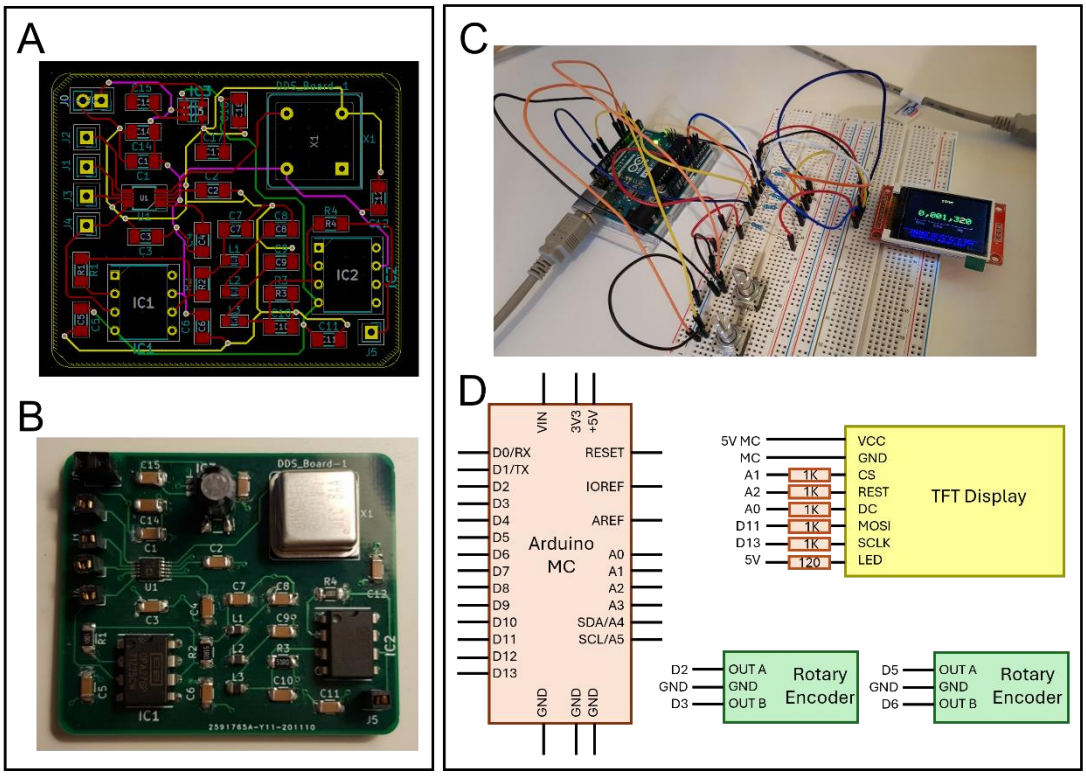

Figure 27: A) KiCAD PCB layout of DDS design chip. B) Printed PCB board of DDS design chip. C) Breadboard circuit of Arduino MC, rotary encoders and TFT display. D) Circuit diagram of Arduino MC, rotary encoders and TFT display. Circuit allows for the frequency to be changed by using the rotary encoders, with the frequency value displayed on the TFT display.

2.5.2 Designing an adjustable amplitude power supply

The amplitude produced by the piezo array depends on the voltage, as observed in Figure 25. However, the current power supply is limited in the voltage it is capable of producing. Figure 28 shows the displacement of the top plate produced by output voltages the current power supply unit is capable of as well as the voltages required for three of the devices used in later experiments.

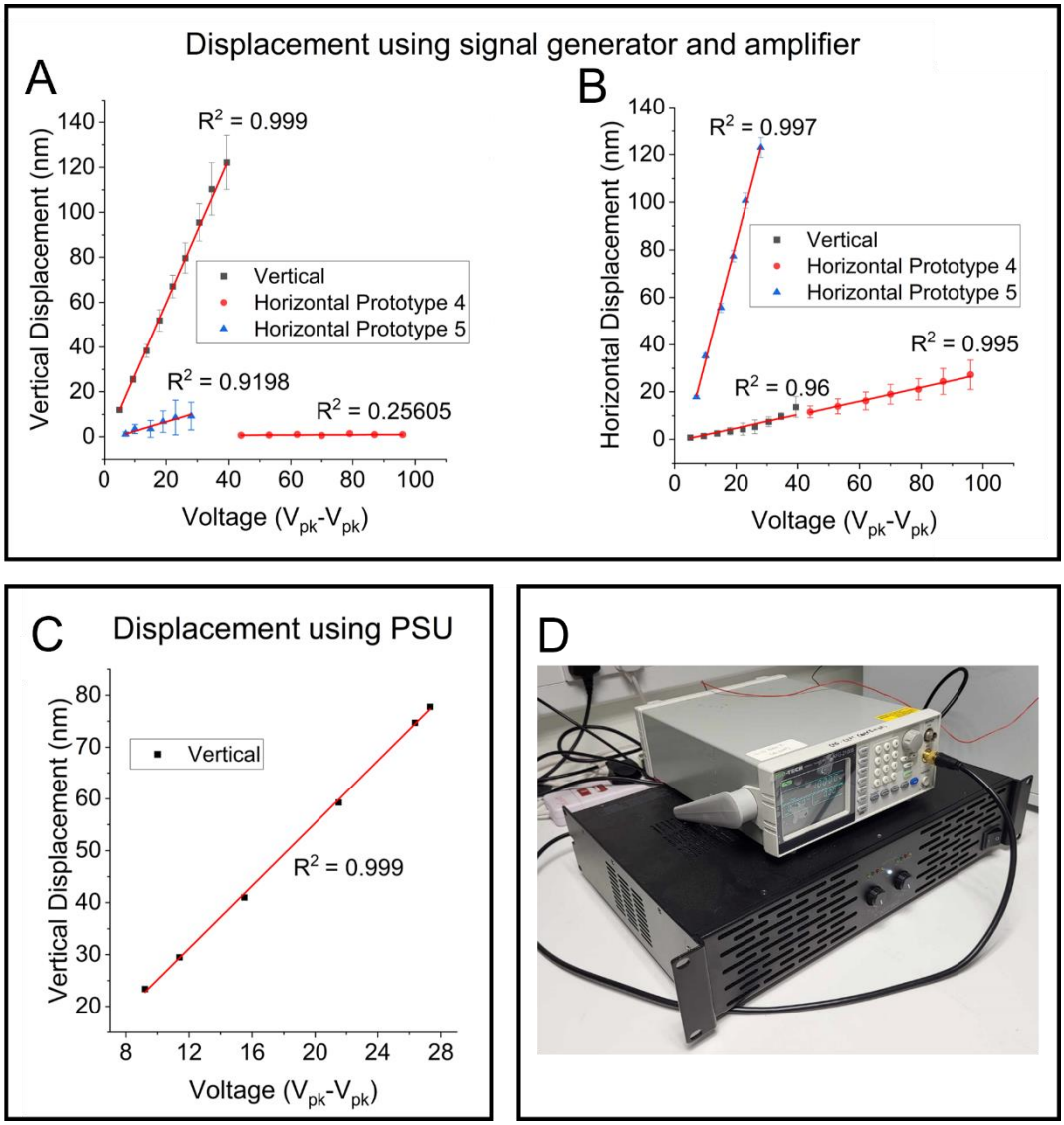

Figure 28: Voltages required to produce average displacements in three devices were *measured*: the standard vertical device and two horizontal prototypes. A) Vertical displacement at a range of voltages. Only the vertical device shows a significant range of vertical displacements. B) Horizontal displacement at a range of voltages. The shear piezo device (Horizontal Prototype 4) required higher voltages and was only capable of a maximum amplitude of around 30 nm, whilst Prototype 5 was capable of a range of displacements are relatively low voltages. C) Limitations of the current PSU showing the voltages required to produce average displacement in the device. D) Signal generator and Behringer amplifier. Data shown in C was collected by Dr. Paul Campsie. N = 12 where each replicate was obtained at different points across the top plate.

The device uses piezo actuators to produce nanoscale amplitudes. When a sinusoidal voltage is applied, the actuators expand and contract in response. For

the system to reach higher amplitudes, a larger voltage is required, however for this a DC offset must be introduced. This is due to the piezo actuators being limited in how much they can contract (i.e. the negative portion of the sine wave), and they can be damaged if too high an electric field is applied in the opposite direction to the poling of the molecules. To achieve these higher voltages, an improved amplifier was proposed. Op-amps are used in the existing power supply design, however these cannot provide a high current (power). A transistor is capable of much more power, and so it was decided to pursue a transistor-based amplifier. Class AB amplifiers use both a negative positive negative (NPN) and a positive negative positive (PNP) transistor. Such a circuit has the advantages of a Class A amplifier, which has a high amplification, with the advantages of a Class B amplifier which has a high DC-AC conversion efficiency. A Class AB amplifier also does not have any signal distortion when switching between transistors, ensuring a clean sinusoidal output signal.

The highest amplitudes the existing power supply is capable of producing are around 90 nm, and it is hoped that a Class AB amplifier design will give amplitudes of upwards of 100 nm, aided by the inclusion of a DC offset ensuring that the electrical signal provided to the actuators is continually positive. The current power supply has a pre-amplifier, which is capable of controlling the level of voltage inputting into the amplifier via a potentiometer. The maximum input available is 0.64 $V_{pk\text{-}pk}$. Therefore, to achieve higher amplitudes, a power supply with a gain of *circa* x50 needed to be produced.

To investigate amplitude combinations in a safe environment, the software LTSpice was used to model such amplifiers. The software also made it possible to predict the output voltage and current from such a device. Based on results in Figure 28C, it was aimed that the new amplifier design would be capable of producing an output voltage of over 40 $V_{pk\text{-}pk}$. Through a number of iterations of resistor and capacitor combinations, the optimal amplifier design is shown in Figure 29.

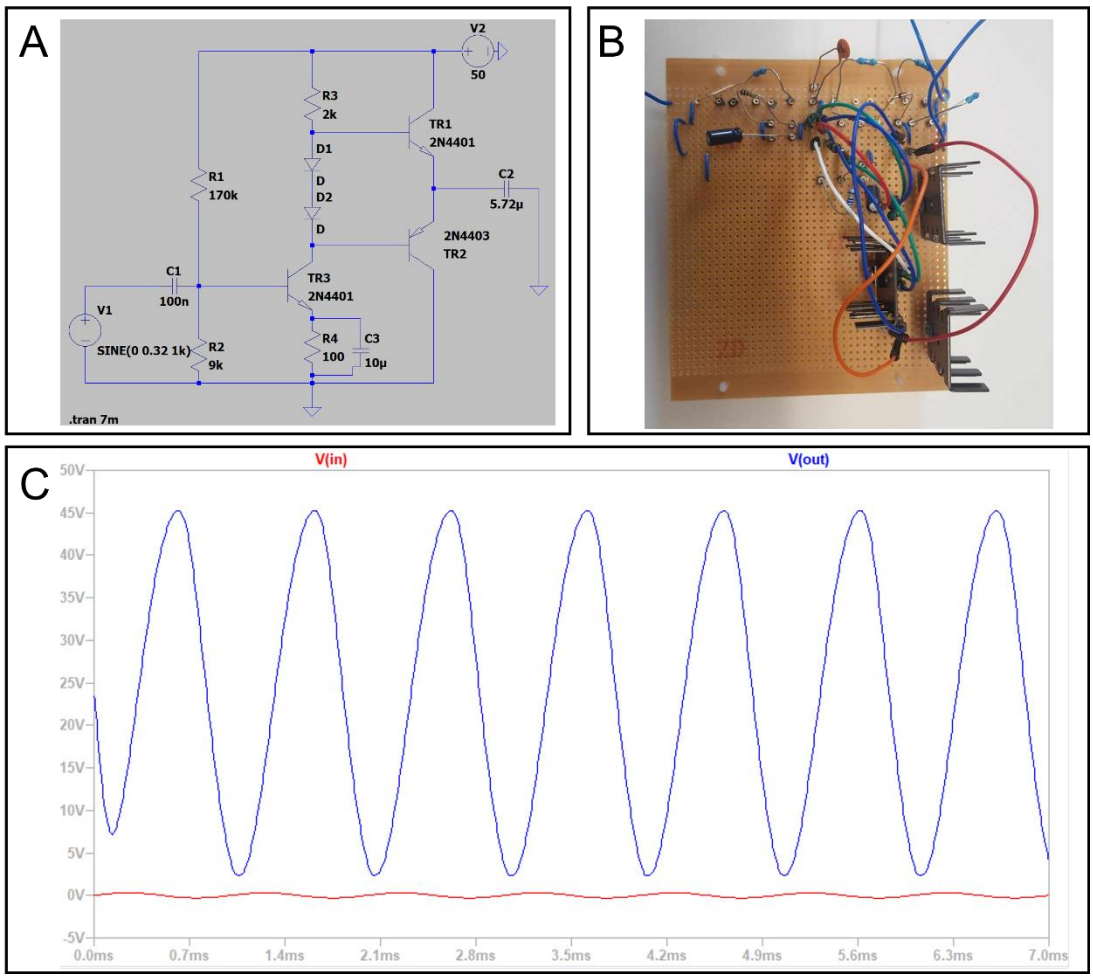

Figure 29: A) Class AB amplifier design in LTSpice. B) Class AB amplifier built on a copper breadboard with heat sinks attached to transistors C) Voltage response as measured in LTSpice where V(n006) is Vin and V(n003) is Vout. Design shows a max peak-to-peak voltage of 50V whilst still maintaining a reliable sine-wave output.

V_1 was set to the maximum value the amplifier within the current PSU was capable of, which was 0.6 $V_{pk\text{-}pk}$. Therefore, the input voltage in the LTSpice model was set to 0.32 V_{pk}. An input coupling capacitor (C1) was used to pass the desired AC signal and block unwanted DC components before entering the transistor. This was connected in series with the signal path and prevented any interference of the transistor's bias voltage. A capacitor of 100 nF was chosen, as this is suitable for signals up to 10kHz in frequency. Resistors R1 and R2 create a bias voltage, creating a DC offset and moving the signal into the positive range. R1 could be switched for a potentiometer to control this offset. TR3 acted as a current source that set up the required DC biasing current. This was also what produced the

voltage gain. Resistor R3 defines the magnitude of the gain (due to Ohms Law) with higher resistances producing higher voltages. TR3 was the pre-amp NPN transistor.

A small current flowed through R3-D1-D2. Across D1-D2 was a constant voltage drop of 1.4 V, biasing the transistors above the cut-off and removing crossover distortion. Crossover distortion produced a zero voltage 'flat-spot' on the output wave as it crossed over from one half of the waveform to the other. This is due to the transition period when transistors switch over, which does not stop/start exactly at the zero crossover point, thus causing a small delay between the first transistor turning off and the second turning on. The diodes are chosen to match the characteristics of the matching transistors. TR1 and TR2 are matching NPN and PNP transistors. These are responsible for the current gain. To amplify the current gain, Darlington pairs may be used instead of single transistors TR1 and TR2. C2 was used simply to represent the piezo array within the device.

The circuit was then tested on a copper breadboard using an external DC power supply and signal generator. The signal generator produced an output of 0.64 $V_{pk\text{-}pk}$, and the external DC power supply produced voltages of up to 50V. The output signal was measured using an oscilloscope, and the measurement was taken just before C2 which represents the piezo array in the circuit. The output signal could then be compared to the input of the signal generator to calculate the gain of the circuit.

Although the modelling work done in LTSpice was promising, when the amplifier design was built on copper breadboards it did not function as expected. Several components melted, although they were capable of enduring the voltages and currents expected. Although several heat sinks were added to the circuit, the heat produced was still too overwhelming for individual components. Due to the complexities of designing a new PSU, the work presented in this section suggests a potential theoretical design that could be developed further in the future. For *in vitro* testing, a signal generator and Behringer amplifier were instead used, enabling the testing of higher frequencies and amplitudes without the need of a new PSU. This option however does not include a DC voltage offset, therefore

limiting the maximum amplitude the piezo actuators may reach (due to limitations in the amount piezo actuators may contract).

2.6 Development of a horizontal nanovibration device

2.6.1 Motivation

During consultation with the literature, it was noted that as well as variations in frequency and amplitude, studies also vary in the direction of applied vibration (see Appendix A). Very few studies compared the effects of horizontal versus vertical vibration and identifying which was more effective in inducing differentiation in cells.

2.6.2 Modelling MSCs in ANSYS

2.6.2.1 Designing cell models

To investigate the stresses and forces experienced by cells when vibrated horizontally compared to vertically, three cell models were designed in ANSYS representing three different levels of adherence to the surface. These were essentially spherical 'caps', with increased stages of adherence corresponding to a lower height and larger radius of the model, mimicking the 'spreading out' of cells as they adhere.

To maintain consistency, the volume of the cell at each adhesion stage was kept as constant as possible. To do this, Equation 2 was used to calculate the volume of the spherical 'cap' at the top of a sphere:

$$V = \frac{\pi h^2(3R-h)}{3} = \frac{\pi h\left(3r^2+h^2\right)}{6}, \tag{2}$$

where h is the height of the model, R is the radius of the original sphere and r is the radius of the base of the model. The models had a volume of around 1033 μm^3, with the radius increasing and the height decreasing in later stages of adhesion. The radius/volume ratio of the nucleus was kept constant. Three models were designed at different levels of adherence as shown in Figure 30.

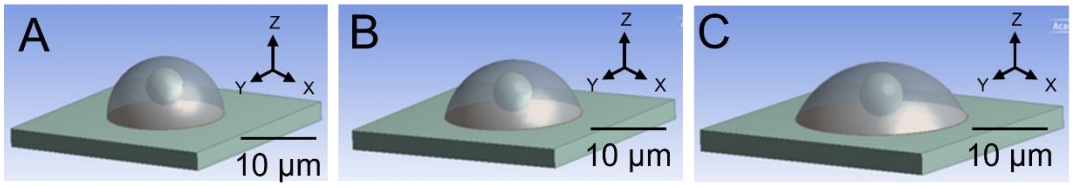

Figure 30: ANSYS models of a cell at different stages of adherence. A) Represents a cell with an area of attachment of 196.1 µm^2 B) Represents a cell with an area of attachment of 243.3 µm^2 C) Represents a cell with an area of attachment of 293.1 µm^2. The dimensions of the different stages of adherence are defined in Table 6.

A square section of culture plate was also added to the model to represent a surface the cells were adhered to. This represents the cultureware the cells would be cultured in. The contact area between the cell membrane and the culture surface was fixed, assuming that the vibration forces would be lower than cell adhesion forces to the surface. The cell membrane, cytoplasm, nucleus and cultureware plate were also defined in the model, with the Young's Modulus and Poisson's Ratio values for each being defined, as is shown in Table 5.

Table 5: Young's Modulus and Poisson Ratios for cell components used in cell models [303, 304].

Material	Young's Modulus (Pa)	Poisson's Ratio
Cell Membrane	1.0×10^6	0.30
Cytoplasm	0.5×10^3	0.30
Nucleus	5×10^3	0.37
Cultureware Plate (structural steel)	2×10^{11}	0.30

The average spherical diameter of an MSC was taken as 15.8 μm and to maintain consistency, the volume of the cell was kept as close to constant as possible for each of the adhesion stages [305]. To do this, equation 2 was used to calculate the volume of the spherical 'cap' at the top of a sphere. This volume was then kept constant and used to calculate the height and radius of the adhered cell models, as shown in Table 6.

Table 6: Dimensions of cell at different stages of adherence. Corresponds to the images of cell models in Figure 30.

Stage	Radius of nucleus (μm)	Thickness of Cell Membrane (μm)	Height (μm)	Radius (μm)	Area of Attachment (μm^2)	Volume (μm^3)
1	2.5	0.01	7.91	7.9	196.1	1034.6
2	2.5	0.01	7.01	8.8	243.3	1033.1
3	2.5	0.01	6.17	9.66	293.1	1027.2

One limitation of the model was that the nucleus was not 'flattened' as it would be during adherence but was instead a perfect sphere. The nucleus is also not representative of an actual MSC's nucleus, which has a diameter of 10.5 μm, whereas the model has a diameter of 5 μm. This discrepancy was simply to allow for the overall cell to be more 'flattened' during the adhesion stages.

2.6.2.2 Measuring the stress on cell models

Default meshing was applied to all cell models. Harmonic analysis was then performed on the models, with the culture plate being displaced by 30 nm either horizontally (x-axis) or vertically (z-axis). A frequency sweep between 0 – 5000 Hz with a step size of 100 Hz was used. The maximum normal stress on the cell membrane was recorded at each stage of vibration (horizontally and vertically) as well as the maximum normal stress on the nucleus (again horizontally and vertically). The strain on both the cell membrane and the nucleus were also measured (both horizontally and vertically) These were all measured in both the x- and z-axis. Stress/strain graphs of the cell membrane and the nucleus in the x- and z-axis are shown in Figure 31.

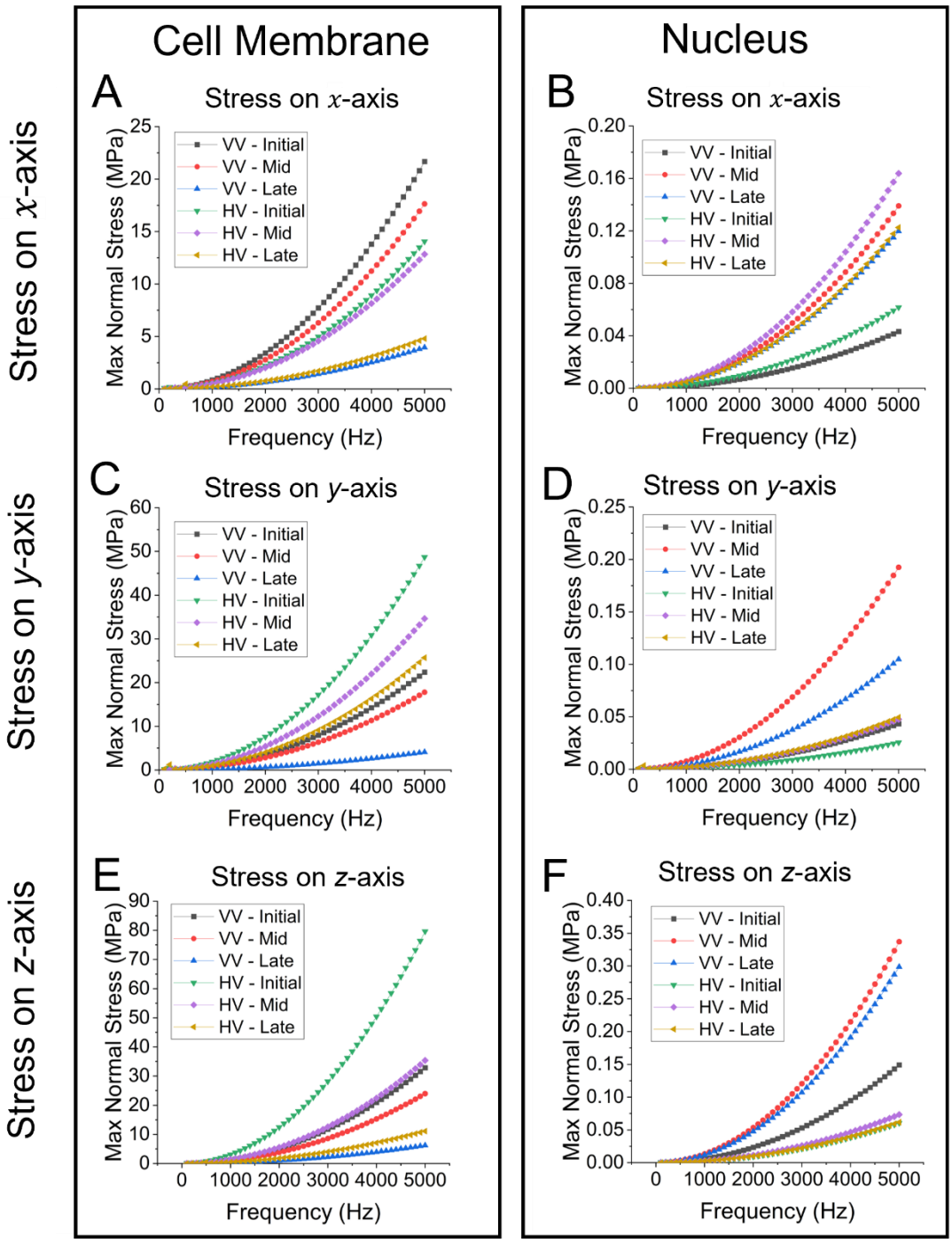

Figure 31: Maximum normal stress experienced by the cell membrane in the A) and B) x– axis, C) and D) y – axis and E) and F) z – axis during a frequency sweep of 0 – 5000 Hz.

The models did not consider the variations in cytoplasm stiffness over time. Therefore, to investigate this, the Young's Modulus of the cytoplasm was varied between 0.5 kPa and 4.0 kPa and the stress experienced by the cell membrane of the late adherence model when vibrated horizontally and vertically was

measured. Again, the frequency sweep was between 0 – 5000 Hz with a step size of 100 Hz, and the results are shown in Figure 32.

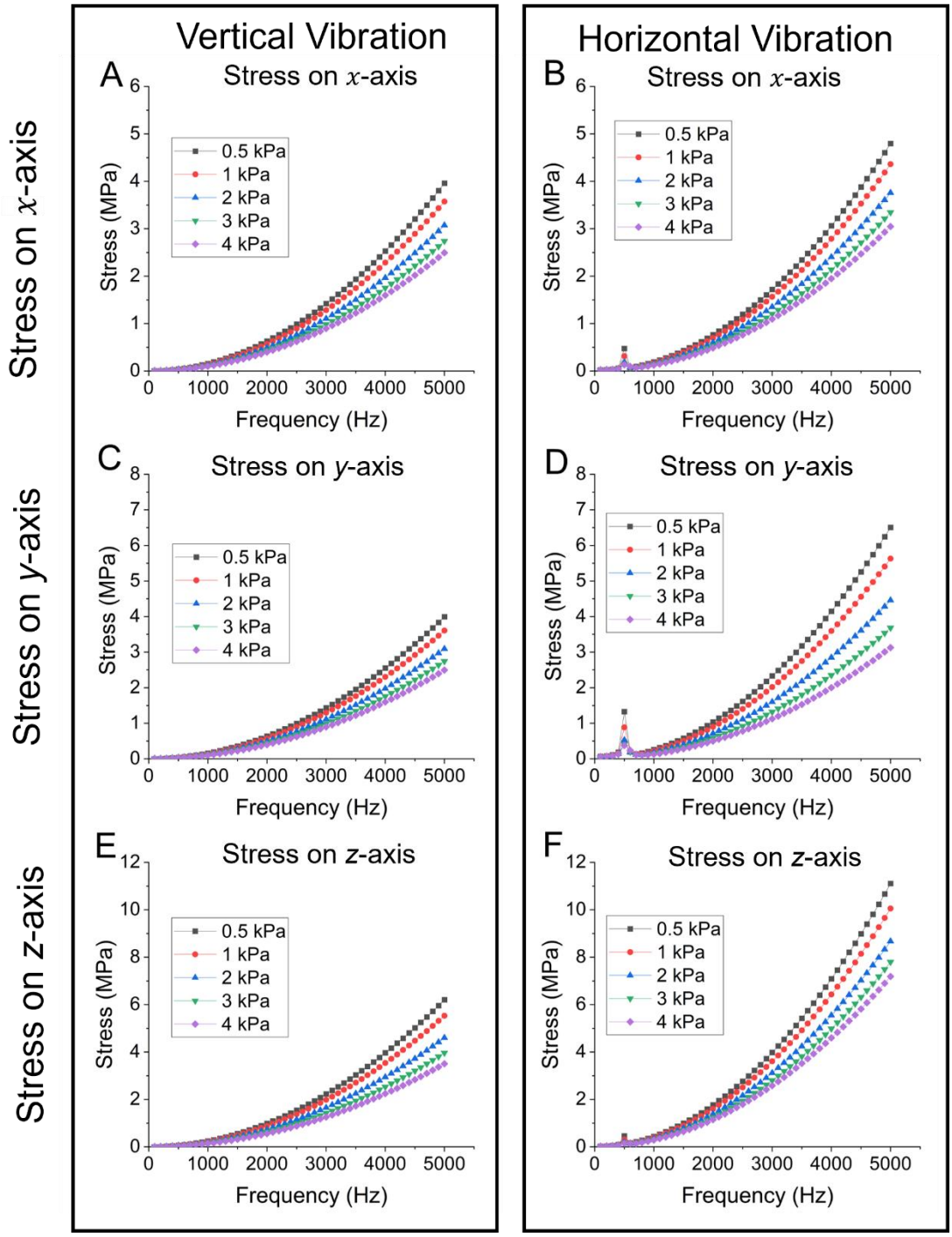

Figure 32: Comparing different Young's Modulus for the cytoplasm. The Young's Modulus varied between 0.5 kPa and 4.0 kPa, and the stress experienced by the cell membrane when vibrated vertically and horizontally in the *x*-axis (A, B), *y*-axis (C, D), and *z* – axis (E, F) was measured. Late adhesion models were used.

Stress on the *y*-axis and *z*-axis were higher during horizontal vibration. A softer cytoplasm resulted in a higher stress during both vertical and horizontal vibration. These results may suggest that the cell experiences more stress during horizontal vibration which may result in a higher stiffness within the cell.

2.6.2.3 Measuring strain hardening of cell models

As well as looking at the stress experienced by the cell membrane and nucleus, the strain of both was also measured and the apparent Young's Modulus (due to applied vibration) was calculated. The Young's Modulus for both the *x*-axis and *z*-axis for the cell membrane and nucleus are shown below in Figure 33.

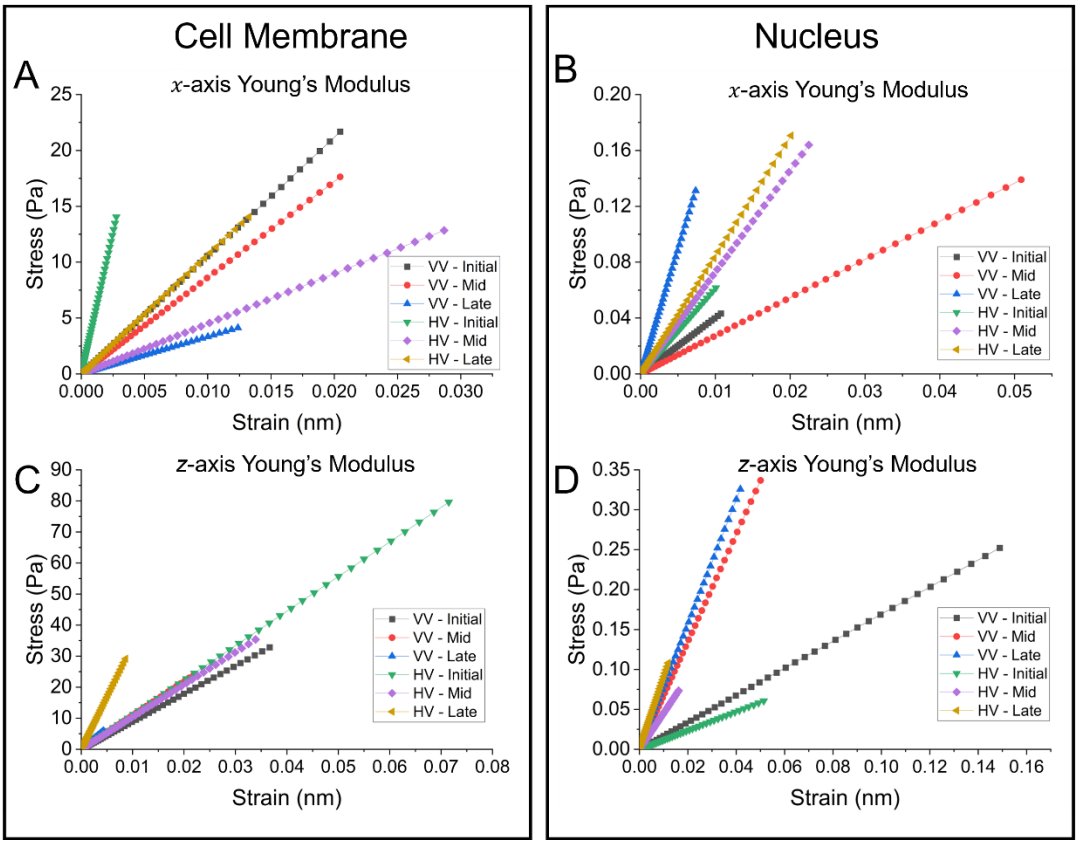

Figure 33: Predicted Young's modulus for the cell membrane and nucleus in the *x*-axis and *z*-axis. A steeper line indicates a higher apparent Young's modulus value and therefore a higher apparent stiffness during vibration. In the *z*-axis, the late adhered model when vibrated horizontally resulted in the highest apparent stiffness in both the cytoplasm and nucleus.

Young's modulus graphs show a higher apparent stiffness in the *z*-axis for the late adhered model when vibrated horizontally in both the cell membrane and the nucleus. In the *x*-axis, the initial adherence model has the highest cell membrane

stiffness when vibrated horizontally. For the nucleus in this axis, it is the late-stage model vibrated vertically which experiences the highest apparent stiffness. Taken together with the previous results measuring stress on the cell membrane and nucleus, it may be that horizontally vibrated cells experience a higher stress during vibration and, as a result, strain harden more.

2.6.2.4 Discussion/hypotheses from cell models

The stress and Young's modulus graphs for the cell models give an indication of the mechanical response the cell may have to vibration. From Figure 31E, the stress on the cell membrane in the *z*-axis (vertical axis) is greatest when the cell is vibrated horizontally, and at an early stage of adhesion. This may also be suggesting that vibrations are transmitted to the cell more effectively before the cell is fully adhered to the culture plate.

The results also show that stress increases at higher frequencies of vibration, and below 1 kHz, there is little variation in stress between different stages of adhesion and direction of vibration. From Figure 32D and Figure 32F, horizontal vibration resulted in higher stress on the cell membrane, which may lead to an increased response from the cell. Figure 33 showed that fully adhered horizontally vibrated cells resulted in more strain hardening in the z-axis. Measuring this response in the *z*-axis would be straight forward using atomic force microscopy (AFM) which obtains measurements in this direction, and as a result, only the z-axis Young's modulus results will be comparable.

These models, combined with previous research suggests that vibrating cells horizontally as opposed to vertically may result in higher cell stiffness and as a result, may provide a higher osteogenic response [271, 274]. Therefore, in vitro studies comparing horizontal and vertical vibration and the effect on mechanical and osteogenic response ought to be investigated. To compare these effects, a horizontal vibration device had to be designed.

2.6.3 Designing a horizontal device

2.6.3.1 Prototype 1

The first initial design for a horizontal vibration device (Prototype 1) was to simply set the device on its side and attach a 'shelf' via magnets. To investigate whether the top plate vibrated the same whilst on its side as it did vertically, interferometry measurements were taken with the device on its side and compared to measurements taken when the device was flat. Results showed that the device (and therefore piezo actuators) performed the same whether flat or at a 90-degree angle (data not shown). Therefore, any discrepancies in interferometry measurements were due to problems in the set up and not in the piezo actuators. Prototype 1 is shown in Figure 34 alongside heatmaps of the interferometry measurements taken.

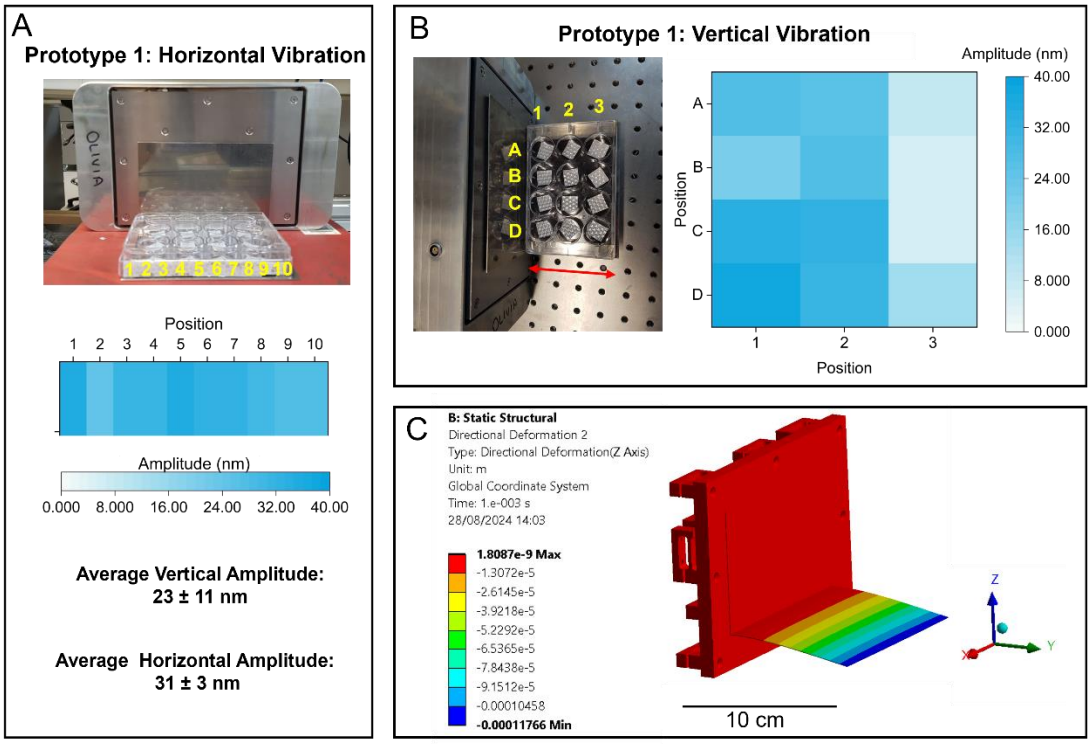

Figure 34: Initial horizontal setup (Prototype 1). A) Device on its side, with a 'shelf' attached via magnets to the top plate. A cultureware plate is then also attached using magnets to the shelf. Interferometry showed an average horizontal amplitude of (31 ± 3) nm. B) Average vertical amplitude was measured at (23 ± 11). C) ANSYS model of prototype 1. For vertical measurements, N = 12, for horizontal measurements N = 10, where each replicate was measured at different positions across the device.

At 1 kHz, and a voltage of 10.56 V the average horizontal amplitude was 31 ± 3 nm. Therefore, horizontally, the amplitude was relatively constant. However, when vertical interferometry was performed, it was found that there was substantial movement in the vertical plane. The average across the wells was 23 ± 11 nm. There was considerably more vibration proximal to the top plate than there was further away.

To further understand the effects of applied vibration on the shelf, ANSYS was used to model the set up as is shown in Figure 34C. A static structural analysis was performed to determine the behaviour of the model under static loading conditions. The device top plate was simulated to have a displacement of 30nm in the *y*-direction and a gravity of 9.8 m/s^2 was also added. The effects show that due to the thinness of the top plate significant bending occurs in the *z*-axis when vibrated horizontally. Interferometry found more vertical vibration closer to the top plate than the edges, contradicting the ANSYS models. This may be due to the shelf not being perfectly parallel to the ground in reality, thus causing additional effects. If the shelf is not parallel, the forces acting in the vertical direction (ie. gravity) will result in variations across the surface when vibrated.

2.6.3.2 Prototype 2

The vertical vibration was far too significant to allow for horizontal vibration to be independently tested and it was therefore concluded that Prototype 1 was unable to suitably minimise vertical vibrations. Therefore, a new set up was designed, this time using piezo clamps outside of the device and bolting them onto steel top plates (Prototype 2). This would ensure that a thicker top plate was used for the cultureware to attach to in an effort to minimize vertical vibrations. Initially, brackets were used to connect piezo clamps to the top plate, however these were found to have a similar problem to the shelf. As the brackets were very thin, they would bend in response to vibrations and would therefore fail to transfer the deformations to the steel top plate. Brackets were replaced with PCB cube connectors, and the piezo clamps were bolted onto the bottom of a device to ensure stability. Cultureware were then attached to the steel top plate using magnets as is shown Figure 35.

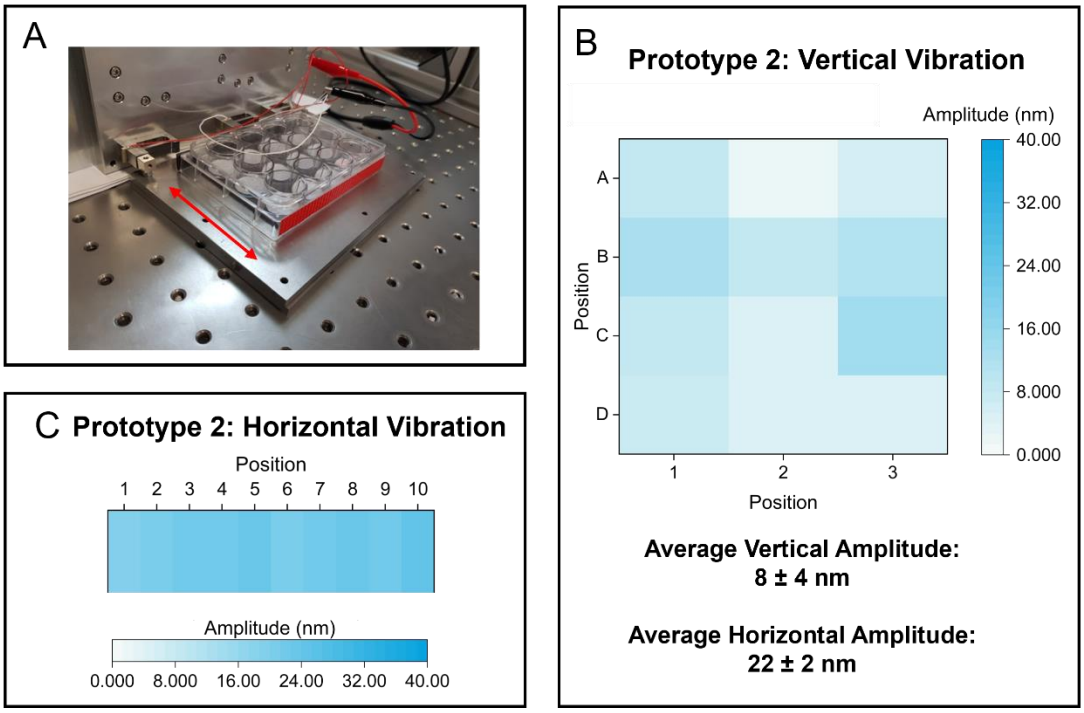

Figure 35: A) Second horizontal setup (Prototype 2), where piezo clamps were bolted onto steel top plates using PCB cube connectors. For stability, piezo clamps were also bolted onto the bottom of a device. Cultureware is then attached to the steel plate via magnets. B) Interferometry measured average vertical amplitude at 8 ± 4 nm. C) The average horizontal amplitude was measured at 22 ± 2 nm. For vertical measurements, N = 12, for horizontal measurements N = 10, where each replicate was measured at different positions across the device.

Interferometry was performed again both vertically and horizontally with measurements shown in Figure 35B and Figure 35C respectfully. At 1 kHz frequency and with an applied voltage of 222.2 $V_{pk\text{-}pk}$, the average horizontal amplitude was 22 ± 2 nm. However, vertically there was an average of 8 ± 4 nm. Although an improvement, vertical vibrations were still too high.

2.6.3.3 Prototype 3

The device base has 45-degree chiselled edges to prevent sharp corners. As a result, when the device is on its side it may not be perfectly stable. Therefore, it was decided to replace the device with a custom designed base block which would provide stability to the piezo actuators (Prototype 3). This block was designed in AutoCAD and manufactured from aluminium. The set-up, along with heatmaps of horizontal and vertical interferometry measurements, is shown in Figure 36.

However, vertical vibrations were still significant at an average of 15 ± 12 nm. Horizontal vibrations were also not as consistent as the previous design, at 18 ± 7 nm. This may have been due to the base block and top plate not lying perfectly flat against the bench top. This was likely due to the cube connectors and bolts not being at a perfect 90-degree right angle. To try and account for this, the right angle was removed all together and the piezo actuators were bolted directly onto the side plate as shown in Figure 36D.

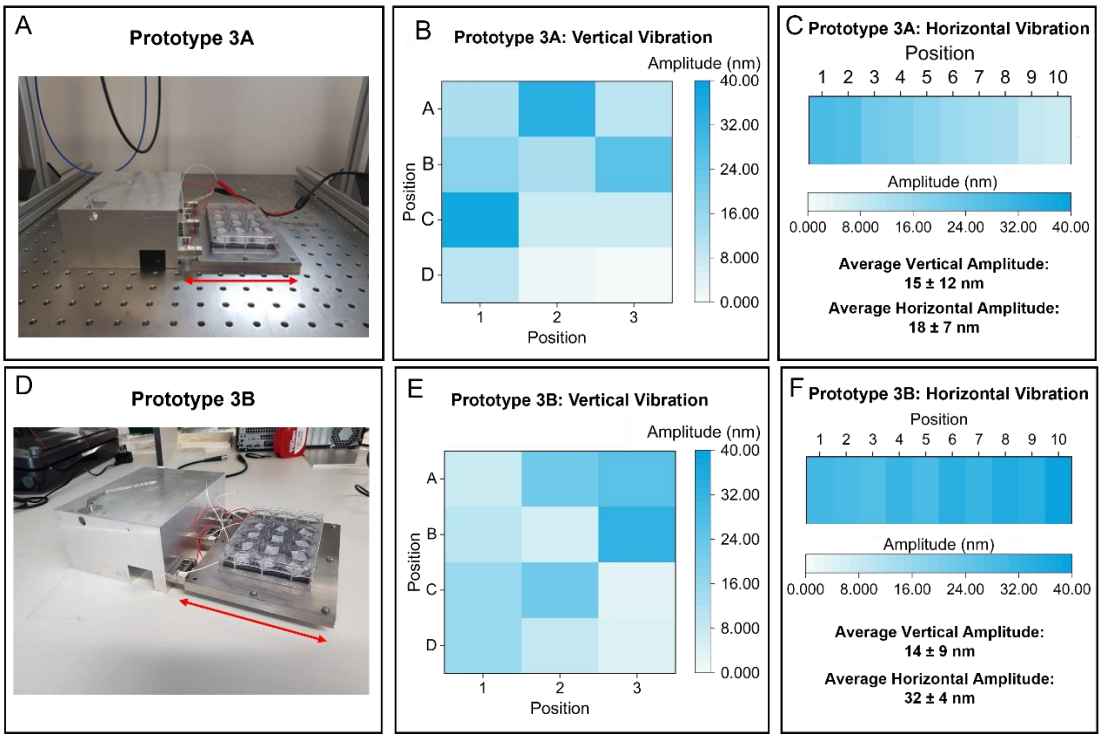

Figure 36: A) Third horizontal set up (Prototype 3A) where piezo actuators were bolted onto an aluminium base block and then secured to a steel top plate via cube connectors. Cultureware was then attached to the steel top plate via magnets. B) Interferometry showed an average vertical vibration of 15 ± 12 nm. C) Average horizontal vibration was measured at 18 ± 7 nm. D) A modification was made to the device bolting the piezo actuators directly onto the side plate (Prototype 3B). E) Average vertical vibration was measured at 14 ± 9 nm. F) Average horizontal vibration was measured at 32 ± 4 nm. For vertical measurements, N = 12, for horizontal measurements N = 10, where each replicate was measured at different positions across the device.

Bolting piezo actuators directly into the side of the top plate did appear to result in better transmission of vibrations. Horizontal vibrations were more consistent at an average of 32 ± 4 nm. However, vertical vibrations were still significant at

14 ± 9 nm. This may have been due to the plate being suspended in air and therefore pulling on the piezo actuators. In an attempt to minimize this, rubber feet were added to the base of the top plate, however this did not significantly reduce vertical vibrations (data not shown).

2.6.3.3 Prototype 4

Using the standard piezo actuator clamp was proving challenging. Despite the ability to produce relatively consistent horizontal vibrations, significant vertical vibrations still remained, and it was proving difficult to dampen this. Therefore, a different type of piezo actuator was proposed. Shear piezoelectric actuators expand laterally as opposed to longitudinally, providing a different method of applying horizontal vibrations.

A device was constructed initially using 3 shear piezo actuators and later another device was built using 4, one in each corner (Prototype 4). Actuators were positioned in the same direction and glued using Araldite (Loctite) to a top plate, with a thin piece of plastic glued in between to prevent wires from short circuiting. This was then left to dry overnight, before a second, smaller top plate was glued on top (again with plastic in between). Due to the fragility of the device, Petri dishes were used for testing and interferometry measurements taken, measuring both horizontal and vertical amplitudes as shown in Figure 37.

The first 3 piezo device showed consistent horizontal vibrations at an average of 34 ±4 nm. Whilst vertical vibrations remained high at an average of 9 ± 9 nm, these were consistently on one side of the dish, where only one shear piezo was in place. In an attempt to make the device more stable, a four piezo actuator device was built, with a shear piezo at each of the four corners of the plate. Interferometry measurements showed that the four piezo actuator device had much lower vertical vibrations at an average of 2 ± 1 nm. Horizontal vibrations were still mainly consistent at an average of 29 nm ± 9, although one side of the device had much lower amplitudes. Although the four piezo device had much lower vertical vibrations, it was only capable of amplitudes of 30 nm using the power supply available. The three piezo device was capable of reaching 60 nm

amplitudes with relatively consistent horizontal vibrations at an average of 62 ± 6 nm. Vertical vibrations were again only on one side of the device.

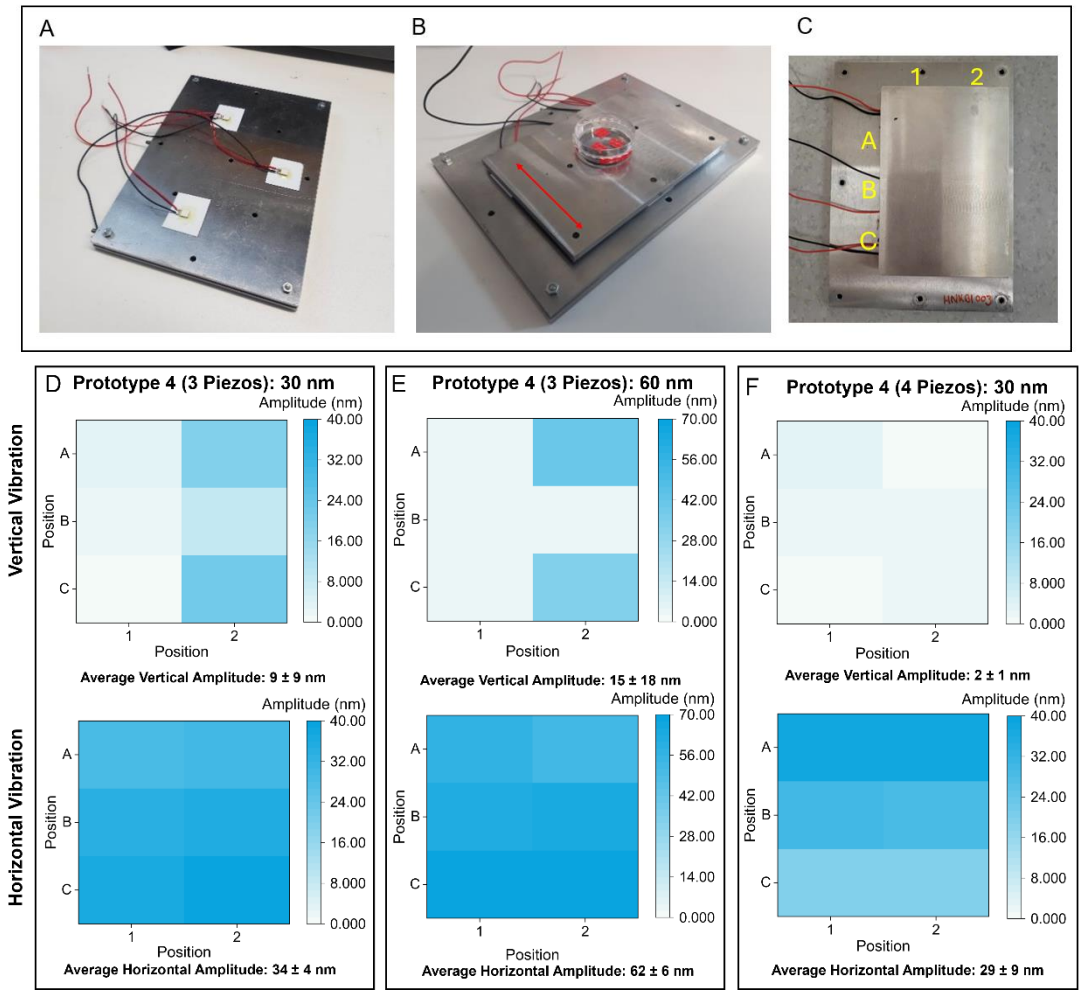

Figure 37: A) Horizontal Prototype 4, shear piezo actuator design with 3 shear piezo actuators (A and B) or 4 piezo actuators (C) glued between two top plates. D) Prototype 4 (3 piezos) set to 30 nm showed an average vertical amplitude of 9 ± 9 nm and an average horizontal amplitude of 34 ± 4 nm. E) Prototype 4 (3 piezos) set to 60 nm showed an average vertical amplitude of 15 ± 18 nm and an average horizontal amplitude of 62 ± 6 nm. F) Prototype 4 (4 piezos) showed an average vertical amplitude of 2 ± 1 nm and average horizontal amplitude of 29 ± 9 nm. N = 6 where each replicate was measured at different positions across the device.

Prototype 4 was used in early horizontal experiments, providing reliable horizontal vibration with minimal vertical vibration to cells *in vitro*. Cultureware was not placed on positions of high vertical vibrations on the three piezo actuator device. Although this device worked well and produced reliable amplitudes, it was not suitable for higher amplitude analysis. Prototype 4 was also not capable of

higher frequencies, and so to enable further work on using higher amplitudes and different frequency combinations, another design was required.

2.6.3.4 Prototype 5

To reach larger amplitudes, the use of the original piezo clamp and piezo actuators was revisited. The base block with bolted piezo clamps were re-employed, however a sturdier top plate was required. For this, a cradle was designed in AutoCAD and 3D printed using PLA, with a slot for a stainless steel top-plate, as shown in Figure 38A (Prototype 5). However, as the 3D printed component was 60% air, this resulted in little transmission of vibration. Therefore, the design was instead cut from aluminium and bolted into place with the final design shown in Figure 38B and Figure 38C. Heat maps illustrating interferometry measurements of the aluminium device are shown in Figure 38D and Figure 38E.

Table 7: Summary of vertical and horizontal interferometry measurements for different horizontal setups, all aimed for a horizontal vibration of 30 nm at 1 kHz.

Setup	Vertical (nm)		Horizontal (nm)		% Vertical vibration
	Average	Std Dev	Average	Std Dev	
Prototype 1	23	11	31	3	74%
Prototype 2	8	4	22	2	35%
Prototype 3	15	12	18	7	85%
Prototype 4 (3 piezos)	9	9	34	4	28%
Prototype 4 (4 piezos)	2	1	29	9	7%
Prototype 5	3	1	30	2	9%

For 30 nm, horizontal vibrations had an average of 29 ± 2 nm. Vertical vibrations were minimal at 3 ± 1 nm. This device was capable of much higher amplitudes than Prototype 4 and could be used at 90 nm amplitudes with horizontal vibrations at an average of 94 ± 8 nm and vertical vibrations were kept minimal at 5 ± 2 nm.

Prototype 5 was used in later experiments comparing the effects of horizontal vibrations at higher amplitudes and vertical vibration. Prototype 4 was used for initial horizontal experiments and for later experiments where two horizontal devices were required. A summary of the average vertical and horizontal vibrations of all horizontal device designs is shown in Table 7.

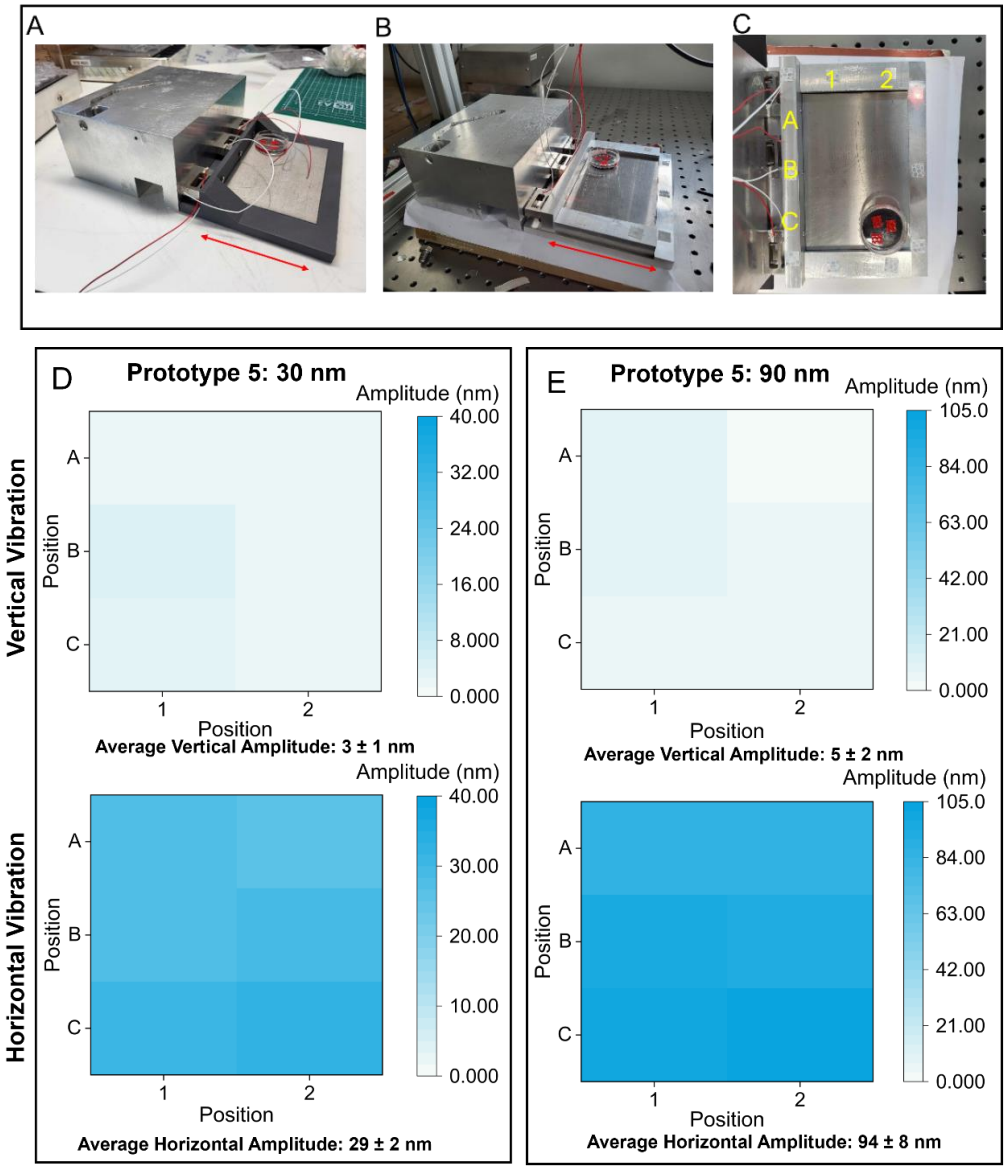

Figure 38: Final horizontal device designed (Prototype 5). A) Initially used a 3D printed cradle. B) Cradle was changed to stainless steel. C) Top view of device showing measurement points. D) At 30 nm, interferometry measured the average vertical amplitude at 3 ± 1 nm and average horizontal amplitude at 29 ± 2 nm. E) At 90 nm, interferometry measured the average vertical amplitude at 5 ± 2 nm and the average horizontal amplitude at 94 ± 8 nm. N = 6 where each replicate was measured at different positions across the device.

2.7 Calibration of Devices

2.7.1 Interferometry calibration

Prior to *in vitro* experiments, all devices were calibrated to the required frequency and amplitude. Vertical devices used at 30 nm and 1 kHz were powered by the original PSU. Vertical vibrations of 1 kHz and 60 or 90 nm were also powered using a previously custom-built PSU capable of amplifying amplitudes of 15, 30, 60 and 90 nm to the device. Horizontal devices and vertical devices requiring frequencies other than 1 kHz were powered using signal generators and a Behringer amplifier. Interferometry measurements for devices used are shown in Table 8.

Table 8: Interferometry measurements of various devices used for *in vitro* experiments. Horizontal vibrations produced by the vertical devices were measured and found to be lower than 2 nm and therefore deemed insignificant (data not shown).

Vibration Conditions	**Average Amplitude (nm)**	
1 kHz, 60 nm	61 ± 3	
1 kHz, 90 nm	96 ± 5	
100 Hz, 30 nm	30 ± 1	
1 kHz, 30 nm	30 ± 1	
6 kHz, 30 nm	30 ± 21	
10 kHz, 30 nm	33 ± 20	
Horizontal Devices	**Horizontal Amplitude (nm)**	**Vertical Amplitude (nm)**
Prototype 4 (4 piezos) 1 kHz, 30 nm	29 ± 9	2 ± 1
Prototype 4 (3 piezos) 1 kHz, 60 nm	62 ± 6	15 ± 18
Prototype 5 1 kHz 90 nm	94 ± 8	5 ± 2

2.7.2 Vibration analysis within incubator

Due to space limitations within incubators, testing of different vibration conditions resulted in devices calibrated to different conditions being within the

same incubator or in some cases on the same shelf. To confirm that there was no transfer of different vibration when in this set up, accelerometers were used to measure vibration when all devices were switched on within the incubator (Figure 39A). Due to differences between accelerometers (ACH-01, TE Connectivity, Schaffhausen, Switzerland) caused during manufacturing, each device gave different voltage outputs for a given amplitude. Therefore, accelerometers were individually calibrated by measuring the displacement of the accelerometer attached to a nanovibrational device using laser interferometry. This enabled calibration curves to be used to calculate displacement from accelerometer voltage output. Calibration had been done previous to the measurements taken here [306]. Results for accelerometery data with four devices of different amplitudes (one horizontal device) are shown in Figure 39.

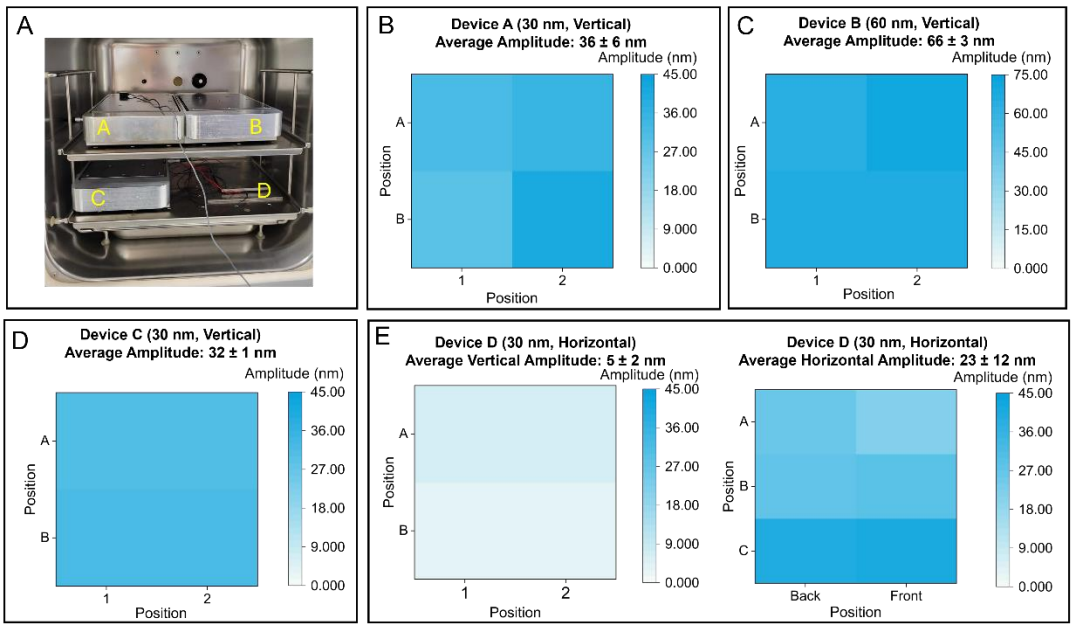

Figure 39: Accelerometer data for several devices within a small incubator. A) Setup with several devices, 3 vertical and 1 horizontal. B) Device A set to 30 nm, vertical measured average amplitude of 36 ± 6 nm. C) Device B set to 60 nm, vertical measured average amplitude of 66 ± 3 nm. D) Device C set to 30 nm, vertical measured average amplitude of 32 ± 1 nm. E) Device D set to 30 nm, horizontal measured average vertical amplitude at 5 ± 2 nm, and average horizontal amplitude at 23 ± 12 nm. For vertical measurements, N = 4, for horizontal measurements N = 6, where each replicate was measured at different positions across the device.

2.7.3 Laser doppler vibrometer measurements

To map vibration across the top plate of both the vertical and horizontal devices, a laser doppler vibrometer (LDV) (Polytec) was used to measure vibration on the two devices. A standard vertical device was used and Prototype 4 horizontal device consisting of 4 shear piezo actuators was also measured. Data is shown in Figure 40.

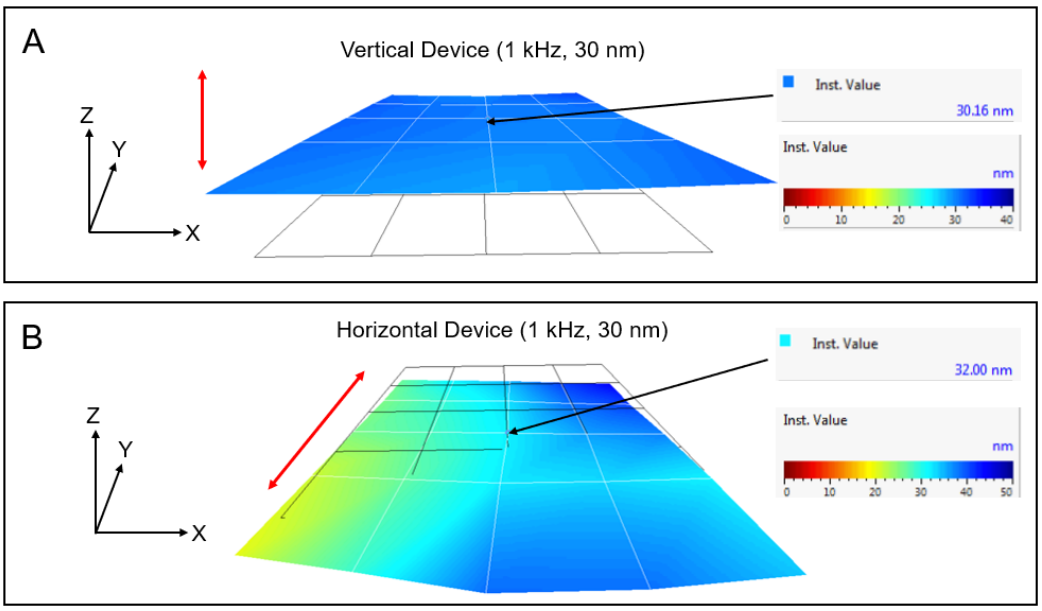

Figure 40: Laser Doppler Vibrometry data for vertical and horizontal devices at 1 kHz, 30 nm. A) Vertical device showed consistent vertical vibration reaching a maximum amplitude of 30.16 nm. B) Horizontal device (Prototype 4) showed some variation in vibration, as had been previously measured by interferometry.

The vertical device showed consistent vertical vibration with minimal horizontal displacement (<6 nm) consistent with previous results [297]. The horizontal device did show some variation across the top plate as had been seen by interferometry (Figure 37). The device showed some lateral movement (<2 nm) likely due to either shear piezo actuators not being aligned precisely in the direction of desired motion or the device being at an angle on the LDV. Vertical movement was also minimal (<2 nm) giving confidence that the device could be used in experiments comparing vertical and horizontal vibration. Whilst horizontal vibration was not consistent across the device, *in vitro* experiments ensured cells were vibrated only on areas with the most consistent vibrations.

2.8 Discussion

This chapter involved the development of several key elements of device design. Initially, it was investigated whether the existing PSU could be modified to produce a variable amplitude and frequency, to make *in vitro* experiments of these parameters possible. Although progress was made in designing a variable frequency circuit, producing a suitable amplifier was much more challenging. As a result, it was determined that an external signal generator connected to a Behringer amplifier would be used to investigate the effects of different amplitudes and frequencies on cell response.

A key parameter to investigate was directionality of vibration. To begin with, FEA models of the cell were designed in ANSYS to determine the effect horizontal and vertical vibration have on the mechanical properties of the cell. These models were very simplified, were not suspended within a liquid (media) and were limited by assuming cells are rigidly attached to a surface, are homogenous and have the same volume. The models suggested that cells vibrated horizontally appear stiffer due to strain hardening than those vibrated vertically, as had been observed in previous studies [271, 274]. To test this hypothesis *in vitro* required the development of a horizontal vibration device.

Through multiple iterations and testing of devices, a shear piezo device was initially developed, capable of consistent horizontal vibrations of 30 nm at a 1 kHz frequency. However, this design was only capable of amplitudes of up to 60 nm and therefore the effects of higher amplitudes in combination with horizontal vibration could not be investigated. Therefore, a new device was designed using a manufactured cradle design and the original piezo actuator clamp. This device was capable of higher amplitudes of 90 nm, allowing for further analysis into the effects of horizontal vibration. The work done here enabled the use of a device capable of horizontal vibration that could be used within *in vitro* experiments to investigate the impact of directionality on cell response.

Chapter 3:

Nanovibrational Stimulation of NIH 3T3 Murine Cells

3.1 Introduction

As well as inducing an osteogenic response in MSCs, nanovibrational stimulation has also been demonstrated to increase gene expression and adhesion in endothelial cells and to even reduce biofilm formation of *Pseudomonas aeruginosa* [66, 300]. In cells, nanovibrational stimulation has been found to result in changes in adhesion, ion channels and gene expression, however the full extent to which cells respond to vibration is still not fully understood, nor the importance of different vibration factors, including frequency and amplitude [66, 139]. In an attempt to further understand the relationship between applying vibration and the resulting physical and functional changes within the cell, nanovibrational stimulation was applied to fibroblastic cells as a model system. Being cells that are involved in producing, maintaining and repairing connective tissue throughout the body, fibroblasts are continuously experiencing forces and there have been several studies that have found fibroblast cells to have mechanoresponsive properties [307-311]. Fluid flow, cyclic stretching, cyclic biaxial tension and cyclic strain have all been found to result in a response from cells, including changes in gene expression and proinflammatory cytokine production, as well as proliferation and fibronectin reorganisation [308-311]. Studies have also found that fibroblasts respond to applied vibration, however the smallest vibrations applied by studies have been on the micron scale [241, 250, 312, 313].

Prior to this study, nanovibrational stimulation had never been applied to fibroblasts. To study the effects, a murine fibroblast cell line, NIH 3T3 cells, were stimulated using vibration of 1 kHz and 30 nm. As these cells play an important

role within connective tissue, the morphology and mechanical properties of the cells were primarily investigated to observe whether there existed a relationship between the two in response to applied vibration. Actin remodelling of cell shape is involved in the differentiation of MSCs, with spread out and flattened MSCs undergoing osteogenesis, whilst rounded up cells result in adipogenesis [103, 314]. Actin also affects the shape of the nucleus during differentiation, with a smaller nuclei being linked to adipogenesis and a large nuclei to osteogenesis [315, 316]. Here, smaller and larger nuclei are due to viewing cells from above via a microscope lens. In addition to nuclear size, adhesion has also been shown to play a role in lineage commitment, with higher levels resulting in osteogenesis, and lower levels in adipogenesis (Figure 7) [103, 106, 126, 127]. As such, morphological changes may be used as indicators for cell differentiation with previous studies having found vibration to result in increased actin formation and reorganisation [245, 255, 317, 318].

Actin plays an important role in maintaining tension within the cell, and changes in actin formation and organisation can have a subsequent effect on the cell's mechanical properties. Cell tension and force transmission to the nucleus are controlled by the interaction between FAK and the cytoskeleton [125]. In NIH 3T3s, the quantity of myosin and actin in stress fibres has been shown to affect cell stiffness [319]. Changes in adhesion and the actin cytoskeleton previously observed following the application of nanovibration, indicate that stimulation leads to changes in the mechanical properties of the cell [67, 302].

Here, fluorescence microscopy was conducted to analyse the morphology of cells, whilst AFM was used to investigate mechanical changes. DAPI was used to investigate changes in nuclear area, whilst actin staining made it possible to observe changes in actin formation. Vinculin staining provided a measurement of focal adhesions, with a higher intensity being assumed to indicate higher focal adhesion formation. The importance of actin in controlling cell shape, differentiation and the mechanical properties of the cell provide relevant parameters to begin investigations into the influence of nanovibrational stimulation on cell response.

3.2 Methodology

3.2.1 Cell Culture Protocol

Mouse NIH-3T3 cells were cultured in Dulbecco's modified essential medium (DMEM, Sigma), supplemented with 10% foetal bovine serum (FBS, Sigma) v/v, 1% minimum essential medium non-essential amino acid solution (MEM NEAA) v/v and 2% antibiotics (penicillin/streptomycin) v/v. Cells were then cultured within an incubator at 37°C with 5% CO_2 and were either passaged or media replaced every 3-5 days. For experiments, cells were seeded at a density of 5000 cells/cm^2 into 35 mm Petri dishes unless otherwise stated (see Table 9). Cells used were all under passage 30.

3.2.2 Nanovibrational stimulation protocol

Prior to experimentation, calibration was performed on the device to ensure vibration was produced at 1 kHz and 30 nm (Table 8) and these vibration conditions were used across all experiments. Cells were left to adhere for 24 hours, unless otherwise stated, before being placed on the device and were vibrated continuously throughout experiments. Non-vibrated control samples were used to compare the effect that nanovibrational stimulation had on cellular morphology and mechanical responses. A summary of the vibration conditions and initial cell seeding densities used for each experiment is shown in Table 9.

Table 9: Summary of nanovibrational stimulation conditions for each experiment described in Chapter 3.

Experiment (Sub section)	Seeding Density (cells/cm^2)	Frequency (kHz)	Amplitude (nm)	Direction	Adhesion Time (hours)
3.3.1: Proliferation	5000	1	30	Vertical	24
3.3.2 Seeding Density	1000 2500 5000	1	30	Vertical	24
3.3.3 Adhesion Time	1000	1	30	Vertical	0 4 24
3.3.4 Timepoints	1000	1	30	Vertical	24
3.3.5 AFM	N/A	1	30	Vertical	4 24

3.2.3 Immunofluorescence Staining

Immunofluorescent staining was carried out on fixed cells, an example of which is shown in Figure 41. Immediately following vibration, cell media was removed, and 4% Formalin solution (Sigma) was used to fix cells at room temperature initially for 15 minutes however in later experiments the shorter fixation time of 8 minutes was eventually adopted to improve staining quality. The fixative was then removed, and cells were washed with phosphate buffered saline (PBS) three times. 1 mL of a Triton X permeabilisation buffer was then added to cells, initially for 5 minutes, then in later experiments for 30 mins to provide more access for antibody binding, at room temperature. The permeabilisation buffer was then removed and cells were blocked, initially for 5 minutes and later for one hour, at room temperature using 1% Bovine Serum Albumin (BSA) dissolved in PBS solution (PBS/BSA), 1g/100mL, w/v, to reduce non-specific antibody binding. Volumes stated here relate to a 35 mm Petri dish.

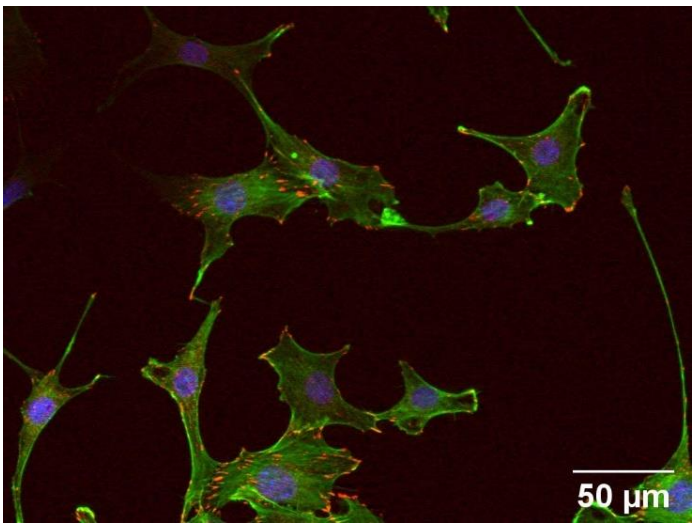

Figure 41: NIH-3T3 cells were stained with phalloidin to image actin (green), DAPI to image the nucleus (blue), and antibodies to image vinculin (red). Images were then analysed in ImageJ where the area of the nucleus was measured and the intensity of both actin and vinculin were quantified. Results were then compared between control and nanovibrated samples.

To investigate the focal adhesion of cells, vinculin, a cytoskeletal protein involved in focal adhesions was imaged. To do so, 100 μL of vinculin recombinant rabbit monoclonal antibody (AB_2532280, ThermoFisher Scientific) was added to cells at a concentration of 1:100 in 10 mg/ml PBS/BSA and cells were incubated at 37°C for 1-2 hours. The primary antibody was then removed, and cells were washed three times for 5 minutes with 0.5% PBS/Tween at room temperature. Details on all primary antibodies used is summarised in Table 10. Following rinsing, 100 μL of a secondary antibody was added to the cells at a concentration of 1:100 with 1 mg/mL PBS/BSA and cells were again incubated at 37°C for one hour. Once the secondary antibody was removed, cells were again washed three times for 5 minutes with PBS/Tween at room temperature.

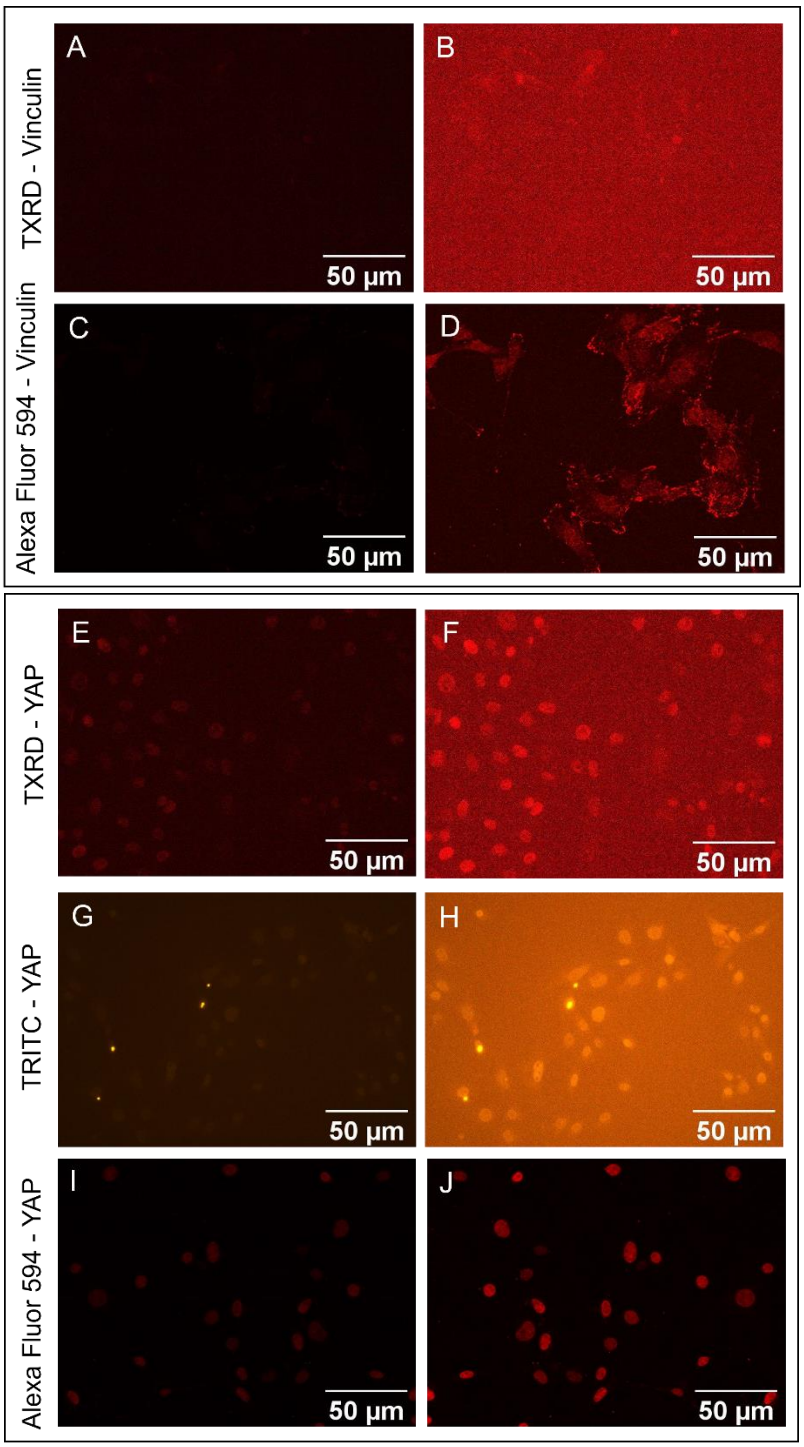

Figure 42: Testing different secondary antibodies. A) Original TXRD staining for vinculin. B) TXRD staining for vinculin image enhanced in ImageJ. C) Alexa Fluor 594 staining for vinculin. D) Alexa Fluor 594 staining for vinculin image enhanced in ImageJ. E) Original TXRD staining for YAP. F) TXRD staining for YAP image enhanced in ImageJ. G) TRITC staining for YAP. H) TRITC staining for YAP image enhanced in ImageJ. I) Alexa Fluor 594 staining for YAP. J) Alexa Fluor 594 staining for YAP image enhanced in ImageJ. All TXRD and Alexa Fluor 594 images taken using Zeiss (Imager Z.1) whilst TRITC images taken using Nikon (Eclipse Ts2).

Different secondary antibodies were tested to optimize the staining protocol. This was done using a vinculin and YAP primary antibody (to investigate YAP translocation to the nucleus following mechanical stimulation). Three secondary antibodies were tested: Goat Anti-Rabbit Texas Red (TXRD) antibody (4010-07, 2B Scientific), Goat Anti-Rabbit tetramethylrhodamine (TRITC) (2B Scientific 4010-03) and Alexa Fluor 594 (FisherScientific). Images of cells stained with each secondary antibody are shown in Figure 42. Upon comparing these stains, Alexa Fluor was determined to be the optimal secondary antibody producing the best resultant stains and was used in later experiments. Experiments where different secondary antibodies were used are stated in figure headings.

Table 10: Primary antibodies used for immunofluorescent staining

Primary Antibody	Supplier Details	Dilution	Response Investigated
Vinculin	AB_2532280, ThermoFisher Scientific	1:100	Focal adhesions
YAP	AB205270, Abcam	1:100	Translocation to nucleus
Sun1	AB103021, Abcam	1:50	LINC proteins
β-tubulin	AB179513, Abcam	1:1000	Neurogenic response
Osteocalcin	PA5-96529, invitrogen	1:100	Osteogenic response

Samples were then stained with 100 μL of Alexa Fluor 488 phalloidin (Thermo Fisher) diluted to a concentration of 1:100 with PBS for one hour at room temperature. Following staining, cells were rinsed once with 1 mL of PBS. PBS was then removed and 100 μL of Invitrogen Fluoromount-G Mounting Medium with DAPI was placed on the cells. Coverslips (18-22 mm diameter, 0.13 – 0.19 mm thick) were then placed over the cells and samples were wrapped in foil and stored at 4°C until ready to image.

3.2.4 Microscopy

Images were taken either using a Zeiss microscope (Imager.Z1) or a Nikon (Eclipse Ts2), both at x20 magnification depending on the use of TXRD or TRITC

respectively. Both excitation intensity and imaging time were kept consistent between images to ensure intensity results were comparable. To investigate the proliferation rate of cells, images were taken of live cells on each day during the experiment using a phase contrast microscope (Motic AE31). All samples were plated in triplicate to represent biological replicates, and three images were obtained per well (or Petri dish), representing technical replicates.

3.2.5 Image Analysis

Image analysis was conducted within ImageJ software. To determine proliferation rate, cell nuclei were counted within each field of view using the multi-point tool. Nuclear area analysis was performed using thresholding, which provided an automated and quick method to measure nuclear area (Figure 43). The images were converted into 8-bit and the brightness/contrast adjusted before thresholding. Once thresholding had been performed, a watershed was performed on the image to ensure cells were separated before the analyse particle function was used to measure nuclear area (pixels converted to μm^2) and count the number of nuclei. All results were plotted as violin plots in OriginPro.

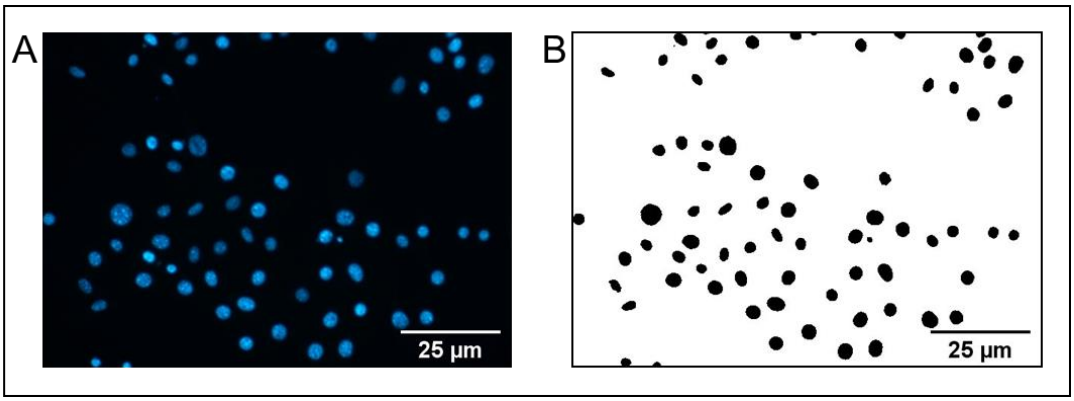

Figure 43: DAPI images were imported into ImageJ and thresholded. The analyse particles function was then used to obtain regions of interests around each nucleus and the area was measured.

To analyse actin and vinculin intensity, only images of isolated cells were used in analysis (to minimise effects from cell-cell contact). Using thresholding and the analyse particle function, the outlines of single cells were defined. These outlines were then used on the original images for both actin and vinculin and both the

grey mean values and integrated density for each were measured (Figure 44). To normalise against the background, the grey mean value of the background in each image was acquired in three empty regions of the image and the average was determined. The background grey mean value was subtracted from the grey mean value of each cell and this value was taken to be the density of actin or vinculin within the cell. To obtain the total intensity of actin and vinculin in each cell, Equation 3 was used:

$$Corrected\ Total\ Cell\ Fluorescence\ (CTCF) = Integrated\ Density - (Cell\ Area\ x\ Background\ Mean) \quad (3)$$

The grey mean value was taken to be the density of the staining within the cell, whilst the CTCF was defined as the total intensity summed over the area of the cell, with background intensity removed. Both density and intensity were plotted for both actin and vinculin staining.

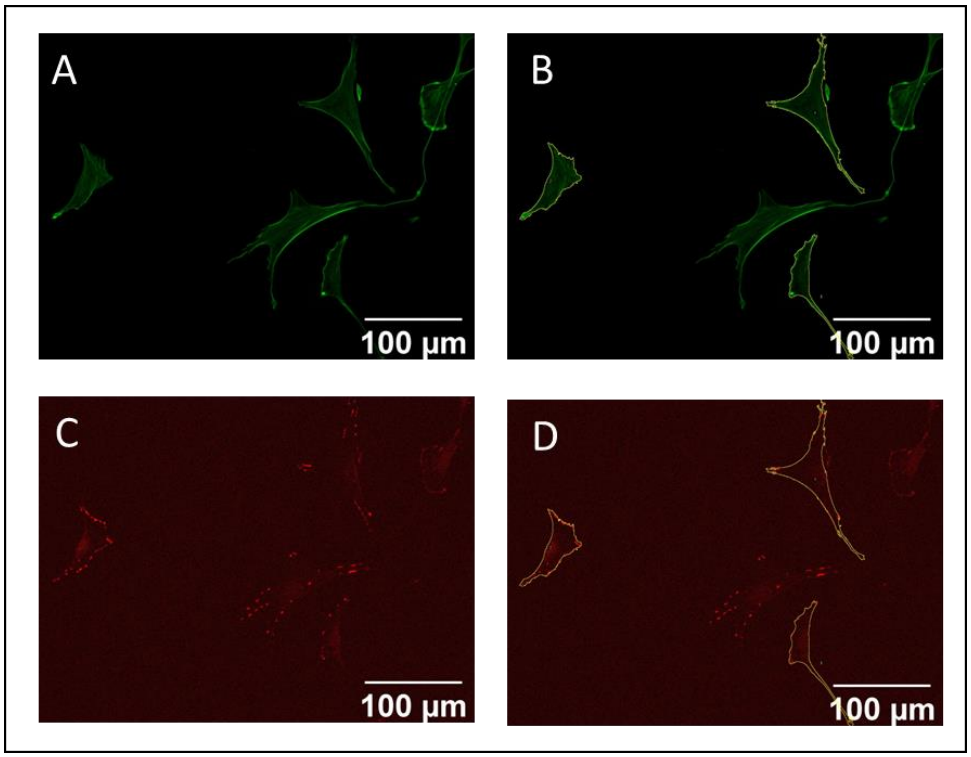

Figure 44: Actin and vinculin intensity were measured in ImageJ (A and C). Cells were thresholded and the analyse particles function was used to obtain outlines of the cells (B and D). These regions of interest (ROIs) were then measured, obtaining quantitative data of the grey mean value (density of staining), the integrated density and the area of each cell. The total intensity of the staining could then be calculated.

3.2.6 Atomic Force Microscopy

Fluorescence microscopy offered a method to obtain morphological and structural information of the cell. To obtain mechanical information, such as cell stiffness, AFM was used. This was done using two AFMs: a JPK Nanowizard 3 (JPK Instruments, Germany) and an Asylum MFP-3D (Oxford Instruments, UK). When obtaining AFM measurements, it is preferable for cells to be isolated on their own, or to at least have minimal contact with surrounding cells. To achieve this, seeding must be done at a very low density (≤ 1000 cells/cm^2). To do this, a suspension of cells was created using trypsin, and a few drops were pipetted into Petri dishes filled with media. Cells were then left to adhere overnight before being stimulated.

To obtain stiffness measurements, a silicon dioxide, spherical tipped cantilever (CP-PNPL-SiO-B, NanoAndMore) with a diameter of 3.5 μm was used. Cells were placed on a heated stage whilst obtaining measurements to ensure cells remained alive whilst stiffness measurements were acquired. Once the system was calibrated, the AFM was set to contact mode. When taking measurements using the Asylum AFM, only a single point on the nucleus and cytoplasm was measured, whilst for the JPK instrument, six points on the nucleus and six points on the cytoplasm of each cell were selected and measured. Force distance curves (FDC) were obtained for each measurement, with measurements being taken prior to stimulation beginning and after 3, 24, 48 and 72 hours of stimulation.

For measurements using the JPK, analysis was done within the JPK Analysis software, using the Hertz/Sneddon model to extract Young's Modulus data from each FDC. On some experiments, further analysis was conducted using power law analysis. Although living cells have viscoelastic properties, elastic expressions such as the Hertz or Sneddon models are commonly used to extract elastic components from AFM measurements on cells. Without considering viscoelasticity, measurements could be inaccurate and incomplete. Cells are also often cultured on rigid surfaces many times stiffer than cells. This combined with the finite-thickness of the cell will result in a bottom-effect that will lead to errors in AFM measurements. Garcia *et al* have previously developed both a method of

extracting viscoelastic parameters from FDCs of cells and algorithms to correct for bottom-effects [320, 321]. The modulus of the cell can be assumed to follow a single power-law dependence with time as can be described by Equation 4,

$$E = E_0 \left(\frac{t}{t_0}\right)^{-\gamma} \quad (4)$$

Where E_0 is the compressive modulus of the material (or cell) at time t_0 whilst γ is the fluidity exponent. When $\gamma = 0$, the material can be considered elastic, whilst $\gamma = 1$ defines a Newtonian liquid. Techniques developed by Garcia have made it possible to extract the parameters E_0 and γ from FDCs obtained during AFM measurements [320, 321]. As such, both the elastic and viscous components of the cell may be obtained. Extraction of fluidity values was performed by Garcia and colleagues at the Materials Science Institute of Madrid. Data was then plotted as a box plot to enable comparisons between samples. Topography images were produced using a rectangular silicon tip on a silicon nitride cantilever (FASTSCAN-D_SS, Bruker) using a JPK instrument.

To inhibit actin formation and contractility, cytochalasin B (14930-96-2, Sigma Aldrich) and blebbistatin (ab120425, Abcam) were used respectively. Inhibitors were added to cell media at a concentration of 5 μM for cytochalasin B and 50 μM for blebbistatin, and cell media was replaced with inhibited media 24 hours after seeding, when starting vibration.

3.2.7 Statistics

Data that contained two or more categorical variables (e.g. two conditions at multiple timepoints) were first subjected to a two-way ANOVA to determine whether any statistical differences existed within the data. Where significant differences did exist, the data was subjected to further statistical tests. Firstly, a normality test was performed to determine whether the data was normally distributed. In cases where $N < 30$ the data was assumed to be normally distributed [322]. When data was normally distributed, either a one-way ANOVA was performed if there were three or more groups, or a t-test when there were only two conditions. For data subjected to a one-way ANOVA a Levene's test was

also performed to test for equal variances. If the data was homogenous, a Tukey post-hoc was used, and when non-homogeneous, a Games Howell post-hoc.

If the data was not normally distributed, either using a Kruskal-Walls test with Dunn post-hoc if there were three of more groups, or a Mann-Whitney when only two conditions existed. A flowchart detailing the decision process for using statistical tests is shown in Figure 45. Any results with a p-value of less than 0.05 were deemed to be significantly different. A single asterisk was used in figures to denote a p-value of ≤ 0.05, two asterisks denoted a p-value of ≤ 0.01 and three asterisks denoted a p-value of ≤ 0.001. Standard deviations were obtained where appropriate, and when necessary, pooled standard deviations were calculated to combine biological replicates together.

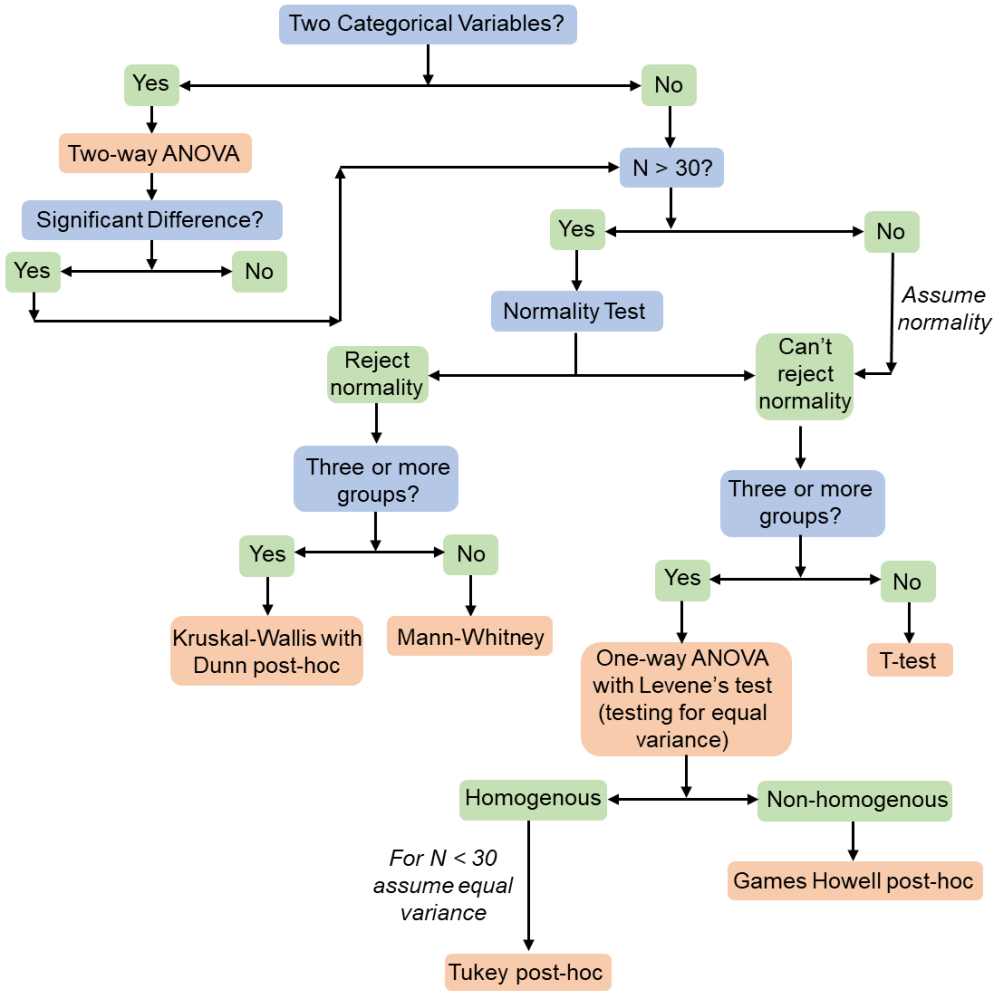

Figure 45: Flowchart detailing the decision making process for statistical tests used. N > 30 required to test for normality [322].

3.3 Results

3.3.1 Nanovibrational stimulation increases cell proliferation

Prior studies of nanovibrational stimulation have shown that stimulation results in an increased proliferation rate in both endothelial cells and MSCs [302, 323]. Applied mechanical stimulation has been found to result in an increased proliferation rate in fibroblasts [310]. To investigate whether this held true for nanovibrated NIH 3T3 cells, cells were seeded into 12 well plates, were stimulated for 2 days and imaged prior to stimulation and following 1 and 2 days of applied vibration. Non-vibrated controls were also measured at each of these timepoints. The percentage of cells per sample showing the growth in proliferation is shown in Figure 46.

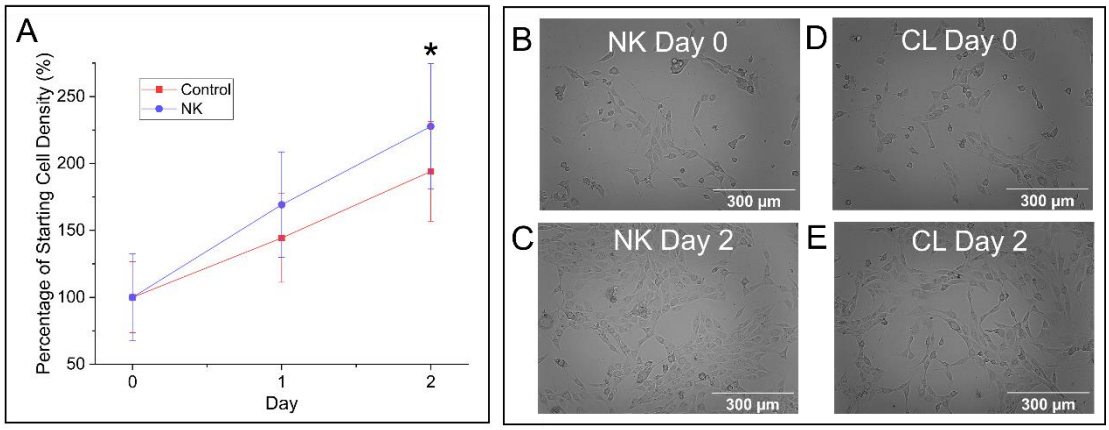

Figure 46: Investigating the proliferation of cells in response to vibration. A) Proliferation data for NIH 3T3 cells over 2 days, with and without nanovibration. Cells were left to adhere for 24 hours prior to first measurement (0 days). Error bars represent standard deviation. N=4, where each replicate is composed of total cells in 3 microscopic fields of view. B) Nanovibrated cells at Day 0 timepoint prior to stimulation. C) Nanovibrated cells after 2 days of stimulation. D) Control cells at Day 0 timepoint. E) Control cells at Day 2 timepoint.

Nanovibrated samples were found to have increased in cell number after 2 days of stimulation compared to non-vibrated controls. Whilst not showing a significant difference, cells stimulated for 1 day also showed an increase in cell number when compared with their relevant control. Although nanovibrational stimulation appeared to result in an increased proliferation rate when compared to non-vibrated controls, due to the nature of seeding within multi-well plates,

there was a large amount of variability between images and samples leading to a high standard deviation. The data was only collected for the first two days of stimulation, and although the trend appears to be that the proliferation rate increases over time in nanovibrated cells, it would be presumptuous to assume the trend would continue at later timepoints.

3.3.2 Initial seeding density affects cell response to nanovibrational stimulation

Vibration application was also optimised by investigating the effects initial seeding density had on morphological response. Initial seeding density has been found to affect gene expression, with higher seeding densities resulting in higher expressions of osteogenic and chondrogenic markers due to increased cell-cell contact required for differentiation and higher matrix deposition [276-279]. Studies have also found seeding density to affect the mechanical properties of 3D constructs, such as tensile strength and Young's Modulus, with higher seeding densities leading to poorer mechanical properties including lower tensile strength [282, 283]. Higher seeding densities may also be affecting nutrient availability, cellular metabolism and cell viability [282, 283]. Although seeding density has a significant effect on cell response, little investigation has been conducted into its effect on cells during vibration.

Three initial densities of NIH 3T3 cells were seeded into 12 well plates: 1000 cells/cm^2, 2500 cells/cm^2 and 5000 cells/cm^2. Nuclear area, cell area, actin intensity and actin density were all analysed after 24 and 72 hours of stimulation in two separate experiments. Nuclear and cell area results are displayed in Figure 47, and actin data in Figure 48.

Nuclear area was found to be consistently higher at all seeding densities in nanovibrated samples compared to non-vibrated controls after 24 hours. After 72 hours, only at the higher seeding densities of 2500 and 5000 cells/cm^2 were nanovibrated samples found to have higher nuclear areas than controls. After 24 hours of stimulation, nanovibrated samples also appeared to have a more bimodal distribution than at the 72-hour timepoint. This suggests that certain

sub-populations of cells were responding differently to vibration, and when compared to the unimodal response seen after 72 hours of vibration, suggests that cells had a higher initial response within the first 24 hours. At earlier timepoints, cells are likely to be more isolated. The bimodal response may be due to cells in cell-cell contact responding differently to vibration than isolated cells. At later timepoints cell-cell contact will be higher in samples, which may be reflected by the unimodal response.

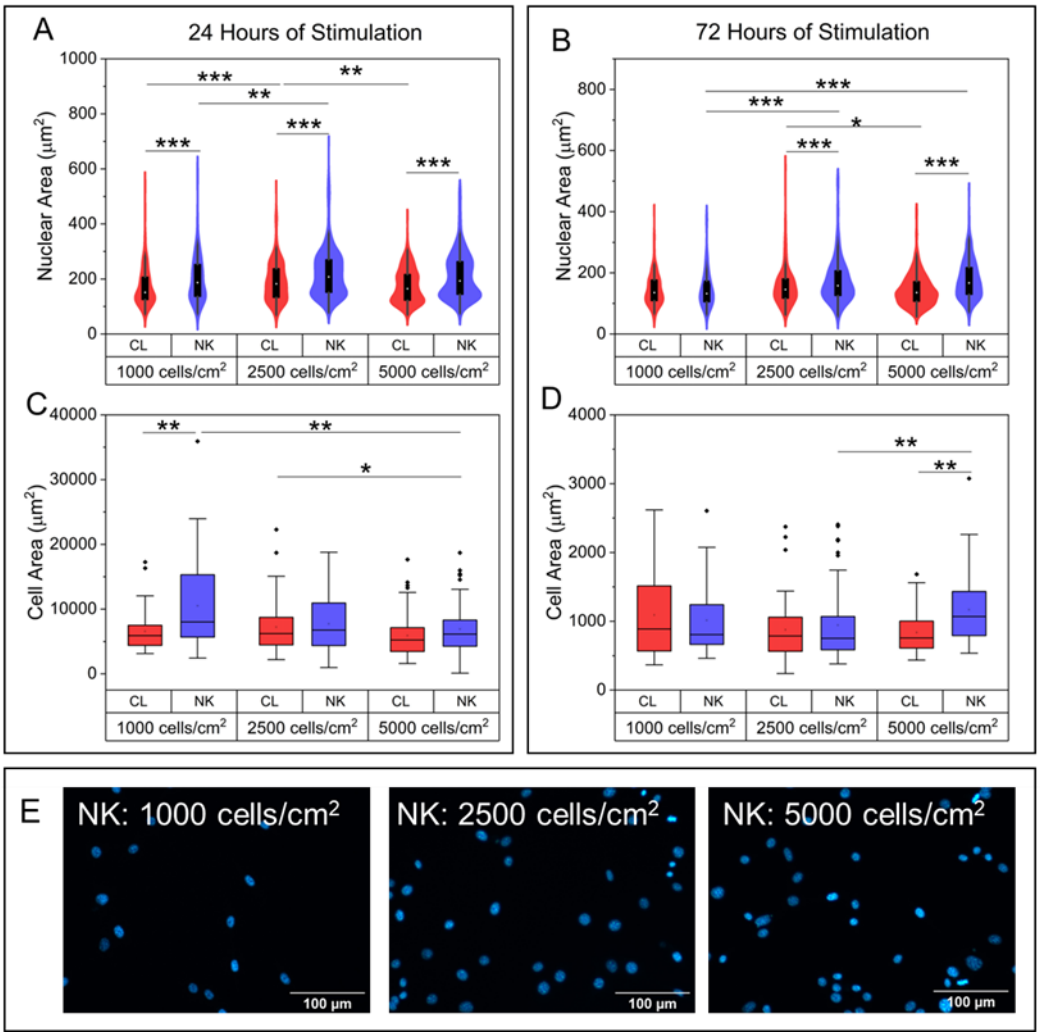

Figure 47: Nuclear and cell area data for cell samples initially seeded at densities of 1000, 2500 and 5000 cells/cm2. A: Nuclear area following 24 hours of stimulation (Number of cells: N > 100). B: Nuclear area following 72 hours of stimulation (N > 100). C: Cell area following 24 hours of stimulation (N ≈ 30). D: Cell area after 72 hours of vibration (N ≈ 30). E) DAPI images after 72 hours of stimulation on cells seeded at different initial seeding densities. Images taken using a Nikon Eclipse Ts2 microscope and brightness was adjusted equally in ImageJ software.

Following 24 hours of stimulation cell area was shown to be significantly higher in nanovibrated samples only at the lowest seeding density of 1000 cells/cm^2 compared to control cells seeded at the same density. After 72 hours of stimulation, it was cells stimulated at the highest seeding density of 5000 cells/cm^2 which had a significantly higher cell area compared to control cells. When comparing both experiments, cell area after 72 hours of stimulation was an order of magnitude lower than after 24 hours, for reasons not fully understood. Whilst nuclear area almost always increased in nanovibrated cells, regardless of seeding density, this did not always correspond with an increase in cell area. Therefore, although the nucleus of nanovibrated cells were often enlarging in response to applied stimulation, the cell itself was not always increasing in size. This may suggest that cell spreading and nuclear tension are not intrinsically related.

Actin intensity and grey mean value were also measured to investigate the effects of initial seeding density on their response with the results shown in Figure 48. After 24 hours of stimulation, actin intensity was found to be significantly higher in nanovibrated cells at the lowest seeding density of 1000 cells/cm^2 compared to controls. Meanwhile, actin grey mean value, representing the density of actin in the cell, was found to be significantly increased in nanovibrated cells at initial seeding densities of 1000 cells/cm^2 and 2500 cells/cm^2. At the highest initial seeding density of 5000 cells/cm^2, actin density was found to be significantly lower in nanovibrated cells.

After 72 hours, the highest initial seeding density resulted in the actin intensity of nanovibrated cells to be significantly higher than non-vibrated controls and stimulated cells at the other two seeding densities. The grey mean value was also found to be significantly higher in nanovibrated cells at this higher initial seeding density. There were no other significant differences found at this timepoint in the other initial seeding density samples compared to their respective controls.

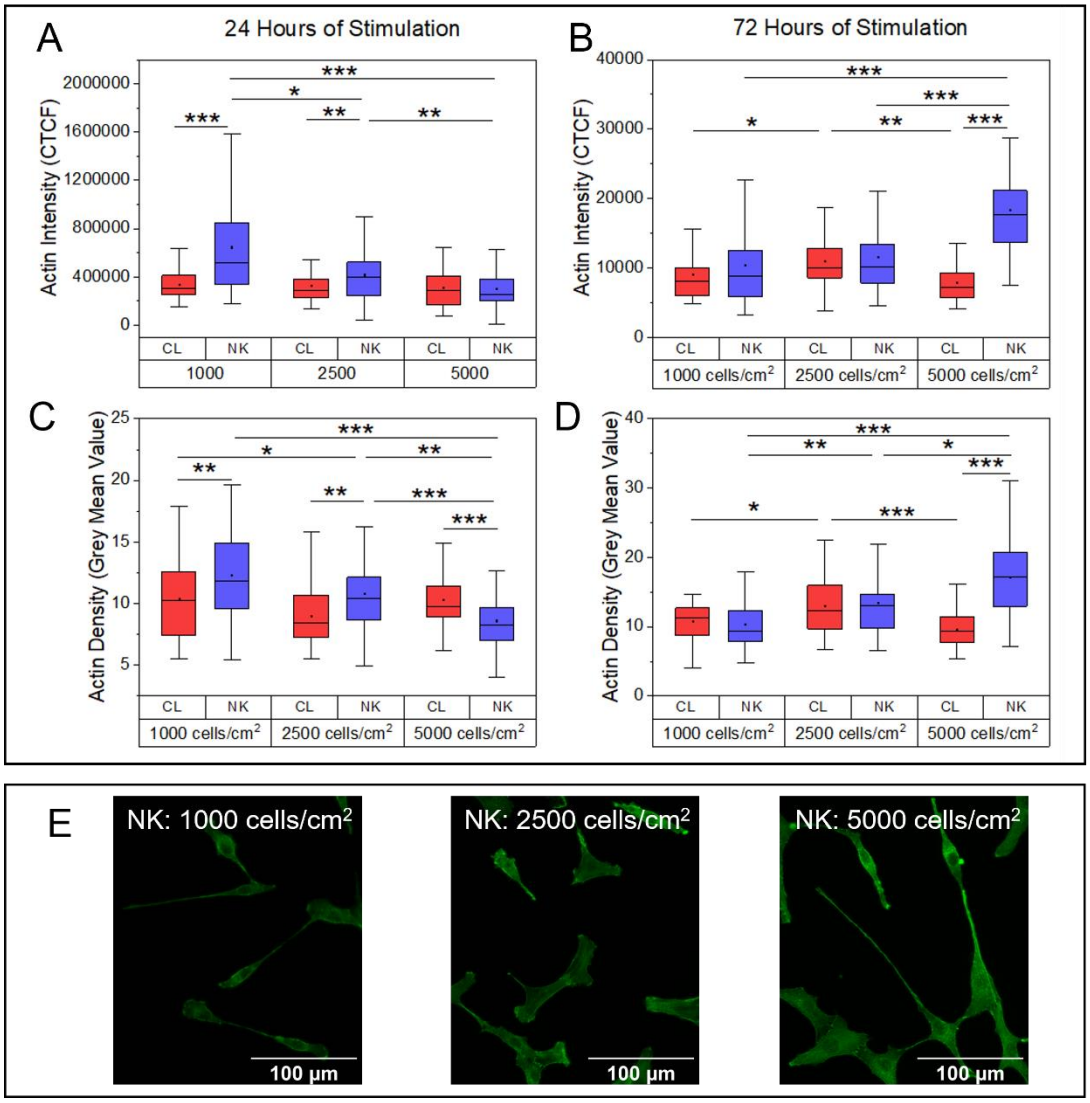

Figure 48: Actin intensity and actin grey mean value data for samples seeded at different seeding densities. A: Actin intensity following 24 hours of stimulation (Number of cells: N ≈ 30). B: Actin intensity after 72 hours of stimulation (N ≈ 30). C: Actin density after 24 hours of stimulation (N ≈ 30). D: Actin density following 72 hours of stimulation (N ≈ 30). E) Actin images after 72 hours of stimulation at each seeding density. Images taken using a Nikon Eclipse Ts2 microscope and brightness was adjusted equally in ImageJ software.

Increases in actin intensity corresponded with increased cell area and actin density, suggesting that the cells were enlarging and forming more actin in response to stimulation. As for comparing between seeding densities, cell area, actin intensity and actin density appeared to increase within the first 24 hours when cells were seeded at a lower initial seeding density. However, at the later timepoint of 72 hours, a higher seeding density showed an increased response

from actin and in cell area compared to controls. This suggests that a lower seeding density may provide cells with an improved initial response to vibration, and as cells become more confluent at later timepoints they would show an increase in cell area, actin intensity and actin density. Therefore, for nanovibrational stimulation, it would appear that a lower initial seeding density would enable single cell analysis, whilst also maximising the cell's initial response to vibration, and allowing cells to culture for longer before becoming fully confluent. Therefore, experiments from here on were seeded at the initial seeding density of 1000 cells/cm^2 unless otherwise stated.

Studies often use different seeding densities for different analysis techniques, such as higher seeding densities for morphology and gene expression analysis, and lower densities for AFM measurements. Given the varied responses seen here as a result of different initial seeding densities, this raises questions as to how much of an impact seeding density may be having upon responses to mechanical stimulation. There is a vital need to keep seeding density consistent throughout an experiment to ensure all responses observed are not being affected by the initial seeding density of cells.

3.3.3 Adhesion time prior to stimulation affects cell response to nanovibrational stimulation

Previous nanovibrational stimulation studies have left cells to adhere for 24 hours prior to vibration [67, 139, 287, 298]. However, for some experimental work such as AFM, it would be beneficial to use different seeding durations prior to applying vibration. This experiment looked to investigate where the time cells are left to adhere prior to vibration affected cell response.

Cells were left to adhere for three lengths of time before beginning stimulation: 0 hours (cells began vibration immediately following seeding, NK0), 4 hours (cells were incubated for 4 hours before vibration begins, NK4) and 24 hours (cells were incubated for 24 hours before vibration began, as had been done previously, NK24). A non-vibrated control sample was incubated in a separate incubator for the duration of the experiment before being fixed alongside NK24. Samples were

measured at two timepoints, after 24 hours of vibration and after 72 hours of vibration in two separate experiments. Nuclear area, cell area, actin data and vinculin data was obtained and is displayed in Figure 49, Figure 50, and Figure 51 respectively.

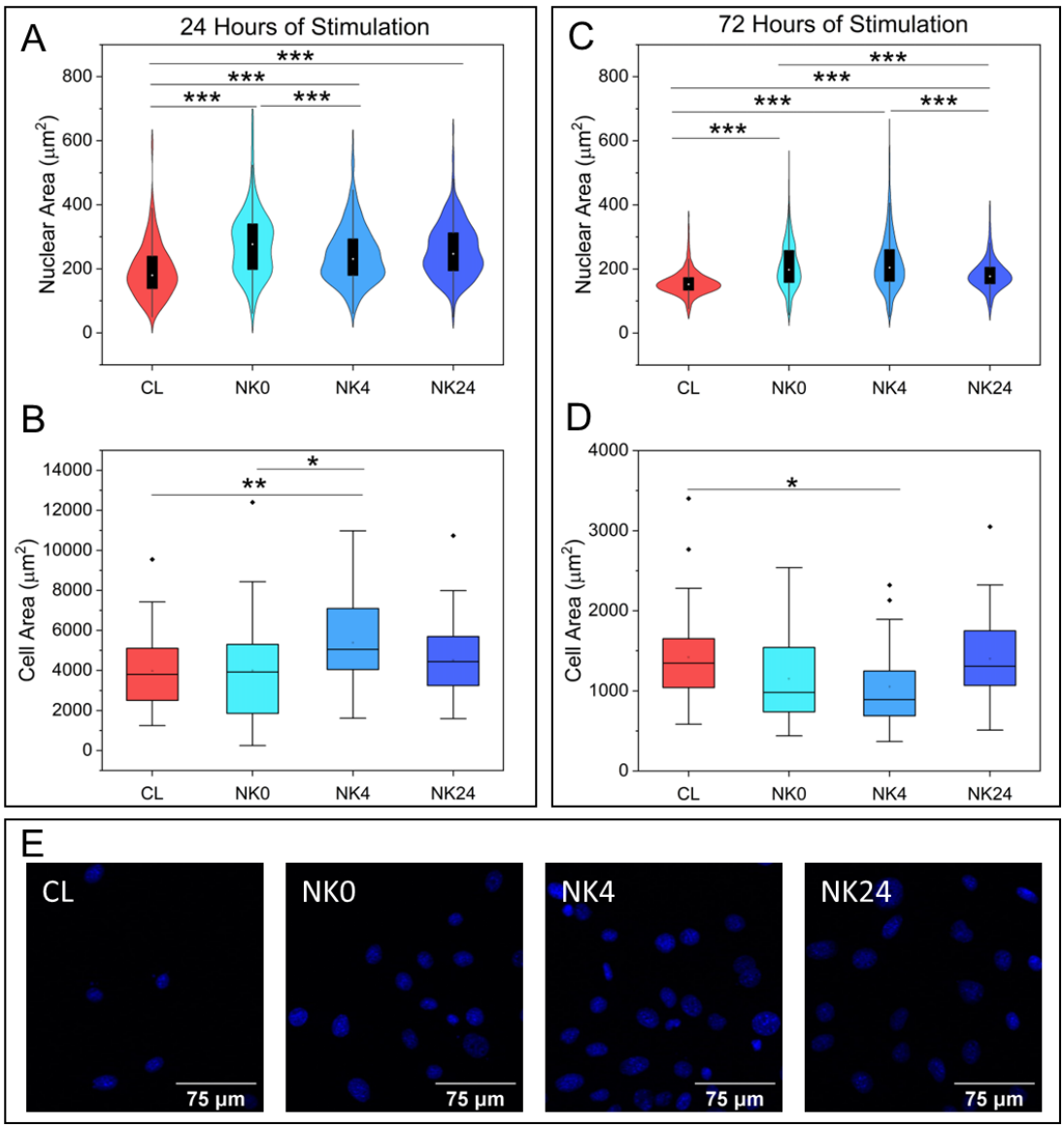

Figure 49: Nuclear area data for cell samples left to adhere for 0 hours (NK0), 4 hours (NK4) and 24 hours (NK24) prior to vibration. A) Nuclear area after 24 hours of vibration (Number of cells: N > 100). B) Cell area after 24 hours of vibration (N ≈ 30). C) Nuclear area after 72 hours of vibration (N > 100). D) Cell area after 72 hours of vibration (N ≈ 30). E) DAPI stained images of cells from all four conditions after 24 hours of stimulation. Images taken using Zeiss (Imager Z.1) and brightness was adjusted equally in ImageJ software.

After both 24 hours and 72 hours of stimulation, the nuclear area of all nanovibrated samples was found to have increased Figure 49A and Figure 49B show control cells to have a unimodal distribution at both timepoints suggesting that the nuclear area was mainly distributed across a small range of values. After 24 hours of stimulation however, the nuclear area of stimulated cells show a bimodal distribution, with the NK0 sample being the most prominent. This suggests that, similarly to the seeding density data shown in Figure 47, cells are responding differently to vibration more at this early timepoint. After 72 hours of stimulation only NK0 has a slight bimodal distribution, suggesting that the NK4 and NK24 samples are responding similarly to vibration at this time.

When measuring cell area, NK4 cells had the largest cell area compared to controls after 24 hours of vibration. NK4 cells were also significantly different from NK0 cells. However, after 72 hours of stimulation, NK4 cells had the smallest cell area, significantly lower than control cells. Similarly, to seeding density experiments, increases in nuclear area did not always correspond to increases in cell area, again showing that nanovibrated cells have an increased nuclear area but not always an increased cell size. This could be due to the nucleus being stretched by actin fibers in response to vibration.

Whilst nuclear area responded similarly across vibrated samples, actin intensity and grey mean value differed far more (Figure 50). Similar to cell area, after 24 hours of stimulation, only the NK4 sample was found to have significantly higher actin intensity when compared to both the non-vibrated control and the NK0 sample. After 72 hours of stimulation, both the NK0 and the NK4 samples had a significantly higher actin intensity when compared to control. This correlation between cell area and actin intensity agrees with previous results that the increase in cell area in response to vibration also results in an increase in actin formation. Actin grey mean value was found to have no significant differences at the 24 hour timepoint, however, after 72 hours it was found to be significantly higher in both NK0 and NK4 compared to control and NK24.

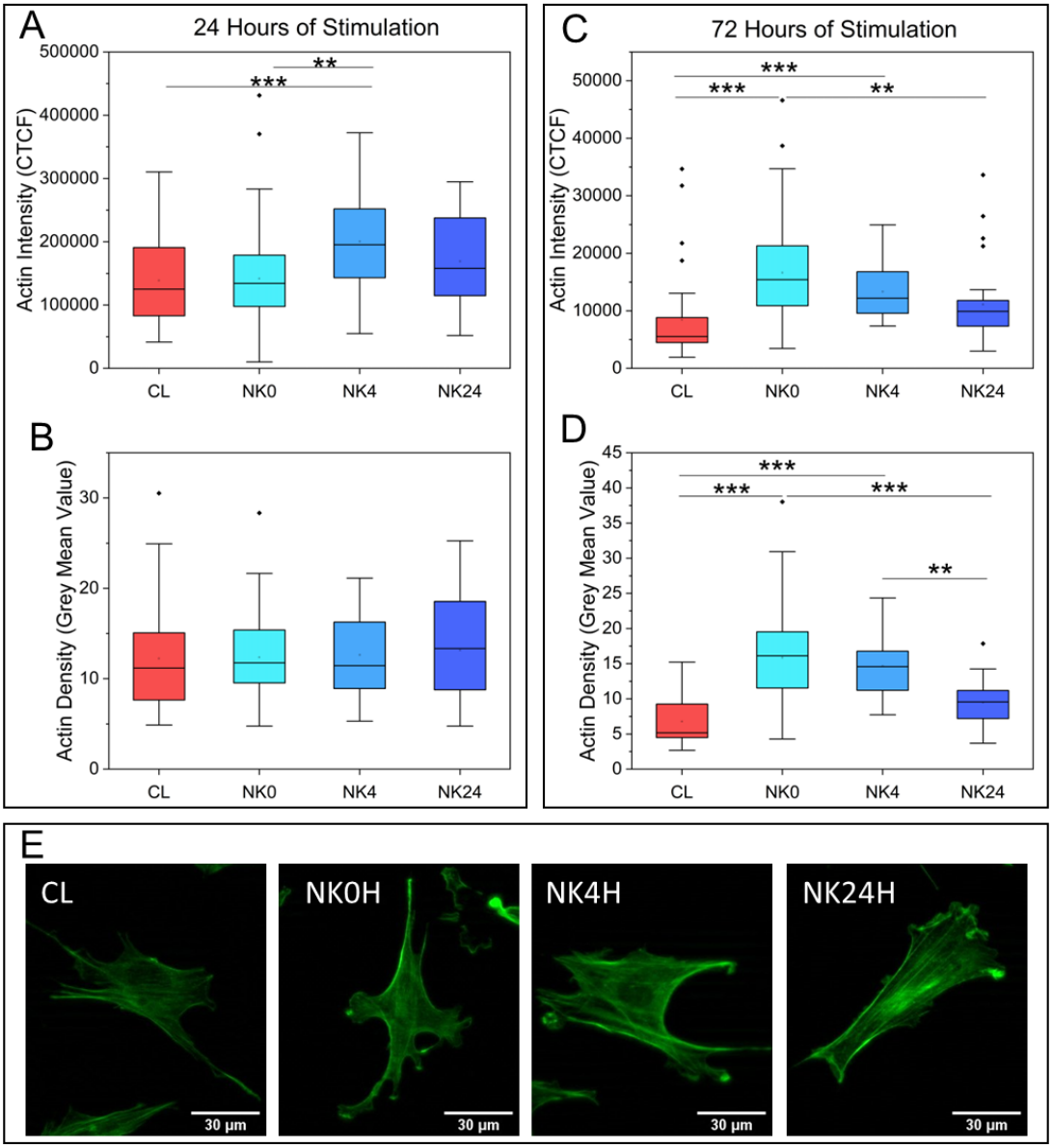

Figure 50: Actin response in cells left to adhere for 0 hours (NK0), 4 hours (NK4) and 24 hours (NK24) prior to vibration (N ≈ 30 per group) . A) Actin intensity data following 24 hours of vibration. B) Actin grey mean value following 24 hours of vibration. C) Actin intensity data following 72 hours of vibration. D) Actin grey mean value following 72 hours of vibration. E) Actin stained images of cells from all four conditions after 24 hours of stimulation. Images taken using Zeiss (Imager Z.1) and brightness was adjusted equally in ImageJ software.

Vinculin data showed a slightly different response after 24 hours of stimulation (Figure 51). Both NK4 and NK24 samples showed significantly higher intensity of vinculin compared to controls. Meanwhile vinculin grey mean value was only found to be significantly higher in NK0 cells. This suggests that cells left to adhere

for 4 hours prior to stimulation appear to have a strong initial response to stimulation which may be diminishing over time.

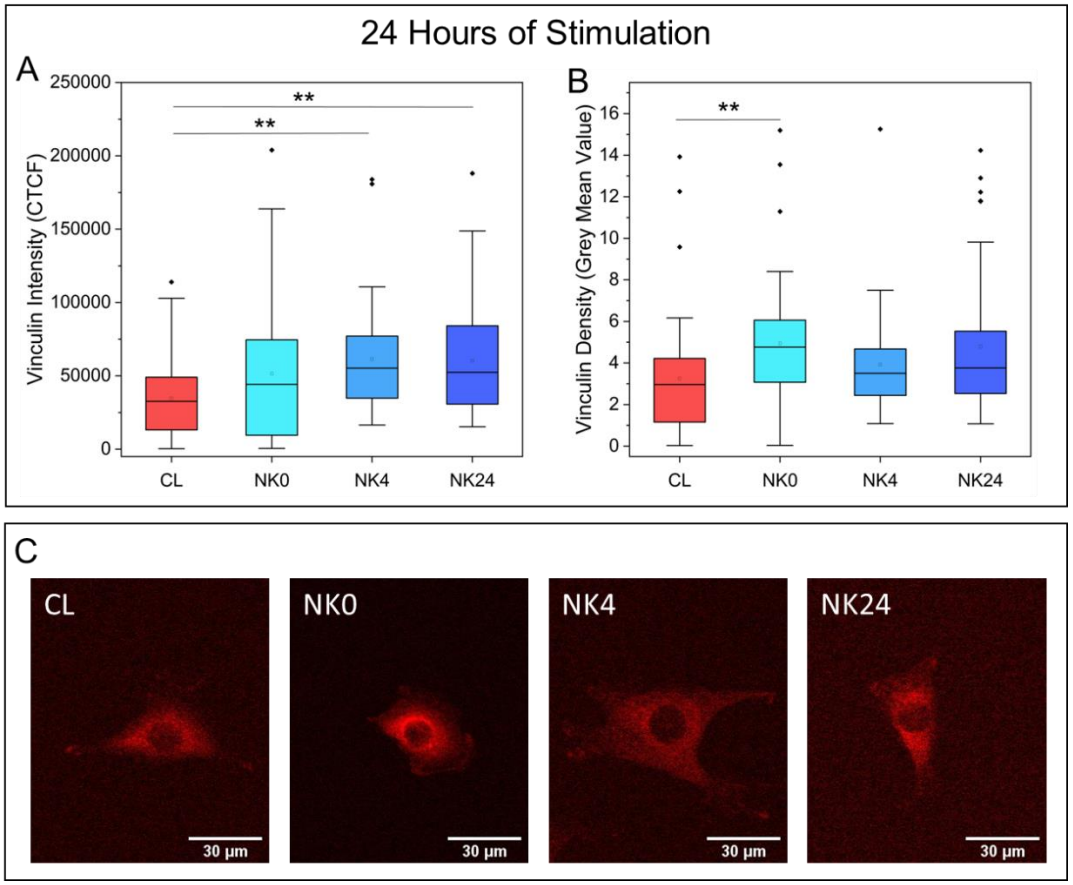

Figure 51: Vinculin response in cells left to adhere for 0 hours (NK0), 4 hours (NK4) and 24 hours (NK24) prior to vibration (N ≈ 30 per group). A) Vinculin intensity following 24 hours of stimulation. B) Vinculin grey mean value following 24 hours of stimulation. C) Vinculin stained images of cells from all four conditions. Images taken using Zeiss (Imager Z.1) and brightness was adjusted equally in ImageJ software.

Adhesion time was found to have a significant effect on cell response to nanovibrational stimulation. NK4 cells resulted in higher nuclear area, cell area, actin intensity and vinculin intensity after 24 hours of stimulation. This higher initial response may suggest cells incubated for 4 hours prior to vibration may respond quicker to stimulation. Nuclear area was consistently higher in all vibrated groups compared to controls as well as being significantly different from each other. Although nuclear area in NK0 has a bimodal response, cell area, actin intensity and vinculin intensity are not higher in NK0 after 24 hours. This

suggests that NK0 may be inhibiting responses due to lack of adhesion prior to stimulation. The increase in both cell area and actin and vinculin intensity in NK4 cells suggest that cells left to adhere for 4 hours prior to stimulation are responding better to applied vibration within the first 24 hours. These varied responses to vibration suggest that the time cells are incubated for prior to stimulation has a significant impact on cell response and as such must be considered when designing vibration experiments. Whilst NK4 did appear to show a strong initial response, later AFM experiments indicated that such cells may have different mechanical properties than cells left to adhere for 24 hours prior to applied stimulation. NK24 cells also showed the highest levels of adhesion which is known to correspond with increased osteogenesis in MSCs (see Figure 7). Due to this, and to keep consistent with previous nanovibration experiments to allow for comparison, subsequent experiments left cells to adhere for 24 hours before applying stimulation.

3.3.4 Morphological changes occur at different timescales for nanovibrated cells

All of the experiments above were run for a maximum of three days (72 hours) of stimulation. To investigate whether cell response was affected at later timepoints, an initial experiment used immunofluorescent analysis after the initial 3 days of stimulation and after 5 days. To ensure cells would not become too overgrown by the later timepoint, cells were seeded at a lower seeding density of 1000 cells/cm^2. Nuclear and cell area as well as actin and vinculin intensity were measured and data is shown in Figure 52 and Figure 53.

Nuclear area was found to be significantly higher in nanovibrated samples following 3 days of stimulation, agreeing with previous results. However, after 5 days of stimulation, the nucleus of nanovibrated cells was found to be significantly smaller than non-vibrated controls. The nuclear area of control cells significantly increased between 3 days and 5 days of stimulation. Cell area showed no significant differences between nanovibrated samples and respective controls, however control cells were found to significantly increase in cell area between

Day 3 and Day 5, and vibrated cells showed a similar though less pronounced response.

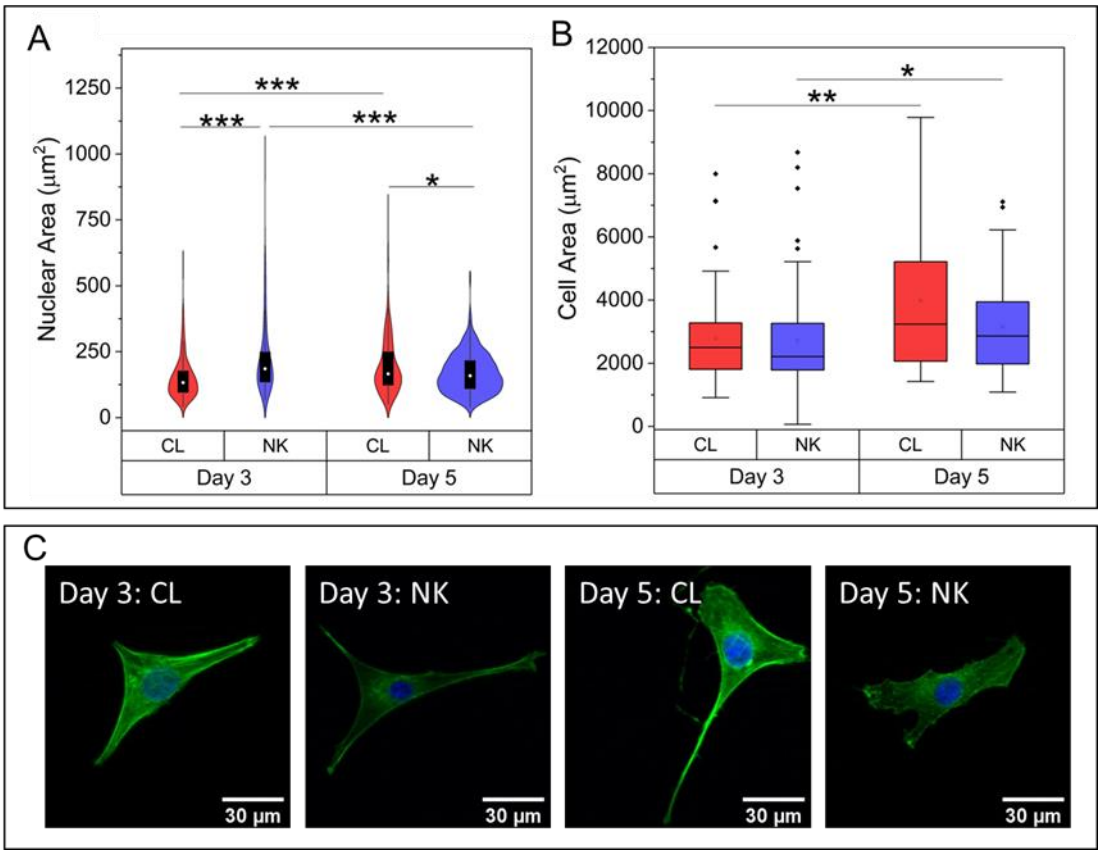

Figure 52: Nuclear and cell area data for cells stimulated for 5 days. A) Nuclear area after 3 and 5 days of stimulation compared to controls (Number of cells per group: N > 100). B) Cell area after 3 and 5 days of stimulation compared to controls (N ≈ 30). C) Combined actin and DAPI images for both samples at both timepoints. Images taken using Zeiss (Imager Z.1) and brightness was adjusted equally in ImageJ software

Nuclear area has consistently been found to be significantly larger in nanovibrated cells compared to control cells after 3 days of stimulation. However, at Day 5, the reverse was found, with the nucleus shrinking in nanovibrated cells. This suggests that the effect of nanovibrational stimulation on the nucleus is only apparent earlier during vibration, and that cells may adapt and change their response the longer vibration is applied for. It may also be due to cells becoming confluent at this later timepoint, resulting in cells have less space to spread, restricting nuclear area. Violin plots shown in Figure 52A show that nanovibrated

cells at Day 3 have a much larger distribution of nuclear area values than vibrated cells at the later timepoint of Day 5 where nuclear areas are more concentrated.

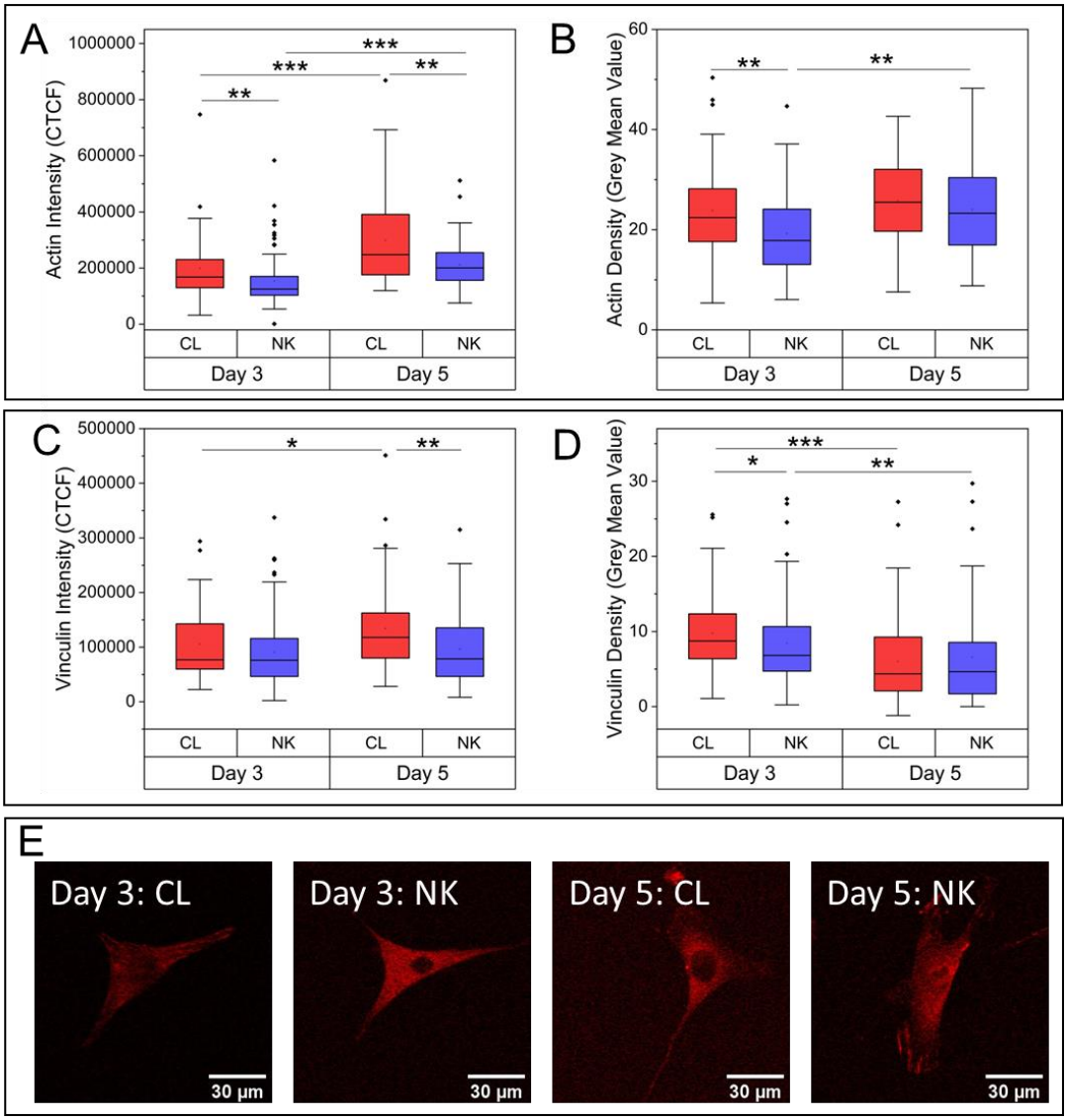

Figure 53: Actin and vinculin data for cells stimulated for 5 days (Number of cells per group: N ≈ 30). A: Nanovibrated cells were found to have a lower actin intensity than non-vibrated control cells. B: Nanovibrated cells were also found to have a lower grey mean value than control cells. C: Vinculin intensity was found to have decreased significantly in nanovibrated cells at day 5. D: There were no significant differences found in vinculin grey mean value at either timepoint. E) Vinculin images of cells. Images taken using Zeiss (Imager Z.1) and brightness was adjusted equally in ImageJ software.

The actin intensity of vibrated cells was found to be significantly lower than non-vibrated controls at both timepoints. However, the actin intensity for vibrated

samples was found to significantly increase between 3 and 5 days of stimulation, with the same being found in non-vibrated controls. The grey mean value of actin was found to be significantly lower in vibrated cells after 3 days of stimulation, however it was found to increase in nanovibrated cells after 5 days of stimulation. There was no significant difference in actin density between stimulated and control cells at this later timepoint. Vinculin intensity was significantly lower in vibrated cells compared to non-vibrated cells after 5 days of stimulation. The grey mean value of vinculin was significantly lower in vibrated cells after 3 days of stimulation and both control and nanovibrated cells significantly decreased in vinculin density at the later timepoint.

Similar to nuclear area, actin and vinculin also appear to be time-dependent, however they consistently show a decrease in both intensity and the density of actin and vinculin in stimulated samples. This contradicts other results which found that actin increases in intensity and grey mean value following nanovibrational stimulation. This inconsistency may highlight that actin response to vibration is less reliable than other responses such as nuclear area and nuclear stiffness. Longer culture times may also override or mask the impact of vibration due to overgrowth of cells and more limited access to nutrients.

3.3.5 Cells stiffen in response to nanovibrational stimulation

3.3.5.1 Initial investigations into stiffening response of nanovibrated cells

Whilst fluorescence microscopy can give in-depth morphological information of the cell, other techniques are required to investigate cellular mechanical properties. AFM can be used to probe these properties, revealing cell characteristics unmeasurable by fluorescence microscopy. Initial investigations seeded cells at a low density, leaving them to adhere for 24 hours before stimulation of 1 kHz, 30 nm was applied for 72 hours. Both the nucleus and cytoplasm of live nanovibrated and non-vibrated control cells were then measured using AFM. This experiment was repeated three times to investigate whether a reliable response could be observed, with the results shown in Figure 54A-C. A fourth experiment investigated the effect of shortening the time cells were left to adhere prior to applied vibration. Cells were seeded and left to adhere

for 4 hours before stimulation began and then measured after 72 hours of stimulation with the results shown in Figure 54D.

Applying stimulation for 72 hours did not appear to result in any reliable mechanical response in 3T3 cells. The first experiment in Figure 54A did show a significant increase in nuclear stiffness in nanovibrated cells. However, a second experiment shown in Figure 54B showed no significant differences between samples. The third experiment shown in Figure 54C showed a significant decrease in cytoplasm stiffness in nanovibrated cells compared to control. The fourth experiment shown in Figure 54D had a shorter adhesion time prior to the start of stimulation. This resulted in an interesting response in nanovibrated cells, which became significantly softer than control cells after 72 hours of stimulation.

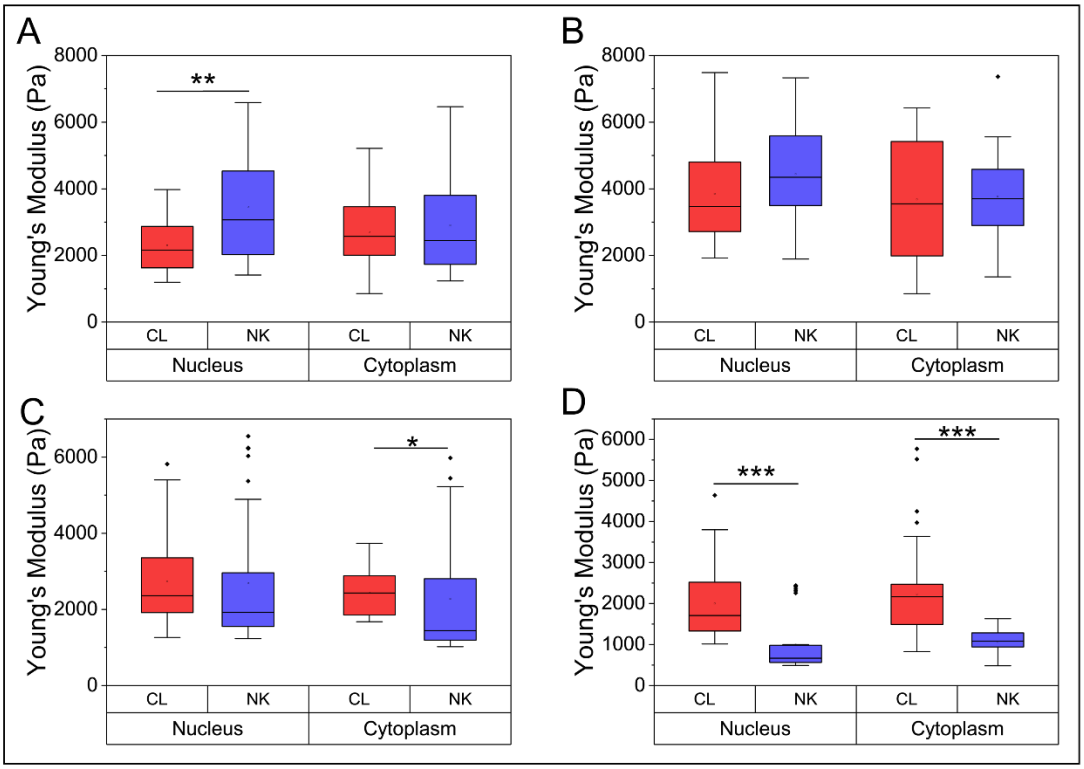

Figure 54: AFM measurements of the nucleus and cytoplasm following 72 hours of stimulation (Number of cells measured: N = 6). A-C) Same experiment repeated three times showing slightly different stiffness results each time as measured by AFM. D) Shorter adhesion time to investigate the effect on cell response. Measurements were all taken using a JPK AFM.

As no consistent response was observed, it was determined that measurements may not be being taken at the correct timepoint to observe a reliable response. Therefore, a timepoint experiment, where measurements would be taken at multiple times throughout the duration of stimulation was conducted.

3.3.5.2 Cell stiffness is time dependent in nanovibrated cells

To investigate the mechanical response of cells over the course of applied vibration, AFM was used to measure cells after 3, 24, 48 and 72 hours of vibration. Initial experiments were conducted using a JPK AFM instrument. The first experiment conducted (Figure 55A and Figure 55B) had two control samples, one which was kept in the same water-jacketed incubator as the vibration device, whilst the other was kept in a separate incubator. This was to identify whether cells were potentially being exposed to a form of stimulation whilst within the same incubator. An additional morphology experiment also incubated control cells separately to ensure morphology results were also unaffected (Figure 58). As is shown in Figure 55A, control cells kept in the same incubator as the device (CL+) were found to be significantly stiffer than control cells kept in a separate incubator (CL 0h and CL 72h). Therefore, the second experiment (Figure 55C and Figure 55D) kept control samples in a separate incubator.

Figure 55A and Figure 55C show the stiffness of the nucleus for both control and nanovibrated samples in each of the two experiments. For the first experiment, the nucleus was significantly stiffer after 3, 48 and 72 hours of vibration compared to the 0 hour timepoint. The second experiment showed similar results, with the stiffness of the nucleus significantly increasing after 24, 48 and 72 hours of vibration, with the most significant increase after 24 hours of vibration. Figure 55B and Figure 55D show the stiffness of the cytoplasm for both control and nanovibrated samples. The first experiment found that the cytoplasm was significantly stiffer after 3 hours of vibration, whilst the second found it to be significantly stiffer after 24 hours of vibration compared to non-vibrated controls. Figure 55E also contains topography images taken by the AFM on cells from the CL, NK 3H and NK 24H samples in the second experiment.

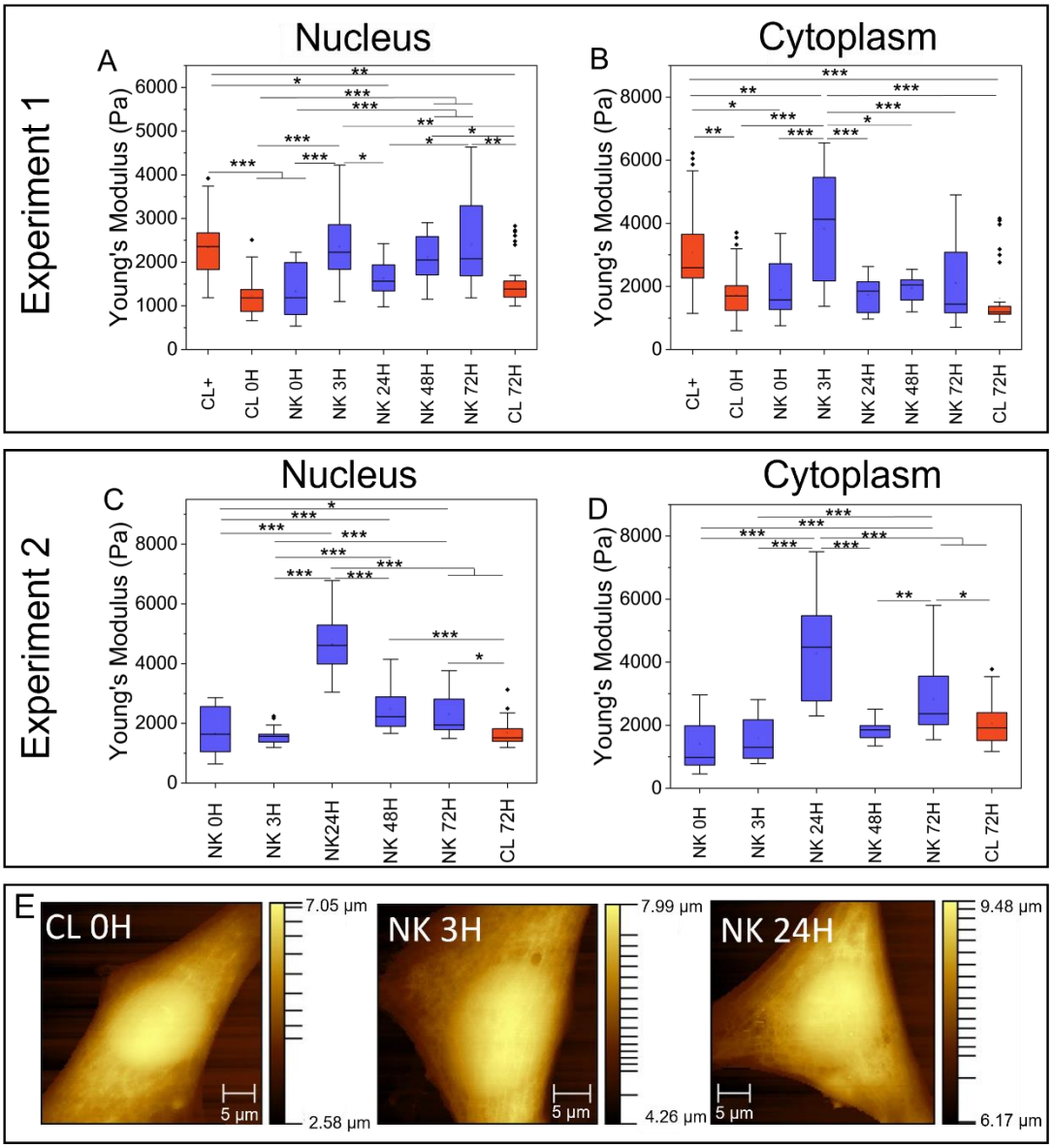

Figure 55: AFM stiffness measurements of both non-vibrated and vibrated cells at multiple timepoints (Number of cells per group: N = 6) taken using a JPK AFM. A and B are from one experiment, C and D are results from a second experiment. A: Young's modulus of the nucleus in Experiment 1 across 72 hours of stimulation. B: Young's modulus of the cytoplasm in Experiment 1 across 72 hours of stimulation. C: Young's modulus of the nucleus in Experiment 2 across 72 hours of stimulation. D: Young's modulus of cytoplasm in Experiment 2 across 72 hours of stimulation. E: Topographical AFM images of CL, NK 3h and NK 24h cells.

As well as conducting the standard analysis on the FDCs obtained from AFM measurements, some experiments were analysed further using bottom-effect correction and power law analysis. This made it possible to separate the elastic and viscous components and analyse both. This was performed upon the

experiment shown in Figure 55A and Figure 55B, with the results shown in Figure 56. Measurements were only taken on the nanovibrated sample, both before stimulation began and during the course of stimulation, and the non-vibrated control sample after 72 hours.

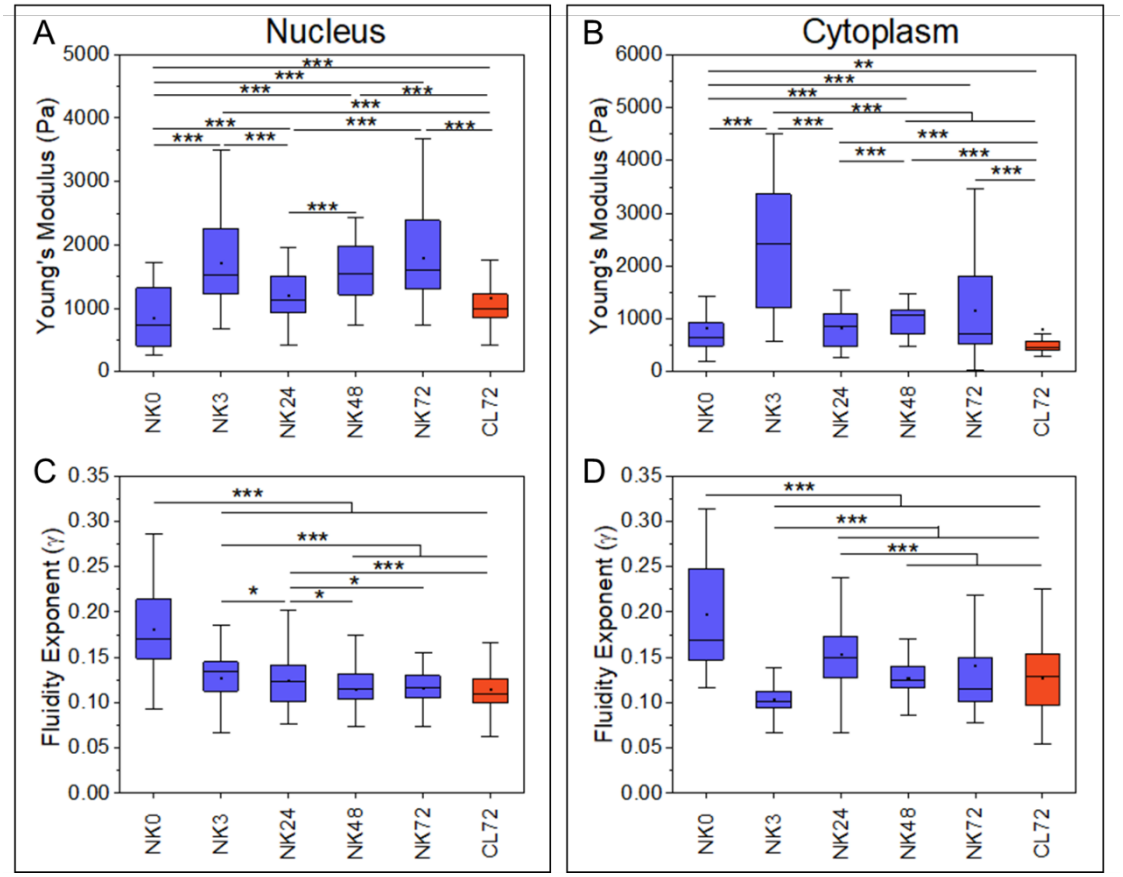

Figure 56: AFM measurements of NIH 3T3 cells at multiple timepoints during nanovibrational stimulation, as measured using a JPK AFM (Number of cells per sample: N = 6). A) Compressive modulus (stiffness) of the nucleus shown to increase due to stimulation. B) Stiffness of the cytoplasm shows a similar response, increasing in stiffness following 3 hours of stimulation. C) Fluidity exponent shown to decrease following stimulation in the nucleus. D) Similarly, the fluidity exponent of the cytoplasm decreases following stimulation. Analysis completed by the Garcia group in Madrid, Spain. Outliers were removed from graphs.

A similar response was observed, with both the nucleus and cytoplasm stiffening within the first 3 hours of stimulation, however this analysis does reduce the stiffness measurements compared to the original data shown in Figure 55. This timepoint showed the highest stiffness response in the cytoplasm, which reduced over time. For the nucleus, the initial stiffness after 3 hours decreased slightly

before increasing at later timepoints. The fluidity exponent was highest prior to applied stimulation and was reduced significantly following applied vibration and in the non-vibrated control sample at the 72 hour timepoint. In the cytoplasm, the fluidity exponent was at its lowest following 3 hours of stimulation. This may suggest that vibration is affecting the elastic properties of the cell more than the viscous properties.

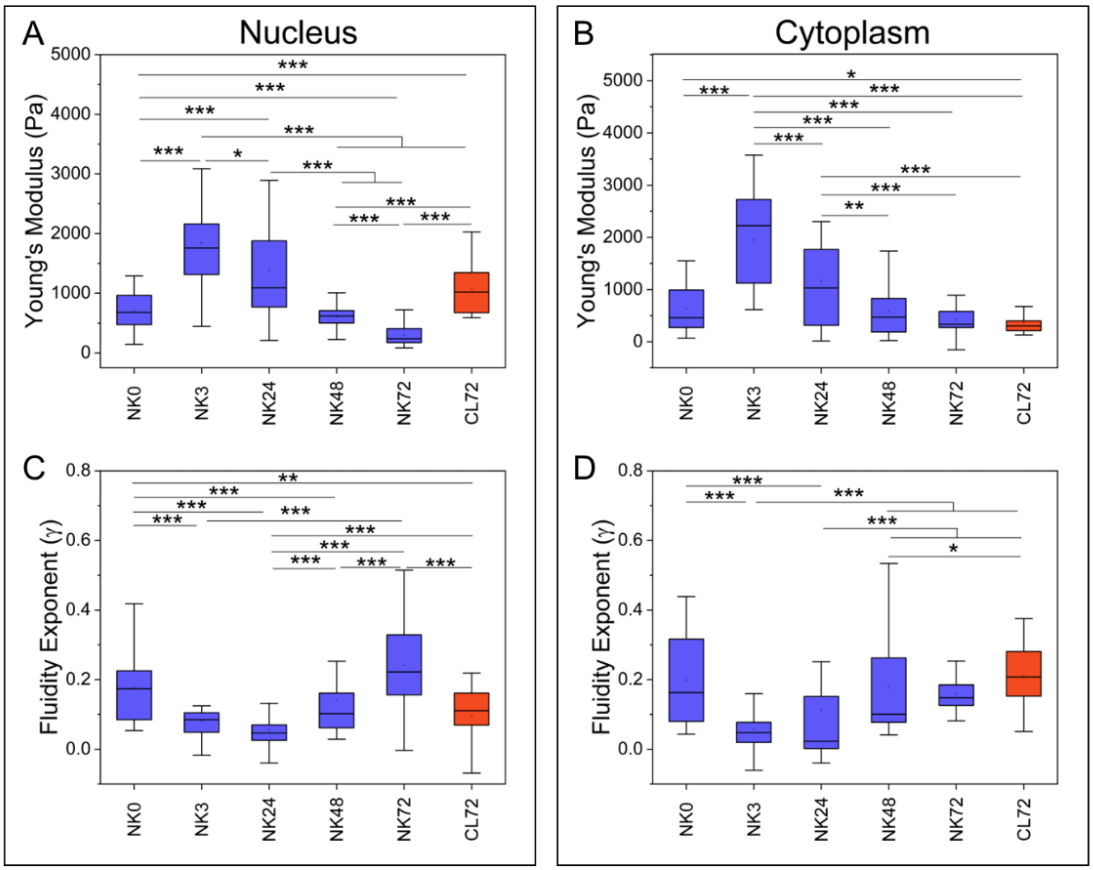

Figure 57: AFM measurements of NIH 3T3 cells at multiple timepoints during nanovibrational stimulation as measured using an Asylum AFM. (Number of cells per sample: N = 6). A) Nuclear stiffness shown to increase significantly during the first 3 hours of stimulation before decreasing at later timepoints. B) Cytoplasm stiffness shows a similar response, stiffening within the first 3 hours before decreasing at later timepoints. C) Fluidity exponent shows an initial decrease in the nucleus in the first 24 hours of stimulation before recovering at later time pints. D) Cytoplasm again showed a similar response, decreasing withing the first 24 hours before again recovering at later timepoints. Analysis completed by the Garcia group in Madrid, Spain. Outliers have been removed.

The same experiment was repeated on an Asylum AFM (Figure 57) to validate that the response could be seen across two AFM systems. Again, the cells showed a high stiffness response following 3 hours of stimulation in both the nucleus and the cytoplasm, however this was not maintained and decayed over time showing a stronger trend than seen previously (Figure 55). The fluidity exponent decreased within the first 24 hours of stimulation, before gradually increasing at later timepoints.

These experiments showed a very early response of cells to nanovibrational stimulation and demonstrated that this response decayed over time as cells were continuously stimulated. The nucleus responded particularly strongly to stimulation, often doubling in stiffness within the first 24 hours and maintaining that response for longer than the cytoplasm in stimulated cells. These results show the earliest stiffening response to vibration seen in nanovibrated cells.

3.3.5.3 Changes in morphology correspond with changes in stiffness in nanovibrated cells

In an attempt to understand the link between morphological and mechanical changes within the cell in response to vibration, the same experiment as outlined for AFM at multiple timepoints was conducted, this time with cells fixed at each timepoint and stained for immunofluorescence analysis. Here, vinculin, actin and DAPI were stained and imaged, with the results shown in Figure 58.

Nuclear area was shown to increase after 3, 24 and 48 hours of stimulation compared to control cells at the same timepoints. Cell area showed unusual results, with the 0 hour control and 3 hour control samples showing a higher cell area than other samples. This may be due to cells being at a low density at this timepoint and therefore having more space to spread. Cell area was significantly higher in vibrated cells at the 24 and 48 hour timepoint compared to relevant controls. Actin intensity was shown to increase after 3 hours of nanovibration as compared to controls. This increased response was significant after 24 hours of stimulation, however the later timepoint of 72 hours showed a significant

decrease in actin intensity. Vinculin intensity was shown to increase after 3 hours of stimulation and again after 72 hours of stimulation.

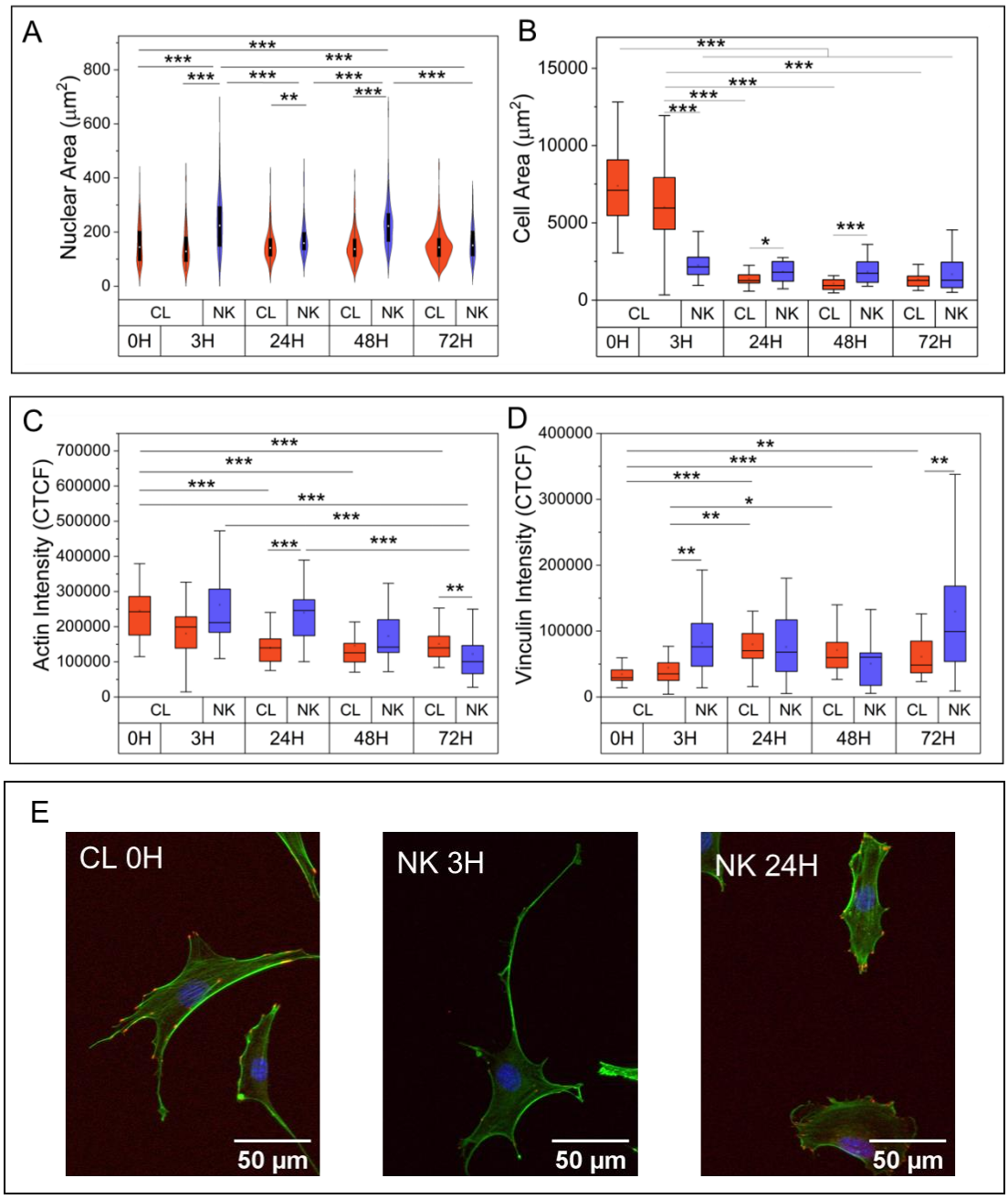

Figure 58: Morphology data for corresponding timepoints in AFM data. A) Nuclear area of cells across 72 hours of stimulation (Number of cells per sample: N > 100). B) Cell area of cells across 72 hours of stimulation (N ≈ 30). C) Actin intensity of cells across 72 hours of stimulation (N ≈ 30). D) Vinculin intensity of cells across 72 hours of stimulation (N ≈ 30). E) Combined actin, DAPI and vinculin images of cells at 0H, and after 3 and 24 hours of vibration. Images taken using Zeiss (Imager Z.1) and brightness was adjusted equally in ImageJ software. Outliers were removed from data.

The nucleus of nanovibrated cells becomes stiffer than non-vibrated controls initially within the first 24 hours of vibration, and again at later timepoints. However, the cytoplasm shows the strongest stiffening response within the first 24 hours of vibration. This initial response to vibration by stiffening suggests that cells respond quickly to applied vibration (within 24 hours) before acclimatizing and no longer responding as strongly to the continuous stimulation. This may suggest that vibration must be applied in doses for only a short period at a time, then allowing cells to relax before more vibration is applied.

3.3.5.4 Inhibiting actin prevents stiffening response of cells to nanovibrational stimulation

Since actin intensity was found to increase in correlation with increased stiffness, the extent of this role was investigated by using actin inhibitors blebbistatin and cytochalasin D to inhibit cell contractility and polymerisation respectively. AFM measurements were taken using an Asylum AFM at the same timepoints as measured previously as shown in Figure 59. Inhibitors were not applied until after measurements were taken at the 0 H timepoint.

Inhibited cells showed a lower stiffness in both the nucleus and cytoplasm in both the nanovibrated and non-vibrated control cells at all timepoints measured. Non-inhibited cells showed a similar response as observed previously, showing a significant increase in both nuclear and cytoplasm stiffness observed after 3 hours of stimulation. Later timepoints did not show a significant increase in stiffness in vibrated cell samples. The fluidity exponent was found to be significantly higher in inhibited cells in both the nucleus and cytoplasm.

Due to the lack of response to vibration in inhibited cells, it could be deduced that actin polymerisation and contractility play an important role in the stiffening response of cells to vibration. This, coupled with the increase in actin intensity observed when conducting morphological analysis indicates that actin tension is one of the main cell responses to vibration, resulting in an increased stiffness within the cell in both the nucleus and cytoplasm.

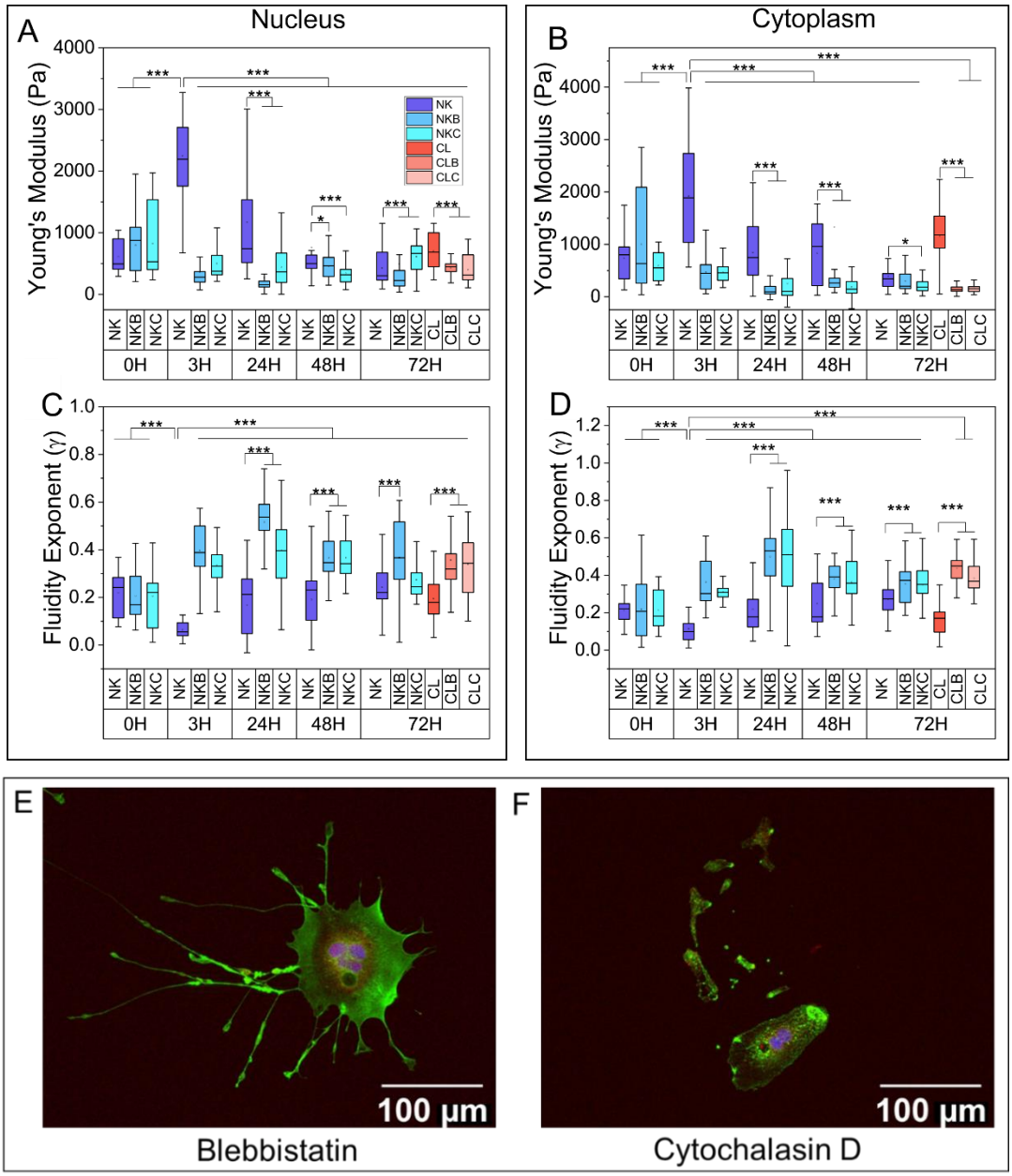

Figure 59: Actin inhibition experiment, where blebbistatin and cytochalasin D were applied to inhibit cell contractility and polymerization respectively. (Number of cells per sample: N = 6) A) Young's modulus of nucleus in both inhibited and uninhibited cells across 72 hours. B) Young's modulus of cytoplasm in both inhibited and uninhibited cells across 72 hours. C) Nuclear fluidity exponent in both inhibited and uninhibited cells across 72 hours. D) Cytoplasm fluidity exponent in both inhibited and uninhibited cells across 72 hours. E) Immunofluorescent image of cell exposed to blebbistatin with actin stained in green, vinculin in red and DAPI in blue. F) Immunofluorescent image of cell exposed to cytochalasin D with actin stained in green, vinculin in red and DAPI in blue. Images taken using a Zeiss (Imager Z.1). Power law analysis completed by the Garcia group in Madrid, Spain.

3.3.5.5 Fixed nanovibrated cells show no changes in stiffness

All AFM experiments had been performed on live cells, with the exception of the topography measurements (Figure 55E) which were performed on fixed cells. To investigate whether fixed nanovibrated cells would still show an increase in stiffness compared to fixed control cells, cells were seeded at a low density, left to adhere for 24 hours and nanovibrated for 24 hours, since cells were seen to stiffen within the first 24 hours of vibration. Following stimulation, cells were fixed for either 2, 5 or 10 minutes. Cells were then measured using an Asylum AFM with results shown in Figure 60.

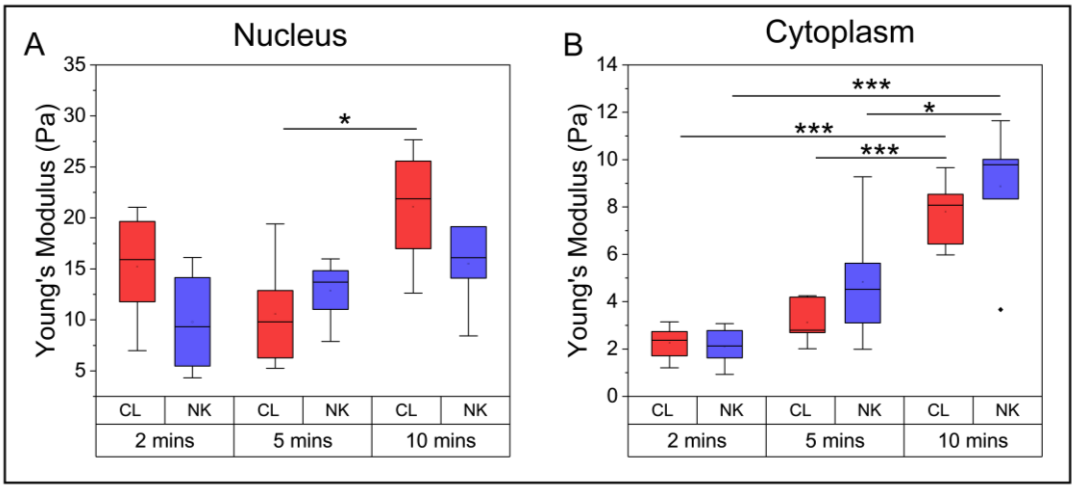

Figure 60: Fixed Asylum AFM experiment showing differences in stiffness following fixation at different lengths of time (N = 6, where N is number of cells measured per sample). A) Nucleus shows no significant increase in stiffness following vibration at any timepoint. B) Cytoplasm shows increased stiffness at longer durations fixation is applied for.

Cells showed no significant increase of stiffness in nanovibrated samples compared to relevant controls as had been seen previously. The cytoplasm also showed no significant differences between nanovibrated and corresponding controls. Longer duration of fixation did result in stiffer cells, as to be expected. However, these results did not reveal the trends observed when measuring live cells, and thus it was decided that future experiments would solely be performed on live cells. Topography experiments (Figure 55E) had been performed on fixed cells, however, given the lack of significant differences observed whilst measuring fixed nanovibrated cells compared to fixed control cells, this type of measurement

was determined to not be as reliable as obtaining single FDCs on live samples. Therefore, further investigation into topography measurements was not explored.

3.4 Discussion

Cells respond to vibration in a multitude of ways. This makes it challenging to understand precisely how cells are responding to stimulation and as a result, makes it difficult to determine the optimal vibration conditions required to produce a desired cell response. This challenge must be addressed before such methods of cell stimulation can be used in a clinical or industrial setting for cell manufacture

This chapter attempted to further understand the effects of nanovibrational stimulation on cell response by applying vibration to murine 3T3 cells. The morphological response of the cell was measured using fluorescence microscopy, whilst the mechanical response was measured using AFM. Nuclear area, cell area, actin and vinculin and cell stiffness were all analysed to determine the response of cells to stimulation.

Findings shown here do show an increased response to vibration in NIH 3T3 cells seen in both the morphological and mechanical properties of the cell. Nuclear area was found to increase in nanovibrated cells, a trend seen in MSCs by Nikukar *et al* [302]. This increase in nuclear area may be due to the cell flattening as it spreads out and forms a stronger attachment to the dish. This would naturally correspond with an increase in cell area, however this isn't always observed consistently alongside an increase in nuclear area. This may suggest that cell spreading and cell tension may not be directly related. Actin may be building stress fibres and reducing other actin processes such as motility and filopodia generation. This may be leading to actin fibres pulling on the cell nucleus, causing it to stretch and elongate. Actin intensity is seen to increase, often alongside nuclear area increases, suggesting that vibration may be inducing an increased response in actin production or fibre formation. Mechanically, cells were found to stiffen following applied vibration, and inhibition of actin contractility and

polymerisation prevented that response. Previous studies have found that an increase in cell stiffness corresponds with actin cytoskeletal reorganisation, as was observed here [324-326]. This indicates the important role actin plays in both the stiffening and morphological response of cells to vibration.

The effects of initial seeding density and adhesion time on nanovibrated cells were investigated here. Initial seeding density has previously been shown to have an effect on phenotypic changes. BM-MSCs and MG63s seeded in 3D scaffolds at high cell densities (10^6-10^7) have been found to exhibit higher mRNA expressions of osteogenic markers [276, 277]. Some studies have also found that seeding density can affect mechanical properties of cells, such as tensile strength and Young's Modulus where a higher seeding density can lead to a reduction in mechanical properties [282, 283]. The results shown here on NIH 3T3 cells did not see any significant differences in the effect of different initial seeding densities on nuclear area at early timepoints, although later timepoints saw a higher seeding density to result in a higher nuclear area. Actin intensity saw a mixed response, with lower seeding densities showing an increased response at earlier timepoints, whilst higher seeding densities showed a higher actin intensity at later timepoints. However, as this cell type did not seem too affected by seeding density, to ensure cells would not become overgrown at later timepoints, and to enable single cell analysis, a lower seeding density of 1000 cells/cm^2 was used for most experiments in this chapter.

AFM experiments showed an increase in cell stiffness within 24 hours of stimulation. However, one experiment investigated the effect of a shorter adhesion time of 4 hours and found cells were softer in response to vibration after 3 days of stimulation as compared to controls (Figure 54D). To further investigate the morphological effects of adhesion time, cells were stimulated either immediately after seeding, 4 hours after, or 24 hours after and fixed following 24 and 72 hours of stimulation. Whilst AFM showed a decrease in cell stiffness, a 4 hour adhesion time resulted in a higher actin intensity, contradicting other AFM results. The shorter adhesion time AFM experiment may therefore have been an outlier experiment.

Leaving cells to adhere for 24 hours resulted in a more consistent response with both nuclear and cell area higher than control at both timepoints, indicating more consistent cell spreading. For actin, at the 24 hour timepoint there was no statistical difference between NK0 and NK24. Therefore, as there was no significant statistical benefit between the two, future experiments left cells to adhere for 24 hours to make results more comparable to previous nanovibrational stimulation studies.

Whilst nuclear area analysis was conducted on a high number of cells ($N > 100$), actin, vinculin and cell area analysis were performed on single cells, resulting in a lower N number ($N < 30$). AFM was lower still with only 6 cells being measured per condition. Due to this, it is difficult to confirm results seen due to the low population number of cells. As measurements were also performed on single cells, rather than a mixed population of cells on their own and in contact with others, it is difficult to understand the effect cell-to-cell contact may be having on the response of cells. The data presented here was also limited to morphological and mechanical changes within the cell, and although the interlink between the two has been investigated, the link between this and phenotypic changes in fibroblast cells in response to nanovibrational stimulation remains to be explored.

Chapter 4:

Optimising osteogenic response using MG63 cells

4.1 Introduction

Whilst fibroblast cells were a mechanically relevant, adherent, cell type to investigate mechanical and morphological changes, they are unable to osteogenically differentiate. To study osteogenesis, ideally mesenchymal stem cells would be used, however, they are slow growing and donor variation can be a confounding factor, hindering optimisation experiments. Previous studies have instead used several cell lines as models for osteogenesis. MC3T3-E1 cells, an immortalised murine osteoblastic cell line have been shown to osteogenically differentiate following vibration, however, as a murine cell line it is difficult to confirm relevance to human cellular response [247, 255, 284, 289, 327, 328]. Some studies have used human osteosarcoma cell lines in osteogenic differentiation, however very few have used them in vibration research [329, 330]. Pre *et al* used SAOS-2 cells to optimise vibration conditions for osteogenic differentiation [235]. These vibration conditions were then later applied to stem cells, successfully inducing osteogenic differentiation [234, 236].

Using human cell lines offers a more direct comparison to human biology. There have been several studies using another osteosarcoma cell line MG63 cells, investigating the effect of applying mechanical stimulation, primarily using cyclic stretch, which has been shown to increase osteogenesis in MG63 cells [331, 332]. However, thus far there has been no thorough investigation into the effects of vibration on the osteogenic response in this cell type.

This chapter used MG63 cells as an osteogenic model to identify optimal vibration conditions to induce an osteogenic response prior to stem cell experiments.

Frequency, amplitude, duration and direction of stimulation were all studied in an attempt to understand their effects on cell response. Immunofluorescence was used to observe morphological changes in cells, whilst AFM and deformability cytometry were used to investigate the mechanical response. Real-time qPCR was employed to investigate the responses of osteogenic and other genes. As far as is known, no study has been conducted that has thoroughly investigated the effects of such a range of vibration parameters on cell response until now.

4.2 Methodology

4.2.1 Cell culture

Human MG63 cells (Sigma) were cultured in Dulbecco's modified essential medium (DMEM, Sigma), supplemented with 10% foetal bovine serum (FBS, Sigma) v/v, 1% minimum essential medium non-essential amino acid solution (MEM NEAA) v/v and 2% antibiotics v/v. Cells were then cultured within an incubator at 37°C with 5% CO_2 and were passaged every 3-5 days. In experiments using osteogenic media (OM), 24 hours after seeding for an experiment, basal medium (BM) consisting of DMEM supplemented with the above, was supplemented with 1% ascorbic acid and 0.1% dexamethasone. Both BM and OM were replaced every 3-4 days during experiments.

4.2.2 Application of nanovibrational stimulation

When applying different frequencies and amplitudes, individual nanovibrational stimulation devices were calibrated to the required vibration conditions using a laser interferometer described previously (section 2.7.1). Experiments requiring 1 kHz, 60/90 nm, vertical vibration used a modified version of the standard nanovibration devices capable of switching between higher amplitudes. When 1 kHz, 30 nm, vertical vibration was required, a standard nanovibrational stimulation device was used (Figure 21). Details on the vibration conditions used for each experiment are summarised in Table 11.

Table 11: Summary of nanovibrational stimulation conditions for each experiment described in Chapter 4

Experiment (Sub section)	Seeding Density (cells/cm²)	Frequency (kHz)	Amplitude (nm)	Direction	Adhesion Time (hours)
4.3: Proliferation	1000	1	30	Vertical	24
4.4: Seeding Density	1000 2500 5000	1	30	Vertical	24
4.5: Adhesion Time	1000	1	30	Vertical	0 4 24
4.6.1: Gene expression	1000	1	30	Vertical	24
4.6.2: LINC and OCN	1000	1	30	Vertical	24
4.7.1: Comparing frequencies	1000	0.1 1 6 10	30	Vertical	24
4.7.2: Comparing frequencies	1000	0.1 1 10	30	Vertical	24
4.8: Intermittent and continuous vibration	1000	1	30 90	Vertical (4 h/d, 5 d/wk)	24
4.9.1: Horizontal vibration	1000 5000	1	30 60	Vertical Horizontal	24
4.9.2: Horizontal Vibration	1000 5000	1	30 90	Vertical Horizontal	24
4.10: AFM	1000	1	30	Vertical Horizontal	24
4.11: Deformability cytometry	5000	1	30	Vertical	24

Devices applying frequencies other than 1 kHz or applying horizontal vibration, used a signal generator and Behringer amplifier. Experiments were calibrated using laser interferometry as described previously, and voltages were supplied using a signal generator attached to a Behringer amplifier. In multi-frequency experiments, four frequencies were used, the original 1 kHz, a lower frequency of 100 Hz, and two higher frequencies of 6 and 10 kHz, chosen as these frequencies had more consistent vibrations across the plate (as verified in Figure 24), and spanned a wide range of values. Device calibrations are summarised in Table 12.

Table 12: Device calibration for multiple frequency experiments. Devices were calibrated using a laser interferometer, with the average displacement calibrated close to 30 nm.

Position	**Amplitude at each frequency**			
	100 Hz	**1 kHz**	**6 kHz**	**10 kHz**
1	30	19	34	44
2	31	28	29	29
3	29	34	17	3
4	30	31	14	65
5	31	29	29	41
6	32	27	69	27
7	31	29	27	12
8	31	30	15	56
9	30	31	10	56
10	31	32	10	31
11	30	31	18	22
12	29	31	26	31
13	29	27	80	26
14	29	29	31	53
15	32	32	12	12
16	34	32	12	69
17	30	29	61	18
18	29	26	43	7
Average	30	29	30	33
Standard Deviation	1	3	21	20

Higher frequencies showed a larger range of amplitudes, as had been seen previously (Figure 24). This is likely due to resonant frequencies of the device from 2 kHz onwards [139]. In all experiments, devices were placed in a single incubator, whilst non-vibrated controls were incubated separately.

4.2.3 Immunofluorescent Staining

Some changes were made to the previously used immunofluorescent staining protocol (detailed in Chapter 3, subsection 3.2.3). For MG63s and MSCs, PBS/BSA dilution was increased to 2% (w/v) and once added, cells were left to incubate for 6-8 hours at 4 °C. Following this, PBS/BSA was removed, and primary antibodies were added, and cells were incubated overnight at 37 °C. Previous protocol detailed in subsection 3.2.3 was then followed to complete immunofluorescent staining.

4.2.4 Gene expression analysis

Quantitative reverse transcription polymerase chain reaction (RT-qPCR) may be used to quantify gene expression in cell samples. The TaqMan Fast Advanced Cells-to-CT Kit (Thermo Fisher Scientific) was used according to the manufacturer's instructions to perform qPCR on samples. Following stimulation, cells were lysed to extract RNA. DNase I was added during lysis to remove any genomic DNA present in the RNA sample. Reverse transcription was then performed using 2x Fast Advanced RT buffer and 20x Fast Advanced RT Enzyme mix and a Thermocycler (Thermo Fisher Scientific) to transcribe the RNA into complimentary DNA (cDNA). TaqMan assays were then used during qPCR to quantify the presence of specific genes in a sample whilst using a QuantStudio 5 (Thermo Fisher Scientific) Real-Time PCR machine. Several assays were used (Thermo Fisher Scientific), including GAPDH and β-Actin as housekeeping genes, with all assays and their ID's shown in Table 13. RUNX2 and ALP were used to indicate early osteogenesis, whilst markers for OCN and ON were used to indicate late osteogenesis. To investigate changes within the nuclear envelope following nanovibrational stimulation Sun1, Sun2 and Lamin A/C gene expression were investigated. Finally, actin remodelling protein Wiskott-Aldrich syndrome (WAS),

a critical regulator involved in rapid actin formation was investigated [333]. Previous studies have observed a high up-regulation in expression of WAS following mechanical stimulation [270].

Automatic thresholding was performed within the software to determine cycle threshold (CT) values. The ΔCT values were then calculated using GAPDH or β-actin as house keeping genes, whilst averages and standard deviations were calculated over three replicates. Three technical replicates were also included for each sample. Data was analysed using the comparative C_T method [334]. The ΔCT values were then normalised to non-vibrated controls within each experiment and plotted as $2^{\Delta CT}$ to give relative expression levels. Statistics were performed on individual delta CT values.

Table 13: Target genes with the type of marker they were used to indicate, alongside TaqMan Assay IDs used during qPCR experiments.

Target Gene	Marker Type	TaqMan Assay ID
RUNX2	Early Osteogenic	Hs01047973_m1 (FAM)
ALP	Early Osteogenic	Hs01029144_m1 (FAM)
BGLAP (OCN)	Late Osteogenic	Hs01587814_g1 (FAM)
SPARC (ON)	Late Osteogenic	Hs00234160_m1 (FAM)
		Hs00234160_m1 (VIC)
Sun1	LINC Gene	Hs00964062_m1 (FAM)
Sun2	LINC Gene	Hs00391446_m1 (FAM)
Lamin A/C	LINC Gene	Hs00153462_m1 (FAM)
WAS	Actin Remodelling	Hs00997437_m1 (FAM)
GAPDH	Housekeeping	Hs02786624_g1 (FAM)
		Hs02786624_g1 (VIC)
ACTB (β-Actin)	Housekeeping	Hs01060665_g1 (FAM)
Col1a	Chondrogenic	Hs00164004_m1 (FAM)
Sox9	Chondrogenic	Hs00165814_m1 (FAM)
β-tubulin	Neurogenic	HS00801390_s1 (FAM)
PPARγ	Adipogenic	Hs01115513_m1 (FAM)

In some cases, duplexing was performed. This enabled the detection of two genes per well, reducing the quantity of reagents and time required to perform qPCR. This required the use of two TaqMan assays within each well, each with different dyes, i.e. FAM and one VIC.

Early qPCR work resulted in high CT values or a lack of any amplification. To investigate whether this was due to impurities inhibiting sample amplification, a spectrophotometer (Implen) was used to quantify the purity of the lysate samples used. Lysate samples used were from a previous experiment with an initial seeding density of 1000 cells/cm^2 cultured for 4 days prior to lysing (stimulated for 3 days), where group A were control samples, group B were cells stimulated vertically at 1 kHz, 30 nm and group C were horizontally vibrated at 1 kHz, 30 nm. A 1 µL droplet was measured via spectrophotometer and both the concentration and 260/280 absorbance ratio were measured. The 260/280 ratio is a measure of how 'pure' the sample is, with a ratio of ~1.8 being accepted as 'pure' for DNA whilst ~2 is accepted as 'pure' for RNA [335]. Spectrophotometer results measuring the lysate samples are shown in Table 14.

Table 14: Spectrophotometer results after measuring the purity of lysate sample both before and after the use of a DNase Kit. 260/280 ratio here is a measure of the sample's purity, with a value of ~2 being accepted as 'pure' for RNA.

Sample	Lysate		Post DNase Kit	
	260/280 Ratio	Concentration (ng/µL)	260/280 Ratio	Concentration (ng/µL)
A2	0.382	41.4	0.588	18.75
A3	0.364	40.75	0.535	17.8
B2	0.451	51.05	0.697	21.4
B3	0.445	51	0.638	16.95
C1	0.609	62.8	0.755	25.5
C2	0.454	52.1	0.664	15.3
C3	0.398	44.3	0.726	20.8

Lysate samples were found to have a low 260/280 ratio indicating a lack of purity for DNA or RNA. This may be as expected since the Cells-to-CT kit does not

separate RNA from lysate (e.g. using spin columns). The impurities may also be affecting concentration values collected via spectrophotometer. In an attempt to purify the samples further, a DNase kit (Thermo Fisher Scientific) was used, according to the manufacturer's instructions to remove any DNA still remaining within the sample. The spectrophotometer measurements were again taken on the new 'purified' samples, with the results again displayed in Table 14. Whilst the DNase kit did increase the 260/280 ratio, it was still well below the approximate value of 2 for 'pure' RNA. The qPCR kit used gave no guidance on the quantification of RNA/cDNA, however later experiments indicated that the kit did appear to be working as the manufacturer intended.

An alternative reason for low CT values may be a low quantity of RNA. The initial seeding density of 1000 cells/cm^2 (~320 cells/well) may be too low to detect the genes of interest (although the kit should be capable of reverse transcription of lysates of 10-10^5 cells), therefore, when lysing, wells were 'doubled-up' when confluency was low (< 50%), i.e. cells in one well were lysed before being moved to a second well where the cells within were lysed also. This meant that samples now had double the number of cells for qPCR. In some experiments, initial seeding density was increased to ensure confluency was high enough for qPCR. To also ensure that all cells were being lysed, the time lysate was applied for was increased from 5 minutes to 8 minutes per well. Following on from this, qPCR generated lower CT values with samples amplifying as expected.

4.2.5 Real-time deformability cytometry

Whilst AFM had previously been used to obtain mechanical data from cells, here another method, real-time deformability cytometry (RT-DC) was also used (Figure 61) [336]. This technique uses controlled hydrodynamic shear stresses to deform cells in suspension [337]. Cells were cultured into T75 flasks (Fisher Scientific, 10364131) at a seeding density of 5000 cells/cm^2. Flasks were then incubated at 37°C with 5% CO_2 for 24 hours before being nanovibrated for 24 hours at 1 kHz, 30 nm. To prepare samples for measurement, cells were detached using 0.05% (w/v) trypsin (Merck, T4674) and an even suspension created. Cells

were then centrifuged and separated from media, and resuspended in CellCarrier B (Zellmechanik Dresden, ZM-C-CC-060) at 1-2 x 10^6 cells/ml.

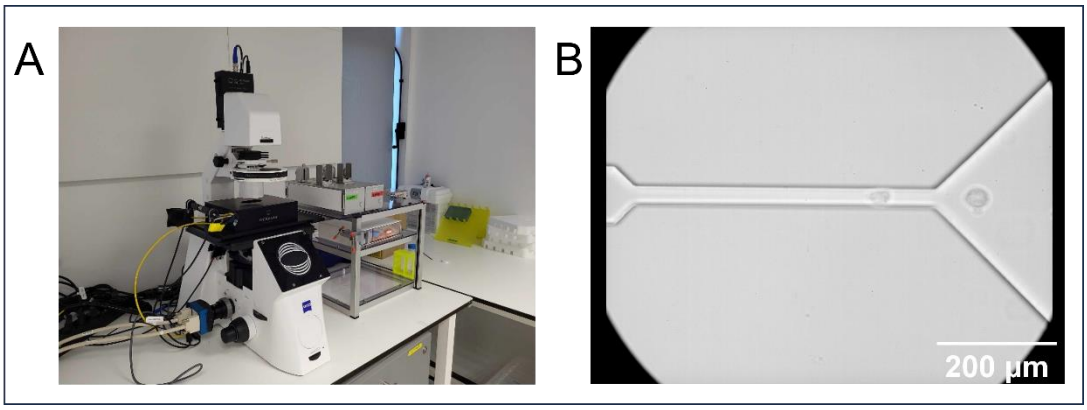

Figure 61: A) Deformability Cytometer set up on Zeiss microscope with high throughput camera (EoSens CL, Mikrotron, Germany). B) View of MG63 cells traversing microfluidic chip, being squeezed into a 'bullet-shape' when within the channel.

Cells were then loaded into a 1 mL syringe and attached to the system. Another syringe was filled with carrier fluid acting as a sheath fluid in the system. Cells then passed through a Polydimethylsiloxane (PDMS) chip (ZellMechanik Dresden, ZM-C-FXX) with a 30 μm × 30 μm cross-section channel at either 0.16 μL/s or 0.24 μL/s (1:3 ratio of sample to sheath fluid), whilst being imaged by a high-speed camera (EoSens CL, Mikrotron, Germany). The RT-DC software used (ShapeOut2, version: 2.13.6) quantified the area and deformability of cells passing through the reservoir and channel respectively. Cells deform whilst passing through the channel, forming a bullet shape as shown in Figure 61B. Deformability is quantified as the amount of deviation from a perfect circle, and was calculated in real time in ShapeIn software [338].

4.2.6 Alizarin Red Staining

Alizarin Red may be used to stain calcium deposits in tissues. Here it was used to measure mineralisation deposition of cells. Following fixation, Alizarin Red solution (40 mM) was added to cells (1 mL for Petri dishes, 50 μL for 96 well plates). Cells were incubated at room temperature for 1 hour before solution was removed. Cells were then rinsed with deionised H_2O (dH_2O) five times to remove excess stain, before dH_2O was left in the well to keep cells hydrated. Cells were

then imaged using a phase contrast (Nikon Eclipse Ts2) or brightfield (Zoe Fluorescent Cell Imager) microscope.

Alizarin Red staining was also quantified using a spectrophotometer (Thermoscientific Multiskan Go, Thermo Fisher). To do so, dH_2O was removed from samples and a solution of 20% methanol, 10% acetic acid and 70% dH_2O was added to each well (100 μL for 96 well plates). Cells were incubated at room temperature for 15 minutes before being quantified using a spectrophotometer (Thermoscientific Multiskan Go, Thermo Fisher). at a wavelength of 450 nm. Blanks were obtained in wells with no cells or stain, filled only with the methanol/acetic acid/dH_2O solution.

4.2.7 Cell/Nuclear Alignment Analysis

To investigate cell alignment, microscopy images of the DAPI channel were obtained on a Zeiss microscope (Imager.Z1) as previously described (section 3.2.4). Dishes were kept at the same angle for each image to ensure any alignment was observed. Analysis was conducted on ImageJ during nuclear area analysis, with minor, major and angle data being obtained. Semicircular polar plots were constructed in MATLAB.

4.2.8 Atomic Force Microscopy

Cells were seeded at a density of 1000 cells/cm^2 into 60 mm Petri dishes and incubated for 24 hours. AFM measurements were taken using an Asylum AFM on the two samples prior to stimulation (VNK and HNK at 0H). Cells were then vibrated at either 1 kHz, 30 nm vertical vibration (VNK) or 1 kHz, 30 nm horizontal vibration (HNK). AFM was performed at multiple timepoints during stimulation, after 3 hours, 24 hours, 48 hours and 72 hours. A non-vibrated control sample was kept in a separate incubator to vibration devices and measured at the final 72 hour timepoint. Nanovibrated samples were measured at each timepoint, ensuring the same population of cells were repeatedly measured. The nucleus and cytoplasm of at least 6 cells were measured in each sample at each timepoint.

4.3 Results

4.3.1 Nanovibrational stimulation does not increase proliferation in MG63 cells

As nanovibrational stimulation was found to increase the proliferation in NIH 3T3 cells, the proliferation rate of MG63 cells was also investigated. Cells were seeded and nanovibrational stimulation was applied as detailed in Table 11 for 72 hours. Cells were imaged prior to stimulation, and following 24, 48 and 72 hours of applied vibration. Non-vibrated controls were also imaged at each of these timepoints. The percentage of cells per sample at each timepoint as compared to the number before beginning stimulation, is shown in Figure 62.

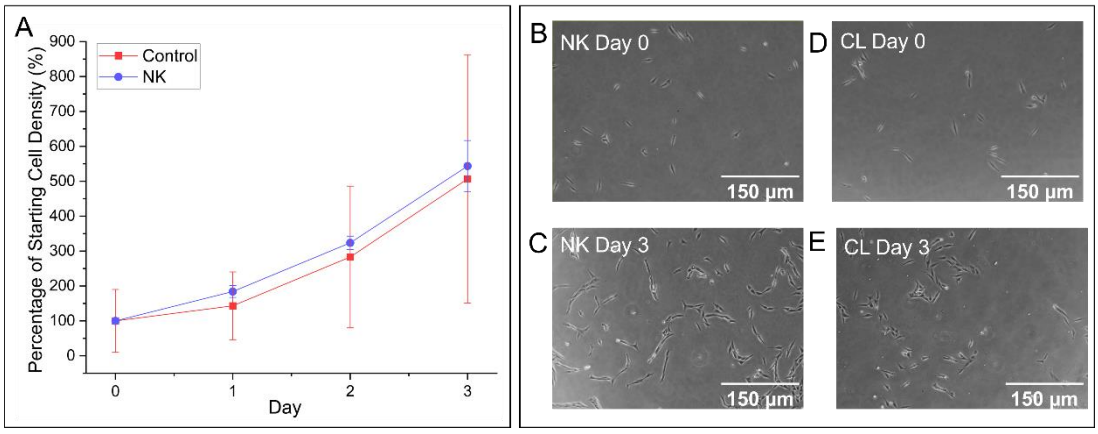

Figure 62: A) Proliferation data for MG63 cells (N > 100). Control cells were incubated in the absence of vibration for 96 hours. Nanovibrated cells (NK) were incubated for 24 hours following seeding before being nanovibrated for 72 hours. Images were obtained on day 0 (24 hours after seeding, no stimulation), day 1 (48 hours after seeding, 24 hours of stimulation), day 2 (72 hours after seeding, 48 hours of stimulation) and day 3 (96 hours after seeding, 72 hours of stimulation). N = 4, where each replicate is composed of total cells in 5 microscopic fields of view. B) Nanovibrated cells at day 0 timepoint prior to stimulation. C) Nanovibrated cells after 3 days of stimulation. Images taken using Nikon Eclipse Ts2.

Whilst no significant differences were found between samples at each timepoint, there was an increased growth rate seen with the NK group. The presence of large standard deviations was a result of the variability between wells.

4.3.2 Initial seeding density affects MG63 morphological response to nanovibrational stimulation

To investigate whether initial seeding density affected MG63 cell response to stimulation, in a similar way to NIH 3T3 cells (section 3.3.2), the same three initial seeding densities as used previously (1000 cells/cm^2, 2500 cells/cm^2 and 5000 cells/cm^2) were used to seed MG63 cells into 12 well plates. Stimulation was applied as detailed in Table 11. Immunofluorescence microscopy was used to obtain morphological data such as nuclear area, cell area, actin intensity and actin density data following 72 hours of stimulation with results shown in Figure 63.

Nuclear area was found to be higher in nanovibrated samples initially seeded at 2500 cells/cm^2 and 5000 cells/cm^2 compared to non-vibrated controls. Meanwhile cell area was found to be higher in nanovibrated samples, although only significantly at lower seeding densities. In NIH 3T3s nuclear area and cell area were also found to be higher in nanovibrated samples, although only at higher seeding densities (Figure 47).

Actin intensity was found to be significantly increased in all nanovibrated samples compared to respective controls, however intensity was lower in cells seeded at a higher initial density. This may have been due to cells becoming more overgrown within the wells, unable to extend and form more cytoskeletal protrusions. Whilst cell area shows no decreasing trend at higher densities, this may have been more due to the low number of cells measured during analysis, and the bias towards isolated cells, where cell boundaries can be distinguished. Actin density was only observed to be significantly higher in nanovibrated samples initially seeded at 2500 cells/cm^2 and 5000 cells/cm^2 compared to non-vibrated controls. Compared to NIH 3T3 cells, actin intensity was only significantly higher in nanovibrated samples seeded at 5000 cells/cm^2, whilst actin density was higher in nanovibrated samples initially seeded at 5000 cells/cm^2 (Figure 48).

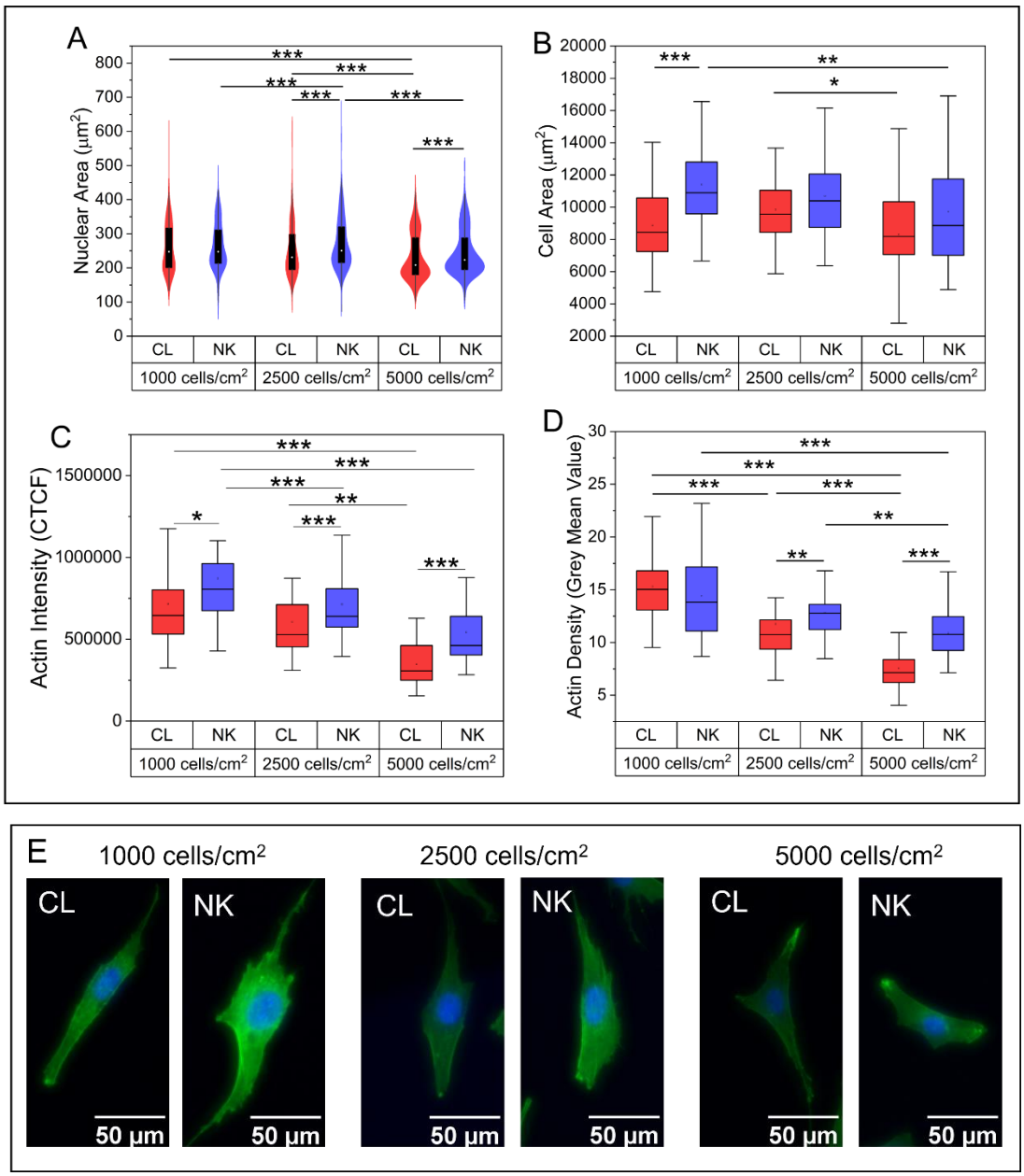

Figure 63: Morphology data for cell samples initially seeded at 1000, 2500 and 5000 cells/cm² and nanovibrated for 72 hours. A) Nuclear area for cells initially seeded at different densities following 72 hours of stimulation (N > 100). B) Cell area for cells initially seeded at different densities (N ≈ 30). C) Actin intensity for cells initially seeded at different densities (N ≈ 30). D) Actin density for cells initially seeded at different densities (N ≈ 30). E) Images of cells at each condition following 72 hours of stimulation. Actin is stained in green and DAPI in blue. Images taken using a Nikon Eclipse Ts2 and intensities adjusted equally within ImageJ software. In graphs, outliers have been removed.

Similarly to NIH 3T3 cells, the lower seeding density was used in morphology experiments unless otherwise stated. Due to their proliferative capabilities and

their larger size, this was concluded to be a better seeding density, particularly as further experiments would culture cells for longer timescales to investigate osteogenic effects of up to 14 days.

4.3.3 Adhesion time affects MG63 cells response to nanovibrational stimulation

To investigate whether adhesion time had a similar effect on MG63s as it did on NIH 3T3s (section 3.3.3), the same conditions were applied to cells, leaving them to adhere for either 0 hours, 4 hours, or 24 hours prior to stimulation. Full stimulation details are shown in Table 11. Here, three timepoints were investigated, 24 hours, 48 hours and 72 hours after stimulation. Morphology data is shown in Figure 64 whilst actin and vinculin intensity data are shown in Figure 65.

Nuclear area was initially found to decrease in nanovibrated MG63 cells left to adhere for 24 hours prior to stimulation (NK24) within the first 24-hour period. However, after 72 hours of stimulation nuclear area was found to increase significantly in all nanovibrated cells, highest in the NK24 group. Nuclear area therefore does appear to increase significantly following nanovibrational stimulation however this effect was most prominently seen after 72 hours of stimulation. Cell area only showed significant differences within the first 24 and 48 hours. After 24 hours, control cells were found to be significantly lower than nanovibrated samples, whilst after 48 hours, NK24 cells showed a higher cell area than control cells. Actin intensity was not found to increase in nanovibrated samples, instead a decrease was observed after 48 and 72 hours in NK24 samples compared to control. This corresponded to a decrease in actin density in the same sample. Vinculin intensity was found to increase at the 72 hour timepoint in the NK24 sample. Vinculin density was found to decrease in nanovibrated samples, significantly in NK24 samples after 24 and 48 hours.

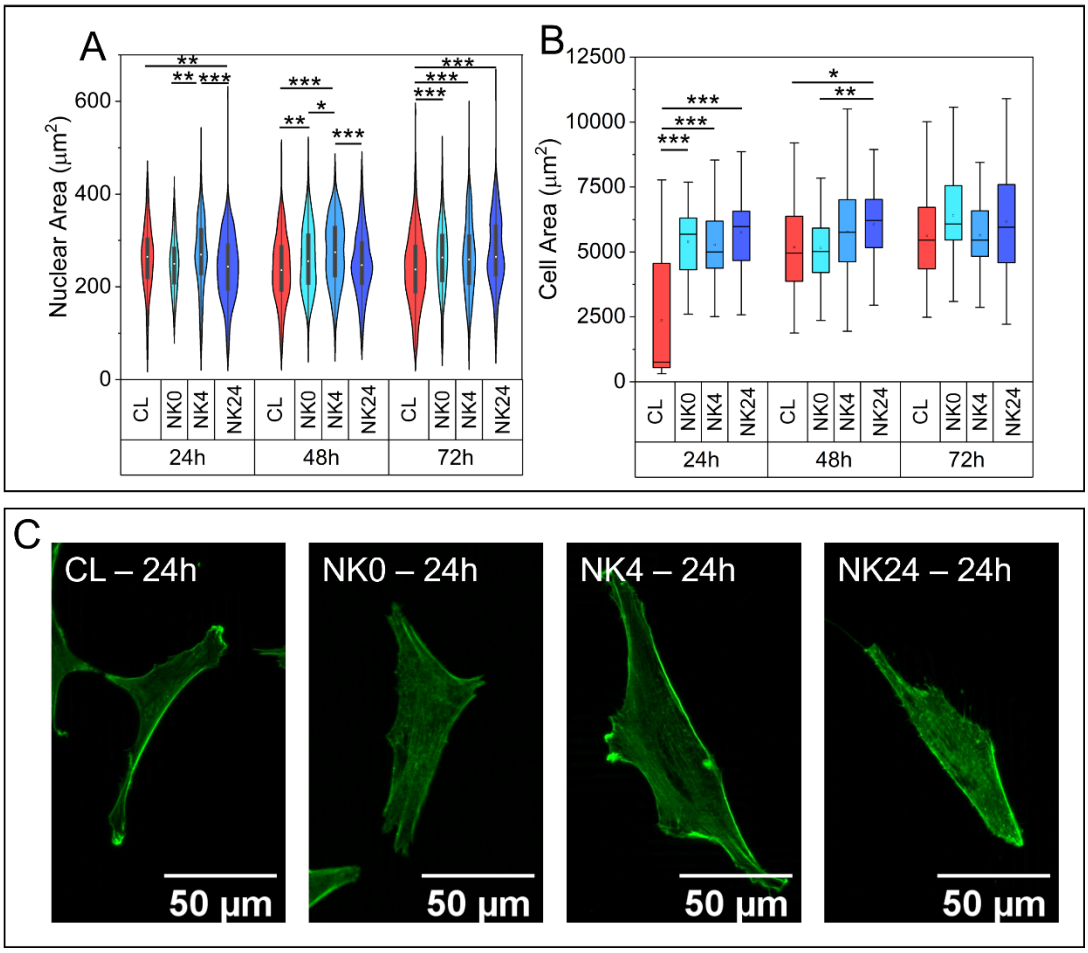

Figure 64: Nuclear and cell area of cells in response to vibration following different adhesion times. A) Nuclear area of cells over 72 hours of stimulation (N > 100) B) Cell area of cells over 72 hours of stimulation (N ≈ 30). C) Images of actin staining in cells after 24 hours of stimulation. Images were taken using a Zeiss microscope (Imager.Z1). Outliers have been removed from data.

It had previously been seen that the lower seeding density of 1000 cells/cm² did not result in any significant differences in nuclear area between samples after 72 hours of stimulation (Figure 63). This contradicts the results seen here (Figure 64) suggesting that nuclear area may not reliably change in MG63 cells in response to vibration and also trends observed in NIH 3T3 cells (Figure 49). Cell area had been found to be higher in MG63 cells following 72 hours of stimulation (Figure 63) however here it was only seen in samples vibrated for 24 hours. In NIH 3T3 cells, cell area only increased in NK4 samples compared to control at this timepoint (Figure 49).

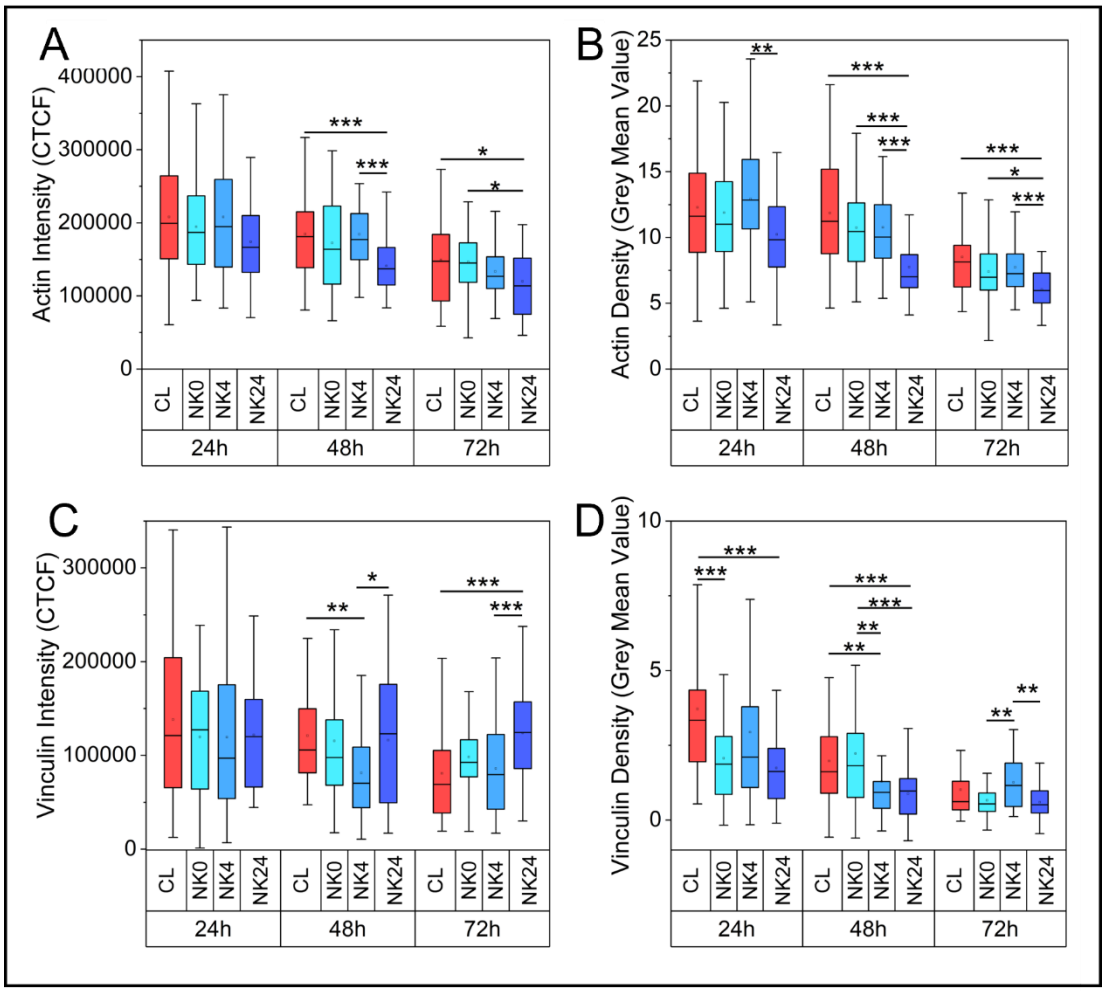

Figure 65: Actin and vinculin response of cells to different adhesion times. A) Actin intensity response across 72 hours (N ≈ 30). B) Actin density (grey mean value) across 72 hours (N ≈ 30). C) Vinculin intensity across 72 hours (N ≈ 30). D) Vinculin density across 72 hours. Outliers have been removed from data (N ≈ 30).

In MG63s, nanovibrated cells showed no increase in actin intensity, contradicting previous results (Figure 63) and not agreeing with increases observed in some nanovibrated NIH 3T3 samples (Figure 50). However, MG63 cells left to adhere for 24 hours prior to vibration showed a significant increase in vinculin intensity following 72 hours of vibration (Figure 65). This suggests stronger adhesion to the cultureware which had also been seen in the NK24 sample in NIH 3T3 cells after 24 hours of stimulation (Figure 50). Therefore, due to this positive response and to again keep consistent with previous nanovibration studies to allow for

comparison, subsequent experiments left MG63 cells to adhere for 24 hours before applying stimulation.

4.3.4 Time course of gene expression for 1 kHz, 30 nm vibration

As an osteosarcoma cell line, MG63 cells are capable of expressing osteogenic genes. Initial experiments aimed to identify key genes modulated following nanovibrational stimulation and how these genes changed over time. Alongside this, links between gene and subsequent protein expression were examined.

4.3.4.1 Nuclear and osteogenic gene expression changes during nanovibrational stimulation

Gene expression over time in response to standard nanovibrational stimulation parameters (1 kHz, 30 nm, vertical, continuous) was investigated to identify key genes that were affected by vibration in this cell type (summary of stimulation conditions shown in Table 11). Cells were stimulated continuously over 7 days, and lysed at three timepoints: Day 3, Day 5 and the final Day 7. A variety of early and late-stage osteogenic markers were investigated as well as genes related to the LINC complex. The results of gene response are shown in Figure 66.

Early-stage marker, RUNX2 did show an increase in expression in nanovibrated cells compared to controls, however none of these were significant. ALP also showed no significant differences, although Day 3 and Day 7 expression in nanovibrated cells was slightly higher than in non-vibrated controls. Late-stage marker OCN showed a steady increase in expression over time although only Day 3 showed a significant increase in the nanovibrated sample. Meanwhile, ON again showed a steady increase in expression over time, and on Day 7, it was shown to be significantly higher in nanovibrated cells compared to controls.

Nuclear envelope gene expression was also investigated at the same timepoints. Sun1 was found to have a decreased expression in nanovibrated cells at each timepoint, significantly at Day 3 and Day 5. Sun2 meanwhile showed an increased expression, although not significantly. It has been seen in previous studies that Sun1 plays a crucial role in the organisation of actin and focal adhesion

maturation [171]. Therefore, to investigate whether the decrease in gene expression was linked to an increase in protein expression, immunofluorescence was used to quantify the protein expression of Sun1 at the Day 5 timepoint.

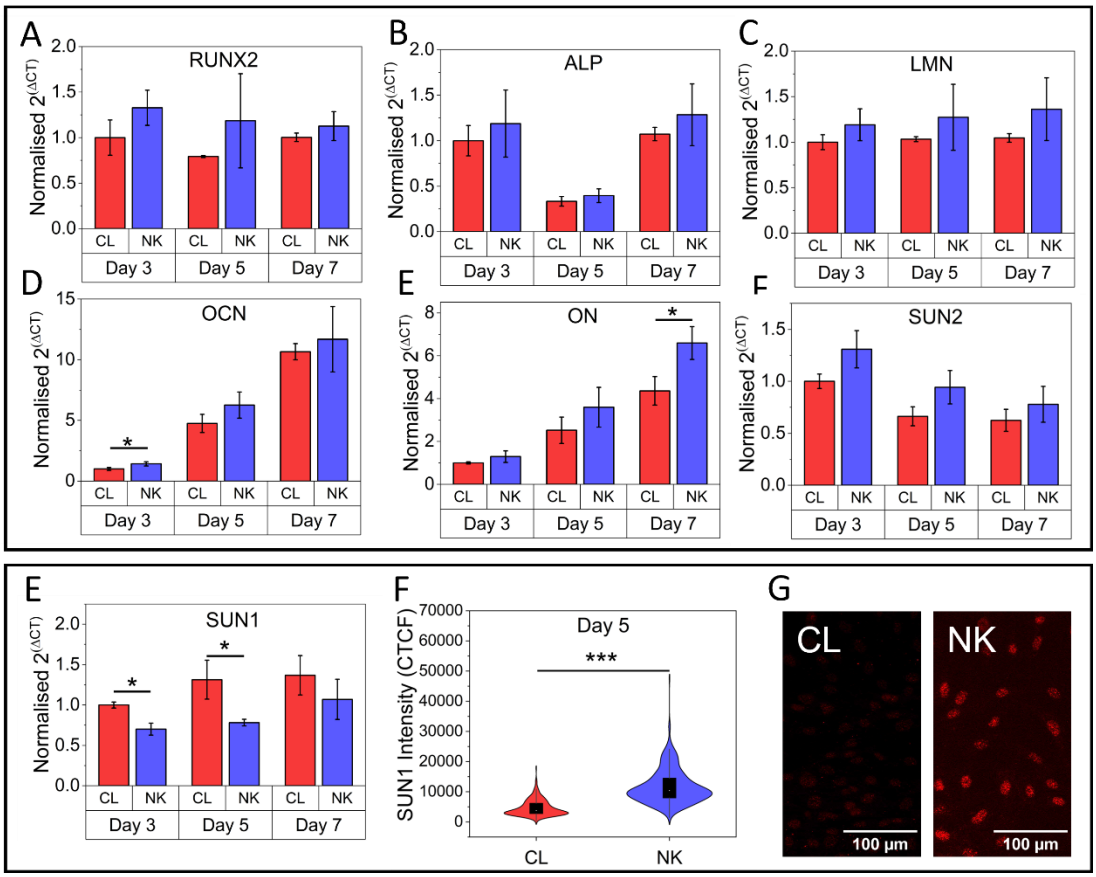

Figure 66: qPCR results for both osteogenic and nuclear genes following 3, 5 and 7 days of stimulation. A-F) Various osteogenic and nuclear gene expressions normalised to Day 3 control. E) Sun1 gene expression changes normalised to Day 3 control. F) Sun1 protein intensity on Day 5. G) Respective images of CL and NK Sun1 expression following 5 days of stimulation. Images taken using Zeiss (Imager.Z1) and intensity modified equally in ImageJ. Error bars show standard deviation (N = 3).

Cells were seeded into Petri dishes, left to adhere for 24 hours, before stimulation was applied for five days. Cells were then fixed and stained for Sun1. Protein expression results following image analysis are shown in Figure 66F. Sun1 protein expression was found to increase significantly in nanovibrated samples following five days of stimulation. This suggests that the decrease in gene expression may be due to translation of protein, as shown by the increase in protein expression. This would indicate that more Sun1 protein is being produced

in response to stimulation, previously shown to be required for actin organisation and playing a role in focal adhesion maturation [171]. The LINC complex is also known to be involved in the mechanosensitivity of the cell [94, 170]. Therefore, observed changes in gene and protein expression of nuclear envelope proteins may be an indication of changes in mechanosensitivity in response to stimulation.

4.3.4.2 Investigating the relationship between LINC and osteogenesis

Nanovibrational stimulation alters the expression of Sun1, however the link to osteogenesis is unknown. To investigate this, cells were stimulated for 7 days according to vibration conditions summarised in Table 11, and fixed at Day 3, Day 5 and Day 7. Samples were either stained for Sun1 or for OCN with intensity results shown in Figure 67.

Sun1 protein expression was found to be the opposite of what had been observed previously with Day 5 showing a decrease in Sun1 intensity in nanovibrated samples compared to non-vibrated controls. As Sun1 is a part of the LINC complex, it was hypothesised that a change in expression may correlate with changes in osteogenic expression. For this, OCN was used as an osteogenic marker, however no changes between control and nanovibrated samples were observed at any timepoint. OCN is a late-stage marker, meaning it may not have been possible to see clear changes in expression in nanovibrated samples compared to controls here. As it is only one marker for osteogenesis, it may be that other proteins involved in osteogenesis are being expressed instead. However, from this study, no definitive link between Sun1 and osteogenesis was observed.

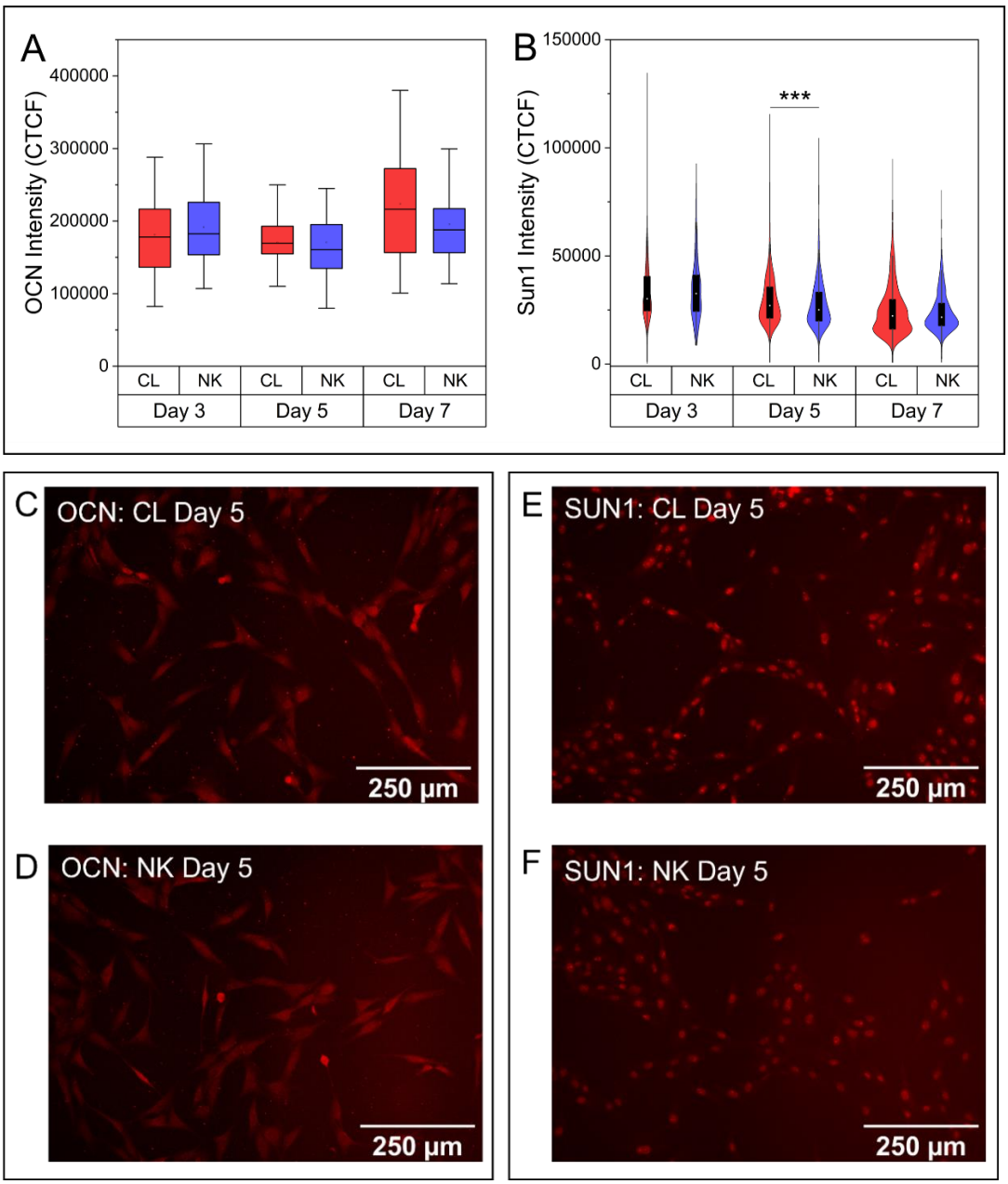

Figure 67: Relationship between osteocalcin and Sun1. A) Osteocalcin intensity following 7 days of stimulation (N ≈ 30). B) Sun1 intensity following 7 days of stimulation. C) Control cells at Day 5 stained for OCN expression (N > 100). D) Nanovibrated cells at Day 5 stained for OCN expression. E) Control cells at Day 5 stained for Sun1 expression. F) Nanovibrated cells at Day 5 stained for Sun1 expression. Images taken using Zoe Fluorescent Cell Imager, with brightness adjusted equally across images in ImageJ. In graphs, significant differences only shown between samples at each timepoint.

4.3.5 Frequency may not influence osteogenic cell response

Nanovibrational stimulation has been shown to affect morphology and gene expression in MG63 cells. Thus far, the only vibration conditions to be tested here have been a 1 kHz frequency and 30 nm amplitude. However, previous vibration studies have found that cells respond differently to different vibration conditions [235, 237, 259, 263, 267, 287]. Studies such as Chen *et al* have demonstrated that lower frequencies (30 Hz) are optimal for driving adipogenesis, whilst higher frequencies promote osteogenesis (800 Hz) [259]. Other studies have tested multiple frequencies on cells to optimise osteogenesis, including Pre *et al* who optimised osteogenesis in SAOS-2 cells by testing multiple frequencies [235, 267]. Recent nanovibrational stimulation studies also found that higher amplitudes (90 nm) increase osteogenesis in MSCs compared to lower amplitudes (30 nm) [287]. This increased response observed when higher amplitudes and frequencies are applied is likely due to cells experiencing higher forces when exposed to these vibration conditions.

Whilst previous nanovibrational studies have observed a higher response when using higher amplitudes, if it is assumed that the cell is responding to the force applied due to vibration, then a larger effect would be observed by altering the frequency applied, as force is related to frequency squared. Therefore, initial experiments investigating the effects of changing vibration conditions focused on altering the frequency applied to samples rather than amplitude.

4.3.5.1 Initial cell response to multiple frequencies

Initial experiments stimulated cells (using devices calibrated in Table 12) for three days, investigating both morphological and gene expression changes after 24 and 72 hours. Cells were seeded into Petri dishes for morphological analysis and 96 well plates for gene expression analysis. Vibration conditions used are summarised in Table 11. Alongside basal media (BM) controls, osteogenic media (OM) controls were also used here to identify whether observed responses induced by vibration mimicked those seen using chemical differentiation. Samples were either fixed or lysed after 24 and 72 hours of stimulation and

analysed. Fixed samples were stained for DAPI, actin and YAP. YAP has been found to translocate to the nucleus in response to mechanical stimulation, therefore it was investigated here to identify whether different frequencies effect the quantity of YAP ratio within the nucleus following stimulation [160-167]. Morphology results are shown in Figure 68 whilst gene analysis is within Figure 69.

Nuclear area was found to be highest in osteogenic media controls at both timepoints. After 24 hours of stimulation, cells stimulated at 10 kHz showed a similar response to OM controls, significant different from BM controls, although not as high as OM samples. Cell area was also found to be particularly high in OM samples after 24 hours, however there were no significant differences amongst vibrated samples at either timepoint. Actin intensity showed a similar response, with OM samples after 24 hours expressing a higher intensity of actin than most other samples. Again, there were no significant differences amongst vibrated samples at either timepoint. YAP was mostly found within the nucleus across all samples, with vibrated samples at 6 kHz showing a higher quantity of YAP within the nucleus than OM controls.

Gene expression analysis was also conducted after 24 and 72 hours of stimulation. Early osteogenic markers RUNX2 and ALP were used to investigate early changes in osteogenic gene expression. RUNX2 in OM samples was found to be significantly higher than other samples by approximately three times following 72 hours of stimulation. ALP was also higher in OM samples in the first 24 hours than other samples, significantly higher than samples stimulated at 6 kHz. Two nuclear genes, Sun1 and Lamin A/C were also investigated. Sun1 showed no significant differences at either timepoint, however Lamin A/C was found to increase after 72 hours in samples stimulated at 6 kHz.

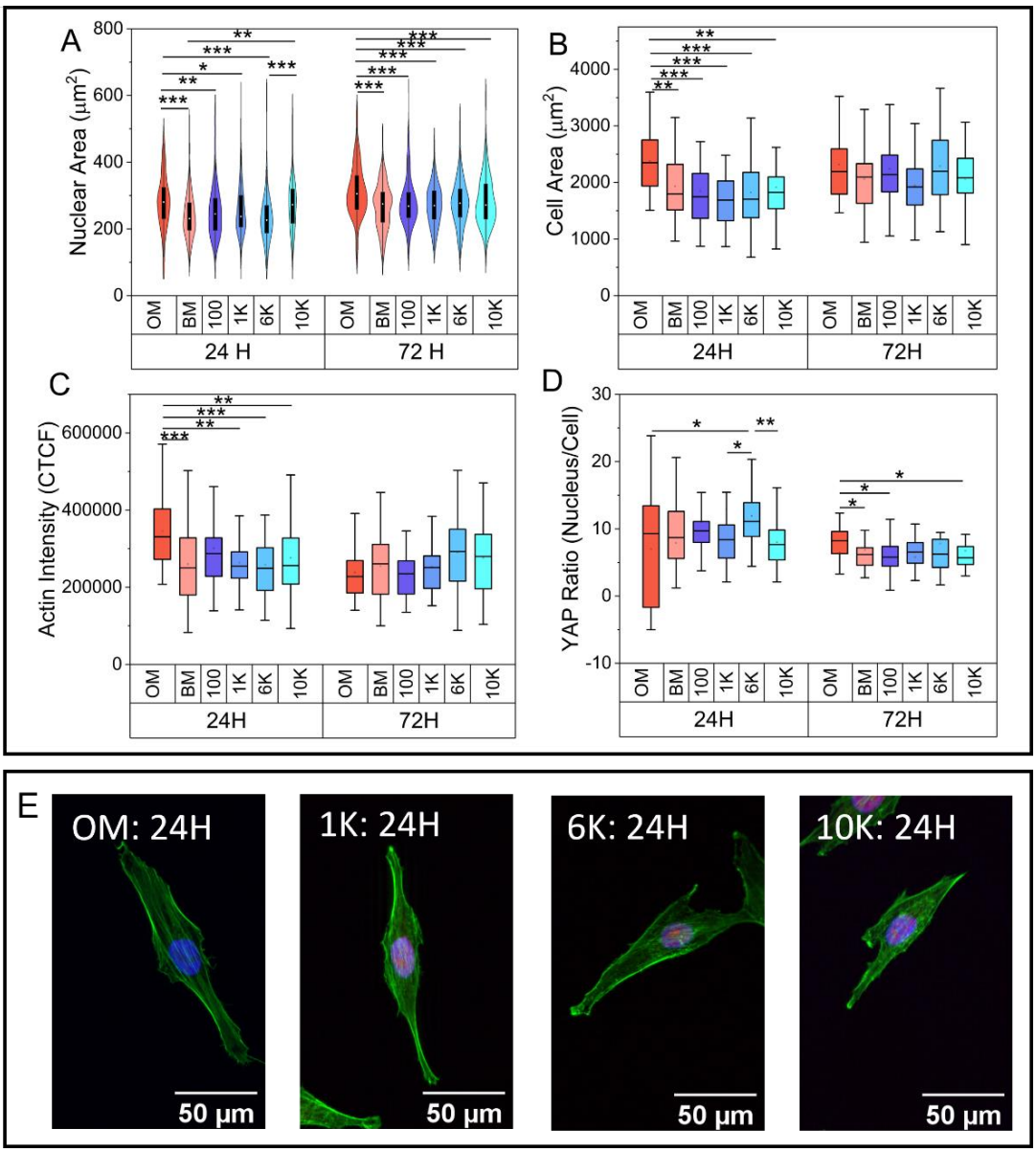

Figure 68: Morphology results showing initial cell response to multiple frequencies. Two control samples were compared, one with basal media (BM) as had been used previously and one with osteogenic media (OM) A) Nuclear area changes after 24 and 72 hours of stimulation (N > 100). B) Cell area results following 24 and 72 hours of stimulation (N ≈ 30). C) Actin intensity data following 24 and 72 hours of stimulation (N ≈ 30). D) YAP ratio (comparing YAP intensity in the nucleus and cell) following 24 and 72 hours of stimulation (N ≈ 30). E) Immunofluorescent images of cells following 24 hours of stimulation, showing actin (green), YAP (red) and DAPI (blue). Images were taken using a Zeiss microscope (Imager.Z1). In graphs, outliers were removed.

The earlier timepoint of 24 hours had high CT values, most likely due to lower cell number and being too early for gene expression changes to be measured. Meanwhile, morphology changes were more noticeable at this earlier timepoint.

Morphological changes may occur quickly in cells responding to stimulation, whilst gene expression changes require more time to become apparent.

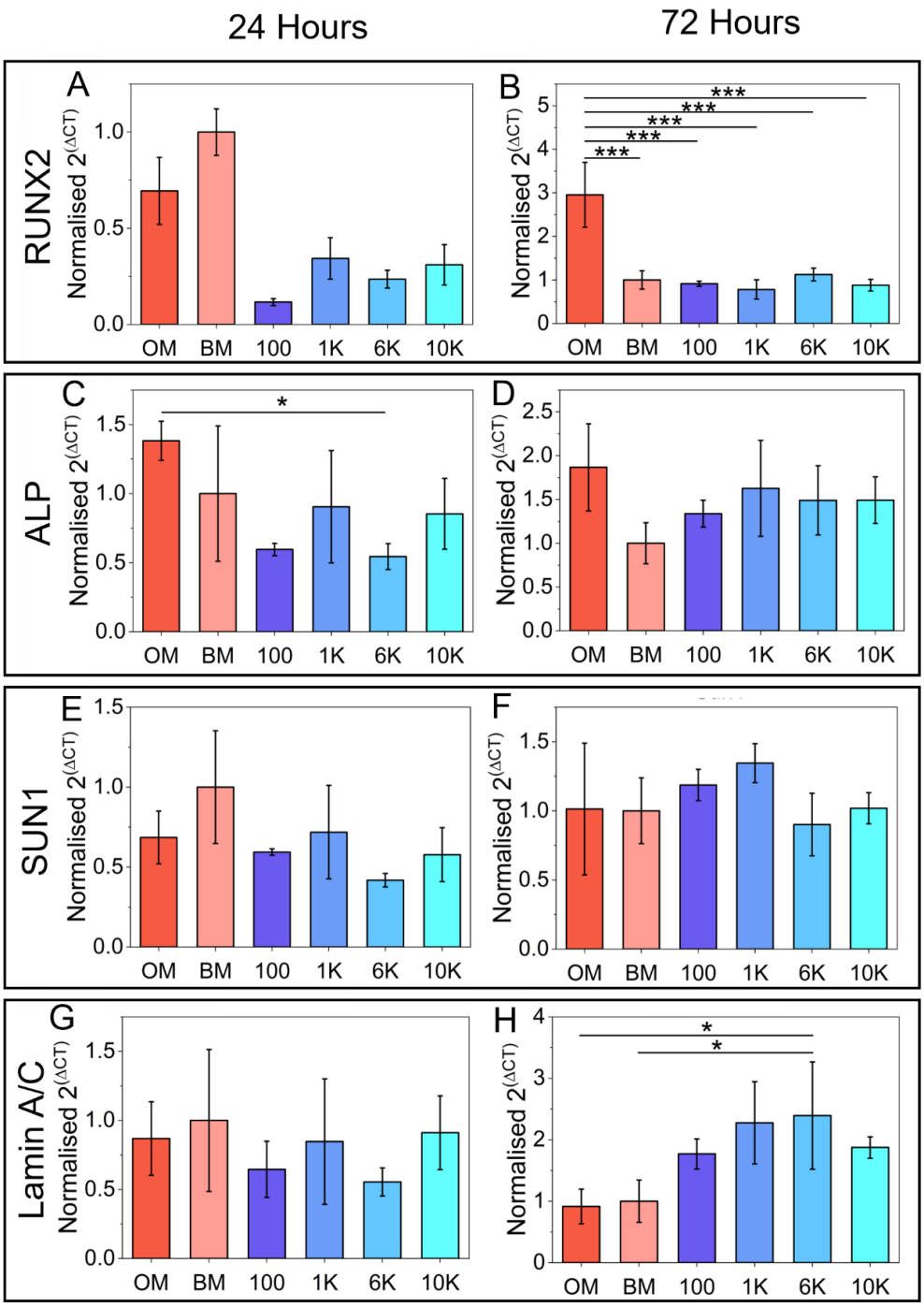

Figure 69: Gene expression results showing cell response at different frequencies. Two control samples were compared, one with basal media (BM) as had been used previously and one with osteogenic media (OM). Two timepoints were measured, following 24 and 72 hours of vibration. Two osteogenic genes were investigated (A-D) and two nuclear genes (E-H). Error bars show standard deviation (N = 3).

Lamin A/C, a protein known to play a vital role in mechanosensitivity, was found to increase in vibrated samples [172]. Lamin A/C proteins have been shown to increase during osteogenic differentiation in stem cells, however no significant increase in osteogenic markers was observed here [172]. The ratio of YAP within the nucleus was found to increase in cells stimulated at 6 kHz compared to BM controls at the same timepoint. However, whilst these responses may indicate a potential increase in mechanosensitivity, this was not observed to correspond with any changes in osteogenic expression within the two early osteogenic markers. Sun1 was also not found to change significantly across groups. This may be due to too early a timepoint being investigated to observe any changes in expression. Due to this, and the lack of changes observed in osteogenic genes, it was decided that later timepoints would be necessary to investigate whether different frequencies would have an effect on cell's osteogenic response.

4.3.5.2 Long-term osteogenic response to multiple frequencies

Up to Day 3, no osteogenic responses were observed following nanovibrational stimulation. Therefore, a longer-term experiment investigated the morphological and osteogenic response up to 7 days of stimulation. Previous results (Figure 68 and Figure 69), showed little difference between 6 and 10 kHz, except where nuclear area was larger following 10 kHz of stimulation and YAP translocation higher following 6 kHz of stimulation after 24 hours. When looking at a longer-term experiment, only one higher frequency of 10 kHz was used to maximise the frequency range that was examined. No osteogenic media controls were used here. Cells were seeded into 96 well plates, at a seeding density of 1000 cells/cm^2 for immunofluorescence analysis and a density of 2500 cells/cm^2 for qPCR analysis. Low seeding densities were chosen to ensure cells could still be measured effectively at a later timepoint of 7 days. Devices that had previously been calibrated (see Table 12) were used with a summary of vibration conditions used in Table 11. For immunofluorescence, cells were also stained for osteocalcin to investigate osteogenic response. Alizarin red staining was also used to investigate mineralisation deposition in cells. Gene expression data and immunofluorescent data were both obtained on Day 3 and Day 7 of stimulation,

whilst Alizarin red was analysed on Day 7. Morphology results, qPCR data and Alizarin red quantification are shown in Figure 70, Figure 71, and Figure 72 respectively.

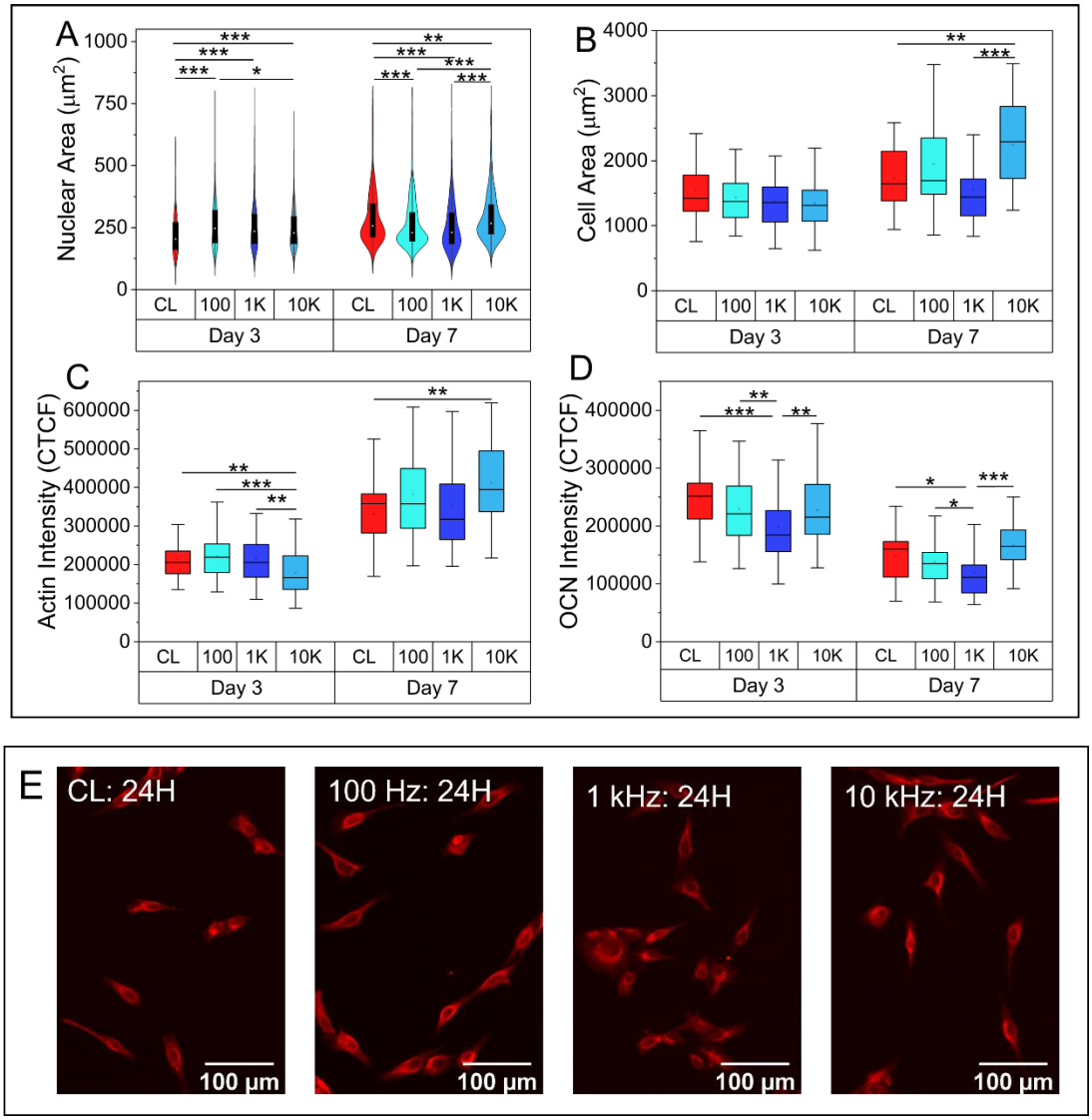

Figure 70: Morphology results showing cell response to multiple frequencies at later timepoints of Day 3 and Day 7. A) Nuclear area response to different frequencies (N > 100). B) Cell area response to different frequencies (N ≈ 30). C) Actin intensity response to different frequencies (N ≈ 30). D) Osteocalcin intensity response to different frequencies (N ≈ 30). E) Osteocalcin stained images following 24 hours of stimulation. Images taken using Zoe Fluorescent Cell Imager and brightness was adjusted equally in ImageJ. In graphs, significant differences between timepoints are not shown.

Nuclear area was found to increase significantly in all vibrated samples at both timepoints. The distributions varied greatly at both timepoints, with the first timepoint showing a much more varied response, whilst Day 7 showed a more condensed distribution. Cell area showed no significant differences on Day 3, similar to the initial experiment (Figure 68), however after 7 days, the 10 kHz sample showed a significant increase in cell area.

Actin intensity showed a similar trend to cell area. As with cell area, actin intensity did increase between Day 3 and Day 7, with the 10 kHz sample showing the highest intensity on Day 7. This was the reverse to that seen on Day 3, where 10 kHz was seen to have a significantly lower actin intensity compared to control. Osteocalcin intensity did not show any significant increases in expression compared to control. Instead, at the earlier timepoint, the 1 kHz sample was found to be significantly lower compared to other conditions. The later timepoint did show a significant increase in expression in the 10 kHz sample compared to the 1 kHz sample.

Gene expression analysis was performed on Day 3 and Day 7 of stimulation. The same two early-stage osteogenic markers as used previously (Figure 69) were again investigated. As before, RUNX2 decreased in all vibrated samples at both timepoints, significantly in the 100 Hz and 10 kHz samples. ALP showed a different trend to before, with the 1 kHz sample showing a decrease in expression at Day 3, although not significantly. The 10 kHz sample showed the highest response in the vibrated samples although not significantly higher than control. At Day 7, all samples showed a decrease in expression compared to the Day 3 timepoint, except the 1 kHz sample, which showed a significantly higher expression than the Day 7 control. This decrease in expression was to be expected as this is an early stage osteogenic marker and may start to be downregulated in favour of later stage markers at this timepoint [339].

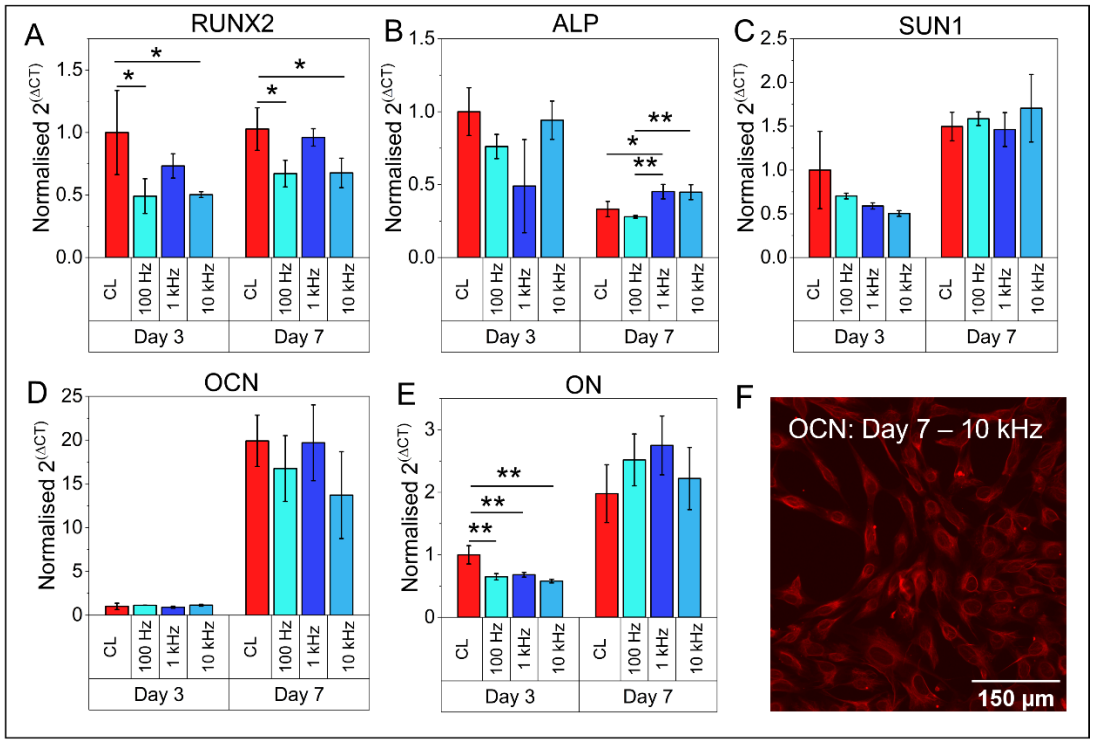

Figure 71: qPCR results showing cell response at different frequencies after 3 days and 7 days of stimulation. Two early osteogenic gene were measured (A-B), one nuclear gene (C) and two late osteogenic markers (D-E). F) OCN staining of 10 kHz stimulated cells on Day 7. Significant differences between timepoints are not shown. Image taken using Zoe Fluorescent Cell Imager microscope. Error bars show standard deviation (N = 3).

Only one nuclear gene was investigated, Sun1, which showed a decrease in nanovibrated samples at the Day 3 timepoint. Expression across all samples increased by Day 7 but there were no significant differences between samples at that timepoint. Two late-stage markers were used to indicate later stages of osteogenesis, osteocalcin (OCN) and osteonectin (ON). OCN was found to increase as expected between the two timepoints. However, all vibrated samples, except 1 kHz, showed a decreased expression compared to control at Day 7, particularly the 10 kHz sample, although no changes were significant. ON also showed an increase between the two timepoints and did show a non-significant increase in expression in vibrated samples with 1 kHz showing the highest expression. OCN gene expression did not correlate with protein intensity measurements (Figure 70). At Day 7, control and the 1 kHz vibrated sample showed a similar gene expression response (Figure 71), whilst protein intensity was lower in the 1 kHz

sample compared to control, significantly at Day 3. The 10 kHz sample was found to have the highest protein intensity at Day 7, however it also had the lowest gene expression, which may be due to genes being transcribed into proteins.

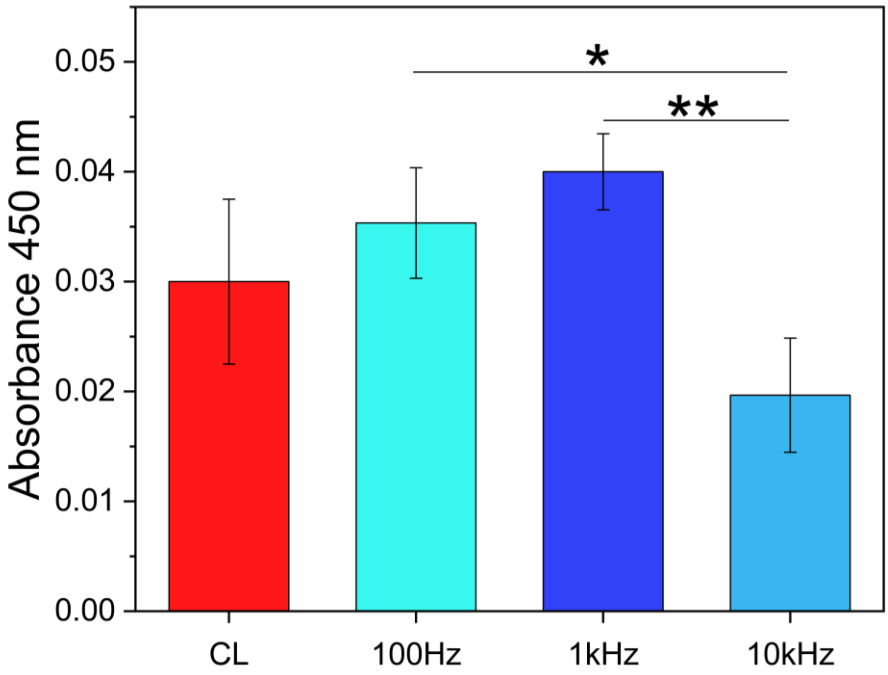

Figure 72: Alizarin red absorbance on Day 7 using a spectrophotometer (Thermoscientific Multiskan Go, Thermo Fisher). Error bars show standard deviation (N = 3).

Alizarin Red was used to stain mineralisation deposition in samples on Day 7 and was analysed using a spectrophotometer (Thermoscientific Multiskan Go, Thermo Fisher). Whilst nanovibrated samples were not found to be significantly higher than control, the 1 kHz vibration sample was found to have the highest level of mineralisation whilst the 10 kHz sample showed significantly lower levels of mineralisation compared to the other nanovibrated samples (Figure 72). This may indicate that 1 kHz results in the highest mineralisation in MG63s.

Whilst Alizarin red analysis and late-stage osteogenic markers showed no significant increases compared to control, this may have been due to looking at early timepoints. Therefore, it was decided that the next experiment would stimulate cells for longer. Both 1 kHz and 10 kHz showed positive osteogenic gene and morphological responses with some markers increased for both frequencies.

Therefore, these two frequencies were selected as optimal frequencies to use in future experiments.

4.3.6 Comparing the effects of intermittent and continuous vibration on cell response

Whilst both 1 and 10 kHz had been identified as giving rise to changes in morphology and gene expression, there are other vibration parameters which can be controlled. To test these parameters in isolation, the same original frequency of 1 kHz was used. In this experiment, the effect of both amplitude and duration of stimulation was investigated. Nanovibrational stimulation has normally been applied to cells continuously throughout an experiment [67, 139, 287]. However, studies have shown that continuous vibration may not be necessary and may even be detrimental to cell response [286]. Equally, for wearable technology, continuous vibration may not be feasible, and shorter periods of vibration would be preferable for animal studies and clinical trials [306]. Therefore, to investigate the effect of intermittent stimulation compared to continuous stimulation, cells were seeded in 96 well plates at 1000 cells/cm^2 and stimulated at two amplitudes (30 nm and 90 nm) either continuously or intermittently (4 hours/day, 5 days/week) for 14 days. These length of these intermittent vibrations were chosen based on an *in vivo* study applying nanovibrational stimulation to rat hind-limbs [306]. This length of time was the maximum that could be practically applied. Previous studies had shown larger amplitudes of 90 nm to induce a higher osteogenic response in MSCs, therefore this amplitude was also tested to investigate whether MG63s would show a similar response [287].

Initial experiments attempted to grow MG63 cells to Day 28, however the cells became very overgrown by this timepoint. Therefore, cells were only stimulated for 14 days and were lysed on both Day 7 and Day 14. Given that previous experiments had not seen a strong, reliable morphological response to nanovibration, only gene expression analysis was performed in this experiment with the results shown in Figure 73. As well as osteogenic and nuclear genes that had been analysed in previous experiments, gene expression analysis was also

performed for the actin remodelling protein WAS. Previous studies have shown this gene to have a high increase in expression following vibration after 7 days [270].

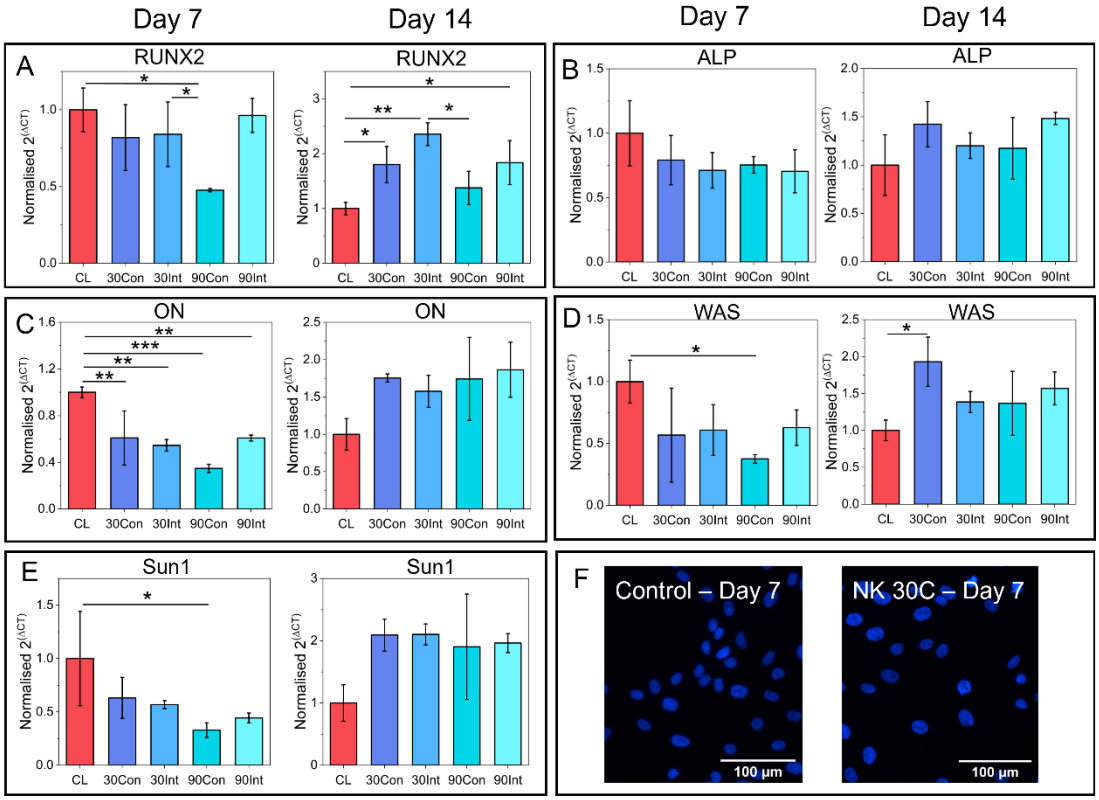

Figure 73: qPCR results for cells vibrated at two amplitudes (30 nm and 90 nm) continuously (NK 30C, NK 90C) or intermittently (NK 30P, NK 90P) and non-vibrated control cells at two timepoints (Day 7 and Day 14). A) Early osteogenic marker RUNX2. B) Early osteogenic marker ALP. C) Late osteogenic marker ON. D) Actin remodelling protein WAS. E) Nuclear envelope gene Sun1. F) DAPI images for control and NK 30C samples on Day 7. Images taken using Nikon Eclipse Ts2. Error bars show standard deviation (N = 3).

Two early osteogenic markers, Runx2 and ALP were investigated. At Day 7, Runx2 was significantly lower in continuously nanovibrated samples, vibrated at 90 nm (90Con). By Day 14, most vibration conditions showed an increase in Runx2 expression following nanovibration, with the highest response in intermittently nanovibrated samples, vibrated at 30 nm (30Int). For this marker, intermittent stimulation appeared to provide a better response than higher amplitude continuous stimulation. The second early marker ALP did not show any significant differences in vibrated samples. Day 7 showed a decrease in vibrated

samples, and whilst this was reversed by Day 14, no vibration condition showed a markedly increased expression. Given that ON had previously responded positively to nanovibrational stimulation (Figure 71E), it was used as a late stage marker here. At Day 7, vibrated samples were instead seen to decrease in ON expression compared to non-vibrated controls. While at Day 14, all vibrated samples increased compared to control, none did so significantly and there was little difference between vibration conditions.

The actin remodelling protein, WAS showed a decrease in expression at Day 7, significantly in the 90Con sample. At Day 14 continuously nanovibrated samples, vibrated at 30 nm (30Con) did show a significant increase in expression. Nuclear envelope gene, Sun1 was also measured. As expected from prior results, Day 7 showed a decrease in expression in all vibrated samples compared to control, significantly in 90Con sample. Day 14 showed an increase in expression in vibrated groups compared to control although not significantly.

Other than Runx2, no significant differences were observed between vibrated groups. Runx2 also showed no significant differences between 30Con and 30Int, or 90Con and 90Int. Due to this, it was decided that continuous vibration would be used in future work to keep experiments consistent with previous studies. As for amplitude response, this was further investigated alongside cell response to different directions of applied vibration.

4.3.7 Comparing horizontal and vertical vibration

Alongside frequency and amplitude, studies also use different vibration directions. Most studies apply vertical vibration, stimulating cells perpendicular to the cell monolayer. Very few studies have directly compared the effects of different directions of vibration, however those that have, observed horizontal vibration (stimulation of cells parallel to the cell monolayer) resulted in an increased osteogenic response in stem cells [271, 274]. Alongside an increase in osteogenic gene expression and mineralisation, Halonen *et al* also observed that cells realign their actin cytoskeleton in the direction of horizontal vibration [274].

Rearrangement of the actin cytoskeleton led to an increase in stiffness in horizontally vibrated cells, as measured by AFM.

ANSYS models previously discussed (section 2.6.2) predicted an increase in stress on the cell membrane when the cell is vibrated horizontally. As a result, horizontally vibrated cells were predicted to have a higher stiffness than vertically vibrated cells. This agrees with previous studies that have linked this increase in stiffness with an osteogenic response in stem cells [274]. To verify whether this effect may also be observed *in vitro*, optimisation experiments were first performed on MG63 cells.

4.3.7.1 Short-term cell response to horizontal vibration

Cells were seeded into Petri dishes at a density of 1000 cells/cm^2 for immunofluorescence analysis and into 96 well plates at a density of 5000 cells/cm^2 for qPCR analysis. A summary of the vibration conditions used are within Table 11. For these experiments, frequency was kept at the original 1 kHz to ensure any differences in response observed were due to changes in direction or amplitude.

4.3.7.1.1 Morphology is not a reliable marker of cell response in MG63 cells

Initial experiments vibrated cells at 30 nm (Figure 74A and C, Figure 75A, Figure 76A and C), however a later experiment compared amplitude as well as directionality, vibrating cells either horizontally or vertically at 30 nm or 60 nm amplitudes (Figure 74B and D, Figure 75B, Figure 76B). Two repeats of the initial experiment comparing directionality only were conducted, with nuclear area, cell area and actin intensity results being combined in Figure 74A and C, and Figure 75A.

Nuclear area was initially found to only significantly increase in horizontally vibrated samples (1 kHz, 30 nm) after 72 hours of stimulation. When comparing amplitude, horizontally vibrated cells at 60 nm (H60) showed a significant increase in nuclear area than at 30 nm (H30), showing a similar response to vertically vibrated cells at 30 nm (V30), and significantly higher than vertically vibrated cells at 60 nm (V60). Initially cell area was not found to significantly

change following stimulation (Figure 74C), however when comparing amplitude, cells stimulated at V30 were found to have a significantly higher area than control and horizontally vibrated cells (Figure 74D).

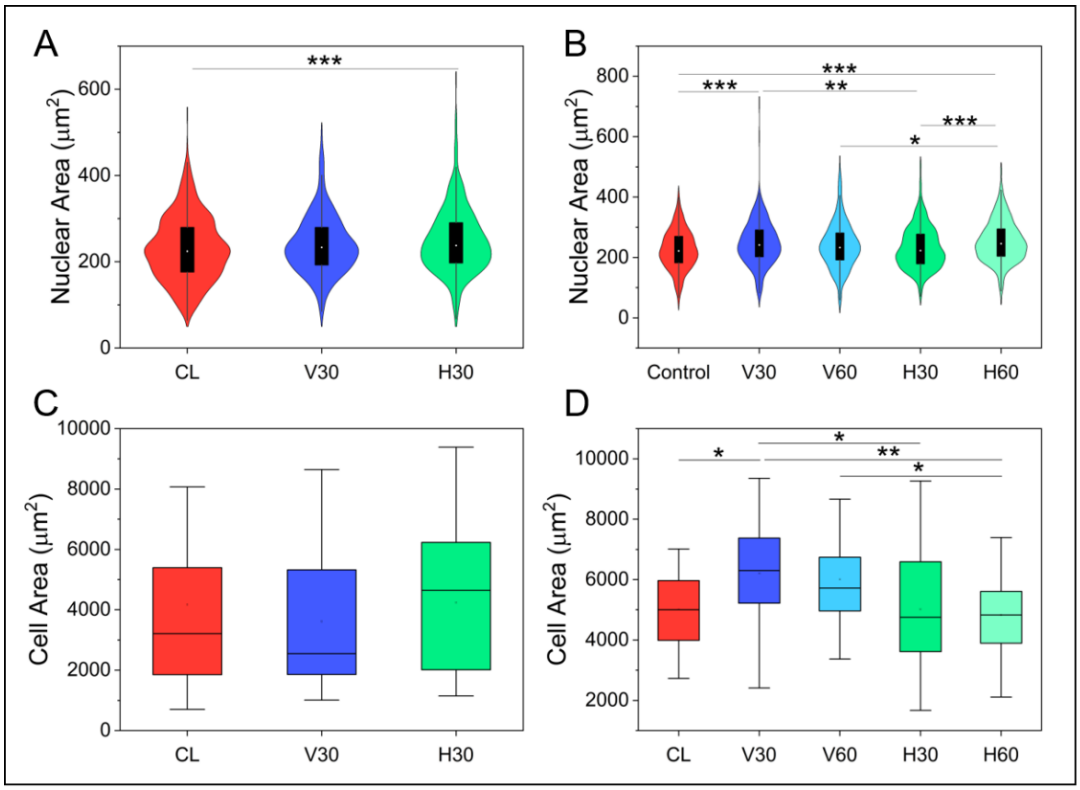

Figure 74: Nuclear area data for initial horizontal experiments following 72 hours of stimulation. A) Nuclear area data comparing directionality only. Two repeats of this experiment are combined here (N > 100). B) Nuclear area data comparing both amplitude and directionality (N > 100). C) Cell area comparing directionality only. Two repeats of this experiment are combined here (N ≈ 60). D) Cell area comparing both amplitude and directionality (N ≈ 30). Outliers have been removed from data.

Actin intensity (Figure 75) did not show many significant differences between samples, only showing a significant increase in the V60 sample compared to the H30 sample. The lack of response observed may be due to the timescale investigated, as actin reorganisation may have occurred much earlier during vibration.

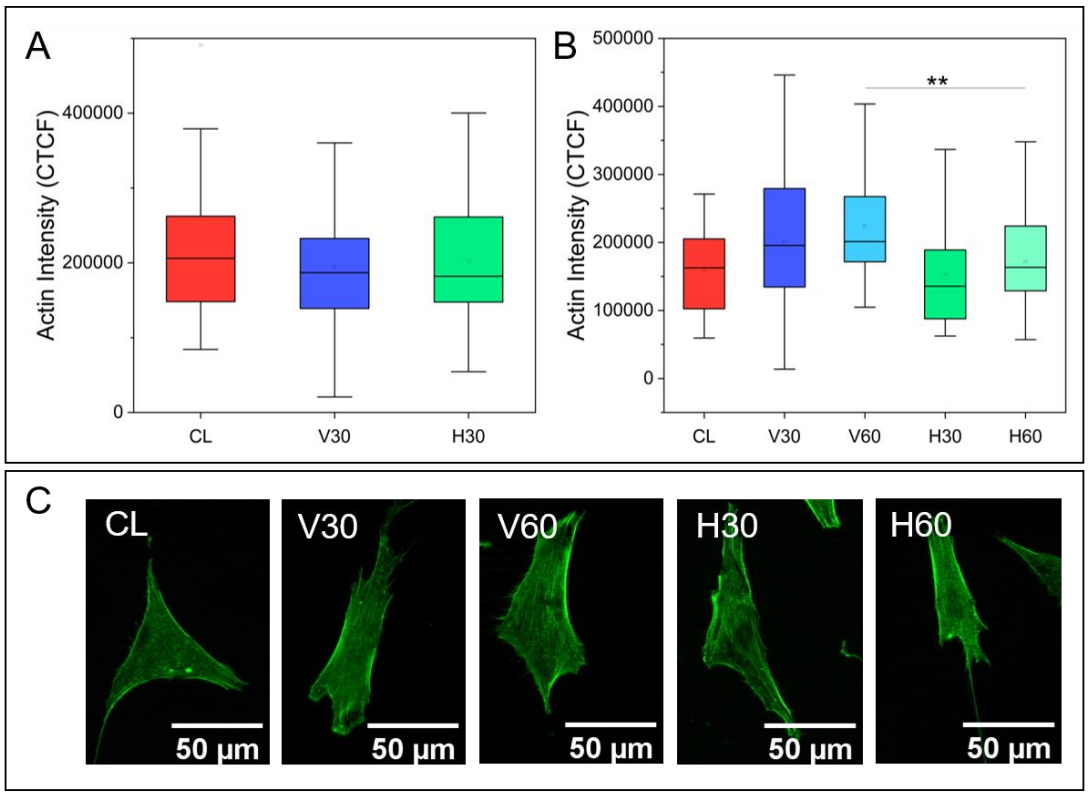

Figure 75: Actin intensity data for initial horizontal experiments. A) Actin intensity data comparing directionality only. Two repeats of this experiment are combined here (N ≈ 60). B) Actin intensity comparing both directionality and amplitude (N ≈ 30). C) Actin stained images for each amplitude and direction. Images taken using Zeiss (Imager.Z1) with brightness of images being adjusted in ImageJ equally. In graphs, all outliers were removed

YAP translocation and vinculin intensity was also investigated (Figure 76). Initially, YAP content was shown to significantly increase within the nucleus in both vertically and horizontally vibrated cells, with the highest response in horizontally vibrated cells. However, when comparing amplitudes in addition to directionality, vertically vibrated cells showed a lower YAP content within the nucleus than non-vibrated control cells (Figure 76B). Horizontally vibrated cells at 30 nm did show a significantly higher YAP content in the nucleus than vertically vibrated samples, however this was not higher than control samples. Vinculin was found to decrease in vibrated samples, most significantly in horizontally stimulated cells (Figure 76C).

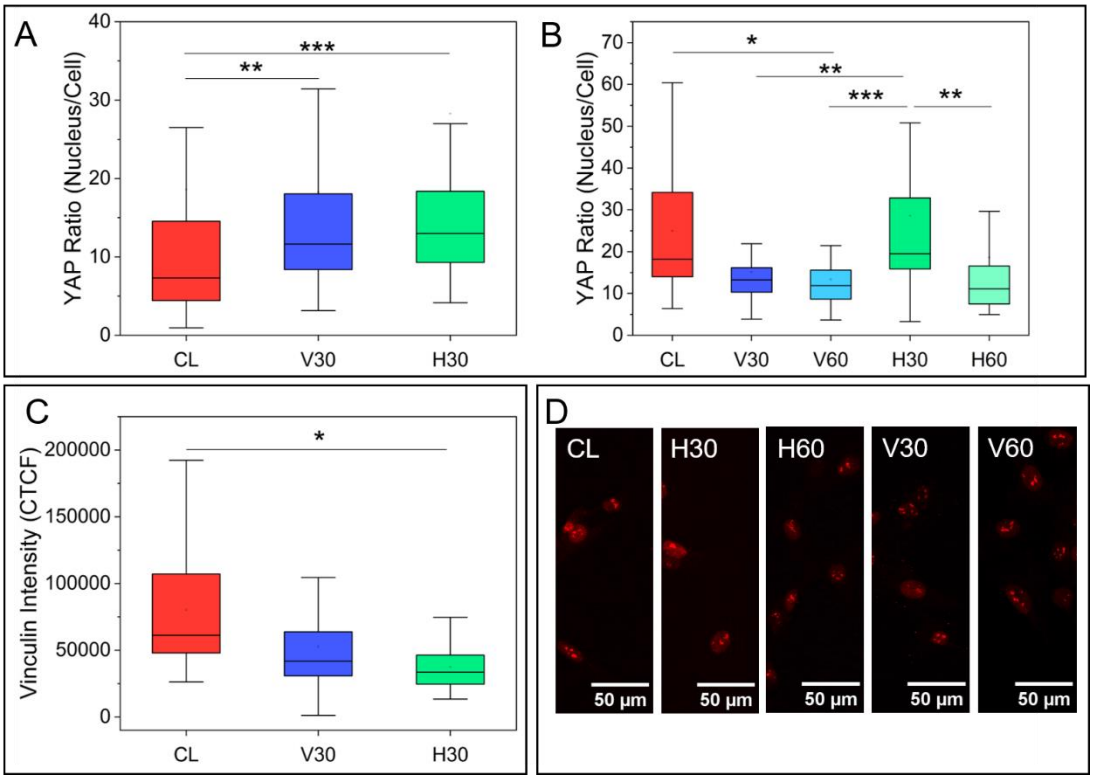

Figure 76: Vinculin intensity and YAP translocation data for initial horizontal studies. A) YAP ratio when comparing directionality only (N ≈ 30). B) YAP ratio when comparing both amplitude and directionality (N ≈ 30). C) Vinculin intensity when comparing directionality only (N ≈ 30). D) Immunofluorescent images of YAP for experiment comparing both amplitude and directionality. Images were taken using a Zeiss (Imager.Z1) and brightness has been adjusted equally in ImageJ. In graphs, all outliers were removed.

Morphological changes in horizontally vibrated samples were mixed after 72 hours of stimulation. Nuclear area increased in horizontally vibrated samples compared to control, although not always more than vertically vibrated samples, and in one experiment not at all. Actin intensity changes did not show much response to vibration, changes in YAP translocation were mixed and vinculin intensity decreased in stimulated samples. It may be that morphological changes are not observable on these timescales, or that morphology is not a reliable marker of cell response in MG63 cells.

4.3.7.1.2 MG63 cells do not align in the direction of horizontal vibration

As previous studies have shown actin alignment in the direction of vibration, it may be that cells realign themselves in the direction of horizontal vibration. This

was investigated by analysing DAPI images in ImageJ, assuming that nuclear alignment follows cell alignment. By keeping the direction of vibration consistent between images, the alignment of nuclei was measured. Results were then plotted as a semi-circular histogram to identify whether there was a bias of cells aligning in the direction of horizontal vibration, as shown in Figure 77 and Figure 78.

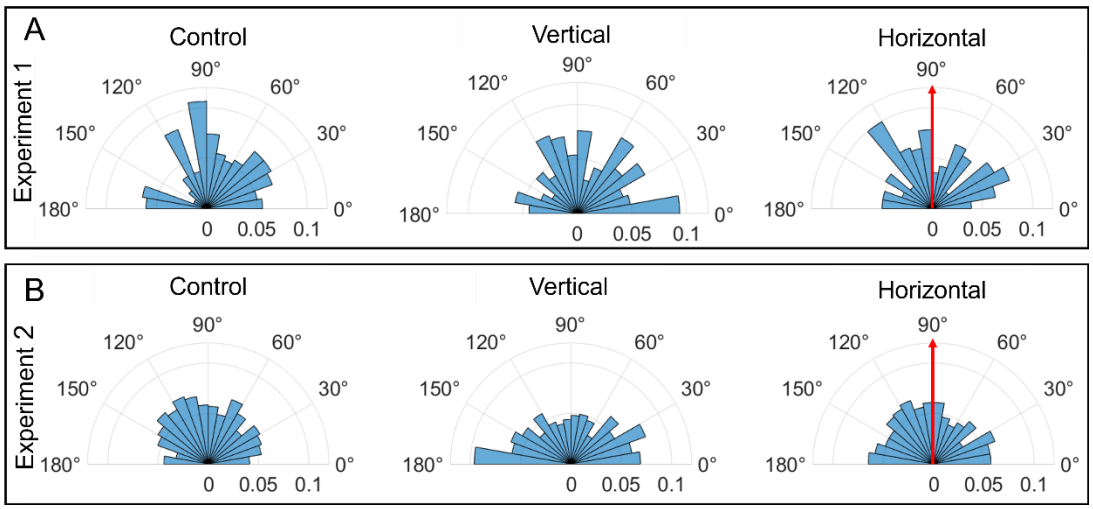

Figure 77: Investigating alignment in stimulated cells following application of 1 kHz, 30 nm vibration either vertically or horizontally in two experiments (N ≈ 30 for each sample in each experiment). Direction of vibration in horizontal results indicated by red arrow. Plots made in MATLAB software.

Initial experiments only comparing horizontal and vertical vibration at the same amplitude did not see a bias in nuclei aligned toward the direction of horizontal vibration, as indicated by the red arrow at 90 degrees. Instead, cells appeared to show no direction bias across vibrated and non-vibrated samples. Similar results were also seen when comparing two amplitudes (30 and 60 nm) both horizontally and vertically, as shown in Figure 78. Cells again did not align themselves in the direction of horizontal vibration.

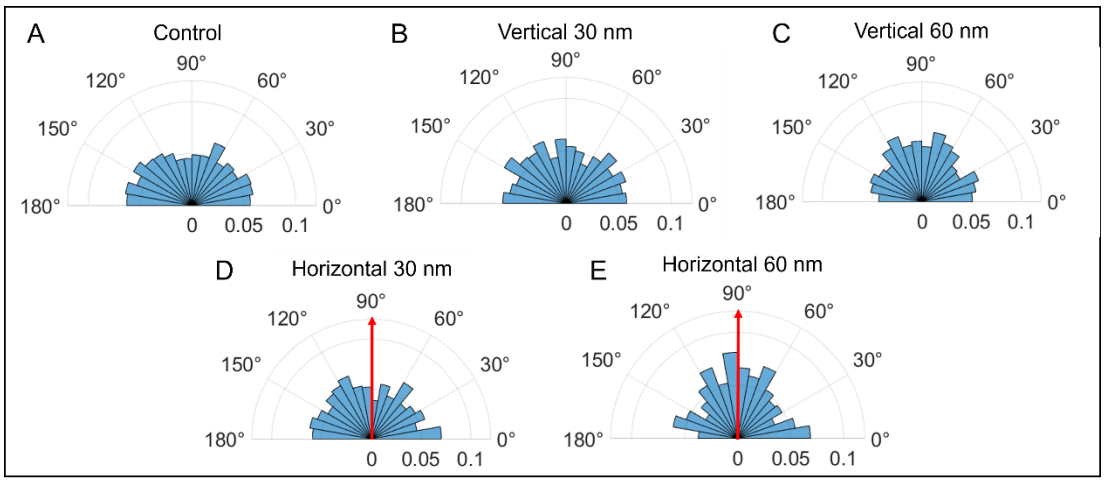

Figure 78: Investigating alignment in stimulated cells at two amplitudes (30 nm and 60 nm) at a 1 kHz frequency, vibrated either vertically or horizontally (N ≈ 30). Direction of vibration in horizontal results indicated by red arrow. Plots made in MATLAB software.

Whilst no alignment in the direction of horizontal vibration was observed, this may have been due to a number of factors. Cells were seeded into round Petri dishes, and whilst the dish was marked to indicate the direction of vibration, due to the geometry of the dish it was particularly difficult to ensure they were aligned correctly on the device and when measuring on the microscope. Being out by a few degrees may have been more consequential for the angle of cells within the images. The method used here for determining the angle of cells was to obtain the angle of the nucleus and assuming this angle was the same for the entire cell. However, this may not be true for actin fibre alignment which was seen to align with the direction of vibration in other studies [274]. This study had also used an intermittent vibration regime of 30 minutes on, 2.5 hours off, repeated 6 times per day for 18 days. Cells also experienced a higher force of 2.5 g compared to around 0.1 g experienced by nanovibrated cells at 1 kHz, 30 nm [297]. These differences may partially explain the lack of alignment observed here.

4.3.7.1.3 Lack of osteogenic response in cells at early timepoints

Gene expression following vertical and horizontal vibration was also measured within the first 72 hours of stimulation. Three osteogenic genes were measured, two early stage (RUNX2 and ALP) and one late stage (OCN), and three nuclear genes (Sun1, Sun2 and Lamin A/C). Results are shown in Figure 79.

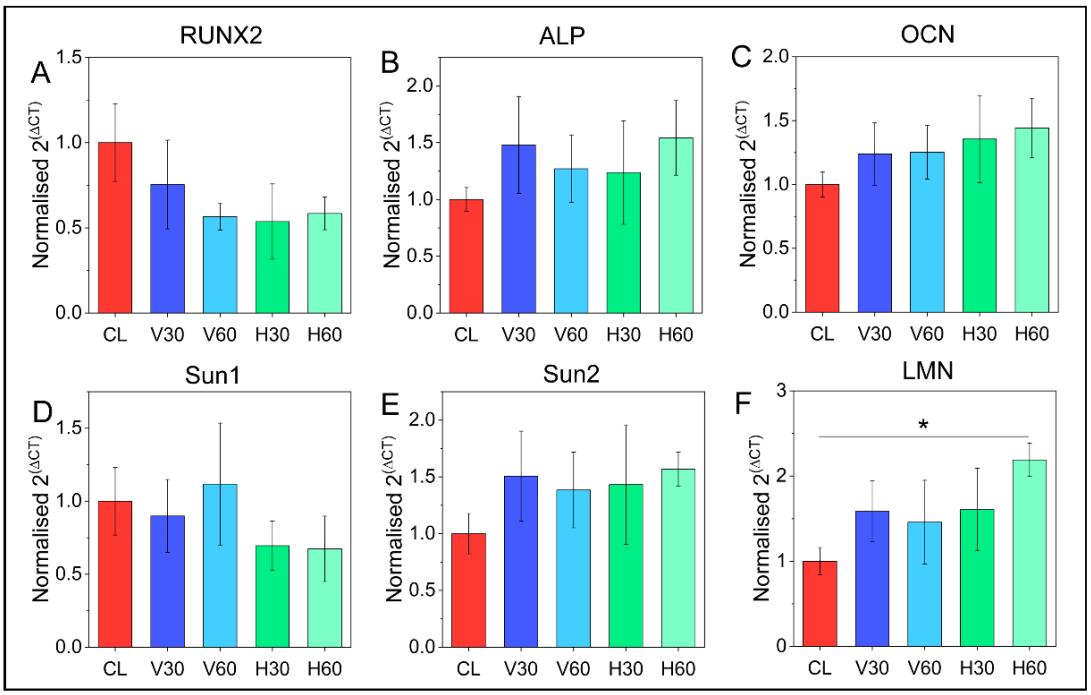

Figure 79: qPCR data for multiple amplitude, multiple directional experiment following 72 hours of stimulation. Three osteogenic genes were investigated (A-C) and three nuclear genes were investigated (D-F). Error bars represent standard deviation (N = 3).

Runx2 showed a decrease in expression in vibrated samples whilst ALP showed the opposite, although no significant differences were observed. OCN also showed an increase in vibrated samples although again no significant differences were observed. Previous experiments (Figure 69) also showed no significant increases in Runx2 and ALP expression after 72 hours of stimulation. OCN, being a late-stage marker, has also not consistently been shown to increase in vibrated samples at this early stage.

Sun1 and Sun2 also showed no significant differences, although Sun2 did show an increase in vibrated samples. Lamin A/C also showed an increase in expression in vibrated samples with horizontal vibration at 60 nm significantly higher than non-vibrated control samples. This has been seen in previous results (Figure 69), with some vibration conditions (1 kHz, 6 kHz) resulting in an increased Lamin A/C expression. As the lack of responses in osteogenic gene expression may be due to too early a timepoint being investigated, cells were stimulated for longer to investigate osteogenic responses.

4.3.7.2 Long-term cell response to horizontal vibration

As cells did not show a significantly increased osteogenic response following 72 hours of stimulation, cells were instead vibrated for 7 days. As there had been some indication that higher amplitudes may lead to an increased response, as seen by a significant increase in Lamin A/C expression, a higher amplitude of 90 nm was also tested alongside the lower amplitude of 30 nm. A summary of vibration conditions used is given in Table 11. Cells were lysed at Day 3 and Day 7 and samples were also fixed for immunofluorescent staining at Day 7. Alizarin red staining was also performed at Day 7. Morphology data, qPCR results and Alizarin Red analysis are shown in Figure 80, Figure 81, and Figure 82 respectively.

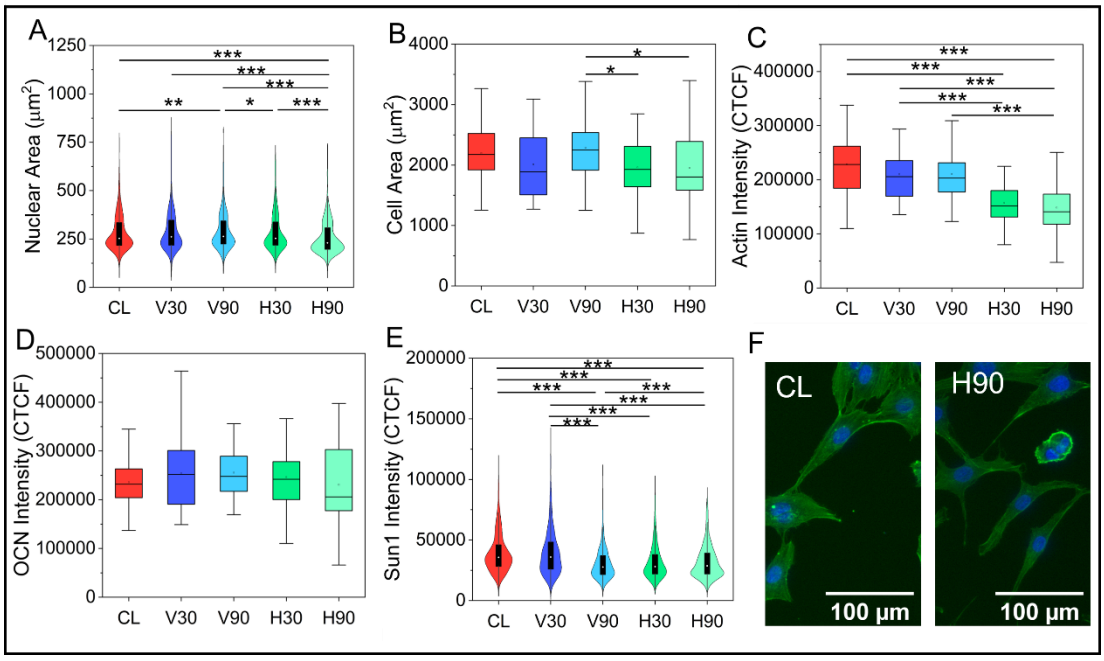

Figure 80: Morphology results after 7 days of stimulation both horizontally and vertically at two amplitudes (30 nm and 90 nm). A) Nuclear area results (N > 100). B) Cell area results (N ≈ 30). C) Actin intensity changes (N ≈ 30). D) OCN intensity changes (N ≈ 30). E) Sun1 intensity changes (N > 100). F) Images of CL and H90 samples stained with actin (green) and DAPI (blue) after 7 days of stimulation. Images taken using Zoe Fluorescent Cell Imager.

Nuclear area showed a significant increase in samples vibrated vertically at 90 nm (V90) compared to control, however horizontally vibrated samples at the same amplitude (H90) showed a significant decrease in nuclear area compared

to control and both vertically vibrated samples. Cell area showed no significant differences between control and vibrated samples, however H90 cells has a significantly smaller cell area compared to V90. Actin intensity was also reduced in horizontally vibrated samples, significantly lower compared to control. OCN showed no change in expression across samples. Sun1 expression was found to be significantly lower in all vibrated samples compared to control except vertically vibrated samples at 30 nm (V30).

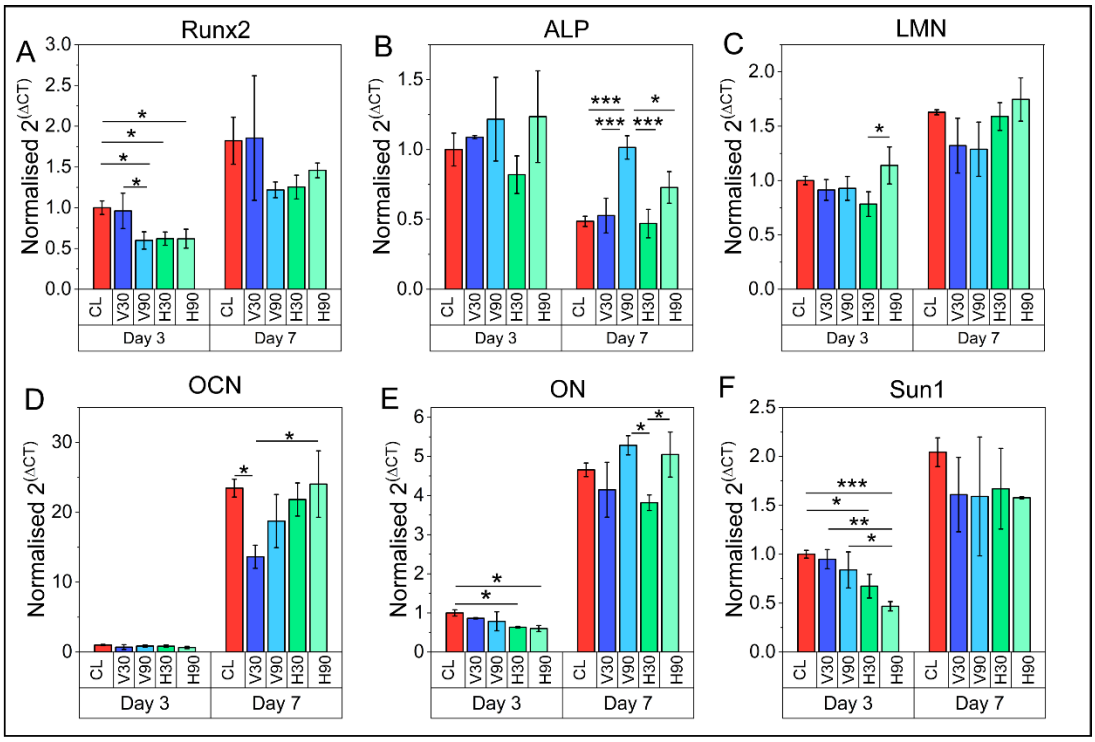

Figure 81: qPCR results after 3 and 7 days of stimulation both horizontally and vertically at two amplitudes (30 nm and 90 nm). Two early osteogenic genes were measured (A, B), two late osteogenic markers (D, E) and two nuclear genes (C, F). Statistical differences are not shown between timepoints. Error bars represent standard deviation (N = 3).

Whilst horizontal vibration did not lead to any significant increases in morphological changes, gene expression analysis did show some increases in osteogenic gene expression following vibration. At Day 3, Runx2 expression was significantly lower in all vibrated samples except V30. At Day 7, although showing the same trend, no significant differences were observed. ALP showed no significant differences at Day 3, however Day 7 showed a significant increase in V90 compared to all other conditions. OCN protein expression showed no

significant differences at Day 7 (Figure 80), however gene expression at the same timepoint showed a significant decrease in V30 samples compared to both control and H90. ON expression was significantly lower in horizontally vibrated samples on Day 3, however V90 and H90 were slightly higher than control by Day 7, though not significantly. Lamin A/C again showed a high response in H 90 samples at both timepoints although not significantly higher than control. Sun 1 was again decreased, with the lowest response in H90 at Day 3.

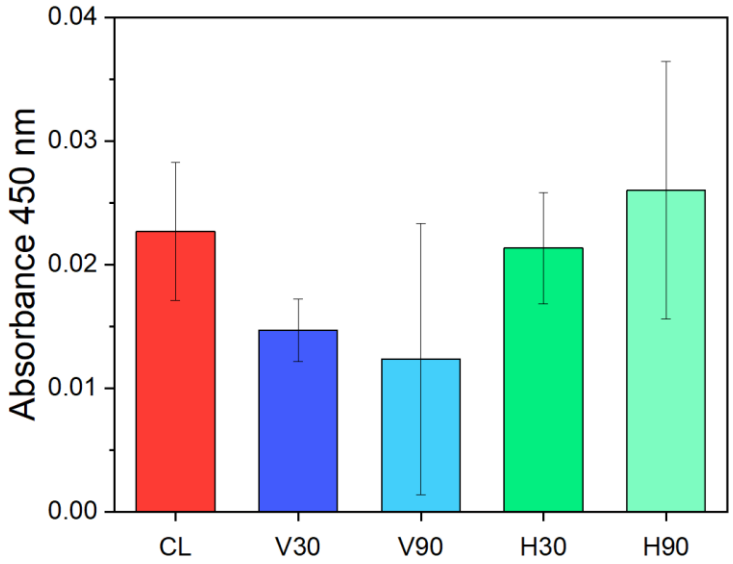

Figure 82: Alizarin red data taken using a spectrophotometer (Thermoscientific Multiskan Go, Thermo Fisher). No significant differences observed, although H90 expressed the highest quantity of Alizarin red of all vibrated samples. Error bars represent standard deviation (N = 3).

Alizarin red was again used to measure mineralisation deposition at Day 7 using a spectrophotometer (Thermoscientific Multiskan Go, Thermo Fisher). Results (Figure 82) did not show any significant differences, however the highest response in vibrated samples was in H90. In both gene expression analysis and Alizarin red data, whilst not significant, H90 often showed the highest osteogenic response of all the vibrated samples.

Morphological data often did not show expected results following stimulation. Actin intensity was expected to increase in response to optimal vibration conditions, as had been observed in previous NIH 3T3 experiments. Cells also did not align with the direction of horizontal vibration however this may have been

more due to flaws within the experiment and suboptimal vibration conditions. It may also be due to the cell type, as MG63s are an osteosarcoma cell line, their behaviour does not naturally tend toward alignment. Applying horizontal vibration to muscle cells or even fibroblasts may result in a more reliable alignment in response to vibration.

YAP translocation to the nucleus has been previously observed following mechanical stimulation [160-167]. However, here it was inconsistent, with horizontal vibration at 30 nm resulting in the highest ratio of YAP within the nucleus compared to other vibration conditions. Vinculin, which had previously been shown to increase in response to vibration in other cells, was found to decrease following stimulation.

Gene expression analysis of OCN and ON showed horizontal vibration at high amplitudes performed as good or better than vertical vibration at the same amplitude. Whilst no osteogenic gene was found to increase significantly in horizontally vibrated samples compared to control, Lamin A/C was found to be highest in horizontally vibrated samples at 90 nm at Day 7. This may be indicating increased mechanosensitivity in horizontally vibrated samples at higher amplitudes, despite the lack of osteogenic response.

4.3.8 The cytoplasm of MG63 cells stiffens within the first 3 hours of stimulation

As morphology results were mixed, and gene expression data did not show any significant increases in osteogenic response, the mechanical response of MG63 cells was investigated using AFM. Following on from NIH 3T3 AFM results, the same experiment was performed on MG63 cells to investigate changes in stiffness following applied stimulation. For this experiment, the effects of both vertical and horizontal stimulation were investigated with a summary of vibration conditions used shown in Table 11. Results are shown in Figure 83.

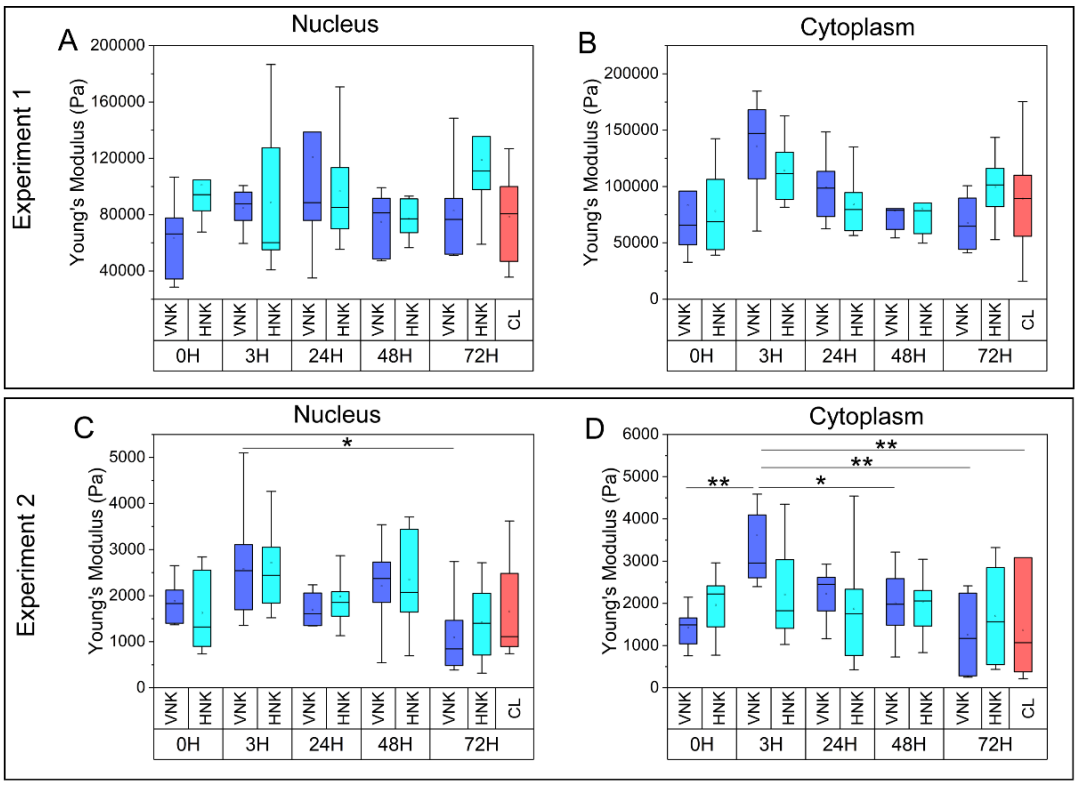

Figure 83: AFM measurements on the nucleus and cytoplasm of MG63 cells. A and B are from an initial experiment, C and D are from a second experiment. A) Measurements of Young's Modulus within the nucleus. B) Measurements of Young's Modulus within the cytoplasm. C) Measurements of Young's Modulus within the nucleus. D) Measurements of Young's Modulus within the cytoplasm. AFM measurements taken using an Asylum AFM, with 6-10 cells measured per condition (N > 6).

The first experimental repeat (Figure 83A and Figure 83B) measured very high Young's modulus values, much higher than expected of a cell, and lower than expected for the polystyrene culture dish. It was concluded that this may have been due to a calibration error prior to data being obtained, and whilst individual values are likely incorrect, an overall trend in the data ought to still be visible. Nuclear stiffness did not show any significant changes before or after vibration at each timepoint. The cytoplasm however did appear to increase in stiffness (not significantly) within the first 3 hours of stimulation, particularly following vertical stimulation, before relaxing at later timepoints, as had been seen previously in NIH 3T3 AFM data.

The second repeat of the experiment (Figure 83C and Figure 83D) showed similar results. The cytoplasm did show significant increases in stiffness in samples vertically vibrated for 3 hours compared to measurements taken before stimulation began. The stiffness of vertically vibrated cells after 3 hours of stimulation were also significantly stiffer than both vibrated and non-vibrated cells at the 72 hour timepoint. The nucleus did not show significant increases in stiffness after 3 hours of stimulation compared to measurements taken immediately prior to vibration, however these measurements were found to be significantly stiffer than vertically vibrated cells following 72 hours of stimulation. This may indicate a subtle increase in nuclear stiffness following applied vibration. There were however no distinct differences observed between horizontal and vertical vibration, and horizontal stimulation did not show any significant increases in stiffness compared to control or vertically vibrated samples.

4.3.9 MG63 cell deformability

Whilst AFM offers a precise, reliable method to measure the mechanical properties of cells, it is still a low throughput technique, only allowing for the measurement of a few dozen cells per hour, all whilst the sample is removed from the incubator, and without the presence of nanovibration. This means that during measurements, it cannot be guaranteed that cells are not responding to their new environment by changing their morphology and mechanical properties.

Real-time deformability cytometry (RT-DC) is a relatively new technique, offering a method of measuring the mechanical properties of >100 000 cells within a few minutes, all within a short period of time of being out of the incubator [336]. Cells must first be detached and are passed through a microfluidic chip at high speeds, deforming due to shear stress effects. By quantifying their deformability, populations of cells may be identified, and as a result the technique has been primarily used in identifying blood cell populations within a sample using this fast high-throughput, label-free approach [340].

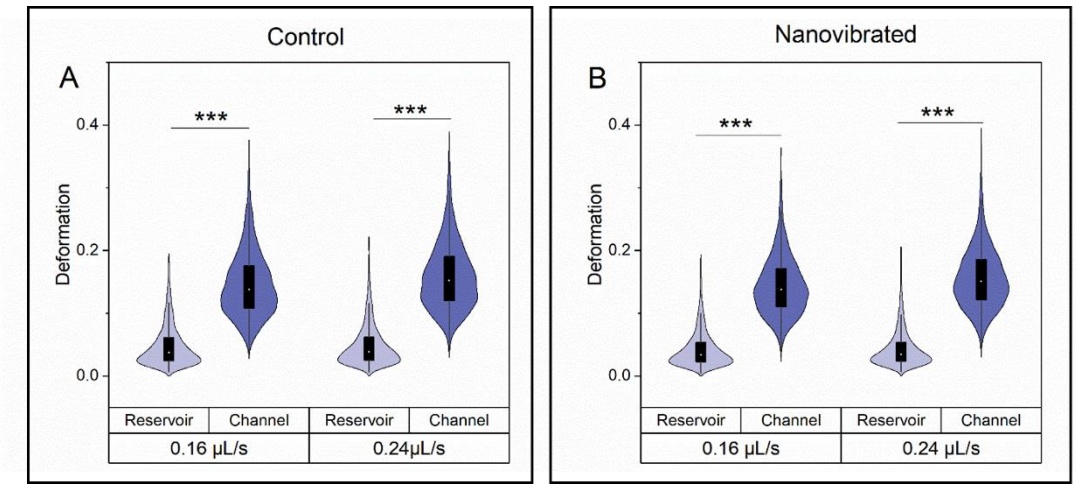

Figure 84: Deformability cytometry data showing proof of concept of experiment. Cells are measured for deformation in both the reservoir and channel at two flow rates. A) Control cells showing increased deformation in channel. B) Nanovibrated cells showing increased deformation in channel. (N > 1000).

The quantity by which cells deform gives an indication into their mechanical stiffness. Stiffer cells would be expected to deform less, whilst softer cells would deform more. Deformability cytometry therefore offers a fast, high-throughput method of quantifying stiffness in large populations of cells. The deformation of MG63 cells is measured both in the reservoir and the channel of the microfluidic device. Cells measured in the reservoir should be rounded and undeformed. The shear flow effects pushing cells through the channel causes deformation, similar to blood cells deforming to squeeze through small capillaries. The graphs in Figure 84 show that MG63 cells are capable of deformation. As the cells are deformable, stiffer cells would not deform as much as soft cells, therefore this would be a valid technique to determine the stiffness of cells.

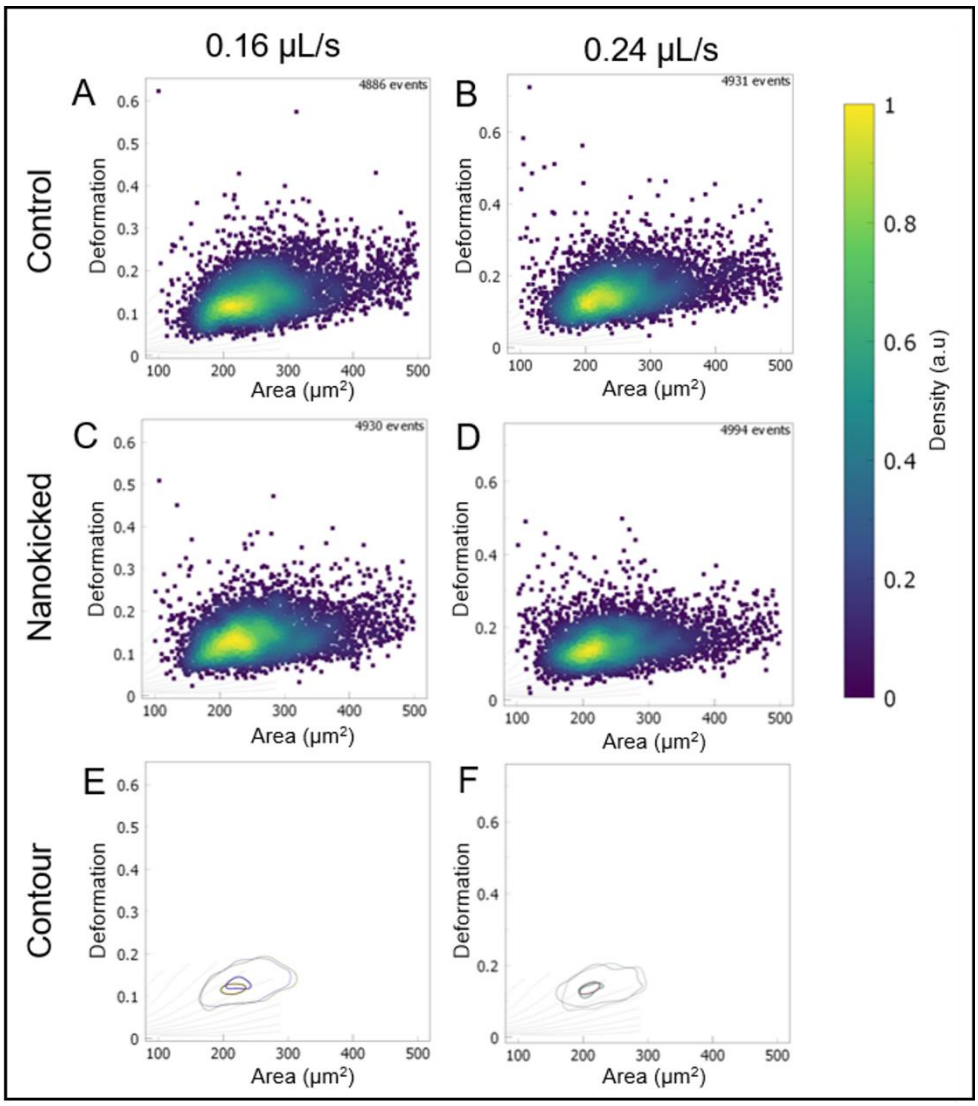

Figure 85: Deformation against area graphs as measured by deformability cytometry at two different flow rates. A) Control cells at 0.16 µL/s. B) Control cells at 0.24 µL/s. C) Nanovibrated cells at 0.16 µL/s. D) Nanovibrated cells at 0.24 µL/s. E) Contour plot comparing control and nanovibrated samples at 0.16 µL/s flow rate. F) Contour plot comparing control and nanovibrated samples at 0.24 µL/s flow rate. Plots made using Shape Out 2 software. (N > 1000).

Cells were stimulated for 24 hours before being prepared for RT-DC. Measurements were made at two flow rates, 0.16 µL/s and 0.24 µL/s. Different flow rates may be necessary to observe deformation depending on the stiffness of cells. The area of cells was measured in the reservoir, whilst deformation was quantified in the channel. Using the ShapeOut2 software, deformation and area of each cell was plotted for each sample as shown in Figure 85. Contour plots were constructed to identify any differences within the cell populations of

nanovibrated and control cells. Violin plots shown in Figure 86 also display distribution of area and deformation measurements.

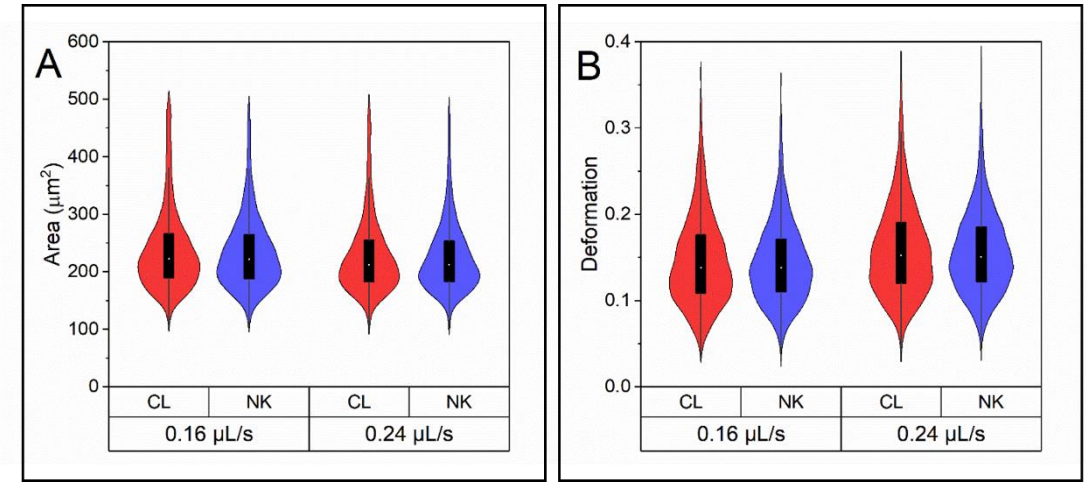

Figure 86: A) Area of cells as measured by deformability cytometry at two flow rates. B) Deformation of cells as measured by deformability cytometry at two flow rates. No significant differences were observed between samples. (N > 1000).

No differences between the contour plots were seen visually (Figure 85) and no significant differences were observed in deformability or the area of nanovibrated and control cells, at each flow rate as shown in Figure 86. Therefore, nanovibration did not appear to be having an effect on either the stiffness or area of the cells at this timepoint and flow rate as measured by real-time deformability cytometry.

4.4 Discussion

Here, MG63 cells were used as an osteogenic model to identify vibration conditions optimising osteogenesis. These cells were used as a precursor to stem cells as they lack donor variability and are capable of performing many experiments with less phenotypic drift, allowing for multiple experiments to be performed during optimisation.

The morphological response of MG63 cells to vibration was varied and inconsistent. As such, these parameters were unreliable in identifying vibration conditions optimising morphological cell responses. YAP translocation to the

nucleus has been observed following mechanical stimulation, however here YAP content within the nucleus was only found to be significantly higher in vibrated cells compared to control in one experiment [160-167]. There is some evidence within the literature that YAP may be more concentrated within the nucleus in cancer cells, and therefore this may be a confounding factor here [341, 342]. OCN, involved in matrix mineralisation, would be expected to increase when osteogenesis is induced, however no significant differences in protein expression in vibrated samples compared to control were observed.

The mechanical response of MG63 cells was also not found to produce as reliable a response as previously observed in NIH 3T3 cells. Whilst AFM measurements revealed a similar trend in the cytoplasm of MG63 cells compared to NIH 3T3s, showing an increase in stiffness within the first 3 hours of vibration, the same response was not observed within the nucleus and there was not a huge distinction between horizontal and vertical vibration. In fibroblast cells, some significant changes in stiffness were only observed within the first 3-24 hours of stimulation, therefore, it may be possible that the timepoint showing the highest stiffness change in MG63 cells was not measured. Changes may also be much more subtle in this cell type, requiring a large number of cells to be measured at each timepoint, which is difficult when using AFM. There were also no distinct stiffness differences between vertical and horizontal vibration, with vertical vibration resulting in a marginally stiffer cell at some timepoints.

RT-DC was also used here to measure the stiffness of MG63 cells. There are many differences between the two techniques which may affect measurements. As AFM uses live cells still attached to cultureware, actin fibres remain intact during measurement, thus enabling stiffness provided by the cytoskeleton to be accurately measured. Morphology analysis can also reveal the spread of cells on the surface in response to vibration making cell area measurements possible. As deformability cytometry requires cells to be detached from the surface, actin fibres may be rearranged during this process and cell area when spread is not the same as cell area when detached. Stiffness may be lost, whilst the area of cells would be expected to show no differences if the volume remained constant.

AFM also allows for the distinct measurements between the nucleus and cytoplasm of the cell and for multiple measurements to be made on the same sample at different timepoints. RT-DC only allows for an end timepoint measurement and does not distinguish between cell components. High volumes of cells are also required for the technique which, as observed in seeding density experiments, may alter cell response.

Whilst no significant differences were observed with RT-DC, this may have been due to a number of factors. The morphology and stiffness of cells may have been affected by the sample preparation. It may also be that the flow rate or channel size used did not allow subtle differences in cell stiffness to be observed. Indeed, without optimisation of the technique, whilst RT-DC holds promising potential for mechanical measurements, it was not explored further here. Meanwhile, AFM, as it had previously revealed significant differences in the stiffness of NIH 3T3 cells, was used in later experiments with MSCs.

Seeding density and adhesion time were also investigated here to investigate whether MG63 cell morphology responded similarly to NIH 3T3 cells. Whilst a higher initial seeding density did show an increased morphological response in vibrated samples, it was decided that a lower initial seeding density would be more beneficial for experiments, due to the fast rate at which the cells grow and concerns of overgrowth at longer timepoints rendering it difficult to conduct analysis. A 24 hour period prior to vibration showed cells to have stronger attachment as measured by vinculin intensity. Therefore, further experiments ensured a 24 hour adhesion time prior to stimulation.

Four key vibration parameters were investigated here: frequency, amplitude, duration and direction. When testing multiple frequencies, 1, 6 and 10 kHz showed increased morphological and osteogenic responses. At longer timescales, 1 and 10 kHz showed good gene response, with 10 kHz showing a higher ALP expression and OCN intensity. OM did increase the expression of osteogenic genes, however it did not have an effect on nuclear genes. Vibration did however increase the expression of nuclear genes, indicating that different signalling processes may be involved here.

After being selected as optimal frequencies, the 1 kHz frequency was used in further vibration parameter optimisation experiments to ensure the response observed was due to different parameters instead of the higher frequency. Only one experiment testing the effects of continuous and intermittent stimulation was conducted, investigating the effects of intermittent (4 hours/day, 5 days/week) compared to continuous stimulation on cell gene response. However, data from this was inconclusive as to whether intermittent or continuous stimulation is preferable. Genes such as WAS have been previously shown by other studies to increase in expression following application of higher forces, however it may have been that the vibration conditions used here were not significant enough to illicit a strong response from this gene [270].

Finally, direction and amplitude were investigated within the same studies. Horizontal vibration had previously been shown to result in actin realignment with the direction of vibration, however cells were not found to align themselves in line with horizontal vibration here [274]. Whilst morphology data of cells horizontally vibrated was mixed, osteogenic gene analysis did show a high response in cells horizontally vibrated at 90 nm (H 90). H90 samples were also found to have an increased expression of Lamin A/C, a LINC complex protein, known to be involved in mechanosensitivity. It may be therefore, that higher amplitudes of horizontal vibrations result in cells becoming more sensitive to stimulation, and that an osteogenic response may not be visible until later timepoints (rather than within 7 days as measured in these experiments). Therefore, higher amplitudes of 90 nm, and horizontal vibration, were chosen to be carried forward to experiments with MSCs with potential to improve osteogenic response beyond 30 nm, vertical vibration.

Throughout this chapter there have been several occasions where MG63s were not behaving as expected following nanovibrational stimulation. Morphology did not have a reliable response, stiffness was not found to significantly increase as had been observed in NIH 3T3 cells and osteogenic gene expression was often not found to increase significantly following vibration. This may be a downside to

using a cell line as a model rather than a primary line that may provide more accurate responses to stimulation.

Chapter 5:

Vibration of Mesenchymal Stem Cells (MSCs)

5.1 Introduction

Stem cells offer the potential for new therapies for a variety of diseases, including many bone-related conditions. Growing cells for clinical use comes with many difficulties, particularly growing enough for implantation and ensuring cells are specifically directed toward desired phenotypes. A variety of techniques have been shown to drive osteogenic differentiation, including using chemical media supplementation[8]. However, osteogenic media contains components such as dexamethasone, a known inducer of adipogenesis. As a result, this leads to mixed differentiation, making it harder to produce a single population of cells. Any supplements used in media for cell therapies would also require testing and removal from the final product before it may be used within patients. Therefore, techniques such as mechanical stimulation offer drug-free therapies that may be more beneficial for the end recipient.

Vibration has been shown to illicit a response in cells and has been used to direct differentiation toward osteogenesis, chondrogenesis, myogenesis, adipogenesis and neurogenesis [42, 286, 287, 291]. Whilst primarily focused on obtaining an osteogenic response in cells, studies have however used a vast range of vibration conditions, often contradicting each other on the vibration conditions resulting in osteogenesis (Appendix A). It may be that there is no general optimal set of vibration conditions, with parameters such as frequency and amplitude often interfering with one another. It may also be that different cell types and donors respond differently to vibration, making it challenging to precisely identify vibration conditions that will maximise an osteogenic response.

Thus far, key responses have been identified in cells exposed to nanovibration, as well as testing a limited range of parameters to identify the optimised conditions to illicit osteogenic responses in cells. Due to limitations within the range of parameters tested here, it is not possible to confidently state that these vibration conditions are the optimal parameters for cell response, but do represent optimisation within the parameter space examined. NIH 3T3 cells were used to identify morphological and mechanical changes in cells exposed to vibration, identifying an initial increase in stiffness within 3-24 hours of stimulation and the links between this and actin fibre formation leading to nuclear stretching. MG63 cells were then used to further understand the osteogenic response of cells to vibration and to optimise vibration conditions for this output. Frequencies of 1 and 10 kHz were found to produce the optimal osteogenic response in cells. Directionality was thoroughly tested, identifying horizontal vibrations of 90 nm to increase the expression of nuclear envelope genes known to be involved in the mechanosensitivity of the cell [94, 170]. Whilst intermittent vibration was tested, results in MG63 cells were inconclusive and so required further testing on MSCs.

This chapter focuses on further testing of intermittent vibration on MSCs before applying the optimised vibration conditions to cells from a range of donors to determine whether such conditions could be used universally to direct stem cell differentiation toward osteogenesis

5.2 Methodology

5.2.1 MSC Donors

Cells from three donors were used in experiments. These were obtained commercially from Merck and Promocell and details regarding age, gender and ethnicity of donors are given in Table 15. When applying optimised vibration conditions, three donors were used to identify if donor variability would impact the response.

Table 15: MSC donor information, giving age, gender, ethnicity of donors, as well as the passage number used in following experiments. Donors were anonymised.

Donor	Age	Gender	Ethnicity	Passage No.
Donor 1	80	Male	Caucasian	P4
Donor 2	28	Male	Caucasian	P4
Donor 3	72	Female	Caucasian	P4

5.3 Comparing the effects of intermittent and continuous vibration on MSCs

Previous experiments testing intermittent vibration on MG63 cells were inconclusive, showing no significant differences between samples simulated continuously or intermittently (Figure 73). Therefore, the same conditions were applied to MSCs to test whether the same response would be observed in this cell type. Cells from Donor 3 (see Table 15) were seeded at 4000 cells/cm^2 in 96 well plates and incubated for 24 hours prior to beginning stimulation. Again, two amplitudes were used, 30 and 90 nm, and cells were stimulated either continuously or intermittently for 4 hours/day, 5 days/week for a total of 28 days. As discussed in section 4.3.6, these parameters were chosen based on an *in vivo* study applying nanovibrational stimulation to rat hind-limbs [306]. Cells were then lysed on Day 28 of stimulation with the gene expression results shown in Figure 87.

Whilst one-way ANOVA statistical tests showed no significant differences, there were some distinct differences between cells vibrated continuously and those vibrated intermittently. Runx2 showed higher expression in the two continuously measured samples, whilst intermittently vibrated samples showed similar levels of expression as control samples. ALP did not show any distinct differences between samples, whilst Col1a showed a higher expression in continuously vibrated samples at 30 nm. The three late osteogenic markers, OCN, OPN and ON, all showed increased expression in continuously vibrated samples compared to those stimulated intermittently.

Non-osteogenic genes also showed some increases in continuously vibrated samples. Adipogenic marker, PPARγ showed an increased expression in cells stimulated continuously at 30 nm. Similarly, chondrogenic marker, Sox9 showed an increase in expression in both continuously stimulated samples. Actin remodelling gene WAS showed the highest expression in samples continuously stimulated at 90 nm.

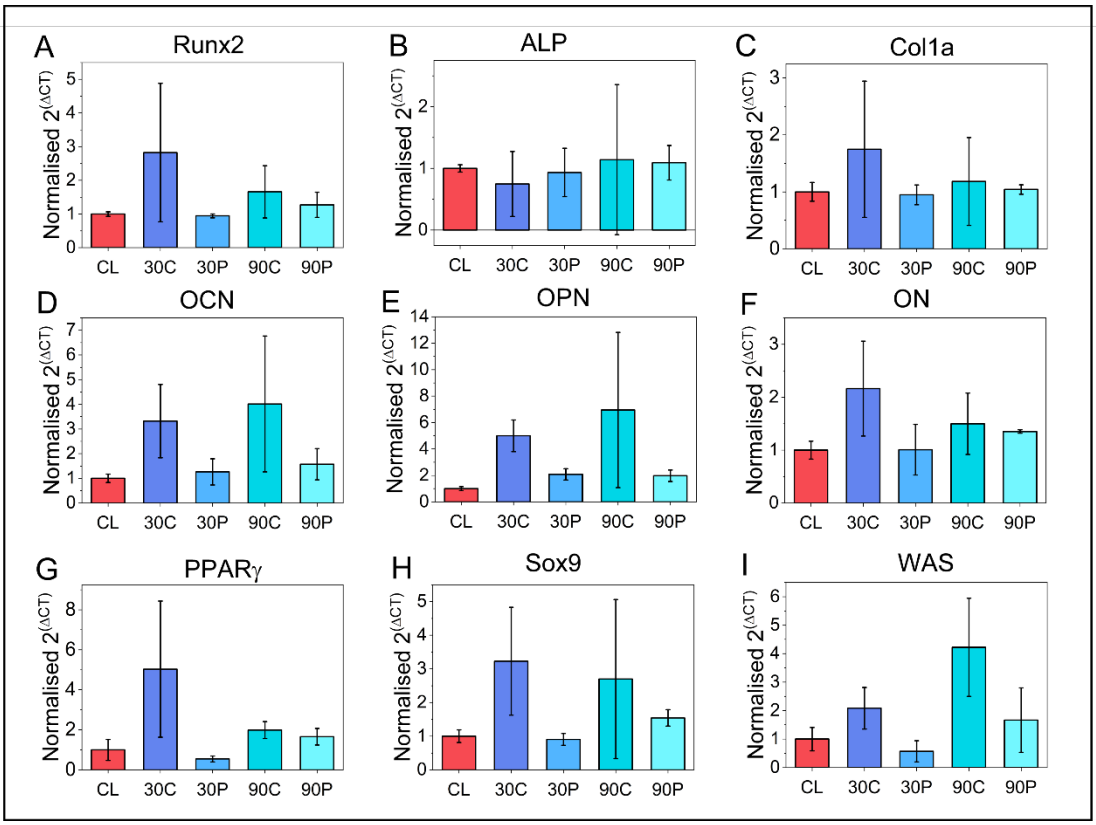

Figure 87: Gene expression results for MSCs vibrated at two amplitudes (30 nm or 90 nm) either continuously or intermittently (4 hours/day, 5 days/week) for 28 days. Two early osteogenic markers Runx2 and ALP (A, B), one mid osteogenic marker Col1a (C), three late osteogenic markers OCN, OPN, ON (D-F), one adipogenic marker PPARγ (G), one chondrogenic marker Sox9 (H) and one actin remodelling gene WAS (I) were investigated. Error bars represent standard deviation (N = 3).

Whilst there were no significant differences observed, continuously vibrated samples showed a distinct increase in osteogenic genes. Although non-osteogenic genes also showed an increase in expression, it may be that continuous stimulation is resulting in a higher response in cells. Intermittent vibration did not seem to induce any increases in gene expression compared to control cells.

Other studies have found intermittent stimulation to produce a higher osteogenic response than continuous stimulation of cells, however, although not observed here, it may be that the stimulation applied during intermittent vibration was insufficient [286]. Equally, only one timepoint was measured, and the benefits of intermittent vibration may have been observable earlier in the vibration regime. Only one donor was also used, and there may be differences between donor response. However, as continuous vibration was observed as the optimal condition here, intermittent vibration was not further investigated, and continuous vibration of cells was used in future experiments.

5.4 Applying optimal vibration conditions to induce osteogenesis in MSCs

Thus far, experiments have endeavoured to identify the optimal vibration conditions for osteogenesis. Experiments done on MG63 cells tested four parameters: frequency, amplitude, direction and duration of vibration. Frequencies of 1 kHz and 10 kHz were found to increase morphological and osteogenic response in cells. Directionality experiments found horizontal vibration resulted in the highest expression of osteogenic genes, particularly at higher amplitudes. Experiments comparing continuous and intermittent vibration were inconclusive on MG63 cells, however when repeated on MSCs (Figure 87), continuous vibration was found to produce the highest osteogenic response. From these experiments the optimal vibration conditions were identified as shown in Table 16.

Two frequencies had been identified as providing a higher osteogenic response. However, when calibrating a device at the optimised conditions described in Table 16, the horizontal device was unable to produce vibration at a 10 kHz frequency. Therefore, 1 kHz was chosen to use in a final experiment applying the optimal vibration conditions to MSCs. Here, three MSC donors were exposed to both the optimal vibration conditions and the original vibration conditions. Three donors of different ages and genders (detailed in Table 15) were chosen to test

whether all three would respond to vibration in the same way. Cells were seeded at 4000 cells/cm^2 into 96 well plates, left to adhere for 24 hours, before being vibrated either at the original vibration conditions of 1 kHz, 30 nm, vertically, continuously (VNK30) or the optimised vibration conditions of 1 kHz, 90 nm, horizontally, continuously (HNK90). Non-vibrated controls were incubated separately. Cells were lysed after 7, 14, 21 and 28 days of stimulation and fixed on Day 28.

Table 16: Summary of optimal vibration conditions identified in previous experiments and details on the responses observed.

Vibration Condition	Optimal Parameter	Cell Type Tested	Response
Frequency	1 kHz and 10 kHz	MG63	10 kHz – Higher ALP expression and OCN intensity 1 kHz – Highest mineralisation and ON expression
Amplitude	90 nm	MG63, MSCs	Increased late osteogenic marker expression
Direction	Horizontal	MG63	Increased expression in LINC proteins known to increase mechanosensitivity
Intermittent/ Continuous	Continuous	MG63, MSCs	Increased late osteogenic marker and WAS gene expression

5.4.1 Morphological changes in MSCs in response to optimal vibration conditions

Morphology changes were investigated on Day 28 following staining and imaging. Nuclear area and cell area were investigated, alongside aspect ratio, the ratio of the minor/major cell length, with results shown in Figure 88.

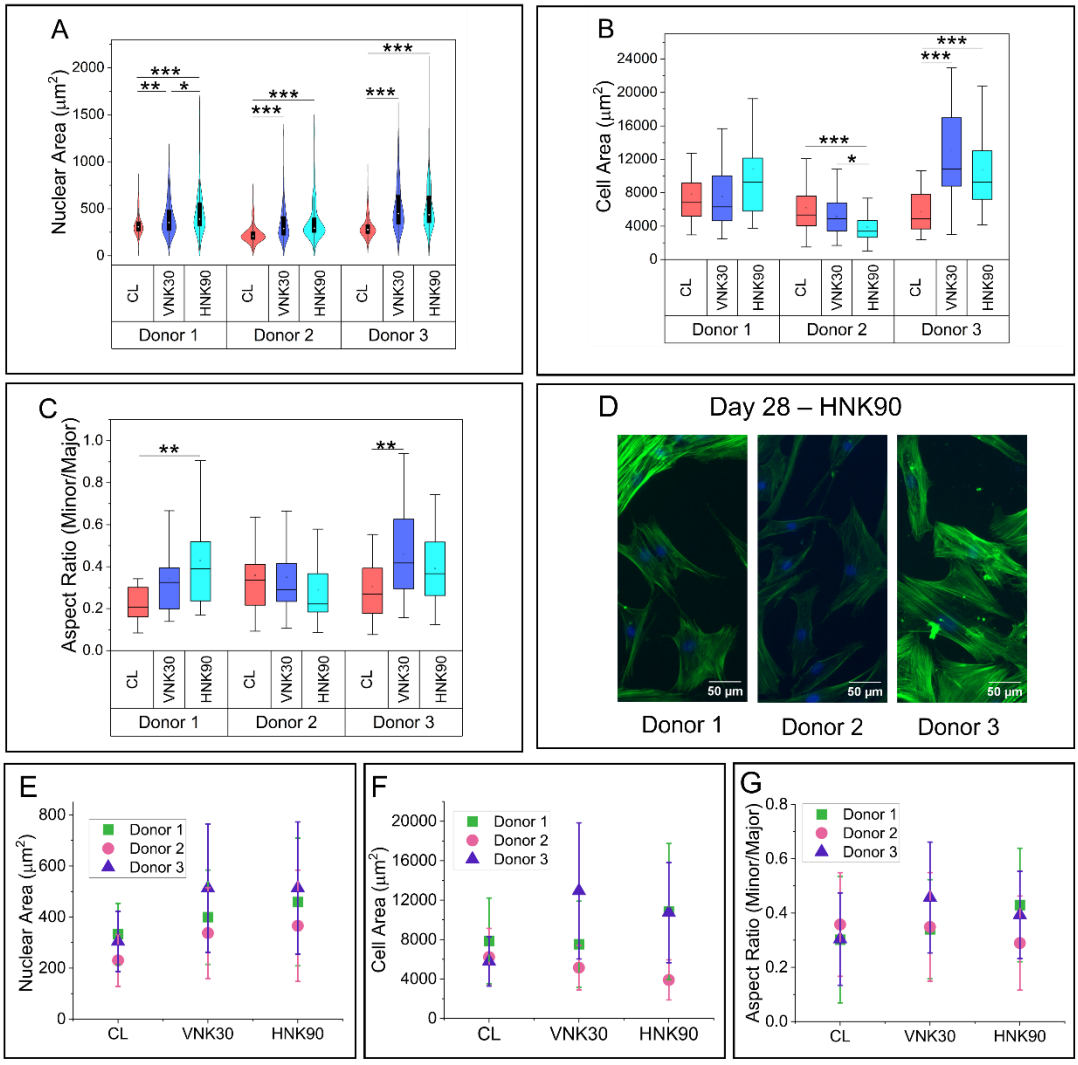

Figure 88: Morphology data for three MSC donors exposed to original nanovibration conditions (1kHz, 30 nm, vertical, VNK30) and optimised conditions (1 kHz, 90 nm, horizontal, HNK90). A) Nuclear area was found to significantly increase in all donors following vibration (N > 100). B) Cell area was only found to significantly increase in Donor 3 at both vibration conditions (N ≈ 30). C) Aspect ratio was found to be significantly increased in Donor 1 HNK90 samples and Donor 3 VNK30 samples (N ≈ 30). D) Combined images of actin (green) and DAPI (blue) staining in all three donors vibrated at optimal vibration conditions. Image brightness and contrast have been adjusted equally. Images taken using Zoe Fluorescent Cell Imager microscope. E) Combined donor replicates showing average nuclear area for each condition. F) Combine donor replicates showing average cell area for each condition. G) Combined donor replicates showing average aspect ratio for each condition. Statistical differences between donors not shown.

Nuclear area was found to significantly increase in all donors following vibration. Cell area was also shown to increase in Donor 3 vibrated samples, whilst

significantly decreasing in Donor 2 vibrated samples. Aspect ratio (the ratio between the minor and major axis of the cell) was also calculated, with an aspect ratio close to 1 indicating round cells with a circular morphology, whilst a ratio close to 0 would indicate longer, thinner cells. Aspect ratio was highest in Donor 1 when vibrated at the optimised conditions (HNK90), whilst in Donor 3, the original vibration conditions resulted in the highest response (VNK30).

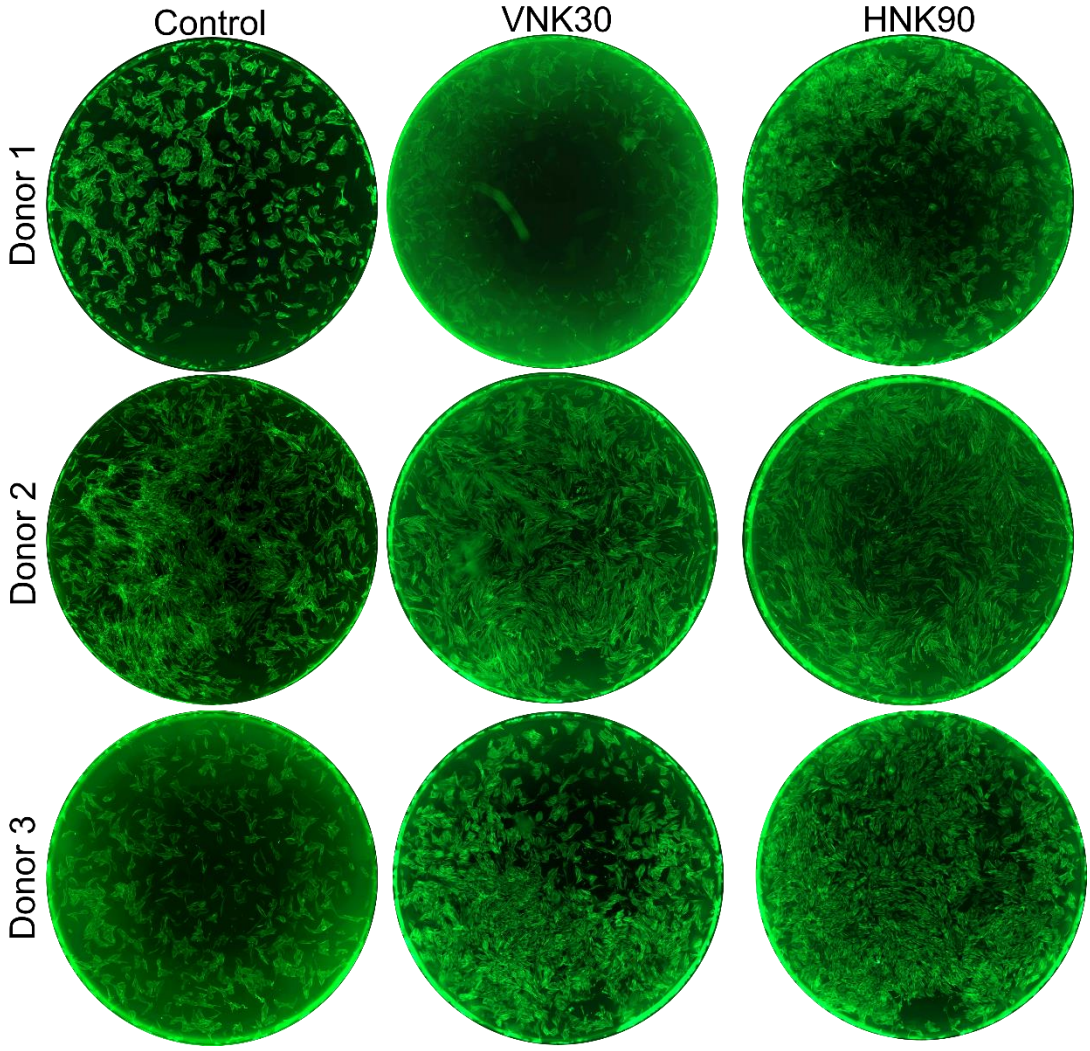

Figure 89: Whole well images for each donor at each condition showing actin staining. Each vibration condition and donor reveal different morphologies and proliferation in response to vibration, highlighting the different responses each donor will have to applied vibration conditions. Donor 1 VNK group shows reduced staining intensity due to actin degradation over time after staining. Images were taken using a Nikon (Eclipse Ts2) and were stitched together using ImageJ plugin Grid/Collection stitching [343]. Intensity of actin has not been enhanced equally in these images.

Nuclear area showed a consistent response across donors following exposure to vibration. This may be indicating that cells are flattening more in response to stimulation and as a result the nucleus is being stretched, increasing in area. Cell area and aspect ratio did not show consistent changes between donors, suggesting that the morphological response may be different between donors.

To illustrate the morphological differences observed between donors, actin and DAPI images of each condition were stitched together to obtain views of the whole well in ImageJ using the plugin Grid/Collection stitching [343]. Actin stained images shown in Figure 89 reveal very different morphologies between donors and at different vibration conditions. Donor 1 appears to have a more cuboidal morphology, whilst Donor 2 is more striated and lengthened. Donor 3 morphology appears to be somewhere between the two with cells showing more filopodia formation than observed in Donor 1. These images also give the opportunity to observe any cell alignment in response to horizontal vibration. Whilst none were observed across an entire well, Donor 2 did appear to show some group alignment across all three conditions. This may be due to the longer filamentous morphologies observed in this donor. It should be noted that the Donor 1 VNK30 image shows a reduction in actin intensity due to a delay between staining the cells and subsequently imaging them.

DAPI stained images, as shown in Figure 90, reveal the differences in proliferation between donors. Donor 2 showed a higher number of cells in each well compared to the other two donors. Vibration did appear to increase the number of cells in Donor 1 and Donor 3 samples, although not to the same levels at those seen in Donor 2. This increase in proliferation in Donor 2 may be due to the younger age of the donor. Previous studies have seen younger cells to tend toward proliferation whilst older cells differentiate in response to vibration [239]. This may explain the increased number of cells observed in Donor 2.

Morphologically, donors appear vastly different, responding to vibration in different ways, with the younger donor appearing to proliferate more than older donors, whilst nuclear area appears to increase consistently in cells vibrated at the optimal vibration conditions, other responses appear to vary across donors.

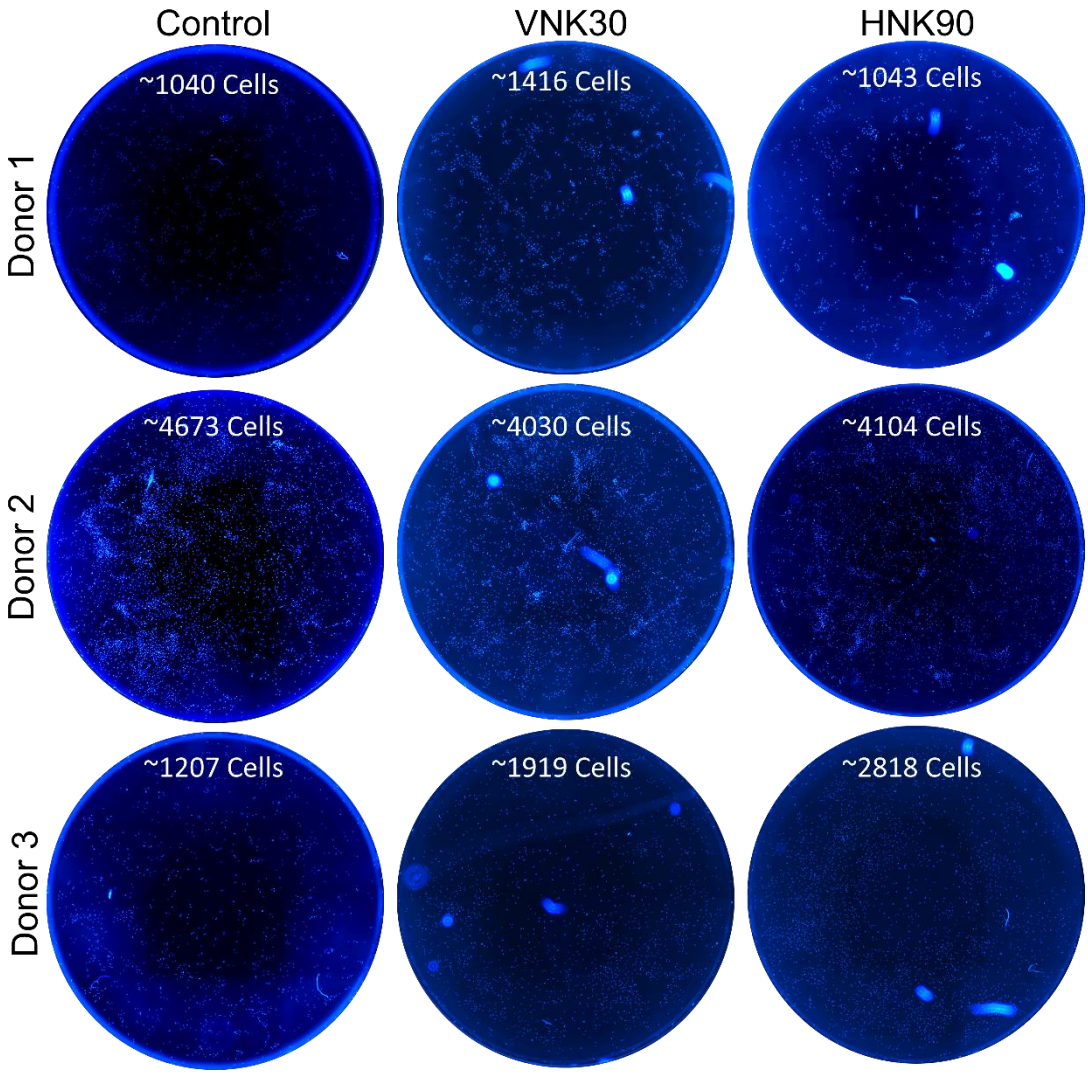

Figure 90: Whole well images of each donor at each vibration condition showing DAPI staining. Images show the range of proliferation response for each condition, highlighting the different responses each donor has to vibration. Images were taken using a Nikon (Eclipse Ts2) and were stitched together using ImageJ plugin Grid/Collection stitching [343]. Intensity of DAPI has not been enhanced equally in these images.

5.4.2 Mechanical response to stiffness across donors

To investigate the mechanical response of cells to vibration, AFM was used to measure the stiffness of the nucleus and cytoplasm in MSC donors prior to vibration and following 3, 24, 48 and 72 hours of stimulation. A non-vibrated control sample was also measured at the final timepoint. Results for all three donors are shown in Figure 91.

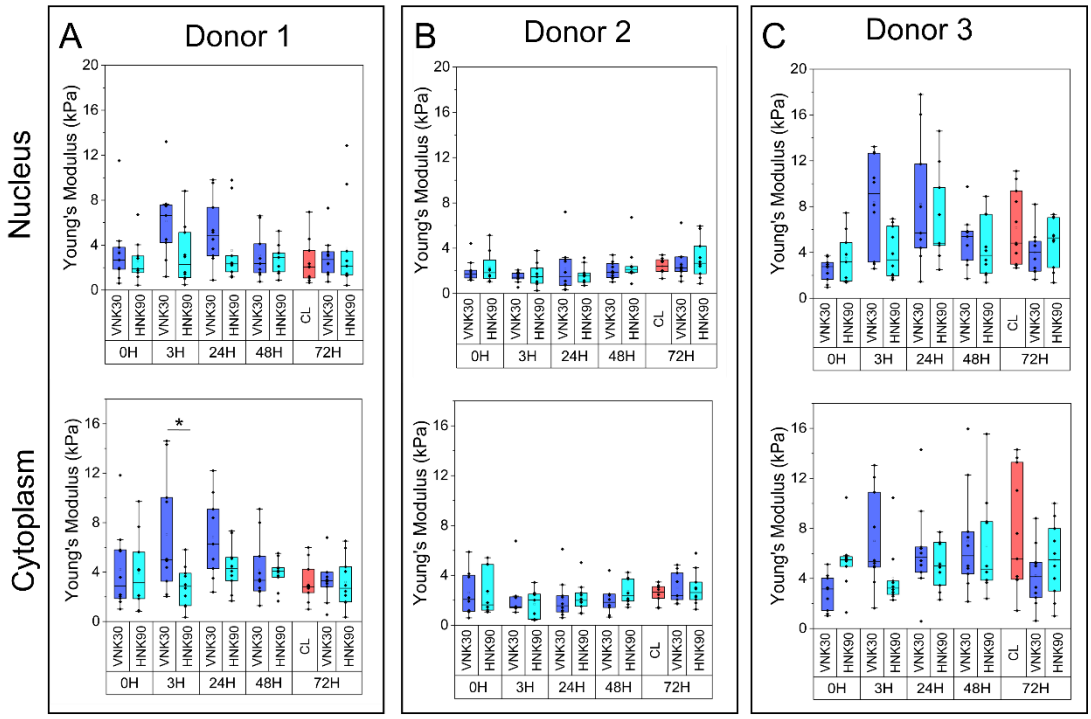

Figure 91: AFM results for three MSC donors measuring the nucleus and cytoplasm prior to vibration and after 3, 24, 48 and 72 hours of stimulation. A) Donor 1 showed a significant difference in the stiffness of the cytoplasm in vertically vibrated cells (VNK30) compared to the optimal horizontal conditions (HNK90). B) Donor 2 showed no significant differences in stiffness following vibration. C) Donor 3, whilst not significant, did show a slight increase in stiffness after 3 hours of stimulation in vertically vibrated samples (VNK30). (N = 10).

Only Donor 1 showed a significant difference between the two vibration conditions after 3 hours of stimulation, with the VNK30 sample resulting in a significantly higher cytoplasm stiffness than the HNK90 sample. Donor 2 did not show any significant changes in stiffness at any timepoint and was observed to have a lower stiffness than the other two donors. Donor 3, whilst not significant, did show a higher cytoplasm stiffness in the VNK30 sample compared to measurements taken prior to beginning stimulation. From these results, it appears that the mechanical properties of the cytoplasm were responding slightly more to vibration than the nucleus of cells. The results here did not show as significant a change in stiffness as had been seen in NIH 3T3 cells, however the stiffness of cells may indicate lineage commitment. Cells may not show mechanical changes until later timepoints during which cells may be committing

to an osteogenic lineage. Future experiments therefore ought to investigate a time-dependant link between mechanical changes in MSCs and lineage commitment to identify such a relationship.

5.4.3 Immunofluorescence data in response to optimised vibration conditions

Following fixation on Day 28, cells were stained for actin, OCN, vinculin and β-tubulin. Actin had been seen to increase in intensity in NIH 3T3 cells in correspondence with increased stiffness and nuclear area. OCN showed mixed results in MG63 cells, with no clear link between increased mechanosensitivity and OCN expression. Here OCN was measured again to observe if MSCs responded differently to MG63s. Vinculin was seen to increase in NIH 3T3 cells in correspondence with increased nuclear area and stiffness, suggesting that adhesion is also vital for a cell responding mechanically to vibration. Finally, β-tubulin, a protein involved in the polymerization of microtubules, is most commonly expressed in neurons and is widely used as a marker for neurogenesis. Here, it was used to indicate whether cells were expressing neurogenesis in response to vibration. Immunofluorescent results are shown in Figure 92.

Actin intensity was highest in Donor 3 at both vibration conditions. However, in Donor 1 it was significantly lower in the VNK30 sample and in Donor 2, in the HNK90 sample. OCN expression was found to be significantly lower at both vibration conditions in Donor 1. Vinculin and β-tubulin expression showed no significant differences within donor samples, however Donor 2 showed a lower expression than Donor 1 and Donor 3.

Here, the different responses between donor samples are evident. Whilst nuclear area was found to increase in all donors following vibration, other responses appear to vary widely between donors, with the younger Donor 2 forming less focal adhesions, actin fibres and expressing less OCN and β-tubulin than the older donors.

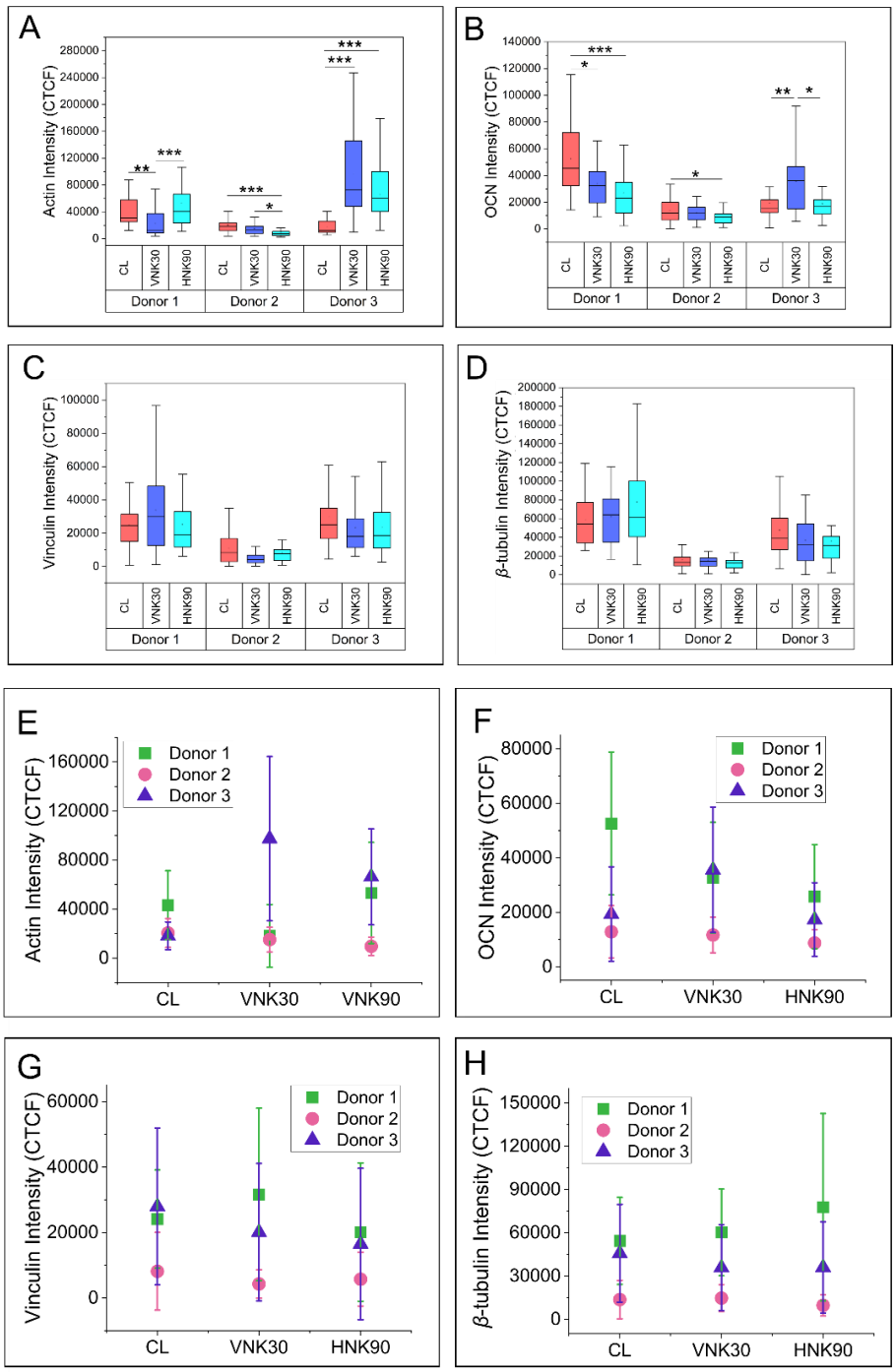

Figure 92: Intensity data for three MSC donors exposed to original nanovibration conditions (1kHz, 30 nm, vertical, VNK30) and optimised conditions (1 kHz, 90 nm, horizontal, HNK90). A) Actin intensity (N ≈ 30). B) OCN intensity (N ≈ 30). C) Vinculin intensity (N ≈ 30). D) *β*-tubulin intensity (N ≈ 30). E) Combined donor replicates showing average actin intensity for each condition. F) Combined donor replicates showing average OCN intensity for each condition. G) Combined donor replicates showing average vinculin intensity for each condition. H) Combined donor replicates showing average *β*-tubulin intensity for each condition. Statistical differences between donors not shown.

5.4.4 Gene expression in MSCs exposed to optimal vibration conditions

To determine the lineage commitment potential of MSCs, gene expression was analysed using qPCR. Cells were lysed at four timepoints: Day 7, Day 14, Day 21 and Day 28. Early osteogenic marker Runx2 was measured at Day 7 alongside neurogenic marker β-tubulin. Late osteogenic marker ON, chondrogenic marker Sox9 and adipogenic marker PPARγ were all measured at Day 28. Gene expression analysis data for these markers is shown in Figure 93. Two late stage osteogenic markers OPN and OCN were also measured at each of the four timepoints throughout the experiment with results shown in Figure 94. All data in Figure 93 and Figure 94 has been normalised to the non-stimulated control for that donor.

On Day 7, Runx2 gene expression was significantly increased in both Donor 1 and Donor 2 vibrated samples, with the highest response in cells vibrated at HNK90. Both donors also showed high expression of β-tubulin on Day 7 in both vibrated conditions, with the highest response again shown at HNK90. At Day 28, ON was not shown to be significantly higher in any vibrated samples compared to controls, however Donor 1 showed a significant decrease in expression in VNK30 samples. PPARγ expression was significantly increased in vibrated samples in Donor 2 with the highest response in the HNK90 samples. Sox9 expression showed a similar response with vibrated samples in Donor 2 showing significantly higher expression compared to controls.

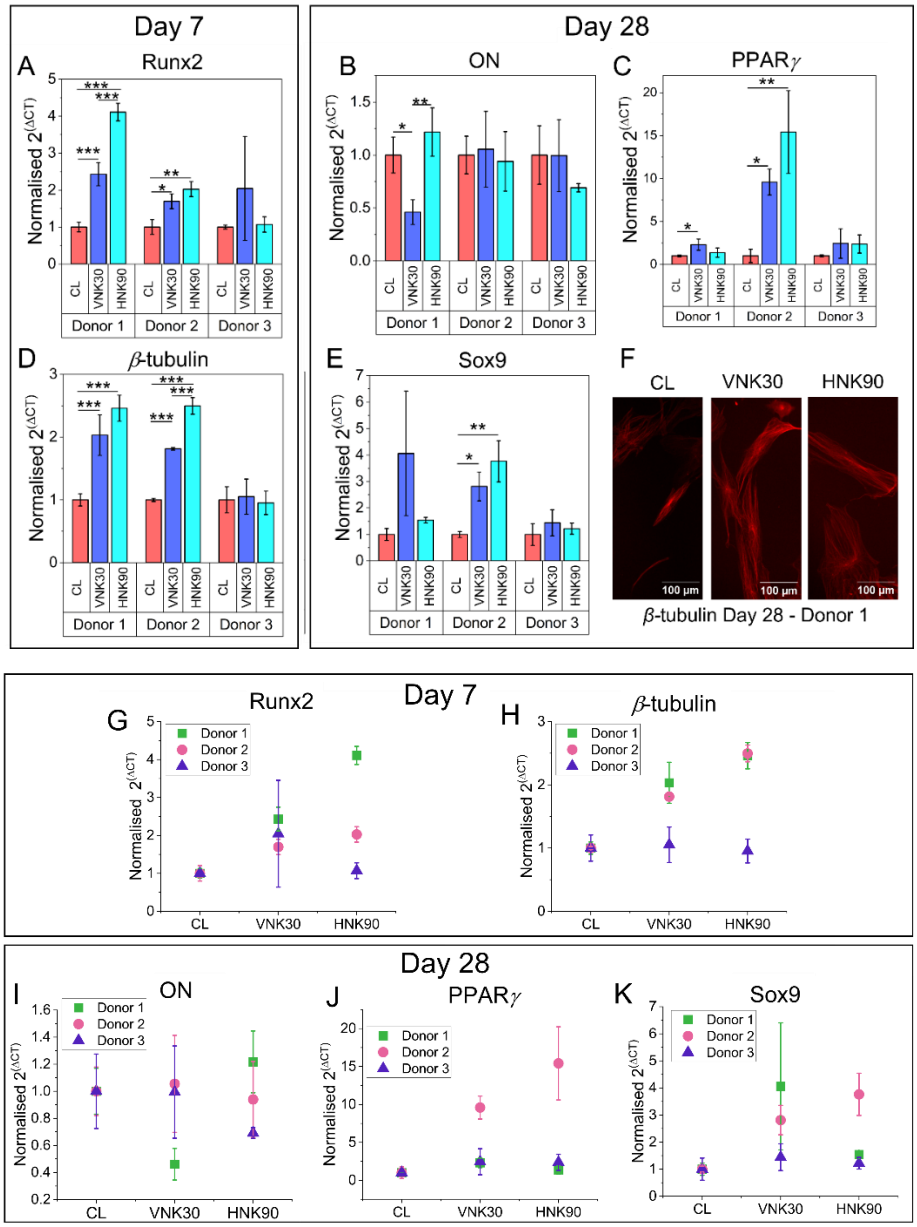

Figure 93: Gene expression data for three MSC donors exposed to original nanovibration conditions (1kHz, 30 nm, vertical, VNK30) and optimised conditions (1 kHz, 90 nm, horizontal, HNK90). Data normalised to each donor's respective control sample. A) Runx2 gene expression. B) *β*-tubulin gene expression. C) ON gene expression. D) PPARγ gene expression. E) Sox9 gene expression. F) *β*-tubulin staining on Day 28 in Donor 1 at all conditions. Images taken using a Zoe Fluorescent Cell Imager microscope, with brightness adjusted equally across images. G) Combined donor replicates showing average Runx2 expression for each condition. H) Combined donor replicates showing average *β*-tubulin expression for each condition. I) Combined donor replicates showing average ON expression for each condition. J) Combined donor replicates showing average PPAR*γ* expression for each condition. K) Combined donor replicates showing average Sox9 expression for each condition. Statistical differences between donors not shown. Error bars represent standard deviation (N = 3).

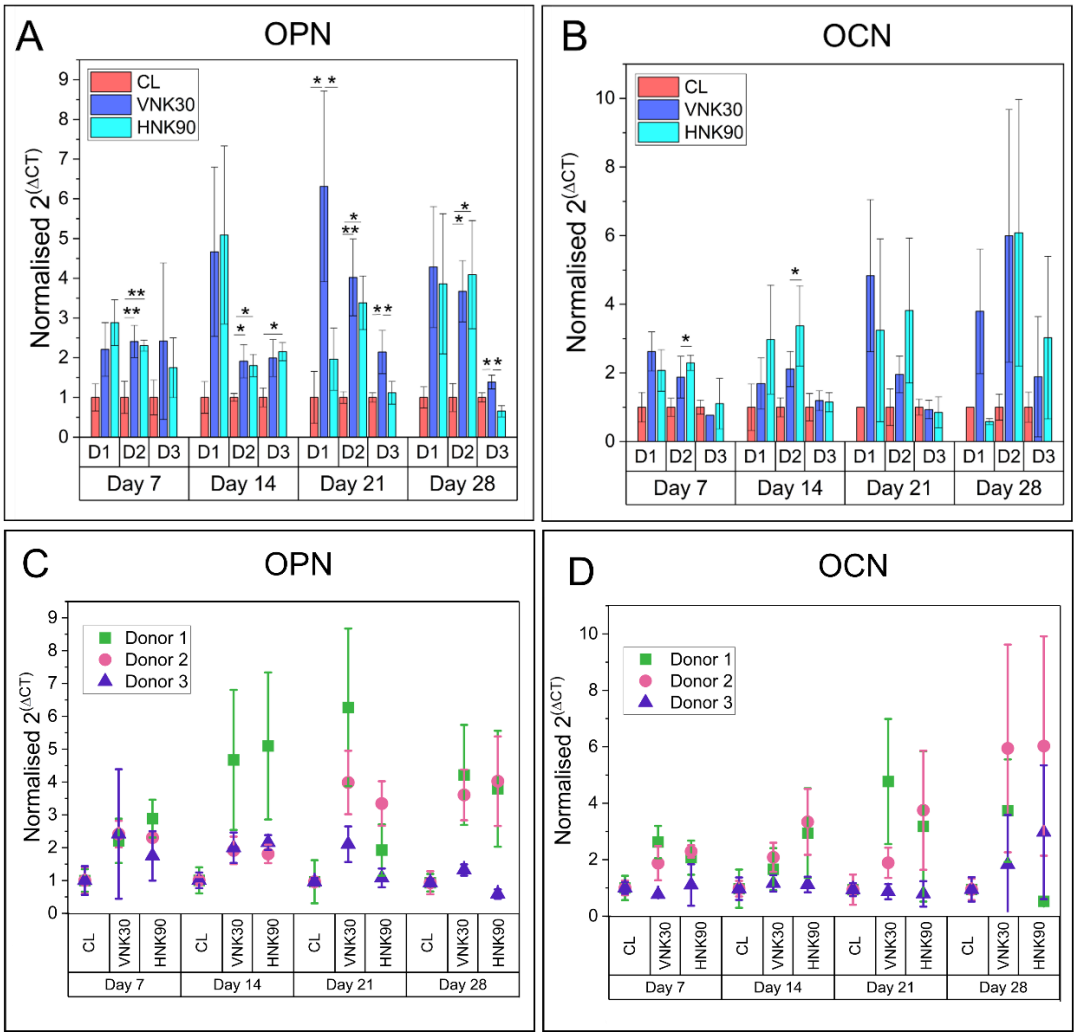

Figure 94: Time course analysis for OPN and OCN gene expression data for three MSC donors exposed to original nanovibration conditions (1kHz, 30 nm, vertical, VNK30) and optimised conditions (1 kHz, 90 nm, horizontal, HNK90). A) OPN gene expression B) OCN gene expression. C) Combined donor replicates showing average OPN expression for each condition. D) Combined donor replicates showing average OCN expression for each condition. Statistical differences between donors not shown. Each timepoint was conducted on one qPCR plate with all samples being normalised to the donor control at each timepoint. Error bars represent standard deviation (N = 3).

OPN was always expressed highly in Donor 1 in the NK30 samples at all timepoints measured, though not always significantly. Donor 2 consistently showed a significant increase in expression following vibration. Donor 3 showed some significant increases in expression following vibration, although it did not show as great a change in expression as Donor 1 and 2. OCN was seen to be

significantly higher in expression in HNK90 samples in Donor 2 compared to VNK30 samples at earlier timepoints. However, no significant differences were observed at later timepoints in any donor. There appears to be no correlation between OCN gene expression and protein expression at Day 28. This may be due to OCN protein expression peaking earlier in stimulation than the final timepoint.

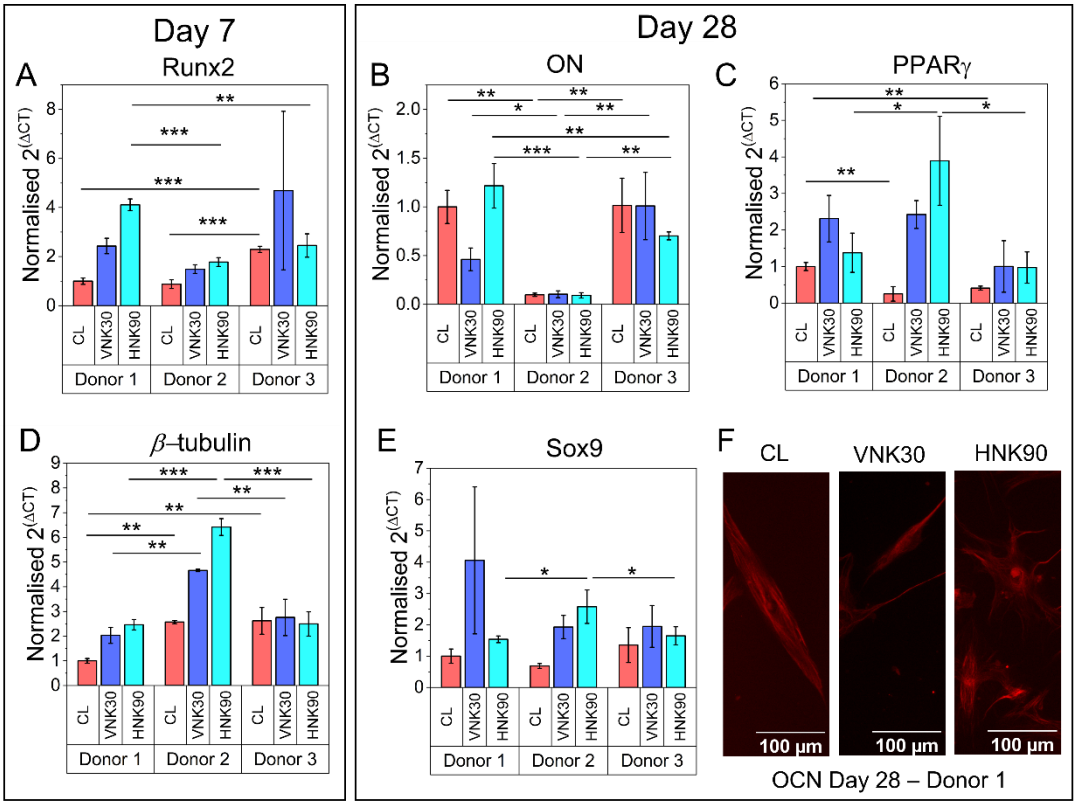

Figure 95: Comparing gene expression between donors. Three MSC donors exposed to original nanovibration conditions (1kHz, 30 nm, vertical, VNK30) and optimised conditions (1 kHz, 90 nm, horizontal, HNK90). A) Runx2 found to express highly in Donor 1 HNK90 samples at Day 7. B) *β*-tubulin highly expressed in Donor 2 vibrated samples at Day 7. C) ON expression much lower in Donor 2 than other donors at Day 28. D) PPARγ expression higher in Donor 2 than other donors on Day 28. E) Sox9 expression on Day 28. F) Immunofluorescent images of OCN on Day 28 in Donor 1. Images taken using a Zoe Fluorescent Cell Imager microscope, with brightness and contrast being adjusted equally in all images. Data has been normalised Donor 1 control. Error bars represent standard deviation (N = 3).

Whilst Figure 93 and Figure 94 are normalised to non-stimulated controls for each individual donor, Figure 95 and Figure 96 normalised all samples to the non-stimulated Donor 1 control sample. This enabled a comparison of gene response

across donors. HNK90 samples were significantly higher in Runx2 expression in Donor 1 than the other two donors on Day 7. β-tubulin showed the highest response in Donor 2 particularly in HNK90 samples. ON however had very low expression in Donor 2 compared to the other two donors. PPARγ was highly expressed in Donor 2 in both vibration conditions. Sox9 expression on Day 28 was significantly higher in HNK90 samples of Donor 2 compared to the other two donors. These results suggest that Donor 2 MSCs respond less osteogenically than other donors, tending toward a more adipogenic or neurogenic lineage in response to vibration.

Donor 1 showed the most consistent osteogenic gene response, with the highest expression of OPN at every timepoint measured in VNK30 samples. Donor 3 however showed the highest expression of OCN at Day 14, although no vibrated samples are significant against controls. Meanwhile Donor 2 showed a lower expression of OPN and OCN at most timepoints, indicating that this donor may have a lower osteogenic potential compared to the older donors.

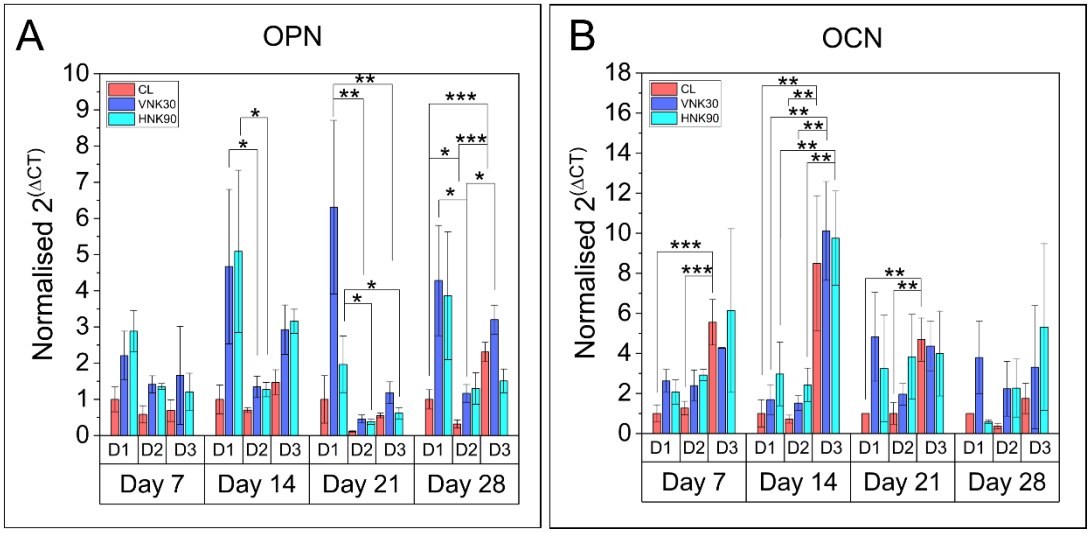

Figure 96: Comparing gene expression between donors. Three MSC donors exposed to original nanovibration conditions (1kHz, 30 nm, vertical, VNK30) and optimised conditions (1 kHz, 90 nm, horizontal, HNK90). A) OPN expression at four timepoints during vibration: Day 7, Day 14, Day 21 and Day 28. B) OCN expression at the same four timepoints. Data has been normalised Donor 1 control. Each timepoint was conducted on one qPCR plate with all samples being normalised to Donor 1 control at each timepoint. Error bars represent standard deviation (N = 3).

Gene expression analysis revealed different responses between donors to different vibration conditions and genes. Donor 1 showed a more osteogenic response to vibration, as observed in increased Runx2 and OPN expression. Whilst an increase in Sox9 expression was observed in cells vibrated at the original vibration conditions (VNK30), the optimised conditions (HNK90) did not show increased expression, indicating that these vibration conditions are more specific to bone, directing cells toward a more specific osteogenic lineage rather than also chondrogenic. Donor 2 meanwhile showed decreased osteogenic gene expression compared to other donors but showed a significantly increased expression of PPARγ following vibration. This may indicate that Donor 2 is more adipogenic than other donors. Finally, Donor 3 showed a lack of response to vibration. This may indicate that the two conditions used were not sufficient to induce any gene expression changes within the cell. To investigate whether the osteogenic responses observed in some samples led to any mineralisation, Alizarin Red analysis was conducted.

5.4.5 Mineralisation in MSC samples

MSCs were stained with Alizarin Red after 28 days of stimulation. Samples were quantified using a plate reader, with results shown in Figure 97. Alizarin red showed no significant differences within donor samples, however Donor 2 showed the highest expression of mineralisation in control samples. Donor 1 did show an increase in samples vibrated at the optimal vibration conditions, although not significantly. Donor 3 showed no increases in mineralisation in vibrated samples.

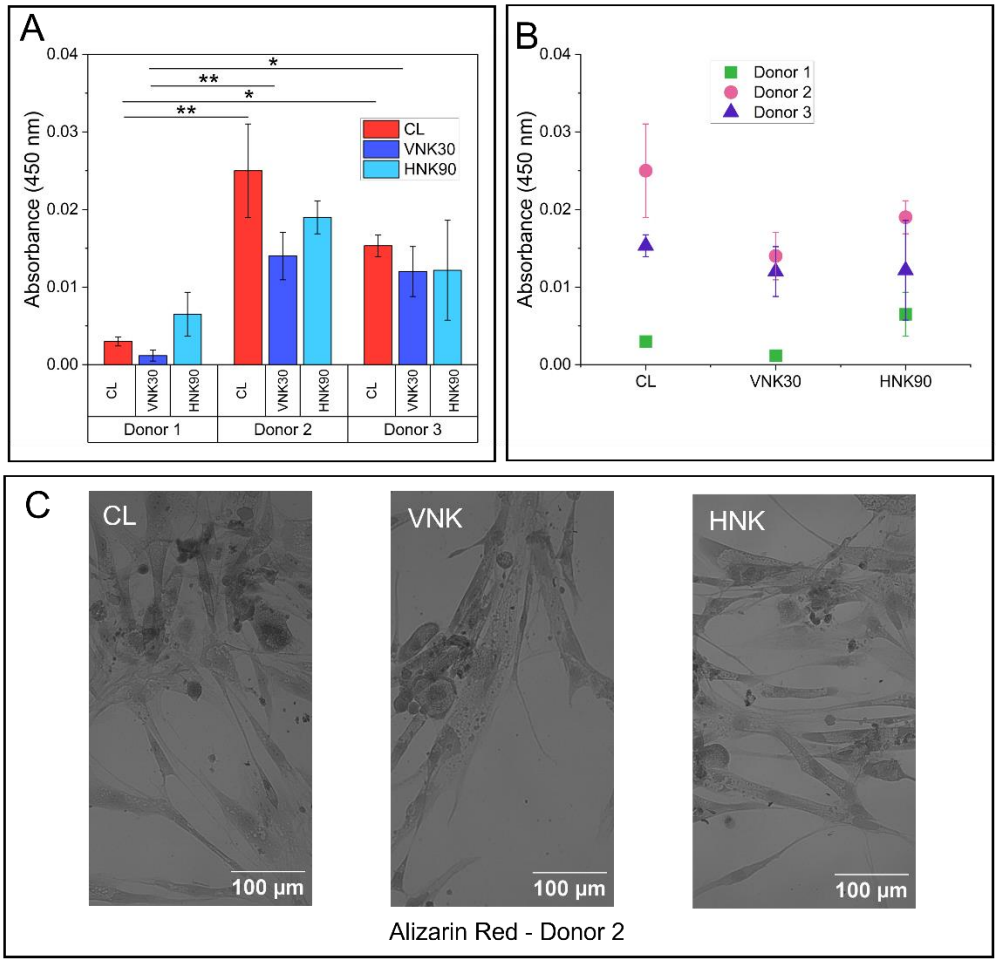

Figure 97: Alizarin Red analysis results for three MSC donors exposed to original nanovibration conditions (1kHz, 30 nm, vertical, VNK30) and optimised conditions (1 kHz, 90 nm, horizontal, HNK90) for 28 days, measured using a spectrophotometer (Thermoscientific Multiskan Go, Thermo Fisher). A) Quantified results of Alizarin Red staining. B) Combined donor replicates showing average Alizarin Red expression for each variable. C) Stained images of Alizarin Red in Donor 2 at each vibration condition. Images taken using a Zoe Fluorescent Cell Imager microscope. Error bars represent standard deviation (N = 3).

Whilst gene analysis of Donor 2 showed little response in osteogenic genes and a higher response in adipogenic and neurogenic genes, Alizarin Red staining shows higher mineralisation in Donor 2 samples. This may suggest that Donor 2 has a higher mineralisation potential than the other donors, which is not revealed in gene analysis. The lack of increase in mineralisation following stimulation in any of the donors may be due to the timepoint measured as mineralisation may be occurring later during vibration. It may also be that the vibration conditions used,

whilst producing an osteogenic response in Donor 1, are not sufficient to induce mineralisation in any of the donors used.

5.5 Discussion

In this chapter, the optimised vibration conditions obtained previously: 1 kHz, 90 nm, horizontal, continuous vibration were applied to three MSC donors. Morphology, immunofluorescence, gene expression and Alizarin Red were all measured to determine whether donors would respond to vibration equally.

Morphologically, nuclear area was found to increase in all donors vibrated at the optimal vibration conditions. Beyond this however, all donors responded differently. Cell area and actin intensity were only found to increase in Donor 3 cells vibrated at the optimal conditions. AFM did not reveal any significant changes in stiffness following vibration. This may be due to cells having not committed to a lineage within the first 72 hours of stimulation, and therefore later timepoints ought to be investigated to identify whether a relationship exists between mechanical changes within the cell and lineage commitment.

Meanwhile vinculin and β-tubulin staining intensity showed no changes in response to vibration. Gene expression did reveal increased Runx2 expression in two donors vibrated at the optimal vibration conditions at Day 7 and increases in OPN at Day 14 and Day 28. β-tubulin gene expression was found to increase in two donors in response to optimal vibration conditions at Day 7, although this did not lead to an increase in protein expression by Day 28. Sox9 was seen to significantly increase in Donor 1 cells vibrated at the original vibration conditions however the optimal conditions did not show a significant increase suggesting that the optimised conditions do not direct cells toward a chondrogenic lineage. Whilst gene expression was positive in promoting osteogenesis in the MSC donors, mineralisation was not found to increase in any vibrated samples within donor groups.

The donors all responded differently to vibration. The younger cells, Donor 2, showed a significant increase in PPARγ expression in response to vibration not

observed in the other two donors. This donor also showed a reduced expression of late osteogenic markers ON, OCN and OPN as compared to the other donors, but did show an increased expression of Runx2 following stimulation. The highest expression of mineralisation was also observed in Donor 2. Donor 2 was also found to proliferate more than older donors, which has been observed previously. The different morphologies observed in Figure 89 between donors also indicates the difference between cell donors in both their potential and response to vibration. Taken together, this may indicate that younger donors may have a higher proliferation potential and may be responding to vibration initially directing towards an osteogenic lineage, however prolonged vibration may be directing cells toward an adipogenic lineage. These cells may also have higher mineralisation capabilities than the older donors which is unaffected by vibration.

Whilst the optimised vibration conditions did induce a positive osteogenic response in Donor 1, the more adipogenic and neurogenic response observed in Donor 2 and the lack of gene expression changes observed in Donor 3 may indicate that the vibration conditions used do not result in a universal response between donors. Whilst no significant gene expression changes were observed in Donor 3, morphologically, actin intensity and cell area were significantly higher in vibrated samples. This may indicate that Donor 3 is more responsive morphologically to vibration, however this does not translate into gene expression changes. This may indicate that changes in actin intensity and nuclear area are not linked with an osteogenic response. Cell morphology has been shown to determine lineage commitment, with rounder cells undergoing adipogenesis and more spread out cells undergoing osteogenesis [103]. Although Donor 3, whilst showing an increased cell area, did not show an increased osteogenic gene expression, Donor 2 did show an increased adipogenic gene expression alongside a smaller cell area following stimulation.

The variability in responses observed between donors underscores the need for a deeper understanding of how factors such as donor age, gender and ethnicity (not explored here) influence cellular responses to vibration stimulation. To

optimise vibration conditions for inducing osteogenesis across different donors, a more comprehensive analysis that considers these differences will be essential. Increasing the number of donors will help determine the extent to which optimised vibration conditions can continuously elicit and osteogenic response. A more detailed understanding of the variations between donor groups will be crucial to maximise the effectiveness of nanovibration to induce osteogenesis across diverse populations.

Chapter 6:

Discussion

6.1 Introduction

Stem cell therapies are quickly becoming realised as a viable method of treatment for a range of conditions, including osteoporosis, cardiovascular disease and neurodegenerative diseases such as Parkinson's and Alzheimer's [1]. Controlling stem cell differentiation *in vitro* may be done using chemical factors, however mechanical stimulation is increasingly being explored, particularly vibrational stimulation. Using vibration to direct cell response may be easier to translate into wearable devices than other forms of mechanical stimulation, and when developing cell therapies, vibrational stimulation enables the use of regular cultureware often within an easy-to-use platform. However, between studies, vibration conditions vary widely, making it difficult to identify parameters leading to desired cell responses. Without this, it is difficult to develop reliable cell engineering techniques using vibrational stimulation, which are effective in directing stem cell differentiation toward specific lineages.

Many vibration studies fail to investigate a range of vibration conditions to optimise differentiation in cells. Pre *et al* did do some amount of optimisation prior to application of vibration on MSCs [235]. SAOS-2 cells were stimulated at multiple frequencies (between 1 and 120 Hz) to determine the optimal frequency for differentiation (30 Hz). Following this, multiple durations of vibration (15, 30, 45 and 60 mins/day) were tested before the optimal durations were selected (45 and 60 mins/day) [235]. These optimised vibration conditions were then applied to human BM-MSCs and ASCs to induce osteogenesis [234, 236]. Whilst showing a level of optimisation, only frequency and duration of stimulation were optimised in these studies. No investigation was conducted into amplitude or direction of stimulation (11 mm, vertical vibration was used). Equally, the two higher durations of vibration were found to illicit the strongest osteogenic

response, and yet no further investigations were carried out into longer durations of stimulation.

Without more thorough investigation into the optimisation of vibration conditions for cell response, it may be that many studies are failing to realise parameters that could be adjusted to maximise a desired response. Indeed, there have been some studies who have inadvertently inhibited a desired cellular response following the application of vibration. Lau *et al* applied vibration of 60 Hz, 0.3 G for 60 minutes/day, for 6 days to rat MSCs and instead of observing an expected increase in osteogenesis, saw matrix mineralisation to be inhibited and a decrease in osterix expression [266]. However, these conditions were not thoroughly tested on cell response and were instead chosen based on *in vivo* animal studies [344-346]. The vibration conditions used in these animal studies applied different frequencies and different durations of vibration (10-20 mins/day) to the limbs of animals. Transmission of vibration through the body would result in different vibration conditions being experienced by cells within the bone [347]. Therefore, the vibration conditions applied *in vitro* by Lau *et al* are not comparable to animal studies, and based on this, it was likely that ideal vibration conditions were not used here [266]. Additionally, cell experiments were only run for a period of 6 days, during which only early osteogenesis would occur, yet the authors investigated late stage osteogenic markers (OPN and OCN) and matrix mineralisation, all of which are unlikely to occur so early in osteogenic differentiation [287, 348]. Without systematic optimisation of vibration conditions in studies, it cannot be expected that the observed results are the optimal response.

Many studies using vibration to induce osteogenesis, only consider vertical vibration (perpendicular to cell monolayer), however studies which have compared horizontal and vertical vibration have found horizontal vibration (parallel to the cell monolayer) to result in a higher osteogenic response in cells [271, 274]. Limiting vibration conditions to a single direction may be restricting the potential responses in cells. When comparing directions of vibration, it is essential to ensure that cells are being stimulated in only the desired direction,

as was done by Halonen *et al* who developed and thoroughly tested a device capable of vertical vibration (with low levels of horizontal vibration) and horizontal vibration (with low levels of vertical vibration) [274].

There may effectively be unlimited combinations of duration, frequency, amplitude and other vibration conditions that could be tested. No singular study would find the optimised settings without 1) determining underpinning trends or 2) working across multiple research groups/settings in a standardised way. It is however essential that vibration conditions are optimised within the limitations of devices being developed to ensure experiments are maximising the potential response of cells.

Alongside the lineage of interest, it is also crucial to investigate multiple responses from cells to identify whether the observed response is singular, or cells are being directed toward multiple lineages. The few studies which have investigated at least two lineages, have also used different vibration conditions to identify whether different conditions result in different responses from cells [237, 259, 263]. However, such studies used chemical factors to induce lineage response alongside vibrational stimulation making it particularly difficult to determine whether the response observed is due to vibration or chemical induction. Studies ought to at least have additional samples stimulated in the absence of chemical factors, whilst also investigating a range of potential lineages. Some studies, such as Safavi *et al* have investigated two lineages (osteogenic and chondrogenic) at a single vibration conditions whilst in the absence of differentiation media, making it more reliable to claim responses observed are due to vibrational stimulation [251].

Once vibration conditions have been optimised (in the absence of chemical factors) it is essential to test multiple stem cell donors to identify whether vibrational stimulation results in the same response. To move the technology forward to a clinical or industrial setting, this must be done *in vitro* to identify whether donors of different ages, genders and ethnicities will respond similarly to vibration. Studies such as Halonen *et al* tested four donors and quantified the effects of vibration on different donor response. Ambattu *et al* went further by

applying vibration conditions to MSCs from three sources, bone marrow, adipose tissue and umbilical cord [285]. This is equally important to determine whether viable tissue sources will respond in the same manner.

Noting the importance of 1) testing multiple vibration conditions to maximise cell response, 2) investigating multiple lineages to ensure the cells are directed as desired and 3) using multiple cell donors, this current study carried out a systematic optimisation (within device limitations) of nanovibrational stimulation.

6.2 Device Development

Whilst a range of frequencies and amplitudes could be easily tested using a signal generator and amplifier, and intermittent vibration could be investigated by only putting cells on a device for short periods of time, for directionality experiments, a new horizontal device had to be designed. ANSYS models of cells identified that the level of stress experienced by cells differs between directions of applied vibration. This may lead to changes in signalling and may indicate that cells respond differently to vibration applied horizontally compared to vertically.

There have been many horizontal devices designed to apply vibration horizontally to cells. Some, early devices were bulky and incompatible with incubators [267]. Devices such as that developed by Lorusso *et al* mounted a horizontal vibration device to an inverted microscope. Whilst this allows for microscopy to be used during applied stimulation, it does involve removing cells from the incubator which may affect their characteristics and as a result, their response to vibration. In line with other horizontal devices that have been developed (and our own vertical device), we decided to design a device that would remain within an incubator throughout stimulation [42, 237, 274, 297].

Some devices, such as that developed by Pre *et al* applied both vertical and horizontal vibration to cells simultaneously, making it impossible to determine whether observed responses are due to vertical, horizontal or a mixture of the two vibrations [235]. Most other studies however did apply vibration only

horizontally, although some studies do not specify whether vertical vibration is quantified during horizontal motion [42]. Halonen *et al* do quantify both horizontal and vertical vibration, ensuring that the opposite is minimized during stimulation [274]. This was deemed to be essential when developing the horizontal nanovibration device to ensure observed responses were due to the direction of applied vibration. Whilst most devices also calibrated using accelerometers, the design described in Chapter 2 instead used laser interferometry, providing a more precise and reliable method of measuring amplitude.

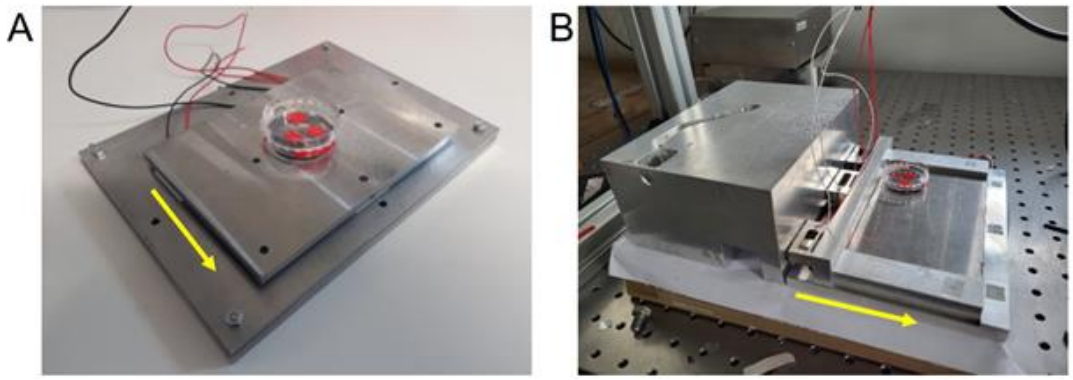

Figure 98: Two final horizontal devices used for directionality experiments. A) Shear piezo device with shear piezoelectric actuators attached between two metal plates, driving vibration horizontally as indicated by arrow. B) Cradle design using standard piezoelectric actuators attached to base block driving horizontal vibration as indicated by arrow.

We developed a novel horizontal vibration device (Figure 98) that represents a significant advancement over previously reported designs, such as that described by Enomoto *et al* [250]. While their devices utilised a piezoelectric stacked actuator positioned between a base block and dish holder, allowing for the horizontal stimulation of a single 35 mm dish or standard 96-well plate, our design offers substantial improvements in functionality and scalability. Specifically, our device employs piezo actuators (with previously designed custom holders) mounted to a base block, which drive vibration through a cradle. Unlike Enomoto's setup, our device supports a larger surface area for vibration, enabling simultaneous stimulation of up to six 35 mm Petri dishes or a single plate using just three piezoelectric actuators [250]. This innovation enhances

experimental efficiency and scalability, facilitating larger-scale studies with fewer components and significantly reducing setup complexity. Importantly, this design addresses a critical gap in horizontal nanovibrational stimulation technology and enables broader applications in cell culture research.

While the prototypes designed successfully produced consistent horizontal vibration and were effectively utilised in cell experiments, both devices were limited by their reliance on an external signal generator and amplifier to supply power, rather than a dedicated, purpose-built PSU. To enhance the practicality and portability of the device, developing an integrated PSU would be highly beneficial, enabling a more compact and user-friendly design. Additionally, the current platform for cultureware attachment is limited in size, accommodating only half the capacity of a standard vertical vibration device. Expanding this platform would allow for larger-scale experiments and increased throughput, which should be a key consideration in future iterations of the device. These improvements will further advance the applicability and versatility of the device for research and clinical purposes.

6.3 The impact of nanovibrational stimulation on cells

To thoroughly test the effects of nanovibrational stimulation, four cell types were used. Initially murine NIH 3T3 cells provided a good model for observing morphological and mechanical changes within the cell, allowing for initial identification of stiffness changes following vibration and for modification of immunofluorescent staining and morphological analysis. Following on from this, human MG63 cells provided a useful model of osteogenesis, allowing the further investigation of cell response in gene expression changes following the vibration. This enabled the testing of multiple vibration conditions to identify key parameters for optimizing osteogenesis. Morphological and mechanical changes previously observed in NIH 3T3 cells were also analysed here to identify any correlation between these visible changes and osteogenic responses. MG63s have limitations, therefore it was important to test vibration conditions on MSCs to confirm cells would respond as expected.

Table 17: Comparison of responses to nanovibrational stimulation between cell types investigated in this study

Cell Type	Observed Responses to Nanovibrational Stimulation
NIH 3T3s	Increased nuclear area Increased actin intensity Increased stiffness within 24 hours
MG63s	Increased nuclear area Increased Lamin A/C following 90 nm horizontal vibration No increase in actin intensity Some increases in cytoplasm stiffness Increased osteogenesis at higher amplitudes
SH-SY5Y	Lower amplitude increases β-tubulin protein intensity after 7 days Decreased expression of NeuroD1
MSCs	Increased nuclear area Higher stiffness in older donors with vertical vibration showing increased response Some donors show increased cell area and actin intensity Mixed adipo/osteo response in younger donors

BM-MSCs from three human donors were subjected to typical nanovibration conditions (1 kHz, 30 nm vertical vibration) and the optimised conditions as identified during MG63 experiments to investigate donor variance [67, 139]. Neuroblastoma cells (SH-SY5Y) were also used to investigate the potential neurogenic effect of nanovibrational stimulation (see Appendix A). A comparison

of the responses to nanovibrational stimulation between all four cell types is summarised in Table 17 whilst a visual summary of the aims/hypotheses and findings of this study is shown in Figure 99.

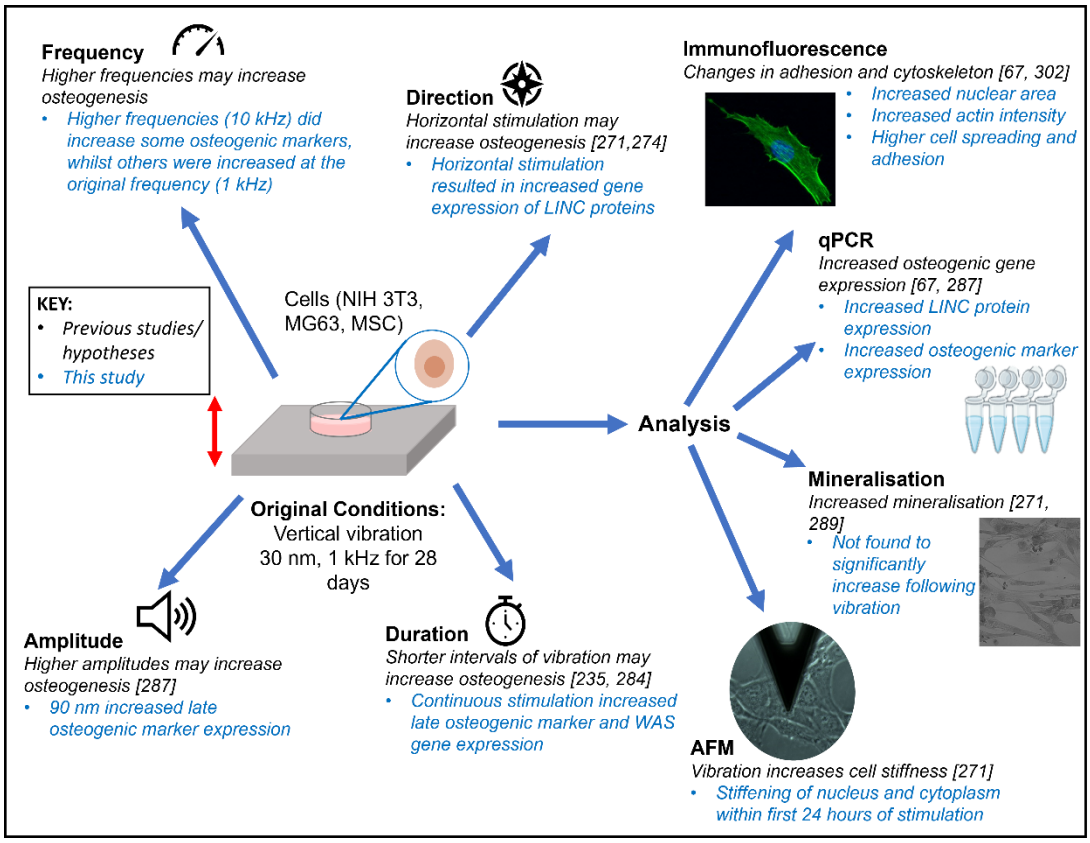

Figure 99: Summary of aims/hypotheses and the findings of this study. Four main parameters were explored: frequency, amplitude, direction and duration of vibration. Analysis was carried out using immunofluorescence, qPCR, mineralisation (Alizarin Red) and AFM.

6.3.1 Relationship between morphological and mechanical changes in cells

In NIH 3T3 cells, nuclear area was seen to increase in response to nanovibrational stimulation, which has been seen previously in MSCs [302]. Increases in nuclear area may indicate increased cellular or cytoskeletal tension within the cell in response to vibration. Whilst nuclear area was not seen to increase as reliably in MG63 cells, optimised vibration conditions did see an increase in nuclear area in all three MSC donors. Previous studies have linked an increase in nuclear size to elevated Lamin A/C expression in human embryonic stem cells [349]. Consistent

with this, this study observed a concomitant increase in both nuclear area and Lamin A/C in MG63 cells stimulated horizontally at higher amplitudes. Lamin A/C expression is known to scale with nuclear stiffness, yet despite the observed increases in Lamin A/C under certain conditions, this did not correlate with increased nuclear stiffness in MG63 cells [173, 350, 351]. Given that reduced Lamin A/C expression inhibits osteogenesis, while increased expression suppresses adipogenesis in BM-MSCs, these findings underscore the critical role of Lamin A/C in MSC differentiation [351-353]. Importantly, this study is the first to explore the response of the LINC complex to nanovibrational stimulation, revealing its potential involvement in mechanotransduction and nuclear remodelling.

Actin staining intensity was also observed to increase in NIH 3T3 cells, indicating enhanced cytoskeletal formation. This corresponded with an increased stiffness within the first 24 hours of stimulation, as well as an increase in nuclear area. These findings suggest that the cell may spread and flatten in response to vibration, generating actin filaments that exert tension on the nucleus, thereby increasing cellular stiffness. This study is the first to observe such rapid stiffness changes in cells following nanovibrational stimulation, whilst also indicating a potential interplay between nuclear morphology, cytoskeletal formation and cell tension.

Conversely, MG63 cells did not show an increase in actin intensity at timepoints measured. Whilst stiffness measurements did show an initial increase in cytoplasm stiffness within the first 3 hours of stimulation, measurements of actin intensity were not taken at this timepoint. The nucleus did not show any increases in stiffness within the first 24 hours of stimulation, corresponding with no observed increases in nuclear area. MG63 cells indicated an alteration of LINC genes in response to vibration which correlated with changes in nuclear morphology. This may be linked to changes within the actin cytoskeleton and overall cell stiffness, however measurements for each of these responses were not taken at the same timepoint. Further investigation into the relationship of the

LINC complex, nuclear morphology and overall cell stiffness may reveal the role of LINC proteins in cell response to nanovibrational stimulation.

In MSCs, Donor 3 showed an increase in nuclear area and actin intensity, which may indicate the potential for increased cellular stiffness. It is well known the importance of the actin cytoskeleton in maintaining cell mechanics [354, 355]. Likewise, drugs disrupting actin formation lead to a decrease in cell stiffness [356]. Here, nanovibrational stimulation was shown to increase both actin formation and nuclear and cytoplasm stiffness within 24 hours of stimulation. The increase in stiffness observed within the nucleus agrees with previous studies showing that the nucleus accounts for 69.7% of the overall stiffness in MSCs, whilst the increased stiffness observed within the cytoplasm may be due to increased actin formation [357]. Additionally, an increase in stiffness has been suggested to correlate with an increased osteogenic response in MSCs [271].

Whilst experiments conducted here did show an elevation in cell stiffness of vibrated MSCs, the changes were not consistently significant. AFM measurements however were only taken within the first 72 hours of stimulation, whilst morphological changes were investigated following 28 days of vibration. This makes it difficult to determine a relationship between morphological and mechanical changes within MSCs in response to vibration. Additionally, the lack of concurrent AFM and gene expression measurements limits the ability to confirm whether early stiffening correlates with increased osteogenic differentiation.

Future investigation should include a full-time course study to determine whether a relationship between morphological and mechanical changes exists in MSCs, and also whether an increased stiffness correlates with increased osteogenic expression. Furthermore, the lower response observed in MG63s compared to MSCs highlights the importance of conducting experiments on primary cell lines and not relying too heavily upon immortalised cell lines.

Sample sizes for all morphological measurements with the exception of nuclear area and Sun1 intensity were $N > 30$. AFM also contained small sample sets of N

= 6. Due to this, it is difficult to obtain an overview of the behaviour of all cells to nanovibrational stimulation. In an attempt to increase the sample set size, deformability cytometry was conducted with a sample set size of N > 1000. However, results showed no significant increase in the stiffness of nanovibrated cells in contradiction to what had been observed previously. Whilst a useful, high throughput technique, deformability cytometry requires further optimisation for it to be used confidently in assessing the mechanical characteristics of adherent nanovibrated cells. In addition to a low sample size, morphological measurements were also conducted on isolated cells (or those with low cell-to-cell contact). This may have an impact on results observed and may not be reflective of all cells within the samples.

6.3.2 Identifying key vibration conditions for osteogenic differentiation

The primary aim of this work was to identify key vibration conditions that promote osteogenesis in MSCs. Previous vibration studies have used a wide range of vibration parameters on a variety of cell types to induce a response (see Appendix A), without a thorough systematic evaluation of vibration conditions being studied. Studies that do test multiple conditions, tend to focus on frequency optimisation, often without fully isolating the effects of amplitude.

The findings here challenge the notion that frequency has a greater effect on cell response than amplitude. Frequencies ranging from 100 Hz – 10 kHz were found to result in little difference in cell responses. This was consistent with the inconsistency observed across the literature. Studies appear to widely disagree on the optimal frequency for osteogenesis, with a wide range of vibrations applied at 25 Hz – 10 MHz showing an osteogenic response (see Appendix A) [257, 285]. However, these studies often simultaneously adjusting amplitude, making it difficult to separate the two components [238, 254, 259, 263, 290]. Studies identifying different lineages at different frequencies, whilst using lineage specific media to induce differentiation, do tend to identify osteogenesis as occurring at the higher frequency tested [237, 259]. Yet, studies often contradict

one another, such as those by Zhao *et al* and Zhou *et al* who, whilst using different vibration durations, found the same vibration conditions to induce both adipogenesis and osteogenesis respectively in rat MSCs [262, 291].

These inconsistencies highlight the importance of systematically investigating lineage-specific responses after stimulation, particularly in the absence of chemical factors that drive both osteogenesis and adipogenesis. The data suggests that frequency alone may not play a dominant role in directly inducing osteogenesis but may exert its effects more strongly when combined with specific amplitudes, with the resultant accelerative force (Equation 1) being a more critical factor.

Here, we demonstrated that whilst frequency did not significantly impact osteogenic differentiation, higher amplitudes were consistently shown to enhance osteogenic responses in MSCs and bone-like cells. This agreed with previous results which had seen an increase in osteogenesis in MSCs exposed to 90 nm compared to 30 nm [287]. Although amplitudes ranging from the nanometre to millimetre scale have been reported to induce osteogenesis, studies applying lower amplitudes often employ higher frequencies [251, 285, 287]. Thus, the combination of higher amplitudes with these frequencies may further enhance the osteogenic effect. To understand this further, future studies should systematically investigate the interplay between frequency and amplitude, testing a broad spectrum of frequencies (eg. 1 Hz to 1 MHz) and amplitudes (nm to mm). Since the force exerted on cells during vibration is a function of both frequency and amplitude, these variables cannot be studies in isolation. Understanding their combined effects is essential for optimising nanovibrational conditions to optimise osteogenic responses.

Nanovibrational stimulation has typically been applied continuously to cells, however few other vibration studies stimulate cells continuously [42, 139, 264, 287]. Most studies typically induce osteogenesis in cells by stimulating them for periods of less than one hour per day [234, 270, 285, 318]. Other studies have more complex vibration regimes involving an off period in between bouts of stimulation [249, 271]. In one study, osteogenesis was found to increase after

only 10 minutes of stimulation [284]. However, no prior research has investigated the effect of intermittent nanovibrational stimulation, making this the first study to explore whether shorter durations of nano-vibration could elicit a comparable or enhanced osteogenic response relative to continual stimulation.

In Chapter 4 and Chapter 5, MG63s and MSCs were stimulated for 4 hours/day, 5 days/week to investigate whether intermittent vibration would increase osteogenesis compared to continuous vibration. Whilst MG63 results were inconclusive, MSCs showed an increased response when vibrated continuously. This suggests that intermittent vibration may not optimise osteogenesis, however tests were not thorough here, and further investigation into intermittent vibration and pulsed vibration ought to be conducted. Development of future wearable vibration devices would ideally not require users to undergo continuous stimulation, and therefore extensive cell experiments investigating whether vibration dosage could be shortened are essential.

Previous studies have also used a range of directions for vibration. Few have compared the effects of vertical and horizontal vibration on cell response, however those that do have found horizontal vibration to drive increased osteogenesis [271, 274]. This study has built upon these findings, demonstrating that horizontal nanovibration not only promotes osteogenesis in MSCs but also upregulates mechanosensitive nuclear genes in MG63 cells. FEA models further support this, predicting higher stress on the cell membrane and nucleus during horizontal vibration. This aligns with increased stiffness in MSCs reported by Pongkitwitoon *et al* [271]. Whilst MG63s and MSCs did not show an increase in stiffness following horizontal vibration compared to vertical, it may be that too early a timepoint was investigated for any mechanical changes to have been observed. Despite this, these findings underscore the importance of further investigation into the effect of horizontal vibration on the mechanical properties of cells.

From these experiments, the optimised vibration conditions were identified as continuous horizontal vibration at a 1 kHz frequency, 90 nm amplitude. As discussed, more systematic optimisation would be necessary across a wider

range of frequencies and amplitudes, as well as further study into duration of vibration and the effects of horizontal vibration to identify whether these vibration conditions may be further optimised.

In addition to investigating osteogenesis in MSCs, this study also marks the first application of nanovibrational stimulation to neurogenic cells, specifically the neuroblastoma cell line SH-SY5Y (see Appendix B), potentially opening a new avenue of research in cellular mechanobiology. While nanovibration has traditionally been explored for its osteogenic effects, these findings reveal its broader applicability, demonstrating that it may also influence neurogenic processes. Here, the neuroblastoma proliferation marker, NeuroD1, was found to significantly decrease in gene expression following 7 days of horizontal nanovibrational stimulation (1 kHz, 30 nm). This suggests a potential therapeutic application for nanovibrational stimulation in regulating neuroblastoma cell proliferation, warranting further investigation in the context of neurodegenerative diseases or neural regeneration.

Additionally, staining the neurogenic marker, β-tubulin revealed increased protein intensity at lower amplitudes of vibration (30 nm) compared to higher amplitudes (60 nm). Interestingly, this appears to be the reverse trend to that observed in osteogenesis, where higher amplitudes lead to increased osteogenesis. These results underscore the potential for nanovibrational stimulation to be tailored for lineage-specific outcomes, highlighting the distinct mechanical cues required for different cellular differentiation processes. By extending the application of nanovibration beyond bone research, this work introduces a new field of study and emphasises the need for further optimisation of vibration parameters to harness its full therapeutic potential across various cell types and lineages.

6.3.3 Impact of donor variability on mechanobiology studies

NIH 3T3 and MG63 cells were found to respond to vibration differently. Whilst NIH 3T3s showed increases in nuclear area, actin intensity and cell stiffness, MG63 cells did not respond as reliably. This suggests that different cell types do

not show the same morphological and mechanical responses to vibration. This was further observed when testing multiple MSC donors. Whilst Donor 3 did show morphological changes in response to vibration, only nuclear area was seen to increase in the other two donors. This appears to contradict the proposition that cytoskeletal changes are responsible for deformation of the nucleus.

Further, gene expression was not found to change equally across donors, with Donor 2 showing a higher adipogenic and neurogenic response, and Donor 1 showing a higher osteogenic response. It has been shown previously that different donors do show different differentiation potentials, including osteogenic and chondrogenic lineage commitment [358, 359]. Such variability represents a growing challenge for the development of autologous stem cell therapies, where consistent and predictable responses are critical. This study highlights the importance of donor variability in the cellular response to nanovibrational stimulation, underscoring the importance of further investigating how age, gender and ethnicity may influence outcomes.

To address this, future research should focus on understanding the underlying factors driving donor-specific responses. Emerging machine learning and computational modelling approaches could play a pivotal role in identifying patterns in donor characteristics and predicting their responses to nanovibrational stimulation [360]. While personalised stem cell therapies may not be feasible on a large scale, optimising vibration conditions to account for donor-specific tendencies based on demographic and biological factors could enhance therapeutic outcomes and reduce off-target differentiation [361]. These findings stress the necessity of broadening the scope of vibration studies to include diverse donor populations, ensuring that therapies can be tailored to maximize efficacy across different patient groups.

6.4 Future Work

6.4.1 Future nanovibrational stimulation devices

The work presented here endeavoured to optimise vibration conditions to induce increased levels of osteogenesis. Whilst osteogenesis was shown to increase at higher vibration amplitudes, neural cells may differentiate more at lower amplitudes, as shown in Appendix B. Equally, as MSC donors did not all show the same response to vibration, it may be that optimisation of vibration is also required for each donor. As such, this indicates a need for an adjustable power supply, which would allow cells to be stimulated at different amplitudes and frequencies.

The development of a horizontal vibration device has opened up the opportunity to further study and understand the effect that directional forces have on cells. Whilst a prototype has been developed, the device would benefit from being enlarged to have the same surface area as the current vertical devices, allowing for more cultureware to be stimulated. The device also does not have an independent power supply unit, which ought to be designed and developed to be similar to the proposed adjustable power supply for the vertical devices. The further development of these designs, and simplification of their use, will allow for uptake of these devices to other labs for new biological applications.

6.4.2 Development of cell therapies

The development of cell therapies for clinical use still requires some major hurdles to be overcome [4]. The work shown here developed an understanding of the effects of vibration on various cell responses and attempted to understand the relationship between morphological and mechanical changes within the cell and lineage commitment. Once this has been established, and following on from additional testing of multiple MSC donors from different sources (including bone marrow, adipose tissue and umbilical cord tissue), the technology will be required to scale-up to account for the millions of MSCs necessary for clinical use [13]. Recently, several reviews have discussed technologies that could be used in the scale-up of MSCs, including multi-layer cell stacks, hollow fibre systems and

microcarriers within stirred tanks [362-364]. Different technologies yield different quantities of cells, as summarised in Figure 100.

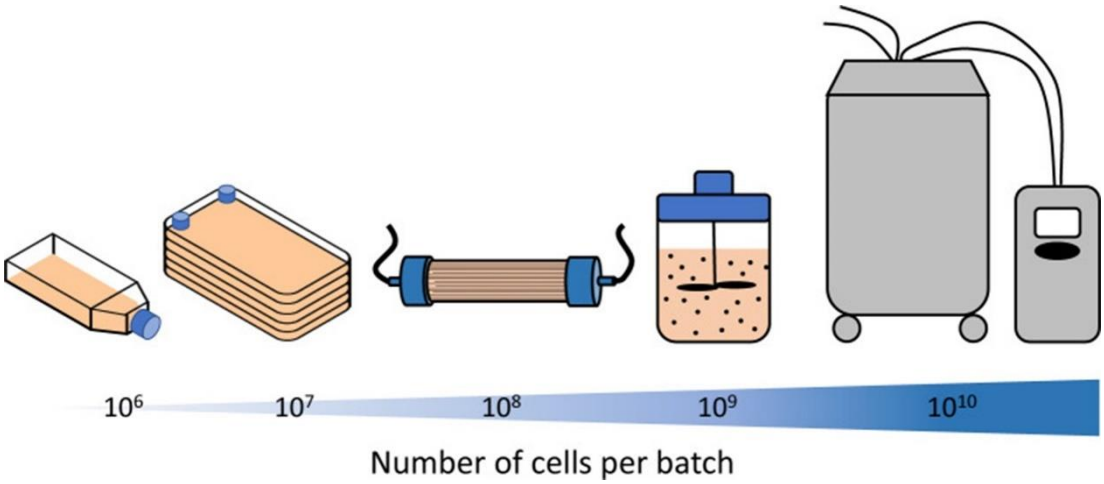

Figure 100: Different culture systems that may be used in the expansion of stem cells. Standard tissue culture flasks may culture several millions of cells, whilst multi-layer stacks may yield tens of millions, hollow fibre systems hundreds of millions, and stirred tank bioreactors upwards of thousands of millions of cells for therapy. Figure reproduced under creative commons licence from [4].

Multi-layer stacks allow for similar culture conditions to standard culture flasks, however they remain bulky and require high quantities of cell media. Hollow-fibre systems yield a higher number of cells whilst requiring less space and could provide multiple benefits over monolayer systems, as has been detailed previously [365]. Beyond this initial scale-up, larger systems will be required, such as stirred tank systems involving the incorporation of microcarriers. The use of different cell culture systems will require calibration to ensure vibration is applied equally to cells within the systems. Particularly within larger systems such as stirred tanks, other mechanical forces may be present (e.g. fluid shear), and it may be that different vibration conditions will be necessary to produce the desired response for cell therapy. This further highlights the need for such technologies to be systematically tested and optimised during early development.

6.4.3 Developing wearable technology

Alongside cell therapies, nanovibrational stimulation also has the potential as a wearable technology. Following on from the optimisation of vibration conditions *in vitro*, it will be necessary to carry out *in vivo* optimisation of nanovibrational stimulation. Vibration applied to the limb on animals in *in vivo* models will be different to that applied to cells *in vitro* due to attenuation effects [306]. Due to this, and to the different environment cells *in vivo* experience compared to *in vitro*, it is likely that different vibration conditions will be necessary to induce an osteogenic response within *in vivo* models.

Prior to optimisation of *in vivo* vibration, intermittent vibration ought to be further explored. Vibrating *in vivo* animal models continuously poses multiple challenges, and the application of continuous vibration on patients is undesirable. Therefore, further exploring the potential benefits of intermittent vibration *in vitro* would enable further optimisation prior to animal experimentation. Once animal studies provide optimal vibration conditions for osteogenesis, clinical trials may be carried out to determine whether nanovibrational stimulation is a potential wearable treatment for patients suffering from reduced bone density conditions. It may be worth exploring frequencies outside the human hearing range, which would be preferable if the device must be worn continuously or for long durations.

6.4.4 Nanovibrational stimulation outside of bone research

Vibration studies have not been limited to bone research, but have investigated chondrogenic, adipogenic, myogenic, neurogenic and other functional responses in cells (See Appendix A). Enomoto *et al* observed horizontal vibration to induce fibroblast cell migration, which may have applications in wound healing [250]. This study, and that by Pongkitwitoon *et al* observed the alignment of cells in the horizontal direction of vibration [250, 271]. This opens up the additional possible application in muscle cell research, where muscle cells require alignment to form skeletal muscle tissues [366]. Whilst the data presented in Chapter 4 did not observe any alignment of cells this ought to be thoroughly explored and tested at

a range of vibration conditions and with skeletal muscle to investigate whether nanovibrational stimulation has the potential to develop skeletal muscle *in vitro*.

As well as skeletal muscle, nanovibration may have cardiovascular applications. Heart disease is one of the leading causes of death worldwide, and stem cell therapies are providing a potential treatment. Stem cells could offer a method of repairing damaged heart tissue to patients suffering from the disease, in an effort to restore healthy cardiovascular function [367].

The neural work shown in Appendix B also shows a potential for using nanovibrational stimulation in brain disease research. The next steps for this work would be to apply nanovibration to neural stem cells to investigate whether neurogenesis could be induced. The applications for this include the treatment of spinal cord injuries and degenerative brain diseases including Parkinson's and Alzheimer's.

Outside of eukaryotic cell research, nanovibrational stimulation may have applications in the reduction of biofilm formation [300]. In healthcare, 65% of all infections are caused by biofilms which are up to 1000 times more resistant to antibiotics than single cell bacteria [368, 369]. The rapid increase in antibiotic resistant biofilms is quickly becoming a health crisis with a rising need for new treatments. Within the food industry, biofilms cause persistent problems in food spoilage and contamination [370]. However, nanovibrational stimulation, may provide a potential solution. Robertson *et al* successfully reduced the formation of *Pseudomonas aeruginosa* biofilms following nanovibrational stimulation. The use of the technology, whilst as yet not well explored, may have potential benefits and applications across healthcare and industry.

6.5 Conclusion

Nanovibrational stimulation is a promising emerging technique in fundamental mechanobiology along with the treatment of bone diseases, as well as showing potential in neurodegenerative brain disease research. It may also have applications in other stem cell therapies, including cardiovascular regeneration

and skeletal muscle development. With an aging population, stem cell therapies are likely to become widely used clinical treatments, if challenges around scalability and cost can be addressed. As highlighted in this study, the use of vibrational stimulation to direct stem cell lineage commitment may require optimisation for donor groups but does hold the potential for treating a wide range of diseases and conditions. Wearable technology could further expand the impact of this technique, having applications for patients on bed rest to avoid reduced bone loss, as well as future space explorers travelling for months in the absence of gravity. Nanovibrational stimulation may indeed play a vital role in maintaining the health of patients worldwide in years to come.

Appendices:

Appendix A

Table 18: Summary of dual chemical-vibration studies applied on a range of cell types investigating cell response. Cell type, culture conditions, differentiation media, vibration conditions and an overview of the response observed are summarised.

Study	Cell Type	Culture Conditions	Media Added	Vibration Conditions	Response
			Osteogenic		
Pré *et al* [235]	SAOS-2 Human	8000 cells/cm^2 2D	Osteogenic Media (β-glycerophosphate, ascorbic acid)	f = 30 Hz Amp = 11 mm Acc = 0.59 g Vel = 5.8 m/s Dura = 45 and 60 mins/day for 4 days Direc = Vertical and Horizontal Combined	After testing multiple frequencies and durations of vibration, 30 Hz applied for 60 minutes/day resulted in the highest expression of osteogenic genes.
Pré *et al* [234]	BM-MSCs Human	5000 cells/cm^2 2D	Osteogenic media*	f = 30 Hz Amp = 11 mm Acc = 0.59 g Dura = 45 mins/day for up to 40 days Direc = Vertical and Horizontal Combined	Late-stage osteogenic genes increased whilst calcium deposition nearly doubled following vibration.
Pré *et al* [236]	ASC Human	1500 cells/cm^2 2D	Osteogenic media*	f = 30 Hz Amp = 11 mm Dura = 45 mins/day for 28 days Direc = Vertical and Horizontal Combined	Found that COLI increased more than 10-fold in vibrated samples compared to osteogenic media controls, suggesting that vibration could be used alone or in combination with osteogenic media.
Uzer *et al* [270]	ASC Human	18000 cells/cm^2 2D	Osteolife Complete Osteogenic Medium, Stemlife Basal Medium	f = 30 and 100 Hz Amp = 3.7 – 552 μm Acc = 0.15, 1 and 2 g	Study investigated effects of fluid shear during horizontal vibration, found that the lowest fluid shear resulted in higher

				Dura = 30 mins/day for 14 days Direc = Horizontal	mineralisation, concluding that fluid shear does not contribute to cell response to vibration.
Kim *et al* [256]	MSC Human	17,000 cells/cm^2 2D Collagen sponge 2.5x10^7 cells/mL 3D	Osteogenic media*	f = 30 Hz Amp = 82.8µm[a] Acc = 0.3 g Dura = 10 mins/day, 5 days/week Direc = Vertical	Compared cell response to vibration in both 2D and 3D, finding that only in 3D were there significant increases in osteogenic gene expression
Lau *et al* [266]	MSC Rat	5000 cells/cm^2 2D	Osteogenic media*	f = 60 Hz Amp = 20.71 µm[a] Acc = 0.3 g Dura = 60 mins/day for 6 days Direc = Vertical	No osteogenic response: Vibration was not found to induce osteogenic differentiation but to instead inhibit osterix expression and decrease matrix mineralisation.
Zhou *et al* [262]	BMSC Rat	20,000 cells/cm^2 2D Human bone-derived scaffold 1x10^7 cells/mL 3D	Osteogenic media*	f = 40 Hz Amp = 50 μm Acc = 0.3 g Dura = 30 mins/day, every 12 hours for up to 26 days	Compared cell response to vibration in both 2D and 3D, finding that cells seeded on scaffolds expressed higher ALP activity than cells cultured in 2D. Also found the ERK1/2 pathway to have a role in inducing osteogenesis in BMSCs during vibrational stimulation.
Lu *et al* [371]	BM-MSC Rat	2D	Osteogenic media*	f = 40 Hz Amp = 50 μm Acc = 0.3 g Dura = 15 mins/day for 14 days	Vibration increased ALP activity, matrix mineralisation and osteogenic gene expression. Found evidence that p38 MAPK signalling is involved in osteogenesis

					following the application of vibration.
Maredziak *et al* [257]	ASC human	4210 cells/cm^2 2D	STEMPRO osteogenic differentiation kit	f = 25, 35, 45 Hz Amp = 119.27 μm[a] Acc = 0.3 g Dura = 10 mins/day for 21 days Direc = Vertical	Found vibration to increase osteogenic differentiation in hASCs obtained from elderly patients (average age of 69). Also observed that frequency had an impact on cell response, highest response observed at 25 Hz.
Halonen *et al* [274]	ASC human	158-167 cells/cm^2 2D	Basal media or osteogenic media*	f = 100 Hz Amp = 62 μm[a] Acc = 2.5 g Dura = 6x30 mins on, 2.5 hrs off for 18 days Direc = Horizontal and Vertical	Compared horizontal and vertical vibration and found that horizontal vibration in combination with osteogenic media resulted in alignment of cells. Horizontal vibration also increased ALP activity whilst vertical vibration decreased it.
Demiray and Ozcivici [317]	D1-ORL-UVA Mouse Bone Marrow Stem Cells	1052 cells/cm^2 2D	Osteogenic Media (β-glycerophosphate, ascorbic acid)	f = 90 Hz Amp = 4.6 μm[a] Acc = 0.15 g Dura = 15 mins/day for 7 days Direc = Vertical	Vibration was found to increase mRNA levels of focal adhesion kinase and RUNX2 whilst also increasing total actin content and thickness of actin fibres. Cell height was also found to increase as well as cytoplasmic membrane roughness.
Pravitharangul *et al* [290]	Osteoblast-like Cells Human (Illiac and mandible)	10,526 cells/cm^2 2D	Osteogenic Media*	f = 30 and 60 Hz Amp = 135 and 34 μm[a] Acc = 0.49 g Dura = 30 mins/day for 27 days	Compared the responses of iliac and mandible osteoblasts to vibration. The two types expressed different levels of osteogenic gene in

				Direc = Vertical	response, with the more mature iliac osteoblasts displaying a higher anti-resorptive response to vibration.
Haffner-Luntzer *et al* [247]	MC3T3-E1	4000 cells/cm^2 2D	Osteogenic Media (β-glycerophosphate, ascorbic acid)	f = 45 Hz Amp = 36.81 μm[a] Acc = 0.3 g Dura = 20 mins/day, 5 days/week Direc = Vertical	Demonstrated that estrogen has a negative effect on osteoblast proliferation following vibration. Findings suggested that estrogen receptor alpha signaling, and cytoskeletal remodelling are critical for osteogenesis in osteoblasts following vibration.
	Primary Osteoblasts Mouse	7000 cells/cm^2 2D			
Lee *et al*[238]	hDPSCs	20,000 cells/well (6 well plate) 2D	Osteogenic Media*	f = 45 and 100 Hz Amp = 137.6 μm and 27.9 μm[a] Acc = 1.12 g Dura = 30 mins/day Direc = Vertical	Vibration resulted in increased expression of osteogenic genes with some proteins increasing the most at 45 Hz. However, the highest number of calcified nodes was found after vibration at 100 Hz.
Li *et al* [327]	MC3T3-E1	Plastic and Glass 200,000 cells/well (6 well plates) 2D	Osteogenic Media*	f = 35 Hz Amp = 50 μm[a] Acc = 0.25 g Dura = 30 mins/day, 5 days/week for 21 days	Morphological analysis found vibration to result in the integration of and crosstalk between primary cilia and the COS2-PGE2-EP4 signalling pathway. Findings suggest that primary cilia may have play a crucial role in osteoblast mineralisation in response to applied vibration

Pongkitwitoon *et al* [271]	BMSCs Human	18,000 cells/cm^2 2D	IGF-1 and FGF-β	f = 30 and 100 Hz Amp = 3.7 – 276 μm Acc = 0.15 or 1 g Dura = 2 x 20 mins/day (2h rest period) for 14 days Direc = Horizontal vs Vertical	Compared horizontal and vertical vibration. Horizontal vibration at 100 Hz produced the highest levels of ALP activity and mineralisation. Horizontal vibration also led to the realignment of the cytoskeleton leading to an increase in cell stiffness. The same was not seen following vertical vibration.
Judex *et al* [254]	Human osteoblasts, periodontal ligament fibroblasts, Osteoclasts	Cultureware 7500 cells/cm^2 2D	Osteogenic media	**AcceleDent** f = 30 Hz Acc = Hori: 0.18 g Vert: 0.15 g Resultant: 0.24 g Amp = 66.26 μm[a] Dura = 20 min/d **VPro5** f = 120 Hz Acc = Hori: 0.41 g Vert: 0.07 g Resultant: 0.41 g Amp = 113.2 μm[a] Dura = 5 min/d	Compared two commercial vibration devices to find the optimal device for increasing osteoclast activity. Higher response from VPro5 treatment, which increased osteoblast proliferation and gene expression, regardless of shorter treatment
Chen *et al* [255]	MC3T3 Osteoblast-like cells	Hydroxyapatite-coated titanium substrate 50,000 cells/cm^2 2D	Osteogenic Media*	f = 40 Hz Amp = 46.6 µm[a] Acc = 0.3 g Dura = 30 mins/day for 14 days	Vibration increased proliferation and osteogenic differentiation. Actin cytoskeleton was observed to rearrange and increased adhesion to the hydroxyapatite coating used.
Macione *et al* [289]	MC3T3 Osteoblas	Glass 8-well 4445 cells/0.8 cm^2	Osteogenic Media (β-glycerophos	10-30 mW/cm^2 for 20	Successfully used ultrasound to induce osteoblast

	t-like cells	2D	phate, ascorbic acid)	mins/day for 16 days	differentiation with increased osteogenic gene expression and mineralisation following vibration.
Chondrogenic					
Takeuchi *et al* [252]	Chondrocyte Pig	Hyaluronic acid cartilage $2x10^6$ cells/mL/well 3D	Hyaluronic acid medium containing ascorbic acid	f = 100 Hz Amp = 0.5 nm Acc = 0.00002 g[a] Dura = Stimulated for 14 days Direc = Vertical	Tested effects of vibration both with and without hyaluronic acid, finding that proteoglycan production was at its highest when vibration was combined with using hyaluronic acid. Vibration also induced MAPK and β-catenin signalling.
Chu *et al* [292]	MSCs	Quartz coverslip	Chondrogenic Media	Inten = 1-20 mW/cm^2 Amp = 0.1μm Dura = 1min of piezoelectric stimulation	Found that vibration alone was sufficient to induce chondrogenesis, however when used in combination with chondrogenic media, chondrogenesis increased.
Hou *et al* [245]	BM-MSC Rat	5000 cells/cm^2 2D	Chondrogenic Media (dexamethasone, ascorbate, sodium pyruvate, proline, TGF-β3)	f = 40 Hz Amp = 7.61 μm[a] Acc = 0.049 g Dura = 30 mins/day for 21 days Direc = Vertical	Vibration increased chondrogenic marker expression along with glycosaminoglycan levels. Found evidence that β-catenin signalling is involved in BM-MSC chondrogenic response to vibration. Following vibration, actin cytoskeleton rearranged, increased F-actin fluorescence intensity.
Adipogenic					

Zhao *et al* [291]	BM-MSC Rat	1 x 10^6 cells/mL 2D	Adipogenic media (dexamethasone, rosiglathazone, isobutyl-methylxanthine, insulin)	f = 40 Hz Amp = 50 μm Acc = 0.3 g Dura = 15 mins/day for 14 days	Vibration resulted in upregulation of adipogenic markers and an increase in lipid droplet formation. Phosphorylation of p38 MAPK was also found to increase.
Baskan *et al* [246]	D1-ORL-UVA Mouse bone marrow pluripotent stem cell line	263 cells/cm^2 2D	Adipogenic media (insulin, indomethacin, dexamethasone)	f = 90 Hz Amp = 3.1 μm^a Acc = 0.1g Dura = 15 mins/day for 7 days Vertical	Saw a decrease in adipogenesis following vibration with a reduced expression of some adipogenic markers.
Baskan *et al* [372]	3T3-L1 Mouse embryo fibroblast cells	2D	Adipogenic media (insulin, indomethacin, dexamethasone)	f = 75 Hz Amp = 4.4 μm Acc = 0.1 g Dura = 10 mins/day for 10 days Direc = Vertical	Tested a range of frequencies (30-120 Hz) to determine the optimal frequency to suppress adipogenesis. 75 Hz was most effective in reducing triglycerides concentration and the PPARγ mRNA levels whilst 45 and 30 Hz were most effective in reducing area, perimeter, mean intensity and integrated density of lipid droplets.
Myogenic					
Sancilio *et al* [239]	Myocytes (Satellite Cells)	Glass coverslips coated in E-C-L collagen 2500-3000 cells/cm^2 2D	Insulin, apo-Transferrin	f = 300 Hz 100 mbar Dura = Increasing time intervals of 10, 20, 30 minutes, then incubated for 72h before analysis	Used mechanoacoustic waves to stimulate both young and old myocytes (23 and 72 years). Cell area and alignment were found to increase in both cell groups. In response to vibration, younger cells tended to proliferate whilst older cells differentiated in

					response to vibration
Neurogenic					
Grosman-Dziewiszek *et al* [258]	SH-SY5Y neuroblastoma cell line used in Alzheimer's Research	Collagen coating 2D	Retinoic acid	f = 40 Hz Amp = 20-30nm Acc = 0.06 – 0.17 g Dura = 8 hours/day for 5 days Direc = Vertical	Compared vibrated cells grown in standard growth medium, with or without a collagen surface, and cells grown in differentiation medium (retinoic acid) with or without collagen. Vibration found to increase neurite length, more in cells grown on collagen surface in differentiation medium. Some analysis found cells to respond better to vibration with addition of differentiation medium, however retinoic acid was found to inhibit cell growth and differentiation.
Multi-lineage response					
Cashion *et al* [237]	UC-MSC Human + Porcine	400,000 cells/cm^2 2D	Chondrogenic Media (ITS-1, ascorbic acid, dexamethasone, TGF-β1, TGF-β3, insulin-like growth factor D, L-proline)	f = 1 Hz Dura = 1 min, 15 min rest, 15h/d for 10 days Direc = Horizontal	Chondrogenic: Glycosaminoglycan content was higher following 1 Hz stimulation, whilst calcium deposition was lower Similar levels of energy (amplitude used for both vibration conditions)
		20,000cells/cm^2 2D	Osteogenic Media*	f = 100 Hz Dura = 1 min, 15 min rest, 15h/d for 10 days Direc = Horizontal	Osteogenic: Increased calcium deposition and BMP2 expression.
Chen *et al* [259]	BM-MSC Human	2D	Adipogenic Media (dexametha	f = 30Hz Amp = 82.8 μm[a]	Adipogenic: Found that osteogenesis was

			sone, isobutyl-1-methylxanthine, insulin, indomethacin)	Acc = 0.3 g Dura = 30 mins/day for 21 days Direc = Vertical	promoted at an early stage at this frequency but was eventually suppressed at later stages. Meanwhile, adipogenic genes were promoted.
			Osteogenic Media (L-ascorbic acid, dexamethasone, β-glycerophosphate disodium salt hydrate)	f = 800 Hz Amp = 116.5 nm[a] Acc = 0.3 g Dura = 30 mins/day for 14 days Direc = Vertical	Osteogenic: Showed the highest level of calcium deposition, and increased expression of osteogenic genes. Adipogenesis was inhibited with lipid accumulation being reduced along with adipogenic gene expression.
Marycz *et al* [263]	ASCs Human	15789 cells/cm^2 2D Tube 50,000 cells per 15mL tube 3D	STEMPRO Chondrogenesis differentiation kit	f = 35 Hz Amp = 40.5 μm[a] Acc = 0.1g Dura = 15 mins/day for 14 days Direc = Vertical	Chondrogenic: Vibration resulted in higher expression of chondrogenic genes. 3D culture at 35Hz vibration resulted in the highest concentrations of BMP-2.
			STEMPRO Adipogenesis differentiation kit	f = 25 Hz Amp = 119.27 μm[a] Acc = 0.3 g Dura = 15 mins/day for 14 days Direc = Vertical	Adipogenesis: Vibration increased lipid droplet formation but no significant changes in adipogenic gene expression were observed.
Other functional responses					
Lin *et al* [240]	MDA-MB-231 metastatic human breast cancer cells	200,000 cells/well (35mm x 10mm dish) 2D	Basal media treated with Yoda1	f = 60 Hz Amp = 20.7 μm[a] Acc = 0.3 g Dura = 60 mins of vibration total Direc = Vertical	Yoda1 and LMHF were used in combination to regulate osteoclastogenesis and breast cancer cell migration
Li *et al* [373]	MC3T3-E1	200,000 cells/well (6 well dish) 2D	Osteogenic Media*	f = 35 Hz Amp = 50.7 μm[a] Acc = 0.25 g	Vibration resulted in a reduction in the density of ciliated osteoblasts

				Dura = 20 mins/day, 5 days/week for 12 days	along with the structural distortion and shortening of primary cilia
Hortobagyi *et al* [241]	hVFF	2D	Pronectin coating ascorbic acid, cytokine treatment (addition of TGF-β1 and IL1β)	f = 50-250 Hz Amp = Average of 82 μm Dura = Continuous vibration for 3 days	Fibrogenesis observed alongside increases in collagen gene expression

[a] acceleration/amplitude calculated with approximations using the following equation: $$Amplitude = \frac{a}{(2\pi f)^2} \quad (5)$$

* Osteogenic media: β-glycerophosphate, ascorbic acid, dexamethasone

Table 19: Summary of vibration only studies. Cell type, culture conditions, vibration conditions and a brief description of cell response are summarised.

Study	Cell Type	Culture Conditions	Vibration Conditions	Response
Osteogenic				
Safavi *et al* [251]	MSCs Rabbit	30,000 cells/cm^2 2D	f = 300 Hz Amp = 10 μm Acc = 3.62 g [a] Dura = 45 mins/day for 14 days Direc = Vertical	Looked at both osteogenic and chondrogenic response, only found a significant osteogenic response and no significant change in chondrogenic markers. Observed higher calcium node formation following vibration whilst no proteoglycan formation was found. F-actin fibres were also found to align in a single direction.
García-López *et al* [248]	BALB/c Mouse Calvarial Osteoblasts Bone marrow derived osteoclasts	10,000 cells in 2mL medium/well (24 well plate) 2D	f = 30 Hz 0.25 N Dura = 20 mins of pulsed vibration	Successfully inhibited osteoclasts whilst promoting apoptosis and activating osteoblasts using vibrational stimulation.
Gao *et al* [260]	Primary Rabbit Osteoblasts	100,000 cells/cm^2 2D	f = 45 Hz Amp = 61.3 μm[a] Acc = 0.5 g	Vibration increased directional cytoskeleton arrangement and significant

			Dura = 60 mins/day for 3 days Direc = Vertical	increases in osteogenic gene expression whilst suppressing sclerostin expression. Increased mineralisation also observed. The protein expression levels of canonical Wnt/β-catenin signaling pathway increased following vibration, suggesting this pathway may be involved
Ota *et al* [284]	MC3T3-E1	Flexible Bottomed (type 1 collagen-coated silicon membrane) 200,000 cells/cm^2 2D	f = 60 Hz Amp = 35 μm Acc = 5 m/s^2 Dura = 10 mins only Direc = Vertical	Found that 10 mins of stimulation resulted in an upregulation of some osteogenic genes.
Rosenberg *et al* [267]	Osteoblasts	20,000 cells/ well (24 wells) 2D	f = 20, 30, 40, and 60 Hz Amp =25 μm (+/- 5) Acc = 1.3 m/sec^2 (+/- 0.1) Dura = 120 seconds every 24 hours for 4 days Direc = Horizontal	Tested a range of frequencies on cells from older donors (55-77 years), finding 60 Hz to be optimal for producing an osteogenic response.
Ambattu *et al* [285]	hMSCs hADSCs hUCSCs	Glass 3000 cells/cm^2 2D	f = 10 MHz Amp =0.248 nm[a] Acc = 10^4 g Dura = 10 mins/day for 4 days Surface Reflected Bulk Waves	Compared vibrating two samples, one with osteogenic media and one without. 10 minutes of vibration increased osteogenic gene expression. Observed the involvement of piezo channel activation and Rho-associated protein kinase signalling.
Kennedy *et al* [288]	CD14+ Blood Cells MSCs	Type I Rat Collagen Gel 30,000 cells/mL 3D	f = 1 kHz Amp = 40 nm Acc = 0.16 g [a] Dura = Continuous vibration for 28 days (7 days for CD14+) Direc = Vertical	Vibration resulted in enhanced osteogenesis and reduced osteoclastogenesis. Akt (protein kinase C) identified as a potential mediator
Sun *et al*[242]	MLO-Y4 Osteocyte	100,000 cells/mL 2D	f = 45 Hz Amp = 61.3 μm[a] Acc = 0.5 g Dura = 1 hour/day for 3 days Direc = Vertical	Exposed cells to high glucose during vibration, investigating applying vibration to reduce the effects of diabetic osteopenia and osteoporosis. Vibration resulted in increased proliferation and viability of MLO-Y4 cells. Also increased cell area, microfilament density and anisotropy, and

				expression of Wnt3a, β-catenin, and osteoprotegerin (OPG) whilst decreasing sclerostin, DKK1 and RANKL expression.
Thompson *et al* [249]	Primary mouse MSCs	1 day experiment: 5200 cells/cm^2 3 day experiment: 1700 cells/cm^2 2D	f = 90 Hz Amp = 21.46 μm[a] Acc = 0.7 g Dura = 2x20 mins, 2h rest period in between, applied every day over 3 days Direc = Horizontal	Induced simulated microgravity whilst applying vibration. Successfully demonstrated that vibration applied daily restore YAP levels within the nucleus and increased YAP translocation to the nucleus in MSCs under stimulated microgravity.
	C2C12s	10000 cells/cm^2 2D		
Orapiriyakul *et al* [287]	MSCs Human	Hydrogel 40,000 cells/mL of hydrogel 3D	f = 1 kHz Amp = 90 nm Acc = 0.36 g[a] Dura = Continuous for 21 days Direc = Vertical	Osteogenesis was increased after vibrational stimulation of 90 nm compared to 30 nm.
Lorusso *et al* [272]	UMR-106 Rat Osteoblast-like cells MC3T3-E1	Glass 20,000 cells/cm^2 2D	f = 30, 45 and 90 Hz Amp = 3 – 83 μm[a] Acc = 0.1, 0.2, 0.3 g Direc = Horizontal	Found that vibration did not increase Ca^{2+} but did desensitise the calcium response to exogenous ATP
Hou *et al* [328]	MC3T3-E1 Mouse	6250 cells/cm^2 2D	f = 40 Hz Amp = 76 μm[a] Acc = 0.49 g Dura = 30 mins/day for 3 days Direc = Vertical	Vibration increased expression of Wnt10B and OPG whilst decreasing sclerostin and RANKL levels. Suggests Wnt signaling may be involved in mechanotransduction following application of vibration
Wu *et al* [318]	Mouse BMSCs	Biphasic Calcium Phosphate Scaffolds 300,000 cells/scaffold 3D	f = 40 Hz Amp = 50 μm Acc = 0.3 g Dura = 30 mins/day for 21 days Direc = Vertical	Vibration increased osteogenic gene expression, F-actin and matrix mineralisation. Evidence that ERK1/2 and Wnt/β-catenin signalling pathways were involved.
Myogenic				
Wang *et al* [293]	C2C12 Mouse	10,000 cells/cm^2 2D	f = 8-10 Hz Amp = 0.4 mm Acc = 0.1 – 0.16 g[a] Dura = 10 mins/day for 3 days Direc = Vertical	Vibration increased expression of myogenic regulatory factors and increased myotube formation.
Lin *et al* [294]	C2C12 Mouse	200,000 cells/cm^2 2D	f = 10 Hz Amp = 0.4 mm Acc = 0.16 g[a]	Vibration resulted in enhanced myotube formation through the P13K/Akt/strathmin

			Dura = 10 mins/day for 3 days Direc = Vertical	pathway. Results also confirmed the importance of stathmin to form myotubes.
Tong *et al* [286]	BM-MSC Human	PCL Scaffold coated in fibronectin $4.5x10^6$ cells/mL, total of 40µL 3D	f = 200 Hz Amp = 40 μm Acc = 65.5 m/s^2 Dura = 12 hours/day for 7 days	Built a bioreactor to mimic the vocal fold and applied vibration to cells at human phonation frequencies. Tested two vibration regimes: 1hr on, 1hr off or continuous for 12h per day. Periodic vibration was found to result in better production of matrix components. Vibration also resulted in reinforcement of actin filaments and increased expression of $\alpha_5\beta_1$ integrin.
Neurogenic				
Choi *et al* [42]	ASCs Human	80,000 cells/cm^2 2D	f = 30 Hz Amp = 379.67 μm^a Acc = 1.376 g Dura = Continuous vibration for 4 days Direc = Horizontal	Found that vibration increased expression of neural markers whilst inhibiting adipogenesis. Vibrated cells achieved elongated and spindle-shape morphologies Analysis showed high potential of cells to differentiate into astrocytes and oligodendrocytes following 30 Hz vibration.
Cho *et al* [264]	UC-MSCs Human	1300 cells/cm^2 2D	f = 40 Hz Amp = 145.627 μm^a Acc = 0.938 g Dura = Continuous vibration for 5 days Direc = Horizontal	Increased expression of neuron-specific markers following vibration alongside cells adopting a neural-like morphology. ERK level also increased following vibration.
Cho *et al* [374]	hUC-MSCs	Low density 2D	f = 30 Hz 13.5 – 14.1g Dura = Continuous vibration for 4 days Direc = Vertical	Found that the PLXNA4 gene is involved in differentiating human UC-MSCs into neural-like cells following vibration.
Multi-lineage response				
Zhang *et al* [375]	PDLSC Human	100,000 cells/well 2D	f = 50 Hz Amp = 29.8 μm^a Acc = 0.3 g Dura = 30 mins/day Direc = Vertical	Osteogenic: Increase in osteogenic genes following vibration.
			f = 50 Hz Amp = 59.61 and 89.42 μm^a Acc = 0.6 and 0.9 g Dura = 30 mins/day	Tendogenic: Scleraxis expression was increased at higher accelerations (and decreased at lower accelerations). Shows magnitude dependent

			Direc = Vertical	response for different lineage commitments.
Other functional responses				
LaGier *et al* [243]	HeLa	10,000 cells/cm^2 2D	f = 20 Hz Dura = 15 mins, vortex mixer	Observed changes in the actin cytoskeleton with filopodia retracting following vibration and actin found to be concentrated in the centre of the cell. Vibration also increased expression of calpain.
Enomoto *et al* [250]	L929 Mouse Fibroblast Line	2D	f = 11.2 kHz Amp = 269 or 538 nm[a] Acc = 136 or 272 g $_{peak}$ Direc = Horizontal	Found that fibroblast cells collectively migrate following vibration in the direction of vibration. When vibration promotes cell migration, cell nuclei become elongated and align at right angles to a gap made using a silicone rubber insert.
Mojena-Medina *et al* [244]	HaCaT Human Keratinocytes	Scratch wound density: 2.03 x 10^7 cells/cm^2 2D	f = 1 and 80 Hz Amp = 0.4 and 0.7 µm Acc = 1.22x10^{-6} and 0.02 g Dura = Continuous for 3 days Direc = Vertical	1 Hz vibration improved conditions for wound healing due to faster proliferation and migration. F-actin was stretched and extended following vibration, and cells were found to have more filopodia and a sparser cell shape. 80 Hz vibration decreased proliferation/migration and resulted in a round smaller morphology.
Benjakul *et al* [376]	Human Periodontal Ligament Cells	100,000 cells/well 2D	f = 30 Hz Amp = 82.8 μm[a] Acc = 0.3 g Dura = 20 mins/day for 3 cycles for a total time of 48h Direc = Vertical	Looked at both vibration and compression and combinations of the two. Found that vibration induced RANKL expression through activation of the cyclooxygenase pathway
Ye *et al* [377]	Human Tonsillar Mononuclear Cells	Culture bottle 2D	f = 60 Hz Dura = Different periods of time used: 1, 3, 5 and 10 minutes, then cultured for 3 days	Study was investigating mimicking the vibration produced by vocal cords and applying these to tonsillar cells. Vibration induced IgA1 secretion by activating BAFF release whilst diverging O-glycosylation IgA1 by suppressing both C1GALT1 and Cosmc expression.
Touchstone *et al* [261]	mMSCs Mouse	1800 cells/cm^2 2D	f = 90 Hz Amp = 21.4 μm Acc = 0.7 g Dura = 2x20 min regimes with 2h	Investigated whether vibration could be used to restore proliferation levels in MSCs exposed to stimulated microgravity. Found that

			rest period in between for 3 days	vibration did restore proliferation levels and levels of nuclear proteins Lamin A/C and Sun-2 all of which had been affected by stimulated microgravity.
Roberts on *et al* [300]	*P. aeruginosa*	2D biofilm	f = 1 kHz Amp = 60 nm Dura = continuous	Nanovibrational stimulation observed to reduce biofilm formation of *P. aeruginosa*

Appendix B

B.1 Introduction

Whilst the majority of vibration studies focus on an osteogenic response, there are a small number which have investigated neurogenesis in cells [42, 258, 264, 374]. Stem cells have been observed to show an increase in neurogenic gene expression following the application of vibration in the absence of lineage specific media [42, 264]. Whilst it remains unclear whether cells are differentiating into functioning neurons, these studies suggest potential for MSCs to be used for neural regeneration and in neurodegenerative brain disease research. Neural stem cells are capable of differentiating into three main neuronal lineages: astrocytes, oligodendrocytes and neurons. Astrocytes are responsible for maintaining a suitable chemical environment for the function of neurons, whilst oligodendrocytes are responsible for myelin synthesis, a lipid-rich insulating layer which forms around the axons of nerve cells. A diagram showing the lineages of neural stem cell differentiation and the markers involved is shown in Figure 101.

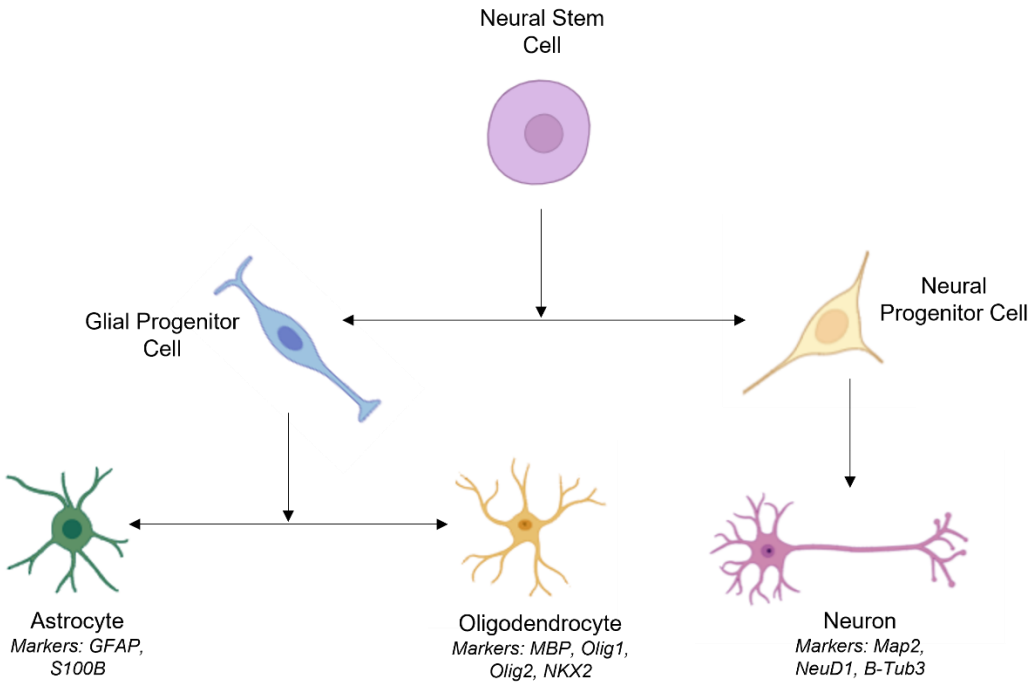

Figure 101: Diagram showing neural stem cell differentiation into three main cell types: astrocytes, oligodendrocytes and neurons and their markers. Image created using BioRender.

The human neuroblastoma cell line SH-SY5Y, has also been shown to respond to an applied vibration of 40 Hz and nanometre amplitudes (20 – 30 nm) resulting in increased neuronal-like differentiation and the proliferation of cells [258]. The use of SH-SY5Y cells enables a model for neurogenesis, in a similar way to the use of MG63s as an osteogenic model in Chapter 4. This study aimed to investigate whether a neurogenic response could be obtained from MSCs and SH-SY5Y cells following the application of nanovibrational stimulation.

B.2 Methods

B.2.1 Cell Culture Protocol

SH-SY5Y cells were cultured in medium composed of a 1:3 ratio of DMEM (Sigma) and Ham's F12 medium (ThermoFisher Scientific), supplemented with 15% FBS (Sigma) v/v, 1% minimum essential medium non-essential amino acid solution v/v and 2% antibiotics v/v. Cells were incubated at 37 °C in a 5% CO_2 environment and were passaged every 3-5 days. All cells used were below passage 30 and following seeding, cells were incubated for 24 hours prior to application of stimulation.

B.2.2 Immunofluorescence Staining

Staining was conducted following the same method as detailed previously (subsection 3.2.3), with the exception of the primary antibody used here: β-Tubulin (Abcam, ab179513), diluted to 1:1000 with PBS/BSA, added to the sample and incubated at 37 °C for two hours.

B.2.3 Gene expression analysis

RT-qPCR was conducted using the same method as detailed previously (subsection 4.2.3). Here, several assays were used (Thermo Fisher Scientific) to investigate differentiation toward several neural-cell lineages as summarised in Figure 101. All assays and their IDs are shown in Table 20.

Table 20: Target genes with the type of marker they were used to indicate, alongside TaqMan Assay ID's (Thermo Fisher Scientific) used during qPCR experiments on both SH-SY5Y cells and MSCs.

Target Gene	Marker Type	TaqMan Assay ID
MAP 2	Neuronal marker	Hs00258900_m1
NeuroD1	Neuronal marker	Hs01922995_s1
β-Tubulin (Tub3)	Neuronal marker	Hs00801390_s1
GFAP	Astrocyte marker	Hs00909233_m1
MBP	Oligodendrocyte marker	Hs00921945_m1

B.2.4 MTT Assay

To investigate cell proliferation following nanovibrational stimulation, an MTT assay was used. Cells were seeded into 96 well plates and measurements were taken following 1, 3, 5 and 7 days of stimulation. At each timepoint, cell media was removed and 100 μL of a 1:1 ratio solution of MTT assay reagent and serum free media was added to each well. Cells were then incubated at 37 °C for three hours after which, 150 μL of MTT solvent (Abcam) was added to each well alongside three empty wells to act as 'blank' controls for background measurements. Samples were then read by a spectrophotometer (Thermoscientific Multiskan Go, Thermo Fisher) at a wavelength of 590 nm.

B.3 Results

B.3.1 Optimising vibration conditions to induce a neural response in SH-SY5Y cells

To optimise vibration conditions to induce a neurogenic response in cells, SH-SY5Y cells were used as a model for neurogenesis as vibration has been shown to increase the neurogenic response in this cell type [258]. Immunofluorescent staining was used to investigate morphological changes, including nuclear area, cell area, actin intensity and β-tubulin intensity, whilst qPCR was used to investigate gene expression changes by measuring neural genes Microtubule-

associated protein 2 (MAP2), NeuroD1 (NeuD) and β-tubulin (B-Tub). Finally, MTT assays were used to indicate the proliferation of cells over time and in response to nanovibrational stimulation.

B.3.1.1 Changes over time

An initial experiment aimed to identify the timepoint at which neurogenic response could be seen. Cells were seeded into 35 mm Petri dishes at 1000 cells/cm^2, as had been used previously for cancerous cell lines (NIH 3T3s and MG63s) due to their fast proliferation rate. Cells were fixed following 1, 3 and 7 days of vertical stimulation at 1 kHz, 30 nm and stained for DAPI, actin and β-tubulin. Image analysis results are shown in Figure 102.

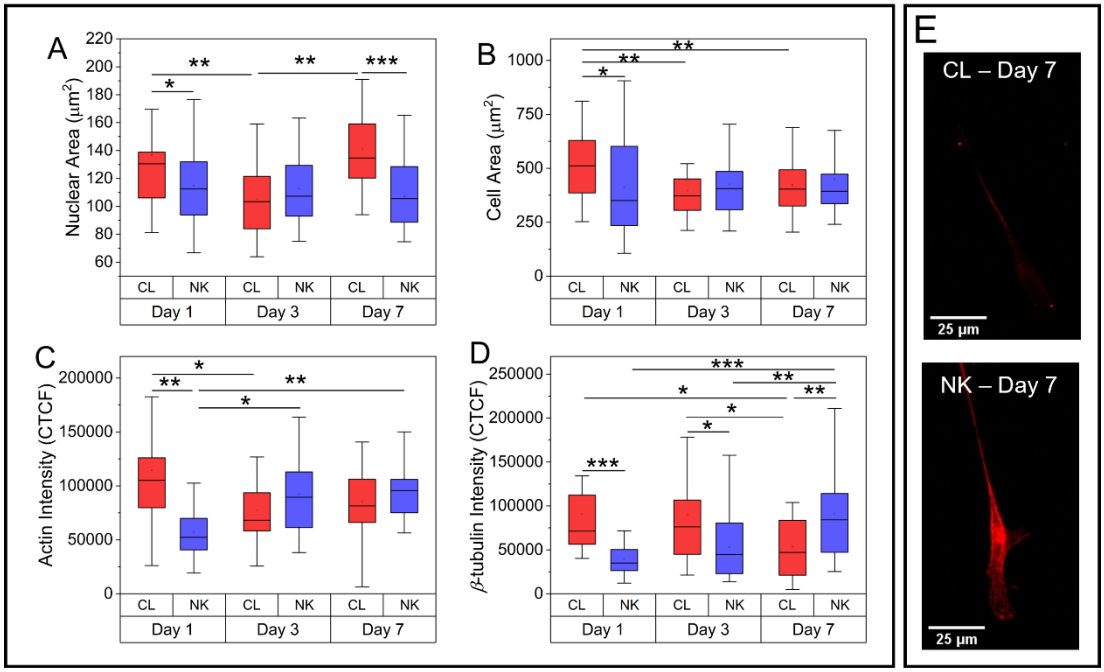

Figure 102: Morphology results of SH-SY5Y cells following 1, 3 and 7 days of vertical vibration of 1 kHz, 30 nm. A) Nuclear area was found to significantly decrease in vibrated cells at the Day 7 timepoint (N > 100). B) Cell area was found to decrease in vibrated cells at the Day 1 timepoint (N ≈ 30). C) Actin intensity was found to decrease in vibrated cells at the Day 1 timepoint (N ≈ 30). D) β-tubulin intensity was initially found to decrease in vibrated cells on Day 1, before showing a significant increase in expression in vibrated cells on Day 7 (N ≈ 30). E) Immunofluorescent images showing β-tubulin intensity in control and nanovibrated cells on Day 7. Image brightness has been enhanced equally in both images. Images taken using a Zeiss (Imager.Z1) microscope.

Nuclear area was seen to decrease in vibrated cells on Day 7. Cell area and actin intensity were also found to decrease in vibrated cells on Day 1. β-tubulin, a known marker of neurogenesis, was initially seen to decrease in vibrated cells on Day 1, before showing a significant increase on Day 7. The increase in β-tubulin intensity may suggest that nanovibrational stimulation may be inducing a neurogenic response in SH-SY5Y cells following 7 days of stimulation, which appears to be the reverse effect at Day 1. Therefore, based on this, Day 7 was chosen as the optimal timepoint during stimulation to investigate neurogenesis.

B.3.1.2 Horizontal vs Vertical Response

Following on from the previous experiment, directionality and amplitude were also optimised. Experiments with MG63s and MSCs suggested that horizontal vibration at higher amplitudes appeared to optimise osteogenesis, and therefore both directionality and amplitude were investigated here to identify any increased neurogenic response in SH-SY5Y cells. Cells were again seeded into Petri dishes at 1000 cells/cm^2 and stimulated either horizontally or vertically at either 30 nm or 50 nm for 7 days. An amplitude of 50 nm was used rather than the higher amplitudes of 60 and 90 nm used in osteogenic experiments due to limitations of the horizontal device used here (Prototype 4). Cells were then fixed and stained for DAPI, actin and β-tubulin. Morphology results are shown in Figure 103.

Nuclear area was found to increase in cells vibrated horizontally at the higher amplitude of 50 nm. There was also no significant decrease in nuclear area as had been observed in the previous experiment (Figure 102) Cell area was also shown to be significantly higher in cells vibrated horizontally at both amplitudes, though more significantly in those vibrated at the lower amplitude of 30 nm. Actin intensity was also shown to increase in cells vibrated vertically at 50 nm and more significantly in cells vibrated horizontally at 30 nm. β-tubulin was shown to be significantly higher in cells vibrated in either direction at 30 nm, with the highest response in cells vibrated horizontally.

The results shown here indicated that horizontal vibration of 30 nm showed the highest neurogenic response as shown by the highest expression of β-tubulin

intensity. There were also some indications of increased cell tension in cells stimulated horizontally at higher amplitudes (as seen by increased nuclear area) which may suggest that higher cell tension inhibits neurogenesis.

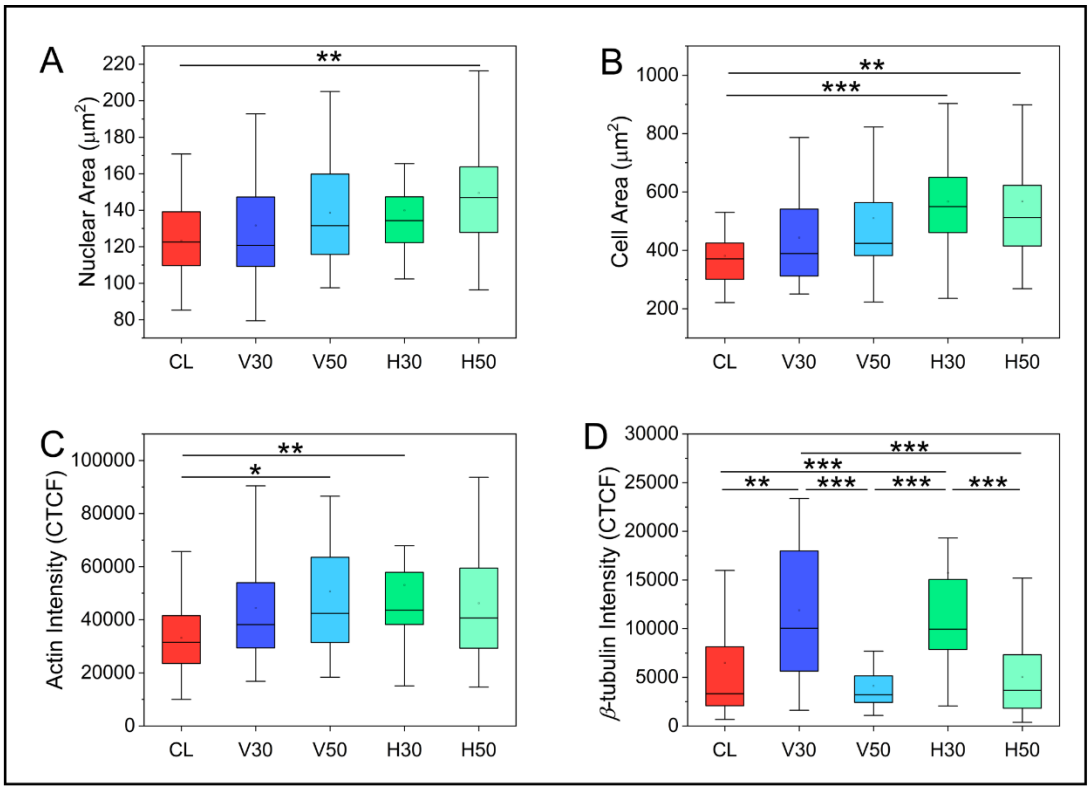

Figure 103: Morphology results for SH-SY5Y cells vibrated either horizontally or vertically at 30 or 50 nm amplitudes. A) Nuclear area was shown to increase in cells vibrated horizontally at 50 nm (N > 100). B) Cell area was found to increase in cells vibrated horizontally at both amplitudes, most significantly at 30 nm (N ≈ 30). C) Actin intensity was found to significantly increase in cells vibrated vertically at 50 nm and horizontally at 30 nm (N ≈ 30). D) β-tubulin intensity was found to be significantly higher in cells vibrated at 30 nm in both directions, though more significantly in cells vibrated horizontally (N ≈ 30).

These results may suggest that optimised osteogenesis vibration conditions are different to optimal neurogenesis vibration conditions, perhaps responding stronger at lower amplitudes. To investigate whether the morphology data observed here reflected changes in gene expression, qPCR was performed to investigate neurogenic markers.

B.3.1.3 qPCR and MTT assay results

The optimised direction and amplitude of horizontal vibration and 30 nm (and the original frequency of 1 kHz) were applied to SH-SY5Y cells for 7 days. Cells were seeded into 96 well plates at 1000 cells/cm^2 and lysed following 7 days of stimulation. Neurogenic marker: MAP2, neuroblastoma proliferation marker: NeuD and β-tubulin encoding gene: β-tubulin 3 were all measured [378]. To investigate the proliferation of cells, an MTT assay was performed following 1, 3, 5 and 7 days of stimulation. Gene expression data and MTT assay results are shown in Figure 104.

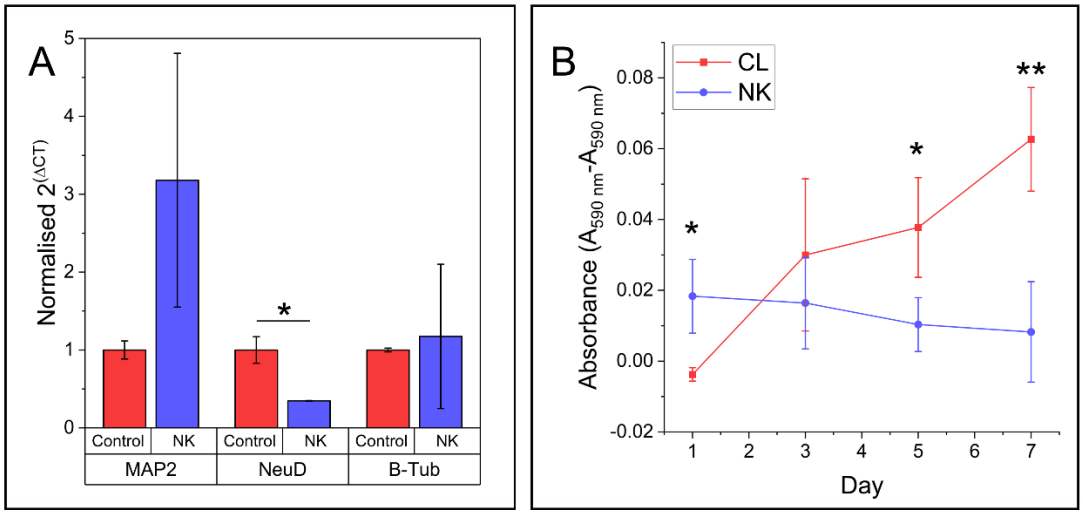

Figure 104: A) Gene expression results following 7 days of horizontal vibration at 1 kHz, 30 nm. NeuD shown to significantly decrease in vibrated cells. B) MTT assay results showing proliferation of cells over time. Nanovibration found to significantly decrease number of cells by Day 5. Error bars represent standard deviation (N = 3).

MAP2 was found to increase in nanovibrated cells although not significantly compared to control. NeuD was found to significantly decrease in cells following vibration, whilst B-Tub showed no differences between control and nanovibrated cells. Nanovibration appeared to reduce proliferation in SH-SY5Y cells compared to control cells, according to preliminary MTT assay results.

Whilst MAP2 data may suggest an increase in neurogenesis following vibration, B-Tub showed no changes. However, β-tubulin protein expression was found to increase under the same conditions at the same timepoint. This may suggest that

gene expression changes of B-Tub occur at a much earlier timepoint before observed protein changes at Day 7. NeuD is known to be involved in the proliferation of neuroblastoma cells. Here, it was found to decrease following nanovibrational stimulation, which may indicate that nanovibrational stimulation is decreasing the proliferative ability of the neuroblastoma cells. MTT assay results appear to agree, showing a decrease in proliferation of vibrated cells compared to non-vibrated control cells. These results may indicate a potential therapeutic application for nanovibrational stimulation, in addition to having a neurogenic effect on cells.

B.3.2 Seeding Density Experiment

All previous experiments shown here were conducted at a seeding density of 1000 cells/cm^2 inline with the majority of previous experiments involving NIH 3T3 and MG63 cells. However, the recommended seeding density for SH-SY5Y cells is 10,000 – 20,000 cells/cm^2. To investigate whether this would have a profound effect on the results observed, cells were seeded at either 1000 cells/cm^2 or 10,000 cells/cm^2 into 12 well plates and vibrated horizontally at 1 kHz, 30 nm for 7 days. Immunofluorescent staining was used to investigate morphology, qPCR to identify neurogenic gene expression changes and an MTT assay to assess proliferation with results shown in Figure 105, Figure 106, and Figure 107, respectively.

Nuclear area was found to decrease in stimulated cells at the lower seeding density. Cells seeded at a higher initial seeding density had a higher nuclear area compared to stimulated cells at the lower seeding density. Cell area was found to be significantly increased in vibrated cells at the higher initial seeding density. Whilst actin intensity showed no significant increases with groups at each seeding density, cells seeded at a higher initial seeding density expressed more actin than cells seeded at the lower initial seeding density. This may be visualised in Figure 105E and Figure 105F. Unlike previously, β-tubulin was not found to increase in stimulated cells, however vibrated cells seeded at a higher initial seeding density did appear to have a higher expression of β-tubulin than non-vibrated cells. Gene expression analysis did not result in any significant

differences being observed. MAP2 did appear to be higher expressed in cells seeded at a lower seeding density whilst NeuD was slightly higher expressed in cells seeded at the higher seeding density.

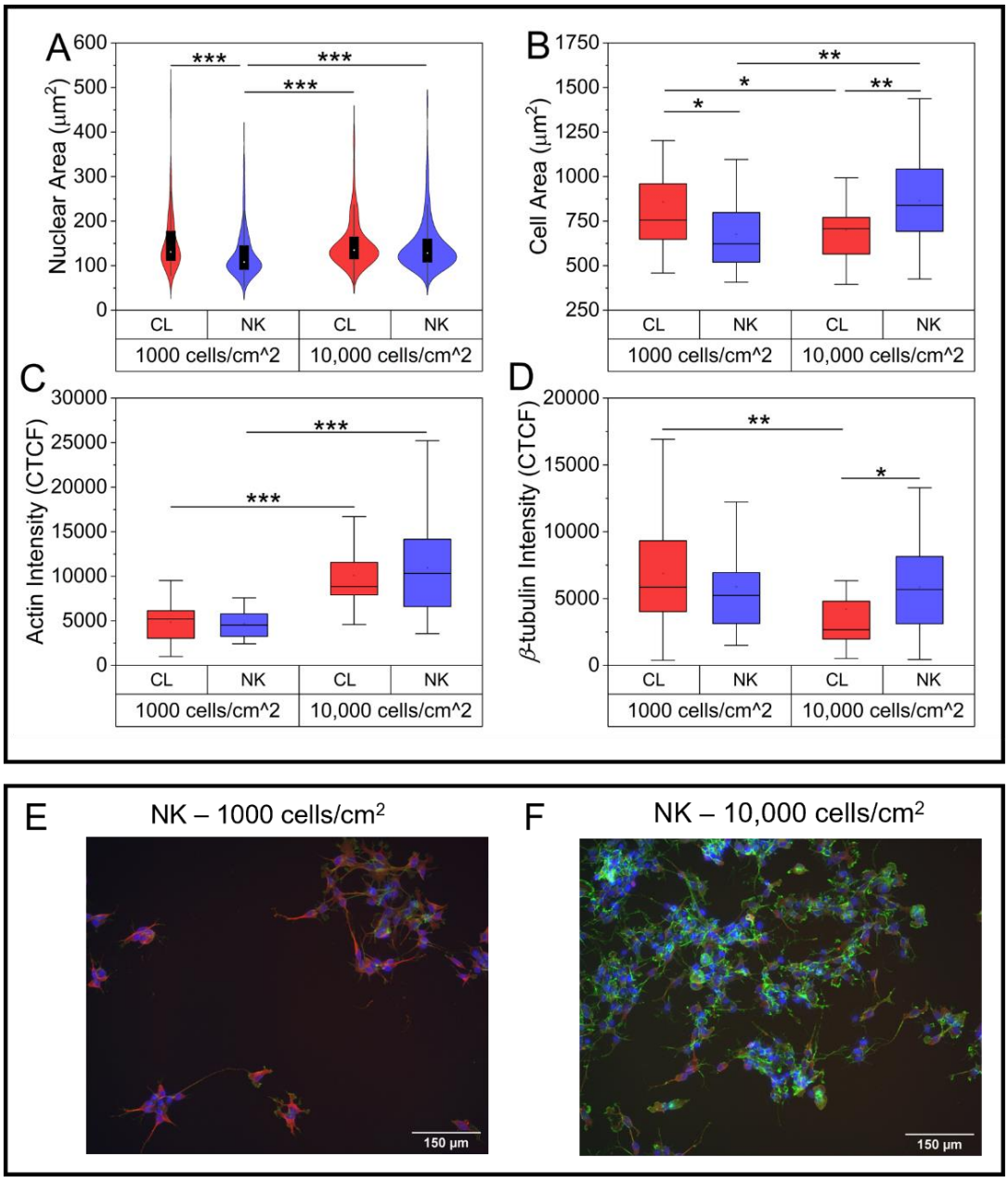

Figure 105: Morphology analysis for SH-SY5Y cells seeded at either 1000 or 10,000 cells/cm² and vibrated horizontally at 1 kHz, 30 nm. A) Nuclear area data (N > 100). B) Cell area data (N ≈ 30). C) Actin intensity data (N ≈ 30). D) β-tubulin intensity data (N ≈ 30). E) Immunofluorescent images showing DAPI (blue), actin (green) and β-tubulin (red). Actin intensity shown to be much higher in cells seeded at the higher seeding density. Images taken using Zoe Fluorescent Cell Imager microscope with image brightness adjusted equally across images.

An MTT assay was again used to quantify the proliferation of cells. The first measurement was taken on Day 0 prior to any applied stimulation, whilst in the previous experiment the first measurement had been after 1 day of vibration. Cells seeded at a lower initial seeding density have large standard deviations, whilst vibrated cells do not seem to follow a trend in proliferation. Meanwhile, cells seeded at a higher initial seeding density appear to increase in proliferation similar to control cells.

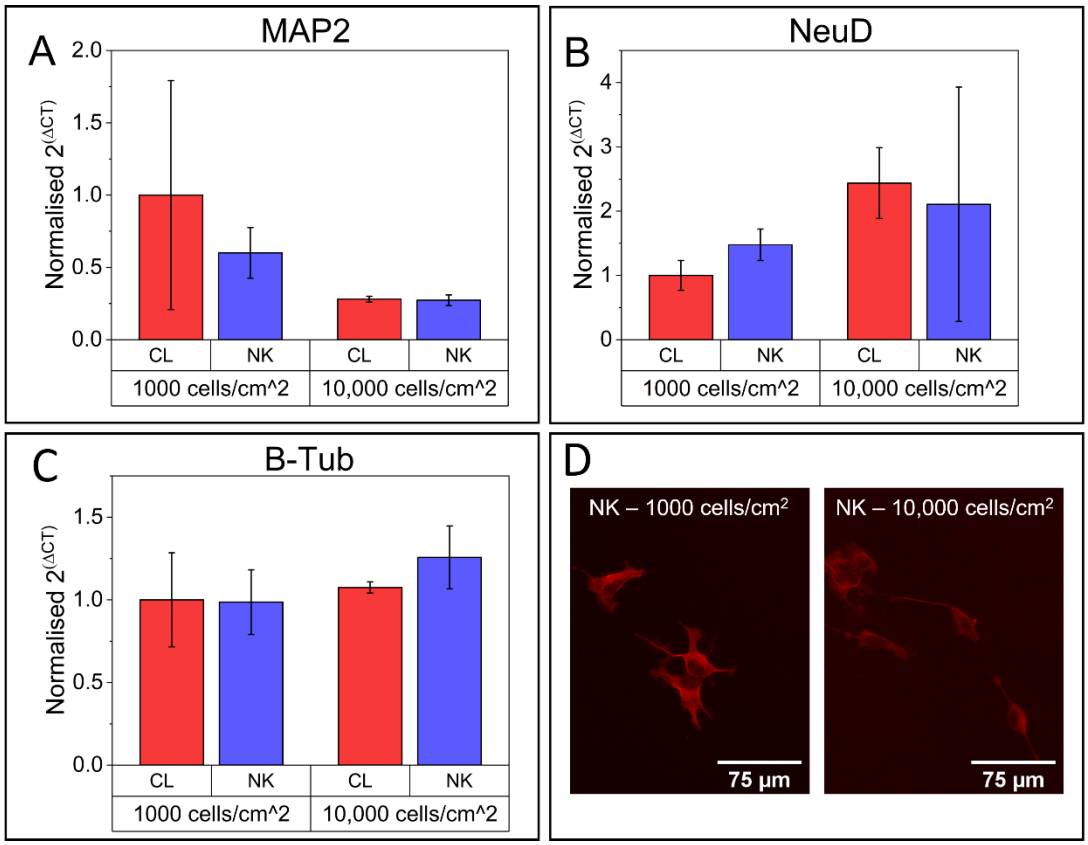

Figure 106: Gene expression data analysis for SH-SY5Y cells seeded at either 1000 or 10,000 cells/cm² and vibrated horizontally at 1 kHz, 30 nm. A) MAP2 gene expression showed no significant differences between samples. B) NeuD increased in expression in cells seeded at a higher initial density however no significant differences were observed between samples. C) B-Tub also showed no significant differences in gene expression between samples. D) Nanovibrated SH-SY5Y cells stained for β-tubulin at each seeding density. Image brightness has been adjusted equally in both images. Images taken using a Zoe Fluorescent Cell Imager microscope. Error bars represent standard deviation (N = 3).

The results shown here largely contradict those seen previously. β-tubulin was not found to significantly increase in protein expression at either initial seeding

densities, and gene expression of NeuD was not observed to significantly decrease in vibrated samples. MTT assays also did not show a similar trend to the prior result. Whilst results were not replicated here, a higher seeding density would be advisable moving forward due to a higher seeding density enabling more cell to cell contact and having a higher neural relevance. Further optimisation experiments may be necessary to optimise cell response at this higher seeding density.

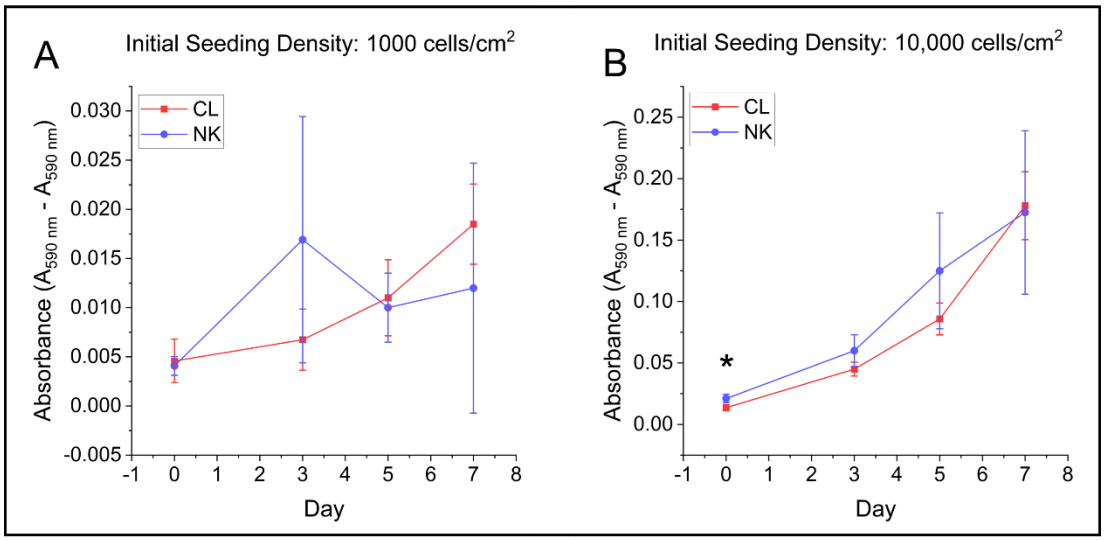

Figure 107: MTT assay results for SH-SY5Y cells seeded at either 1000 or 10,000 cells/cm^2 and vibrated horizontally at 1 kHz, 30 nm. A) MTT assay for cells initially seeded at 1000 cells/cm^2. B) MTT assay for cells initially seeded at 10,000 cells/cm^2. Error bars represent standard deviation (N = 3).

B.3.3 Investigating a neural lineage commitment in MSCs

Whilst an osteogenic response was the focus of this overall project, previous studies had found that following vibration, MSCs expressed increased neurogenic markers in the absence of differentiation specific media [42, 264]. Therefore, to investigate whether nanovibration could be used to illicit a similar response, Donor 3 MSCs (see Table 15) were stimulated for 7 days. Previous studies had seen neurogenic marker expression after 4 and 5 days, and so this timepoint was chosen as it was likely changes would be observed [42, 264]. Cells were seeded at a high initial density of 35,000 cells/cm^2 as increase cell-to-cell contact may increase chances of neurogenic markers being expressed. Cells were then

stimulated at either 100 Hz or 1 kHz frequencies and an amplitude of 30 nm. A lower frequency was tested here, as it would expose cells to a lower force which may induce a neurogenic response. As neural tissue is not load bearing like bone, a lower force may result in a higher neurogenic response. After 7 days of stimulation, cells were either lysed for gene expression analysis or fixed for immunofluorescent staining. Fixed cells were stained for β-tubulin, a known marker of neuronal cells.

Three neural genes were investigated: MAP2, GFAP and MBP. MAP2 is a marker of neuronal differentiation. Glial fibrillary acidic protein (GFAP) is a marker for glia whilst myelin basic protein (MBP) is considered to be a marker for oligodendrocyte differentiation. All three neuronal markers have been seen to be expressed in MSCs previously [379, 380]. Two osteogenic genes were also investigated (RUNX2 and ALP) to identify whether MSCs were favouring specific lineages at each frequency. Cells were also stained with DAPI, phalloidin and for β-tubulin. Gene expression results and immunofluorescent images are shown in Figure 108.

No significant differences were observed in gene expression at the timepoint measured. For qPCR, 40 cycles were run for each gene measured. GFAP showed a very weak expression, resulting in high CT values (>37), often resulting in unobtainable results. This led to samples NK 100 Hz and NK 1 kHz only having one measurement each instead of three, from which error bars could be constructed. GFAP did show an increase in the two vibrated groups, however due to the high CT values, this is likely to be unreliable. MBP showed little difference between samples whilst MAP2 showed a decrease in samples stimulated at 1 kHz. Early osteogenic markers, Runx2 and ALP also showed no differences between samples. Immunofluorescence staining, revealed that cells were too densely packed for individual measurements of cells, making it impossible to obtain single cell intensity data for β-tubulin staining.

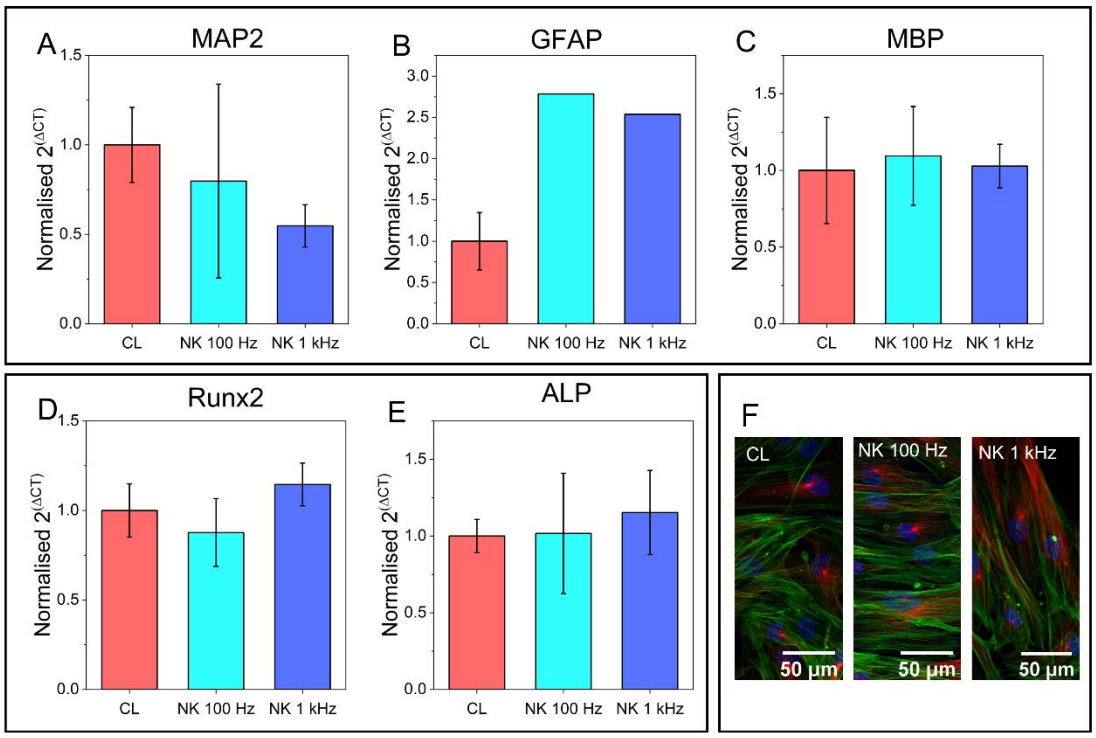

Figure 108: Gene expression results of MSCs stimulated at either 100 or 1 kHz and 30 nm for 7 days. Three neural genes were analysed to investigate any expression of neurogenesis in vibrated cells (A-C). Two early osteogenic genes were also analysed (D, E). F) Composite image of MSCs with actin shown in green, DAPI in blue and β-tubulin in red. Image taken using a Zeiss (Imager Z.1) microscope. Error bars represent standard deviation (N = 3).

The lack of neurogenic response may have been due to a number of factors. As was observed when testing multiple donors for osteogenesis in Chapter 5, Donor 3 did not show any significant differences in either osteogenic or neurogenic gene expression, which may also explain the lack of response in early osteogenic markers and neurogenic markers here. It may be that the donor used here does not have a high capacity for differentiation into certain lineages. Only two vibration conditions were tested here, as well as a single timepoint and a single seeding density. In the absence of optimisation, and without testing multiple donors, it is not possible to fully rule out the potential for neurogenic response.

B.4 Discussion

Nanovibrational stimulation has been widely used within bone research, however vibrational stimulation has been previously shown to induce a neural response in

stem cells [42, 264]. Applying nanovibrational stimulation to MSCs did not show any significant changes in neurogenic gene expression, unlike previous studies which have found 40 Hz, 0.938 – 1.376 g to increase expression in several neurogenic genes in both ASCs and UC-MSCs [42, 264]. It may be that the nanovibration conditions used were not sufficient to induce a neurogenic response in cells, or that the MSC donor used did not have a neurogenic differentiation potential.

Alongside MSCs, nanovibrational stimulation was also applied to SH-SY5Y cells. Previous studies applied vibration at 40 Hz, 20-30 nm and observed a higher average length of neurites in SH-SY5Y cells grown on collagen surfaces in differentiation medium. Authors also found neuronal nuclei (NeuN) expression, a marker of differentiated neurons to be higher in stimulated cells. Although neither NeuN expression on neurite length were investigated here, stimulated SH-SY5Y cells showed a significant increase in β-tubulin expression after 7 days of vibration at 1 kHz, 30 nm. Here, two amplitudes were investigated, with the lower amplitude resulting in the highest neurogenic response in SH-SY5Y cells. This contrasts with a higher amplitude resulting in an increased osteogenic response in MG63 cells and MSCs.

The reduced expression of NeuD observed in vibrated SH-SY5Y cells alongside the decrease in proliferation as shown by an MTT assay does indicate the potential application of nanovibrational stimulation in the halting, or potential reduction of neuroblastoma cell proliferation. The increased expression of β-tubulin in some experiments may be an indicator of increased neurogenesis. Whilst preliminary, this data does indicate the potential for further exploration into the use of nanovibrational stimulation in neural research. Further analysis techniques ought to be investigate, such as measuring neurite and dendrite length, which has been shown to increase in cells following applied vibration [258]. Nanovibrational stimulation ought to be applied directly to neural stem cells to investigate whether the neurogenic responses observed here could be replicated in a more physiologically relevant neural model. The results showing a

potential decrease in NeuD expression could also be further investigated in testing with glioblastoma.

Appendix C

There were several papers published and drafted during the completion of this project. These have been listed here as follows.

C.1 Published journal articles

Jonathan A Williams, Paul Campsie, Richard Gibson, Olivia Johnson-Love, Anna Werner, Mark Sprott, Ryan Meechan, Carmen Huesa, James F C Windmill, Mariel Purcell, Sylvie Coupaud, Matthew J Dalby, Peter Childs, John S Riddell, Stuart Reid. Developing and Investigating a Nanovibration Intervention for the Prevention/Reversal of Bone Loss Following Spinal Cord Injury. *ACS Nano*, 18(27):17630-17641, 2024 [306].

This paper investigates the use of nanovibrational stimulation in the prevention/reversal of bone loss following spinal cord injury in rats. Some preliminary cell data was gathered by Olivia Johnson-Love on comparing continuous and intermittent vibration on MG63 and MSC cells in vitro.

C.2 Unpublished journal articles

Olivia Johnson-Love, Manuel Salmeron-Sanchez, Stuart Reid, Peter G. Childs, Matthew J. Dalby. Vibration-based cell engineering. *Nature Reviews Bioengineering. In press.*

This paper reviews the current state of vibration-based cell engineering, comparing vibration studies used across a range of cells investigating a range of responses. The bulk of the literature searches were carried out by Olivia Johnson-Love, as well as the construction of tables summarising vibration studies and discussions around the importance of different vibration conditions.

Olivia Johnson-Love, Francisco Espinosa, Jamie Tejedor, Paul Campsie, Matthew Dalby, Stuart Reid, Ricardo Garcia and Peter G. Childs. Mechanical evolution of murine 3T3 cells exposed to nanovibrational stimulation. *In draft*.

This paper investigates the mechanical response of NIH 3T3 cells to nanovibrational stimulation, identifying the relationship between morphological and mechanical changes over time. The main lab work for this paper was conducted by Olivia Johnson-Love alongside Dr. Francisco Espinosa.

References

1. Farini, A., *et al.*, *Clinical applications of mesenchymal stem cells in chronic diseases.* Stem Cells Int, 2014. **2014**: p. 306573.
2. Qu, G., *et al.*, *Current status and perspectives of regulatory T cell-based therapy.* Journal of Genetics and Genomics, 2022. **49**(7): p. 599-611.
3. Cofano, F., *et al.*, *Mesenchymal Stem Cells for Spinal Cord Injury: Current Options, Limitations, and Future of Cell Therapy.* Int J Mol Sci, 2019. **20**(11).
4. Childs, P.G., *et al.*, *Hurdles to uptake of mesenchymal stem cells and their progenitors in therapeutic products.* Biochemical Journal, 2020. **477**(17): p. 3349-3366.
5. Dominici, M., *et al.*, *Minimal criteria for defining multipotent mesenchymal stromal cells. The International Society for Cellular Therapy position statement.* Cytotherapy, 2006. **8**(4): p. 315-7.
6. *Available Products: Alliance for Regenerative Medicine*. 2019; Available from: https://alliancerm.org/available-products/.
7. Catapult, C.a.G.T. *Cell and gene therapy GMP manufacturing in the UK: Capability and capacity analysis*. 2019; Available from: https://ct.catapult.org.uk/sites/default/files/publication/2019%20GMP%20Manufacturing%20Report_v6_0.pdf.
8. Almalki, S.G. and D.K. Agrawal, *Key transcription factors in the differentiation of mesenchymal stem cells.* Differentiation; research in biological diversity, 2016. **92**(1-2): p. 41-51.
9. Mitchell, K.E., *et al.*, *Matrix cells from Wharton's jelly form neurons and glia.* Stem Cells, 2003. **21**(1): p. 50-60.
10. Marędziak, M., *et al.*, *The Influence of Aging on the Regenerative Potential of Human Adipose Derived Mesenchymal Stem Cells.* Stem Cells International, 2016. **2016**: p. 1-15.

11. Zhu, M., *et al.*, *The effect of age on osteogenic, adipogenic and proliferative potential of female adipose-derived stem cells.* Journal of Tissue Engineering and Regenerative Medicine, 2009. **3**(4): p. 290-301.
12. Karantalis, V., *et al.*, *Allogeneic cell therapy: a new paradigm in therapeutics.* Circ Res, 2015. **116**(1): p. 12-5.
13. Heathman, T.R.J., *et al.*, *The translation of cell-based therapies: clinical landscape and manufacturing challenges.* Regenerative Medicine, 2015. **10**(1): p. 49-64.
14. Mennan, C., *et al.*, *A comprehensive characterisation of large-scale expanded human bone marrow and umbilical cord mesenchymal stem cells.* Stem Cell Res Ther, 2019. **10**(1): p. 99.
15. Nekanti, U., *et al.*, *Optimization and scale-up of Wharton's jelly-derived mesenchymal stem cells for clinical applications.* Stem Cell Research, 2010. **5**(3): p. 244-254.
16. Santos, F., *et al.*, *Toward a clinical-grade expansion of mesenchymal stem cells from human sources: a microcarrier-based culture system under xeno-free conditions.* Tissue Eng Part C Methods, 2011. **17**(12): p. 1201-10.
17. Hassan, M., *et al.*, *Large-Scale Expansion of Human Mesenchymal Stem Cells.* Stem Cells Int, 2020. **2020**: p. 9529465.
18. Suuronen, E.J., *et al.*, *Tissue-engineered injectable collagen-based matrices for improved cell delivery and vascularization of ischemic tissue using CD133+ progenitors expanded from the peripheral blood.* Circulation, 2006. **114**(1 Suppl): p. I138-44.
19. Roche, E.T., *et al.*, *Comparison of biomaterial delivery vehicles for improving acute retention of stem cells in the infarcted heart.* Biomaterials, 2014. **35**(25): p. 6850-6858.
20. Mao, A.S., J.W. Shin, and D.J. Mooney, *Effects of substrate stiffness and cell-cell contact on mesenchymal stem cell differentiation.* Biomaterials, 2016. **98**: p. 184-91.
21. Saha, K., *et al.*, *Substrate modulus directs neural stem cell behavior.* Biophysical journal, 2008. **95**(9): p. 4426-4438.

22. Olivares-Navarrete, R., *et al.*, *Substrate Stiffness Controls Osteoblastic and Chondrocytic Differentiation of Mesenchymal Stem Cells without Exogenous Stimuli.* PLoS One, 2017. **12**(1): p. e0170312.
23. Yu, H., *et al.*, *Insights into the role of focal adhesion modulation in myogenic differentiation of human mesenchymal stem cells.* Stem Cells Dev, 2013. **22**(1): p. 136-47.
24. Engler, A.J., *et al.*, *Matrix elasticity directs stem cell lineage specification.* Cell, 2006. **126**(4): p. 677-89.
25. Robert, A.W., *et al.*, *Adipogenesis, Osteogenesis, and Chondrogenesis of Human Mesenchymal Stem/Stromal Cells: A Comparative Transcriptome Approach.* Frontiers in cell and developmental biology, 2020. **8**: p. 561-561.
26. Birru, B., *et al.*, *Role of Signaling Pathways in Mesenchymal Stem Cell Differentiation.* Current stem cell research & therapy, 2014. **9**(6): p. 508-12.
27. Hayrapetyan, A., J. Jansen, and J. van den Beucken, *Signaling Pathways Involved in Osteogenesis and Their Application for Bone Regenerative Medicine.* Tissue engineering. Part B, Reviews, 2014. **21**(1): p. 75-87.
28. Moursi, A.M., R.K. Globus, and C.H. Damsky, *Interactions between integrin receptors and fibronectin are required for calvarial osteoblast differentiation in vitro.* J Cell Sci, 1997. **110** (18): p. 2187-96.
29. Wang, Y.-K., *et al.*, *Bone morphogenetic protein-2-induced signaling and osteogenesis is regulated by cell shape, RhoA/ROCK, and cytoskeletal tension.* Stem cells and development, 2012. **21**(7): p. 1176-1186.
30. Wang, Y.K. and C.S. Chen, *Cell adhesion and mechanical stimulation in the regulation of mesenchymal stem cell differentiation.* J Cell Mol Med, 2013. **17**(7): p. 823-32.
31. Mizrahi, O., *et al.*, *BMP-6 is more efficient in bone formation than BMP-2 when overexpressed in mesenchymal stem cells.* Gene Therapy, 2013. **20**(4): p. 370-377.
32. Luo, Z., *et al.*, *Notch Signaling in Osteogenesis, Osteoclastogenesis, and Angiogenesis.* The American journal of pathology, 2019. **189**(8): p. 1495-1500.

33. Bianco, P., *et al.*, *Bone sialoprotein (BSP) secretion and osteoblast differentiation: relationship to bromodeoxyuridine incorporation, alkaline phosphatase, and matrix deposition.* J Histochem Cytochem, 1993. **41**(2): p. 183-91.
34. James, A.W., *Review of Signaling Pathways Governing MSC Osteogenic and Adipogenic Differentiation.* Scientifica, 2013. **2013**: p. 684736-684736.
35. Zhou, S., *et al.*, *Determinants of stem cell lineage differentiation toward chondrogenesis versus adipogenesis.* Cell Mol Life Sci, 2019. **76**(9): p. 1653-1680.
36. Tang, Q.Q. and M.D. Lane, *Adipogenesis: from stem cell to adipocyte.* Annu Rev Biochem, 2012. **81**: p. 715-36.
37. Hesslein, D.G., *et al.*, *Ebf1-dependent control of the osteoblast and adipocyte lineages.* Bone, 2009. **44**(4): p. 537-46.
38. Kozhemyakina, E., A.B. Lassar, and E. Zelzer, *A pathway to bone: signaling molecules and transcription factors involved in chondrocyte development and maturation.* Development, 2015. **142**(5): p. 817-31.
39. Seifert, A., *et al.*, *Role of Hox genes in stem cell differentiation.* World J Stem Cells, 2015. **7**(3): p. 583-95.
40. George, S., M.R. Hamblin, and H. Abrahamse, *Differentiation of Mesenchymal Stem Cells to Neuroglia: in the Context of Cell Signalling.* Stem cell reviews and reports, 2019. **15**(6): p. 814-826.
41. Bengoa-Vergniory, N. and R.M. Kypta, *Canonical and noncanonical Wnt signaling in neural stem/progenitor cells.* Cell Mol Life Sci, 2015. **72**(21): p. 4157-72.
42. Choi, Y.K., *et al.*, *Stimulation of sub-sonic vibration promotes the differentiation of adipose tissue-derived mesenchymal stem cells into neural cells.* Life Sci, 2012. **91**(9-10): p. 329-37.
43. Kang, S., *et al.*, *Wnt signaling stimulates osteoblastogenesis of mesenchymal precursors by suppressing CCAAT/enhancer-binding protein alpha and peroxisome proliferator-activated receptor gamma.* J Biol Chem, 2007. **282**(19): p. 14515-24.

44. Ross, S.E., *et al.*, *Inhibition of adipogenesis by Wnt signaling.* Science, 2000. **289**(5481): p. 950-3.
45. Bennett, C.N., *et al.*, *Regulation of osteoblastogenesis and bone mass by Wnt10b.* Proc Natl Acad Sci U S A, 2005. **102**(9): p. 3324-9.
46. Thomas, S. and B.G. Jaganathan, *Signaling network regulating osteogenesis in mesenchymal stem cells.* J Cell Commun Signal, 2022. **16**(1): p. 47-61.
47. Niehrs, C., *The complex world of WNT receptor signalling.* Nature Reviews Molecular Cell Biology, 2012. **13**(12): p. 767-779.
48. Day, T.F., *et al.*, *Wnt/β-Catenin Signaling in Mesenchymal Progenitors Controls Osteoblast and Chondrocyte Differentiation during Vertebrate Skeletogenesis.* Developmental Cell, 2005. **8**(5): p. 739-750.
49. Baht, G.S., *et al.*, *Activation of hedgehog signaling during fracture repair enhances osteoblastic-dependent matrix formation.* Journal of Orthopaedic Research, 2014. **32**(4): p. 581-586.
50. Zou, S., *et al.*, *Mesenchymal stem cells overexpressing Ihh promote bone repair.* Journal of Orthopaedic Surgery and Research, 2014. **9**(1): p. 102.
51. Kuwahara, S.T., *et al.*, *On the horizon: Hedgehog signaling to heal broken bones.* Bone Research, 2022. **10**(1): p. 13.
52. Zheng, H., *et al.*, *Cbfa1/osf2 Transduced Bone Marrow Stromal Cells Facilitate Bone Formation In Vitro and In Vivo.* Calcified Tissue International, 2004. **74**(2): p. 194-203.
53. Lee, M.H., *et al.*, *Transient upregulation of CBFA1 in response to bone morphogenetic protein-2 and transforming growth factor beta1 in C2C12 myogenic cells coincides with suppression of the myogenic phenotype but is not sufficient for osteoblast differentiation.* J Cell Biochem, 1999. **73**(1): p. 114-25.
54. Xu, J., *et al.*, *Potential mechanisms underlying the Runx2 induced osteogenesis of bone marrow mesenchymal stem cells.* Am J Transl Res, 2015. **7**(12): p. 2527-35.
55. Mu, T., *et al.*, *In Vitro Neural Differentiation of Bone Marrow Mesenchymal Stem Cells Carrying the FTH1 Reporter Gene and Detection with MRI.* Biomed Res Int, 2018. **2018**: p. 1978602.

56. Gong, M., *et al.*, *Retinoic acid receptor beta mediates all-trans retinoic acid facilitation of mesenchymal stem cells neuronal differentiation.* The International Journal of Biochemistry & Cell Biology, 2013. **45**(4): p. 866-875.
57. Shafiee, A., *et al.*, *A comparison between osteogenic differentiation of human unrestricted somatic stem cells and mesenchymal stem cells from bone marrow and adipose tissue.* Biotechnology Letters, 2011. **33**(6): p. 1257-1264.
58. Köllmer, M., *et al.*, *Markers Are Shared Between Adipogenic and Osteogenic Differentiated Mesenchymal Stem Cells.* J Dev Biol Tissue Eng, 2013. **5**(2): p. 18-25.
59. Manokawinchoke, J., *et al.*, *Mechanical loading and the control of stem cell behavior.* Arch Oral Biol, 2021. **125**: p. 105092.
60. Heng, W., *et al.*, *Effects of Electrical Stimulation on Stem Cells.* Curr Stem Cell Res Ther, 2020. **15**(5): p. 441-448.
61. Amin, S., *et al.*, *Comparing the effect of equiaxial cyclic mechanical stimulation on GATA4 expression in adipose-derived and bone marrow-derived mesenchymal stem cells.* Cell Biol Int, 2014. **38**(2): p. 219-27.
62. Foster, N.C., *et al.*, *Dynamic 3D culture: models of chondrogenesis and endochondral ossification.* Birth Defects Res C Embryo Today, 2015. **105**(1): p. 19-33.
63. Meier, E. and M. Lam, *Role of Mechanical Stimulation in Stem Cell Differentiation.* Biotechnology and Bioengineering, 2016. **3**: p. 1069.
64. Vining, K.H. and D.J. Mooney, *Mechanical forces direct stem cell behaviour in development and regeneration.* Nat Rev Mol Cell Biol, 2017. **18**(12): p. 728-742.
65. Janmey, P.A. and R.T. Miller, *Mechanisms of mechanical signaling in development and disease.* J Cell Sci, 2011. **124**(Pt 1): p. 9-18.
66. Curtis, A.S., *et al.*, *Cell interactions at the nanoscale: piezoelectric stimulation.* IEEE Trans Nanobioscience, 2013. **12**(3): p. 247-54.
67. Nikukar, H., *et al.*, *Osteogenesis of mesenchymal stem cells by nanoscale mechanotransduction.* ACS Nano, 2013. **7**(3): p. 2758-67.

68. Atala A, L.R., Thomson J et al., *Foundation of regenerative medicine*. 2010, San Diago: Elsevier.

69. Delaine-Smith, R.M. and G.C. Reilly, *The effects of mechanical loading on mesenchymal stem cell differentiation and matrix production.* Vitam Horm, 2011. **87**: p. 417-80.

70. Najrana, T. and J. Sanchez-Esteban, *Mechanotransduction as an Adaptation to Gravity.* Frontiers in pediatrics, 2016. **4**: p. 140-140.

71. Kelly, D.J. and C.R. Jacobs, *The role of mechanical signals in regulating chondrogenesis and osteogenesis of mesenchymal stem cells.* Birth Defects Res C Embryo Today, 2010. **90**(1): p. 75-85.

72. Deguchi, S., T. Ohashi, and M. Sato, *Tensile properties of single stress fibers isolated from cultured vascular smooth muscle cells.* J Biomech, 2006. **39**(14): p. 2603-10.

73. Tsuda, Y., *et al.*, *Torsional rigidity of single actin filaments and actin-actin bond breaking force under torsion measured directly by in vitro micromanipulation.* Proc Natl Acad Sci U S A, 1996. **93**(23): p. 12937-42.

74. Robertson, S., *et al.*, *Control of cell behaviour through nanovibrational stimulation: nanokicking.* Philosophical transactions. Series A, Mathematical, physical, and engineering sciences, 2018. **376**.

75. Holick, M.F., *Perspective on the impact of weightlessness on calcium and bone metabolism.* Bone, 1998. **22**(5 Suppl): p. 105s-111s.

76. Miyamoto, A., *et al.*, *Medical baseline data collection on bone and muscle change with space flight.* Bone, 1998. **22**(5 Suppl): p. 79s-82s.

77. Stavnichuk, M., *et al.*, *A systematic review and meta-analysis of bone loss in space travelers.* npj Microgravity, 2020. **6**(1): p. 13.

78. Baker, J.M., M. De Lisio, and G. Parise, *Endurance exercise training promotes medullary hematopoiesis.* The FASEB Journal, 2011. **25**(12): p. 4348-4357.

79. Marędziak, M., *et al.*, *Physical Activity Increases the Total Number of Bone-Marrow-Derived Mesenchymal Stem Cells, Enhances Their Osteogenic Potential, and Inhibits Their Adipogenic Properties.* Stem Cells Int, 2015. **2015**: p. 379093.

80. Zhang, L., *et al.*, *The effects of different intensities of exercise and active vitamin D on mouse bone mass and bone strength.* Journal of Bone and Mineral Metabolism, 2017. **35**(3): p. 265-277.
81. Pagnotti, G.M., *et al.*, *Combating osteoporosis and obesity with exercise: leveraging cell mechanosensitivity.* Nature Reviews Endocrinology, 2019. **15**(6): p. 339-355.
82. Fritton, S.P., K. J. McLeod, and C.T. Rubin, *Quantifying the strain history of bone: spatial uniformity and self-similarity of low-magnitude strains.* Journal of Biomechanics, 2000. **33**(3): p. 317-325.
83. Frost, H.M., *Bone "mass" and the "mechanostat": a proposal.* Anat Rec, 1987. **219**(1): p. 1-9.
84. Knapik, D., *et al.*, *Mechanosignaling in Bone Health, Trauma and Inflammation.* Antioxidants & redox signaling, 2013. **20**(6): p. 970-985.
85. Nagaraja, S., *Microstructural Stresses and Strains Associated with Trabecular Bone Microdamage*. 2006, Georgia Institute of Technology.
86. Delaine-Smith, R.M. and G.C. Reilly, *Mesenchymal stem cell responses to mechanical stimuli.* Muscles, ligaments and tendons journal, 2012. **2**(3): p. 169-180.
87. Gurkan, U.A. and O. Akkus, *The mechanical environment of bone marrow: a review.* Ann Biomed Eng, 2008. **36**(12): p. 1978-91.
88. Ingber Donald, E., *Mechanical Signaling and the Cellular Response to Extracellular Matrix in Angiogenesis and Cardiovascular Physiology.* Circulation Research, 2002. **91**(10): p. 877-887.
89. Selig, M., *et al.*, *Mechanotransduction and Stiffness-Sensing: Mechanisms and Opportunities to Control Multiple Molecular Aspects of Cell Phenotype as a Design Cornerstone of Cell-Instructive Biomaterials for Articular Cartilage Repair.* Int J Mol Sci, 2020. **21**(15).
90. Jansen, K.A., P. Atherton, and C. Ballestrem, *Mechanotransduction at the cell-matrix interface.* Seminars in Cell & Developmental Biology, 2017. **71**: p. 75-83.
91. Mitchison, T. and M. Kirschner, *Cytoskeletal dynamics and nerve growth.* Neuron, 1988. **1**(9): p. 761-772.

92. Elosegui-Artola, A., X. Trepat, and P. Roca-Cusachs, *Control of Mechanotransduction by Molecular Clutch Dynamics.* Trends in Cell Biology, 2018. **28**(5): p. 356-367.
93. Lewis, A.H. and J. Grandl, *Mechanical sensitivity of Piezo1 ion channels can be tuned by cellular membrane tension.* eLife, 2015. **4**: p. e12088.
94. Martino, F., *et al.*, *Cellular Mechanotransduction: From Tension to Function.* Frontiers in physiology, 2018. **9**: p. 824-824.
95. Wang, J.H.C. and B. Li, *Mechanics rules cell biology.* BMC Sports Science, Medicine and Rehabilitation, 2010. **2**(1): p. 16.
96. Park, J.S., *et al.*, *The effect of matrix stiffness on the differentiation of mesenchymal stem cells in response to TGF-β.* Biomaterials, 2011. **32**(16): p. 3921-30.
97. Vincent, L.G., *et al.*, *Mesenchymal stem cell durotaxis depends on substrate stiffness gradient strength.* Biotechnol J, 2013. **8**(4): p. 472-84.
98. Huebsch, N., *et al.*, *Harnessing traction-mediated manipulation of the cell/matrix interface to control stem-cell fate.* Nat Mater, 2010. **9**(6): p. 518-26.
99. Choquet, D., D.P. Felsenfeld, and M.P. Sheetz, *Extracellular matrix rigidity causes strengthening of integrin-cytoskeleton linkages.* Cell, 1997. **88**(1): p. 39-48.
100. Solon, J., *et al.*, *Fibroblast adaptation and stiffness matching to soft elastic substrates.* Biophys J, 2007. **93**(12): p. 4453-61.
101. Chowdhury, F., *et al.*, *Material properties of the cell dictate stress-induced spreading and differentiation in embryonic stem cells.* Nat Mater, 2010. **9**(1): p. 82-8.
102. Steward, A.J. and D.J. Kelly, *Mechanical regulation of mesenchymal stem cell differentiation.* J Anat, 2015. **227**(6): p. 717-31.
103. McBeath, R., *et al.*, *Cell Shape, Cytoskeletal Tension, and RhoA Regulate Stem Cell Lineage Commitment.* Developmental Cell, 2004. **6**(4): p. 483-495.
104. Gao, L., R. McBeath, and C.S. Chen, *Stem cell shape regulates a chondrogenic versus myogenic fate through Rac1 and N-cadherin.* Stem Cells, 2010. **28**(3): p. 564-72.

105. Lin, X., *et al.*, *Recent progress in stem cell differentiation directed by material and mechanical cues.* Biomed Mater, 2016. **11**(1): p. 014109.
106. Dalby, M.J., *et al.*, *The control of human mesenchymal cell differentiation using nanoscale symmetry and disorder.* Nature Materials, 2007. **6**(12): p. 997-1003.
107. Dalby, M.J., N. Gadegaard, and R.O. Oreffo, *Harnessing nanotopography and integrin-matrix interactions to influence stem cell fate.* Nat Mater, 2014. **13**(6): p. 558-69.
108. McNamara, L.E., *et al.*, *Skeletal stem cell physiology on functionally distinct titania nanotopographies.* Biomaterials, 2011. **32**(30): p. 7403-10.
109. Martinac, B., *Mechanosensitive ion channels: molecules of mechanotransduction.* J Cell Sci, 2004. **117**(Pt 12): p. 2449-60.
110. Campbell, J.J., D.L. Bader, and D.A. Lee, *Mechanical loading modulates intracellular calcium signaling in human mesenchymal stem cells.* J Appl Biomater Biomech, 2008. **6**(1): p. 9-15.
111. Pathak, M.M., *et al.*, *Stretch-activated ion channel Piezo1 directs lineage choice in human neural stem cells.* Proceedings of the National Academy of Sciences of the United States of America, 2014. **111**(45): p. 16148-16153.
112. Malek, A.M. and S. Izumo, *Mechanism of endothelial cell shape change and cytoskeletal remodeling in response to fluid shear stress.* J Cell Sci, 1996. **109** (4): p. 713-26.
113. Sachs, F., *Stretch-activated ion channels: what are they?* Physiology (Bethesda, Md.), 2010. **25**(1): p. 50-56.
114. Hayakawa, K., H. Tatsumi, and M. Sokabe, *Actin stress fibers transmit and focus force to activate mechanosensitive channels.* Journal of Cell Science, 2008. **121**(4): p. 496-503.
115. Dienes, B., *et al.*, *The Role of the Piezo1 Mechanosensitive Channel in the Musculoskeletal System.* Int J Mol Sci, 2023. **24**(7).
116. Alberts B, J.A., Lewis J, *et al.*, *Molecular Biology of the Cell*. 4th Edition ed. 2002, New York: Garland Science.

117. Henke, M., *et al.*, *Biomimetic Polymers (for Biomedical Applications)*, in *Reference Module in Materials Science and Materials Engineering*. 2017, Elsevier.
118. Giancotti, F.G. and E. Ruoslahti, *Integrin signaling.* Science, 1999. **285**(5430): p. 1028-32.
119. Wang, N., J.P. Butler, and D.E. Ingber, *Mechanotransduction across the cell surface and through the cytoskeleton.* Science, 1993. **260**(5111): p. 1124-7.
120. Clark, E.A. and J.S. Brugge, *Integrins and signal transduction pathways: the road taken.* Science, 1995. **268**(5208): p. 233-9.
121. Carthew, J., *et al.*, *Physical Stimulation in Tissue-Engineering*, in *Tissue Engineering in Oral and Maxillofacial Surgery*, R. Seppänen-Kaijansinkko, Editor. 2019, Springer International Publishing: Cham. p. 35-52.
122. Burridge, K., *et al.*, *Focal adhesions: transmembrane junctions between the extracellular matrix and the cytoskeleton.* Annu Rev Cell Biol, 1988. **4**: p. 487-525.
123. Chastney, M.R., J.R.W. Conway, and J. Ivaska, *Integrin adhesion complexes.* Current Biology, 2021. **31**(10): p. R536-R542.
124. Seok, S.H., *Structural Insights into Protein Regulation by Phosphorylation and Substrate Recognition of Protein Kinases/Phosphatases.* Life (Basel), 2021. **11**(9).
125. Zhou, J., *et al.*, *Mechanism of Focal Adhesion Kinase Mechanosensing.* PLoS Comput Biol, 2015. **11**(11): p. e1004593.
126. Kilian, K.A., *et al.*, *Geometric cues for directing the differentiation of mesenchymal stem cells.* Proc Natl Acad Sci U S A, 2010. **107**(11): p. 4872-7.
127. Tsimbouri, P.M., *et al.*, *Using nanotopography and metabolomics to identify biochemical effectors of multipotency.* ACS Nano, 2012. **6**(11): p. 10239-49.
128. Mierke, C.T., *et al.*, *Mechano-coupling and regulation of contractility by the vinculin tail domain.* Biophys J, 2008. **94**(2): p. 661-70.

129. Yoshigi, M., *et al.*, *Mechanical force mobilizes zyxin from focal adhesions to actin filaments and regulates cytoskeletal reinforcement.* J Cell Biol, 2005. **171**(2): p. 209-15.
130. Zhang, J., W.-h. Guo, and Y.-L. Wang, *Microtubules stabilize cell polarity by localizing rear signals.* Proceedings of the National Academy of Sciences, 2014. **111**.
131. Fletcher, D.A. and R.D. Mullins, *Cell mechanics and the cytoskeleton.* Nature, 2010. **463**(7280): p. 485-492.
132. Fink, J., *et al.*, *External forces control mitotic spindle positioning.* Nat Cell Biol, 2011. **13**(7): p. 771-8.
133. Khan, A.U., *et al.*, *A glance on the role of actin in osteogenic and adipogenic differentiation of mesenchymal stem cells.* Stem Cell Research & Therapy, 2020. **11**.
134. McGough, A., *et al.*, *Cofilin Changes the Twist of F-Actin: Implications for Actin Filament Dynamics and Cellular Function.* Journal of Cell Biology, 1997. **138**(4): p. 771-781.
135. Hayakawa, K., H. Tatsumi, and M. Sokabe, *Actin filaments function as a tension sensor by tension-dependent binding of cofilin to the filament.* Journal of Cell Biology, 2011. **195**(5): p. 721-727.
136. Murrell, M., *et al.*, *Forcing cells into shape: the mechanics of actomyosin contractility.* Nature Reviews Molecular Cell Biology, 2015. **16**(8): p. 486-498.
137. Khatau, S.B., *et al.*, *A perinuclear actin cap regulates nuclear shape.* Proceedings of the National Academy of Sciences, 2009. **106**(45): p. 19017.
138. Goffin, J.M., *et al.*, *Focal adhesion size controls tension-dependent recruitment of alpha-smooth muscle actin to stress fibers.* J Cell Biol, 2006. **172**(2): p. 259-68.
139. Tsimbouri, P.M., *et al.*, *Stimulation of 3D osteogenesis by mesenchymal stem cells using a nanovibrational bioreactor.* Nature Biomedical Engineering, 2017. **1**(9): p. 758-770.

140. Jiu, Y., *et al.*, *Bidirectional Interplay between Vimentin Intermediate Filaments and Contractile Actin Stress Fibers.* Cell Rep, 2015. **11**(10): p. 1511-8.
141. Burridge, K. and M. Chrzanowska-Wodnicka, *Focal Adhesions, Contractility, and Signaling.* Annual Review of Cell and Developmental Biology, 1996. **12**(1): p. 463-519.
142. Cai, Y., *et al.*, *Cytoskeletal coherence requires myosin-IIA contractility.* Journal of Cell Science, 2010. **123**(3): p. 413-423.
143. Even-Ram, S., *et al.*, *Myosin IIA regulates cell motility and actomyosin–microtubule crosstalk.* Nature Cell Biology, 2007. **9**(3): p. 299-309.
144. Ingber, D.E., N. Wang, and D. Stamenovic, *Tensegrity, cellular biophysics, and the mechanics of living systems.* Reports on progress in physics. Physical Society (Great Britain), 2014. **77**(4): p. 046603-046603.
145. Ingber, D.E., *Tensegrity and mechanotransduction.* Journal of bodywork and movement therapies, 2008. **12**(3): p. 198-200.
146. Ingber, D.E., *Tensegrity I. Cell structure and hierarchical systems biology.* Journal of Cell Science, 2003. **116**(7): p. 1157.
147. Ingber, D.E., *Tensegrity: The Architectural Basis of Cellular Mechanotransduction.* Annual Review of Physiology, 1997. **59**(1): p. 575-599.
148. Wang, L. and W. Chen, *Modelling Cell Origami via a Tensegrity Model of the Cytoskeleton in Adherent Cells.* Appl Bionics Biomech, 2019. **2019**: p. 8541303.
149. Bansod, Y.D., *et al.*, *A Finite Element Bendo-Tensegrity Model of Eukaryotic Cell.* Journal of Biomechanical Engineering, 2018. **140**(10).
150. Xu, G.K., *et al.*, *A Tensegrity Model of Cell Reorientation on Cyclically Stretched Substrates.* Biophys J, 2016. **111**(7): p. 1478-1486.
151. Vassaux, M. and J.L. Milan, *Stem cell mechanical behaviour modelling: substrate's curvature influence during adhesion.* Biomech Model Mechanobiol, 2017. **16**(4): p. 1295-1308.
152. De Santis, G., *et al.*, *How can cells sense the elasticity of a substrate? An analysis using a cell tensegrity model.* Eur Cell Mater, 2011. **22**: p. 202-13.

153. Kardas, D., U. Nackenhorst, and D. Balzani, *Computational model for the cell-mechanical response of the osteocyte cytoskeleton based on self-stabilizing tensegrity structures.* Biomech Model Mechanobiol, 2013. **12**(1): p. 167-83.
154. Brangwynne, C.P., *et al.*, *Microtubules can bear enhanced compressive loads in living cells because of lateral reinforcement.* J Cell Biol, 2006. **173**(5): p. 733-41.
155. Wang, N., J.D. Tytell, and D.E. Ingber, *Mechanotransduction at a distance: mechanically coupling the extracellular matrix with the nucleus.* Nature Reviews Molecular Cell Biology, 2009. **10**(1): p. 75-82.
156. Cho, S., J. Irianto, and D.E. Discher, *Mechanosensing by the nucleus: From pathways to scaling relationships.* The Journal of cell biology, 2017. **216**(2): p. 305-315.
157. Crisp, M., *et al.*, *Coupling of the nucleus and cytoplasm: role of the LINC complex.* J Cell Biol, 2006. **172**(1): p. 41-53.
158. Dahl, K.N., A.J.S. Ribeiro, and J. Lammerding, *Nuclear shape, mechanics, and mechanotransduction.* Circulation research, 2008. **102**(11): p. 1307-1318.
159. Raices, M. and M.A. D'Angelo, *Nuclear pore complex composition: a new regulator of tissue-specific and developmental functions.* Nat Rev Mol Cell Biol, 2012. **13**(11): p. 687-99.
160. Aragona, M., *et al.*, *A Mechanical Checkpoint Controls Multicellular Growth through YAP/TAZ Regulation by Actin-Processing Factors.* Cell, 2013. **154**(5): p. 1047-1059.
161. Benham-Pyle, B.W., B.L. Pruitt, and W.J. Nelson, *Mechanical strain induces E-cadherin–dependent Yap1 and β-catenin activation to drive cell cycle entry.* Science, 2015. **348**(6238): p. 1024-1027.
162. Calvo, F., *et al.*, *Mechanotransduction and YAP-dependent matrix remodelling is required for the generation and maintenance of cancer-associated fibroblasts.* Nat Cell Biol, 2013. **15**(6): p. 637-46.
163. Chaudhuri, O., *et al.*, *Hydrogels with tunable stress relaxation regulate stem cell fate and activity.* Nature Materials, 2016. **15**(3): p. 326-334.

164. Dupont, S., *et al.*, *Role of YAP/TAZ in mechanotransduction.* Nature, 2011. **474**(7350): p. 179-183.
165. Elosegui-Artola, A., *et al.*, *Mechanical regulation of a molecular clutch defines force transmission and transduction in response to matrix rigidity.* Nature Cell Biology, 2016. **18**(5): p. 540-548.
166. Nakajima, H., *et al.*, *Flow-Dependent Endothelial YAP Regulation Contributes to Vessel Maintenance.* Developmental Cell, 2017. **40**(6): p. 523-536.e6.
167. Wada, K.-I., *et al.*, *Hippo pathway regulation by cell morphology and stress fibers.* Development, 2011. **138**(18): p. 3907-3914.
168. Driscoll, Tristan P., *et al.*, *Cytoskeletal to Nuclear Strain Transfer Regulates YAP Signaling in Mesenchymal Stem Cells.* Biophysical Journal, 2015. **108**(12): p. 2783-2793.
169. Starr, D.A. and H.N. Fridolfsson, *Interactions Between Nuclei and the Cytoskeleton Are Mediated by SUN-KASH Nuclear-Envelope Bridges.* Annual Review of Cell and Developmental Biology, 2010. **26**(1): p. 421-444.
170. Uzer, G., *et al.*, *Cell Mechanosensitivity to Extremely Low-Magnitude Signals Is Enabled by a LINCed Nucleus.* Stem Cells, 2015. **33**(6): p. 2063-76.
171. Ueda, N., *et al.*, *Inner Nuclear Membrane Protein, SUN1, is Required for Cytoskeletal Force Generation and Focal Adhesion Maturation.* Frontiers in Cell and Developmental Biology, 2022. **10**.
172. Lammerding, J., *et al.*, *Lamin A/C deficiency causes defective nuclear mechanics and mechanotransduction.* J Clin Invest, 2004. **113**(3): p. 370-8.
173. Swift, J., *et al.*, *Nuclear Lamin-A Scales with Tissue Stiffness and Enhances Matrix-Directed Differentiation.* Science, 2013. **341**(6149): p. 1240104.
174. Uhler, C. and G.V. Shivashankar, *Regulation of genome organization and gene expression by nuclear mechanotransduction.* Nature Reviews Molecular Cell Biology, 2017. **18**(12): p. 717-727.
175. Zhao, H., *et al.*, *Specific Intensity Direct Current (DC) Electric Field Improves Neural Stem Cell Migration and Enhances Differentiation towards βIII-Tubulin+ Neurons.* PLoS One, 2015. **10**(6): p. e0129625.
176. Thrivikraman, G., G. Madras, and B. Basu, *Intermittent electrical stimuli for guidance of human mesenchymal stem cell lineage commitment towards*

neural-like cells on electroconductive substrates. Biomaterials, 2014. **35**(24): p. 6219-35.

177. Naskar, S., *et al.*, *Neurogenesis-on-Chip: Electric field modulated transdifferentiation of human mesenchymal stem cell and mouse muscle precursor cell coculture.* Biomaterials, 2020. **226**: p. 119522.
178. Guo, W., *et al.*, *Self-Powered Electrical Stimulation for Enhancing Neural Differentiation of Mesenchymal Stem Cells on Graphene-Poly(3,4-ethylenedioxythiophene) Hybrid Microfibers.* ACS Nano, 2016. **10**(5): p. 5086-95.
179. Gupta, A.K., K.P. Srivastava, and S. Avasthi, *Pulsed electromagnetic stimulation in nonunion of tibial diaphyseal fractures.* Indian J Orthop, 2009. **43**(2): p. 156-60.
180. Liu, H.-F., *et al.*, *Pulsed electromagnetic fields on postmenopausal osteoporosis in southwest China: A randomized, active-controlled clinical trial.* Bioelectromagnetics, 2013. **34**(4): p. 323-332.
181. Cebrián, J.L., *et al.*, *Role of Electromagnetic Stimulation in the Treatment of Osteonecrosis of the Femoral Head in Early Stages.* Journal of Biomedical Science and Engineering, 2014. **7**(5): p. 252-257.
182. Hronik-Tupaj, M., *et al.*, *Osteoblastic differentiation and stress response of human mesenchymal stem cells exposed to alternating current electric fields.* BioMedical Engineering OnLine, 2011. **10**(1): p. 9.
183. Bagheri, L., *et al.*, *Notch pathway is active during osteogenic differentiation of human bone marrow mesenchymal stem cells induced by pulsed electromagnetic fields.* Journal of Tissue Engineering and Regenerative Medicine, 2018. **12**(2): p. 304-315.
184. Martini, F., *et al. Bone Morphogenetic Protein-2 Signaling in the Osteogenic Differentiation of Human Bone Marrow Mesenchymal Stem Cells Induced by Pulsed Electromagnetic Fields*. International Journal of Molecular Sciences, 2020. **21**, 2104.
185. Khaw, J.S., *et al.*, *Electrical stimulation of titanium to promote stem cell orientation, elongation and osteogenesis.* Acta Biomaterialia, 2022. **139**: p. 204-217.

186. Baek, S., *et al.*, *Electrical Stimulation of Human Adipose-Derived Mesenchymal Stem Cells on O(2) Plasma-Treated ITO Glass Promotes Osteogenic Differentiation.* Int J Mol Sci, 2022. **23**(20).
187. Yong, Y., *et al.*, *Electromagnetic fields promote osteogenesis of rat mesenchymal stem cells through the PKA and ERK1/2 pathways.* Journal of Tissue Engineering and Regenerative Medicine, 2016. **10**(10): p. E537-E545.
188. Pietronave, S., *et al.*, *Monophasic and Biphasic Electrical Stimulation Induces a Precardiac Differentiation in Progenitor Cells Isolated from Human Heart.* Stem Cells and Development, 2013. **23**(8): p. 888-898.
189. Ma, R., *et al.*, *Electrical Stimulation Enhances Cardiac Differentiation of Human Induced Pluripotent Stem Cells for Myocardial Infarction Therapy.* Antioxidants & Redox Signaling, 2016. **28**(5): p. 371-384.
190. Nazari, H., *et al.*, *Electrical stimulation induces differentiation of human cardiosphere-derived cells (hCDCs) to committed cardiomyocyte.* Molecular and Cellular Biochemistry, 2020. **470**(1): p. 29-39.
191. He, X., *et al.*, *Biomimetic electrical stimulation induces rat bone marrow mesenchymal stem cells to differentiate into cardiomyocyte-like cells via TGF-beta 1 in vitro.* Progress in Biophysics and Molecular Biology, 2019. **148**: p. 47-53.
192. Vaca-González, J.J., *et al.*, *Effect of electrical stimulation on chondrogenic differentiation of mesenchymal stem cells cultured in hyaluronic acid – Gelatin injectable hydrogels.* Bioelectrochemistry, 2020. **134**: p. 107536.
193. Finger, A.R., *et al.*, *Differential effects on messenger ribonucleic acid expression by bone marrow-derived human mesenchymal stem cells seeded in agarose constructs due to ramped and steady applications of cyclic hydrostatic pressure.* Tissue Eng, 2007. **13**(6): p. 1151-8.
194. Elder, B.D. and K.A. Athanasiou, *Hydrostatic pressure in articular cartilage tissue engineering: from chondrocytes to tissue regeneration.* Tissue Eng Part B Rev, 2009. **15**(1): p. 43-53.
195. Grad, S., *et al.*, *Physical stimulation of chondrogenic cells in vitro: a review.* Clin Orthop Relat Res, 2011. **469**(10): p. 2764-72.

196. Puetzer, J., *et al.*, *The effects of cyclic hydrostatic pressure on chondrogenesis and viability of human adipose- and bone marrow-derived mesenchymal stem cells in three-dimensional agarose constructs.* Tissue Eng Part A, 2013. **19**(1-2): p. 299-306.
197. Angele, P., *et al.*, *Cyclic hydrostatic pressure enhances the chondrogenic phenotype of human mesenchymal progenitor cells differentiated in vitro.* J Orthop Res, 2003. **21**(3): p. 451-7.
198. Huang, C.Y., *et al.*, *Effects of cyclic compressive loading on chondrogenesis of rabbit bone-marrow derived mesenchymal stem cells.* Stem Cells, 2004. **22**(3): p. 313-23.
199. Kong, Z., *et al.*, *Dynamic compression promotes proliferation and neovascular networks of endothelial progenitor cells in demineralized bone matrix scaffold seed.* J Appl Physiol (1985), 2012. **113**(4): p. 619-26.
200. Sim, W.Y., *et al.*, *A pneumatic micro cell chip for the differentiation of human mesenchymal stem cells under mechanical stimulation.* Lab on a Chip, 2007. **7**(12): p. 1775-1782.
201. Ouyang, X., Y. Xie, and G. Wang, *Mechanical stimulation promotes the proliferation and the cartilage phenotype of mesenchymal stem cells and chondrocytes co-cultured in vitro.* Biomed Pharmacother, 2019. **117**: p. 109146.
202. Baker, B.M., *et al.*, *Dynamic tensile loading improves the functional properties of mesenchymal stem cell-laden nanofiber-based fibrocartilage.* Tissue engineering. Part A, 2011. **17**(9-10): p. 1445-1455.
203. Subramony, S.D., *et al.*, *The guidance of stem cell differentiation by substrate alignment and mechanical stimulation.* Biomaterials, 2013. **34**(8): p. 1942-53.
204. McMahon, L.A., *et al.*, *Regulatory effects of mechanical strain on the chondrogenic differentiation of MSCs in a collagen-GAG scaffold: experimental and computational analysis.* Ann Biomed Eng, 2008. **36**(2): p. 185-94.
205. McMahon, L.A., V.A. Campbell, and P.J. Prendergast, *Involvement of stretch-activated ion channels in strain-regulated glycosaminoglycan synthesis in*

mesenchymal stem cell-seeded 3D scaffolds. J Biomech, 2008. **41**(9): p. 2055-9.

206. Sumanasinghe, R.D., S.H. Bernacki, and E.G. Loboa, *Osteogenic differentiation of human mesenchymal stem cells in collagen matrices: effect of uniaxial cyclic tensile strain on bone morphogenetic protein (BMP-2) mRNA expression.* Tissue Eng, 2006. **12**(12): p. 3459-65.
207. Ward, D.F., Jr., *et al.*, *Mechanical strain enhances extracellular matrix-induced gene focusing and promotes osteogenic differentiation of human mesenchymal stem cells through an extracellular-related kinase-dependent pathway.* Stem Cells Dev, 2007. **16**(3): p. 467-80.
208. Byrne, E.M., *et al.*, *Gene expression by marrow stromal cells in a porous collagen-glycosaminoglycan scaffold is affected by pore size and mechanical stimulation.* J Mater Sci Mater Med, 2008. **19**(11): p. 3455-63.
209. Hanson, A.D., *et al.*, *Osteogenic effects of rest inserted and continuous cyclic tensile strain on hASC lines with disparate osteodifferentiation capabilities.* Ann Biomed Eng, 2009. **37**(5): p. 955-65.
210. Kearney, E.M., *et al.*, *Tensile strain as a regulator of mesenchymal stem cell osteogenesis.* Ann Biomed Eng, 2010. **38**(5): p. 1767-79.
211. Rui, Y.F., *et al.*, *Mechanical loading increased BMP-2 expression which promoted osteogenic differentiation of tendon-derived stem cells.* J Orthop Res, 2011. **29**(3): p. 390-6.
212. Qi, M.C., *et al.*, *Mechanical strain induces osteogenic differentiation: Cbfa1 and Ets-1 expression in stretched rat mesenchymal stem cells.* Int J Oral Maxillofac Surg, 2008. **37**(5): p. 453-8.
213. Koike, M., *et al.*, *Effects of mechanical strain on proliferation and differentiation of bone marrow stromal cell line ST2.* J Bone Miner Metab, 2005. **23**(3): p. 219-25.
214. Lohberger, B., *et al.*, *Effect of cyclic mechanical stimulation on the expression of osteogenesis genes in human intraoral mesenchymal stromal and progenitor cells.* Biomed Res Int, 2014. **2014**: p. 189516.

215. Qi, M.C., *et al.*, *Expression of bone-related genes in bone marrow MSCs after cyclic mechanical strain: implications for distraction osteogenesis.* Int J Oral Sci, 2009. **1**(3): p. 143-50.
216. Wu, Y., *et al.*, *Osteoclastogenesis accompanying early osteoblastic differentiation of BMSCs promoted by mechanical stretch.* Biomed Rep, 2013. **1**(3): p. 474-478.
217. Tannaz, N.A., *et al.*, *Comparing the effect of uniaxial cyclic mechanical stimulation and chemical factors on myogenin and Myh2 expression in mouse embryonic and bone marrow derived mesenchymal stem cells.* Mol Cell Biomech, 2014. **11**(1): p. 19-37.
218. Bayati, V., *et al.*, *The evaluation of cyclic uniaxial strain on myogenic differentiation of adipose-derived stem cells.* Tissue Cell, 2011. **43**(6): p. 359-66.
219. Li, Z., *et al.*, *Mechanical load modulates chondrogenesis of human mesenchymal stem cells through the TGF-beta pathway.* J Cell Mol Med, 2010. **14**(6a): p. 1338-46.
220. Saha, S., *et al.*, *TGFbeta/Activin/Nodal pathway in inhibition of human embryonic stem cell differentiation by mechanical strain.* Biophys J, 2008. **94**(10): p. 4123-33.
221. Khani, M.M., *et al.*, *Mechanical characterization of human mesenchymal stem cells subjected to cyclic uniaxial strain and TGF-β1.* J Mech Behav Biomed Mater, 2015. **43**: p. 18-25.
222. Teramura, T., *et al.*, *Mechanical stimulation of cyclic tensile strain induces reduction of pluripotent related gene expressions via activation of Rho/ROCK and subsequent decreasing of AKT phosphorylation in human induced pluripotent stem cells.* Biochem Biophys Res Commun, 2012. **417**(2): p. 836-41.
223. Bai, K., *et al.*, *Endothelium oriented differentiation of bone marrow mesenchymal stem cells under chemical and mechanical stimulations.* J Biomech, 2010. **43**(6): p. 1176-81.

224. Huang, Y., *et al.*, *Effect of fluid shear stress on cardiomyogenic differentiation of rat bone marrow mesenchymal stem cells.* Arch Med Res, 2010. **41**(7): p. 497-505.
225. Kim, D.H., *et al.*, *Shear stress magnitude is critical in regulating the differentiation of mesenchymal stem cells even with endothelial growth medium.* Biotechnol Lett, 2011. **33**(12): p. 2351-9.
226. Dong, J.D., *et al.*, *Response of mesenchymal stem cells to shear stress in tissue-engineered vascular grafts.* Acta Pharmacol Sin, 2009. **30**(5): p. 530-6.
227. Knippenberg, M., *et al.*, *Adipose tissue-derived mesenchymal stem cells acquire bone cell-like responsiveness to fluid shear stress on osteogenic stimulation.* Tissue Eng, 2005. **11**(11-12): p. 1780-8.
228. Li, Y.J., *et al.*, *Oscillatory fluid flow affects human marrow stromal cell proliferation and differentiation.* J Orthop Res, 2004. **22**(6): p. 1283-9.
229. Riddle, R.C., *et al.*, *MAP kinase and calcium signaling mediate fluid flow-induced human mesenchymal stem cell proliferation.* Am J Physiol Cell Physiol, 2006. **290**(3): p. C776-84.
230. Datta, N., *et al.*, *In vitro generated extracellular matrix and fluid shear stress synergistically enhance 3D osteoblastic differentiation.* Proceedings of the National Academy of Sciences of the United States of America, 2006. **103**(8): p. 2488-2493.
231. Arnsdorf, E.J., *et al.*, *Mechanically induced osteogenic differentiation--the role of RhoA, ROCKII and cytoskeletal dynamics.* Journal of cell science, 2009. **122**(Pt 4): p. 546-553.
232. Luo, W., *et al.*, *Laminar shear stress delivers cell cycle arrest and anti-apoptosis to mesenchymal stem cells.* Acta Biochim Biophys Sin (Shanghai), 2011. **43**(3): p. 210-6.
233. Bancroft, G.N., *et al.*, *Fluid flow increases mineralized matrix deposition in 3D perfusion culture of marrow stromal osteoblasts in a dose-dependent manner.* Proceedings of the National Academy of Sciences of the United States of America, 2002. **99**(20): p. 12600-12605.

234. Prè, D., *et al.*, *High-Frequency Vibration Treatment of Human Bone Marrow Stromal Cells Increases Differentiation toward Bone Tissue.* Bone Marrow Res, 2013. **2013**: p. 803450.
235. Prè, D., *et al.*, *Effects of low-amplitude, high-frequency vibrations on proliferation and differentiation of SAOS-2 human osteogenic cell line.* Tissue Eng Part C Methods, 2009. **15**(4): p. 669-79.
236. Prè, D., *et al.*, *The differentiation of human adipose-derived stem cells (hASCs) into osteoblasts is promoted by low amplitude, high frequency vibration treatment.* Bone, 2011. **49**(2): p. 295-303.
237. Cashion, A.T., *et al.*, *Programmable mechanobioreactor for exploration of the effects of periodic vibratory stimulus on mesenchymal stem cell differentiation.* BioResearch open access, 2014. **3**(1): p. 19-28.
238. Lee, W., *et al.*, *The Osteogenic Differentiation of Human Dental Pulp Stem Cells through G0/G1 Arrest and the p-ERK/Runx-2 Pathway by Sonic Vibration.* Int J Mol Sci, 2021. **22**(18).
239. Sancilio, S., *et al.*, *Effects of Focused Vibrations on Human Satellite Cells.* Int J Mol Sci, 2022. **23**(11).
240. Lin, C.Y., *et al.*, *Yoda1 Enhanced Low-Magnitude High-Frequency Vibration on Osteocytes in Regulation of MDA-MB-231 Breast Cancer Cell Migration.* Cancers (Basel), 2022. **14**(14).
241. Hortobagyi, D., *et al.*, *In vitro mechanical vibration down-regulates pro-inflammatory and pro-fibrotic signaling in human vocal fold fibroblasts.* PLOS ONE, 2020. **15**(11): p. e0241901.
242. Sun, T., *et al.*, *Effects of mechanical vibration on cell morphology, proliferation, apoptosis, and cytokine expression/secretion in osteocyte-like MLO-Y4 cells exposed to high glucose.* Cell Biol Int, 2019. **44**(1): p. 216-228.
243. LaGier, A.J., *et al.*, *Vibration, a treatment for migraine, linked to calpain driven changes in actin cytoskeleton.* PLoS One, 2022. **17**(4): p. e0262058.
244. Mojena-Medina, D., *et al.*, *Design, Implementation, and Validation of a Piezoelectric Device to Study the Effects of Dynamic Mechanical Stimulation on Cell Proliferation, Migration and Morphology.* Sensors (Basel), 2020. **20**(7).

245. Hou, W., *et al.*, *Low magnitude high frequency vibration promotes chondrogenic differentiation of bone marrow stem cells with involvement of β-catenin signaling pathway.* Archives of Oral Biology, 2020. **118**: p. 104860.
246. Baskan, O., G. Mese, and E. Ozcivici, *Low-intensity vibrations normalize adipogenesis-induced morphological and molecular changes of adult mesenchymal stem cells.* Proceedings of the Institution of Mechanical Engineers. Part H, Journal of engineering in medicine, 2017. **231**(2): p. 160-168.
247. Haffner-Luntzer, M., *et al.*, *Effects of low-magnitude high-frequency vibration on osteoblasts are dependent on estrogen receptor α signaling and cytoskeletal remodeling.* Biochemical and Biophysical Research Communications, 2018. **503**(4): p. 2678-2684.
248. García-López, S., *et al.*, *Micro-vibrations at 30 Hz on bone cells cultivated in vitro produce soluble factors for osteoclast inhibition and osteoblast activity.* Archives of Oral Biology, 2020. **110**: p. 104594.
249. Thompson, M., *et al.*, *Low-intensity vibration restores nuclear YAP levels and acute YAP nuclear shuttling in mesenchymal stem cells subjected to simulated microgravity.* npj Microgravity, 2020. **6**(1): p. 35.
250. Enomoto, U., C. Imashiro, and K. Takemura, *Collective cell migration of fibroblasts is affected by horizontal vibration of the cell culture dish.* Engineering in Life Sciences, 2020. **20**(9-10): p. 402-411.
251. Safavi, A.S., *et al.*, *Efficacy of mechanical vibration in regulating mesenchymal stem cells gene expression.* In Vitro Cellular & Developmental Biology - Animal, 2019. **55**(5): p. 387-394.
252. Takeuchi, R., *et al.*, *Effects of vibration and hyaluronic acid on activation of three-dimensional cultured chondrocytes.* Arthritis Rheum, 2006. **54**(6): p. 1897-905.
253. Lauffenburger, D.A. and A.F. Horwitz, *Cell Migration: A Physically Integrated Molecular Process.* Cell, 1996. **84**(3): p. 359-369.
254. Judex, S. and S. Pongkitwitoon, *Differential Efficacy of 2 Vibrating Orthodontic Devices to Alter the Cellular Response in Osteoblasts,*

Fibroblasts, and Osteoclasts. Dose Response, 2018. **16**(3): p. 1559325818792112.

255. Chen, B., *et al.*, *Low-magnitude, high-frequency vibration promotes the adhesion and the osteogenic differentiation of bone marrow-derived mesenchymal stem cells cultured on a hydroxyapatite-coated surface: The direct role of Wnt/β-catenin signaling pathway activation.* Int J Mol Med, 2016. **38**(5): p. 1531-1540.
256. Kim, I.S., *et al.*, *Human mesenchymal stromal cells are mechanosensitive to vibration stimuli.* J Dent Res, 2012. **91**(12): p. 1135-40.
257. Marędziak, M., *et al.*, *The Effect of Low-Magnitude Low-Frequency Vibrations (LMLF) on Osteogenic Differentiation Potential of Human Adipose Derived Mesenchymal Stem Cells.* Cell Mol Bioeng, 2017. **10**(6): p. 549-562.
258. Grosman-Dziewiszek, P., *et al.*, *Influence of 40 Hz and 100 Hz Vibration on SH-SY5Y Cells Growth and Differentiation-A Preliminary Study.* Molecules, 2022. **27**(10).
259. Chen, X., *et al.*, *Acoustic-Frequency Vibratory Stimulation Regulates the Balance between Osteogenesis and Adipogenesis of Human Bone Marrow-Derived Mesenchymal Stem Cells.* BioMed Research International, 2015. **2015**: p. 1-10.
260. Gao, H., *et al.*, *Low-level mechanical vibration enhances osteoblastogenesis via a canonical Wnt signaling-associated mechanism.* Mol Med Rep, 2017. **16**(1): p. 317-324.
261. Touchstone, H., *et al.*, *Recovery of stem cell proliferation by low intensity vibration under simulated microgravity requires LINC complex.* NPJ Microgravity, 2019. **5**: p. 11.
262. Zhou, Y., *et al.*, *Osteogenic differentiation of bone marrow-derived mesenchymal stromal cells on bone-derived scaffolds: effect of microvibration and role of ERK1/2 activation.* Eur Cell Mater, 2011. **22**: p. 12-25.

263. Marycz, K., *et al.*, *Low-frequency, low-magnitude vibrations (LFLM) enhances chondrogenic differentiation potential of human adipose derived mesenchymal stromal stem cells (hASCs).* PeerJ, 2016. **4**: p. e1637.
264. Cho, H., *et al.*, *Neural differentiation of umbilical cord mesenchymal stem cells by sub-sonic vibration.* Life sciences, 2012. **90**: p. 591-9.
265. Zhang, C., *et al.*, *Effects of mechanical vibration on proliferation and osteogenic differentiation of human periodontal ligament stem cells.* Arch Oral Biol, 2012. **57**(10): p. 1395-407.
266. Lau, E., *et al.*, *Effect of low-magnitude, high-frequency vibration on osteogenic differentiation of rat mesenchymal stromal cells.* Journal of orthopaedic research : official publication of the Orthopaedic Research Society, 2011. **29**(7): p. 1075-1080.
267. Rosenberg, N., M. Levy, and M. Francis, *Experimental model for stimulation of cultured human osteoblast-like cells by high frequency vibration.* Cytotechnology, 2002. **39**(3): p. 125-30.
268. Uzer, G., *et al.*, *Separating Fluid Shear Stress from Acceleration during Vibrations in Vitro: Identification of Mechanical Signals Modulating the Cellular Response.* Cell Mol Bioeng, 2012. **5**(3): p. 266-276.
269. Bacabac, R.G., *et al.*, *Bone cell responses to high-frequency vibration stress: does the nucleus oscillate within the cytoplasm?* Faseb j, 2006. **20**(7): p. 858-64.
270. Uzer, G., *et al.*, *Vibration induced osteogenic commitment of mesenchymal stem cells is enhanced by cytoskeletal remodeling but not fluid shear.* J Biomech, 2013. **46**(13): p. 2296-302.
271. Pongkitwitoon, S., *et al.*, *Cytoskeletal Configuration Modulates Mechanically Induced Changes in Mesenchymal Stem Cell Osteogenesis, Morphology, and Stiffness.* Sci Rep, 2016. **6**: p. 34791.
272. Lorusso, D., *et al.*, *Vibration of osteoblastic cells using a novel motion-control platform does not acutely alter cytosolic calcium, but desensitizes subsequent responses to extracellular ATP.* Journal of Cellular Physiology, 2020. **235**(6): p. 5096-5110.

273. Coughlin, T.R. and G.L. Niebur, *Fluid shear stress in trabecular bone marrow due to low-magnitude high-frequency vibration.* J Biomech, 2012. **45**(13): p. 2222-9.
274. Halonen, H.T., *et al.*, *Cell adhesion and culture medium dependent changes in the high frequency mechanical vibration induced proliferation, osteogenesis, and intracellular organization of human adipose stem cells.* J Mech Behav Biomed Mater, 2020. **101**: p. 103419.
275. Venugopal, B., *et al.*, *Cell density overrides the effect of substrate stiffness on human mesenchymal stem cells' morphology and proliferation.* Biomaterials Science, 2018. **6**(5): p. 1109-1119.
276. Yassin, M.A., *et al.*, *Cell seeding density is a critical determinant for copolymer scaffolds-induced bone regeneration.* Journal of Biomedical Materials Research Part A, 2015. **103**(11): p. 3649-3658.
277. Bitar, M., *et al.*, *Effect of Cell Density on Osteoblastic Differentiation and Matrix Degradation of Biomimetic Dense Collagen Scaffolds.* Biomacromolecules, 2008. **9**(1): p. 129-135.
278. Francioli, S.E., *et al.*, *Effect of three-dimensional expansion and cell seeding density on the cartilage-forming capacity of human articular chondrocytes in type II collagen sponges.* Journal of Biomedical Materials Research Part A, 2010. **95A**(3): p. 924-931.
279. Cao, C., *et al.*, *Effects of cell phenotype and seeding density on the chondrogenic capacity of human osteoarthritic chondrocytes in type I collagen scaffolds.* J Orthop Surg Res, 2020. **15**(1): p. 120.
280. Olderøy, M., *et al.*, *Biochemical and structural characterization of neocartilage formed by mesenchymal stem cells in alginate hydrogels.* PLoS One, 2014. **9**(3): p. e91662.
281. Sukho, P., *et al.*, *Effect of Cell Seeding Density and Inflammatory Cytokines on Adipose Tissue-Derived Stem Cells: an in Vitro Study.* Stem Cell Reviews and Reports, 2017. **13**(2): p. 267-277.
282. Issa, R.I., *et al.*, *The Effect of Cell Seeding Density on the Cellular and Mechanical Properties of a Mechanostimulated Tissue-Engineered Tendon.* Tissue Engineering Part A, 2011. **17**(11-12): p. 1479-1487.

283. Mauck, R.L., *et al.*, *The role of cell seeding density and nutrient supply for articular cartilage tissue engineering with deformational loading.* Osteoarthritis and Cartilage, 2003. **11**(12): p. 879-890.
284. Ota, T., M. Chiba, and H. Hayashi, *Vibrational stimulation induces osteoblast differentiation and the upregulation of osteogenic gene expression in vitro.* Cytotechnology, 2016. **68**(6): p. 2287-2299.
285. Ambattu, L.A., A. Gelmi, and L.Y. Yeo, *Short-Duration High Frequency MegaHertz-Order Nanomechanostimulation Drives Early and Persistent Osteogenic Differentiation in Mesenchymal Stem Cells.* Small, 2022. **18**(8): p. 2106823.
286. Tong, Z., R. Duncan, and X. Jia, *Modulating the Behaviors of Mesenchymal Stem Cells Via the Combination of High-Frequency Vibratory Stimulations and Fibrous Scaffolds.* Tissue engineering. Part A, 2013. **19**(15-16): p. 1862-78.
287. Orapiriyakul, W., *et al.*, *Nanovibrational Stimulation of Mesenchymal Stem Cells Induces Therapeutic Reactive Oxygen Species and Inflammation for Three-Dimensional Bone Tissue Engineering.* ACS nano, 2020. **14**(8): p. 10027-10044.
288. Kennedy, J.W., *et al.*, *Nanovibrational stimulation inhibits osteoclastogenesis and enhances osteogenesis in co-cultures.* Scientific Reports, 2021. **11**(1): p. 22741.
289. Macione, J., *et al.*, *Stimulation of osteoblast differentiation with guided ultrasound waves.* J Ther Ultrasound, 2015. **3**: p. 12.
290. Pravitharangul, A., S. Suttapreyasri, and C. Leethanakul, *Iliac and mandible osteoblasts exhibit varied responses to LMHF vibration.* Cell Biol Int, 2018. **42**(10): p. 1349-1357.
291. Zhao, Q., *et al.*, *Low magnitude high frequency vibration promotes adipogenic differentiation of bone marrow stem cells via P38 MAPK signal.* PLoS One, 2017. **12**(3): p. e0172954.
292. Chu, Y.C., *et al.*, *Piezoelectric stimulation by ultrasound facilitates chondrogenesis of mesenchymal stem cells.* J Acoust Soc Am, 2020. **148**(1): p. El58.

293. Wang, C.-Z., *et al.*, *Low-magnitude vertical vibration enhances myotube formation in C2C12 myoblasts.* Journal of Applied Physiology, 2010. **109**(3): p. 840-848.
294. Lin, Y.H., *et al.*, *The Essential Role of Stathmin in Myoblast C2C12 for Vertical Vibration-Induced Myotube Formation.* Biomolecules, 2021. **11**(11): p. 1583.
295. Pierres, A., *et al.*, *Do membrane undulations help cells probe the world?* Trends in Cell Biology, 2009. **19**(9): p. 428-433.
296. Voelkner, C., *et al.*, *The nanomorphology of cell surfaces of adhered osteoblasts.* Beilstein J Nanotechnol, 2021. **12**: p. 242-256.
297. Campsie, P., *et al.*, *Design, construction and characterisation of a novel nanovibrational bioreactor and cultureware for osteogenesis.* Sci Rep, 2019. **9**(1): p. 12944.
298. Pemberton, G.D., *et al.*, *Nanoscale stimulation of osteoblastogenesis from mesenchymal stem cells: nanotopography and nanokicking.* Nanomedicine (Lond), 2015. **10**(4): p. 547-60.
299. Håkansson, B., *et al.*, *Resonance frequencies of the human skull in vivo.* J Acoust Soc Am, 1994. **95**(3): p. 1474-81.
300. Robertson, S.N., *et al.*, *Reduction of Pseudomonas aeruginosa biofilm formation through the application of nanoscale vibration.* Journal of Bioscience and Bioengineering, 2020. **129**(3): p. 379-386.
301. Simakou, T., R. Freeburn, and F.L. Henriquez, *Gene expression during THP-1 differentiation is influenced by vitamin D3 and not vibrational mechanostimulation.* PeerJ, 2021. **9**: p. e11773.
302. Nikukar, H., *et al.*, *Production of Nanoscale Vibration for Stimulation of Human Mesenchymal Stem Cells.* J Biomed Nanotechnol, 2016. **12**(7): p. 1478-88.
303. Bansod, Y., *Computational simulation of mechanical tests of isolated animal cell*. 2016, Brno Unviersity of Technology.
304. McGarry, J.G. and P.J. Prendergast, *A three-dimensional finite element model of an adherent eukaryotic cell.* Eur Cell Mater, 2004. **7**: p. 27-33.

305. Lipowsky, H.H., *et al.*, *Mesenchymal Stem Cell Deformability and Implications for Microvascular Sequestration.* Annals of biomedical engineering, 2018. **46**(4): p. 640-654.
306. Williams, J.A., *et al.*, *Developing and Investigating a Nanovibration Intervention for the Prevention/Reversal of Bone Loss Following Spinal Cord Injury.* ACS Nano, 2024. **18**(27): p. 17630-17641.
307. Wang, H.-B., *et al.*, *Focal adhesion kinase is involved in mechanosensing during fibroblast migration.* Proceedings of the National Academy of Sciences, 2001. **98**(20): p. 11295.
308. Steward, R.L., Jr., *et al.*, *Mechanical stretch and shear flow induced reorganization and recruitment of fibronectin in fibroblasts.* Scientific reports, 2011. **1**: p. 147-147.
309. Kurulgan Demirci, E., *et al.*, *Genome-Wide Gene Expression Analysis of NIH 3T3 Cell Line Under Mechanical Stimulation.* Cellular and Molecular Bioengineering, 2011. **4**(1): p. 46-55.
310. Wahlsten, A., *et al.*, *Mechanical stimulation induces rapid fibroblast proliferation and accelerates the early maturation of human skin substitutes.* Biomaterials, 2021. **273**: p. 120779.
311. Anloague, A., *et al.*, *Mechanical stimulation of human dermal fibroblasts regulates pro-inflammatory cytokines: potential insight into soft tissue manual therapies.* BMC research notes, 2020. **13**(1): p. 400-400.
312. Jiang, Y.-Y., *et al.*, *Enhancing Proliferation and ECM Expression of Human ACL Fibroblasts by Sonic Vibration.* Preparative Biochemistry & Biotechnology, 2015. **45**(5): p. 476-490.
313. Wolchok, J.C., *et al.*, *The effect of bioreactor induced vibrational stimulation on extracellular matrix production from human derived fibroblasts.* Biomaterials, 2009. **30**(3): p. 327-335.
314. Mishra, P., *et al.*, *Fluorescence Imaging of Actin Turnover Parses Early Stem Cell Lineage Divergence and Senescence.* Scientific Reports, 2019. **9**(1): p. 10377.
315. McColloch, A., *et al.*, *Correlation between Nuclear Morphology and Adipogenic Differentiation: Application of a Combined Experimental and*

Computational Modeling Approach. Scientific Reports, 2019. **9**(1): p. 16381.

316. Liu, E., *et al.*, *Parsing the early cytoskeletal and nuclear organizational cues that demarcate stem cell lineages.* Cell Cycle, 2010. **9**(11): p. 2108-2117.
317. Demiray, L. and E. Ozcivici, *Bone marrow stem cells adapt to low-magnitude vibrations by altering theircytoskeleton during quiescence and osteogenesis.* Turkish Journal of Biology, 2015. **39**: p. 88-97.
318. Wu, J., *et al.*, *Joint construction of micro-vibration stimulation and BCP scaffolds for enhanced bioactivity and self-adaptability tissue engineered bone grafts.* Journal of Materials Chemistry B, 2020. **8**.
319. Gavara, N. and R.S. Chadwick, *Relationship between cell stiffness and stress fiber amount, assessed by simultaneous atomic force microscopy and live-cell fluorescence imaging.* Biomech Model Mechanobiol, 2016. **15**(3): p. 511-23.
320. Garcia, P.D., C.R. Guerrero, and R. Garcia, *Nanorheology of living cells measured by AFM-based force–distance curves.* Nanoscale, 2020. **12**(16): p. 9133-9143.
321. Sanchez, J.G., *et al.*, *The viscoelasticity of adherent cells follows a single power-law with distinct local variations within a single cell and across cell lines.* Nanoscale, 2021. **13**(38): p. 16339-16348.
322. Moore, D.S., G.P. McCabe, and B.A. Craig, *Introduction to the Practice of Statistics*. 2014: W. H. Freeman.
323. Childs, P.G., *et al.*, *Use of nanoscale mechanical stimulation for control and manipulation of cell behaviour.* Acta Biomater, 2016. **34**: p. 159-168.
324. Jaasma, M.J., *et al.*, *Adaptation of cellular mechanical behavior to mechanical loading for osteoblastic cells.* Journal of Biomechanics, 2007. **40**(9): p. 1938-1945.
325. Hu, J., *et al.*, *Mechanical Point Loading Induces Cortex Stiffening and Actin Reorganization.* Biophys J, 2019. **117**(8): p. 1405-1418.
326. Becerra, N., *et al. AFM and Fluorescence Microscopy of Single Cells with Simultaneous Mechanical Stimulation via Electrically Stretchable Substrates*. Materials, 2021. **14**, 4131.

327. Li, Y.H., *et al.*, *Crosstalk between the COX2-PGE2-EP4 signaling pathway and primary cilia in osteoblasts after mechanical stimulation.* J Cell Physiol, 2021. **236**(6): p. 4764-4777.
328. Hou, W.W., *et al.*, *Involvement of Wnt activation in the micromechanical vibration-enhanced osteogenic response of osteoblasts.* Journal of Orthopaedic Science, 2011. **16**(5): p. 598-605.
329. Chen, Y.-J., *et al.*, *Mechanoregulation of osteoblast-like MG-63 cell activities by cyclic stretching.* Journal of the Formosan Medical Association, 2014. **113**(7): p. 447-453.
330. Tsai, M.H., *et al. Enhanced Osteogenesis Potential of MG-63 Cells through Sustained Delivery of VEGF via Liposomal Hydrogel*. Gels, 2023. **9**, 562.
331. Gao, J., *et al.*, *Cyclic stretch promotes osteogenesis-related gene expression in osteoblast-like cells through a cofilin-associated mechanism.* Mol Med Rep, 2016. **14**(1): p. 218-24.
332. Wang, D., *et al.*, *The interactions between mTOR and NF-κB: A novel mechanism mediating mechanical stretch-stimulated osteoblast differentiation.* Journal of Cellular Physiology, 2021. **236**(6): p. 4592-4603.
333. Machesky, L.M. and R.H. Insall, *Scar1 and the related Wiskott-Aldrich syndrome protein, WASP, regulate the actin cytoskeleton through the Arp2/3 complex.* Curr Biol, 1998. **8**(25): p. 1347-56.
334. Schmittgen, T.D. and K.J. Livak, *Analyzing real-time PCR data by the comparative CT method.* Nature Protocols, 2008. **3**(6): p. 1101-1108.
335. Hassan, R., *et al.*, *Guidelines for nucleic acid detection and analysis in hematological disorders.* Malays J Pathol, 2015. **37**(2): p. 165-73.
336. Otto, O., *et al.*, *Real-time deformability cytometry: on-the-fly cell mechanical phenotyping.* Nature Methods, 2015. **12**(3): p. 199-202.
337. Fregin, B., *et al.*, *High-throughput single-cell rheology in complex samples by dynamic real-time deformability cytometry.* Nat Commun, 2019. **10**(1): p. 415.
338. Guzniczak, E., *et al.*, *Deformability-induced lift force in spiral microchannels for cell separation.* Lab on a Chip, 2020. **20**(3): p. 614-625.

339. Lian, J.B., *et al.*, *Regulatory Controls for Osteoblast Growth and Differentiation: Role of Runx/Cbfa/AML Factors.* 2004. **14**(1&2): p. 42.
340. Guzniczak, E., *et al.*, *High-throughput assessment of mechanical properties of stem cell derived red blood cells, toward cellular downstream processing.* Sci Rep, 2017. **7**(1): p. 14457.
341. Luo, J., *et al.*, *The oncogenic roles and clinical implications of YAP/TAZ in breast cancer.* British Journal of Cancer, 2023. **128**(9): p. 1611-1624.
342. Avruch, J., D. Zhou, and N. Bardeesy, *YAP oncogene overexpression supercharges colon cancer proliferation.* Cell Cycle, 2012. **11**(6): p. 1090-6.
343. Preibisch, S., S. Saalfeld, and P. Tomancak, *Globally optimal stitching of tiled 3D microscopic image acquisitions.* Bioinformatics, 2009. **25**(11): p. 1463-5.
344. Rubin, C., *et al.*, *Quantity and Quality of Trabecular Bone in the Femur Are Enhanced by a Strongly Anabolic, Noninvasive Mechanical Intervention.* Journal of Bone and Mineral Research, 2002. **17**(2): p. 349-357.
345. Garman, R., *et al.*, *Low-level accelerations applied in the absence of weight bearing can enhance trabecular bone formation.* Journal of Orthopaedic Research, 2007. **25**(6): p. 732-740.
346. Judex, S., *et al.*, *Low-magnitude mechanical signals that stimulate bone formation in the ovariectomized rat are dependent on the applied frequency but not on the strain magnitude.* Journal of Biomechanics, 2007. **40**(6): p. 1333-1339.
347. McLeod, R.W.J., *et al.*, *Scanning laser Doppler vibrometry of the cranium when stimulated by a B71 bone transducer.* Applied Acoustics, 2018. **142**: p. 53-58.
348. Boskey, A.L., F.H. Wians, Jr., and P.V. Hauschka, *The effect of osteocalcin on in vitro lipid-induced hydroxyapatite formation and seeded hydroxyapatite growth.* Calcif Tissue Int, 1985. **37**(1): p. 57-62.
349. Butler, J.T., *et al.*, *Changing nuclear landscape and unique PML structures during early epigenetic transitions of human embryonic stem cells.* J Cell Biochem, 2009. **107**(4): p. 609-21.

350. Burke, B. and C.L. Stewart, *The nuclear lamins: flexibility in function.* Nat Rev Mol Cell Biol, 2013. **14**(1): p. 13-24.
351. Buxboim, A., *et al.*, *Matrix elasticity regulates lamin-A,C phosphorylation and turnover with feedback to actomyosin.* Curr Biol, 2014. **24**(16): p. 1909-17.
352. Bermeo, S., *et al.*, *Lamin A/C Acts as an Essential Factor in Mesenchymal Stem Cell Differentiation Through the Regulation of the Dynamics of the Wnt/β-Catenin Pathway.* J Cell Biochem, 2015. **116**(10): p. 2344-53.
353. Alcorta-Sevillano, N., *et al.*, *Crucial Role of Lamin A/C in the Migration and Differentiation of MSCs in Bone.* Cells, 2020. **9**(6): p. 1330.
354. Vakhrusheva, A.V., *et al.*, *Role of actin-binding proteins in the regulation of cellular mechanics.* European Journal of Cell Biology, 2022. **101**(3): p. 151241.
355. Ramos, J.R., *et al.*, *The softening of human bladder cancer cells happens at an early stage of the malignancy process.* Beilstein Journal of Nanotechnology, 2014. **5**: p. 447-457.
356. Rotsch, C. and M. Radmacher, *Drug-Induced Changes of Cytoskeletal Structure and Mechanics in Fibroblasts: An Atomic Force Microscopy Study.* Biophysical Journal, 2000. **78**(1): p. 520-535.
357. Newberg, J., *et al.*, *Isolated nuclei stiffen in response to low intensity vibration.* Journal of Biomechanics, 2020. **111**: p. 110012.
358. Kolliopoulos, V., *et al.*, *Donor Variability in Human Mesenchymal Stem Cell Osteogenic Response as a Function of Passage Conditions and Donor Sex.* bioRxiv, 2023.
359. Kim, M., *et al.*, *Donor Variation and Optimization of Human Mesenchymal Stem Cell Chondrogenesis in Hyaluronic Acid.* Tissue Eng Part A, 2018. **24**(21-22): p. 1693-1703.
360. Mehrian, M., *et al.*, *Predicting in vitro human mesenchymal stromal cell expansion based on individual donor characteristics using machine learning.* Cytotherapy, 2020. **22**(2): p. 82-90.

361. Patel, S.A., *et al.*, *Personalizing Stem Cell Research and Therapy: The Arduous Road Ahead or Missed Opportunity?* Curr Pharmacogenomics Person Med, 2010. **8**(1): p. 25-36.
362. Couto, P.S., A. Bersenev, and Q.A. Rafiq, *Chapter 2 - Process development and manufacturing approaches for mesenchymal stem cell therapies*, in *Engineering Strategies for Regenerative Medicine*, T.G. Fernandes, M.M. Diogo, and J.M.S. Cabral, Editors. 2020, Academic Press. p. 33-71.
363. Robb, K.P., *et al.*, *Mesenchymal stromal cell therapy: progress in manufacturing and assessments of potency.* Cytotherapy, 2019. **21**(3): p. 289-306.
364. Moutsatsou, P., *et al.*, *Automation in cell and gene therapy manufacturing: from past to future.* Biotechnol Lett, 2019. **41**(11): p. 1245-1253.
365. Bell, M., *et al.*, *A semi-automated cost-efficient process for the closed expansion and harvest of pluripotent stem cells using a hollow fibre bioreactor and continuous centrifugation.* Cytotherapy, 2017. **19**: p. S158.
366. Shimizu, K., H. Fujita, and E. Nagamori, *Alignment of skeletal muscle myoblasts and myotubes using linear micropatterned surfaces ground with abrasives.* Biotechnol Bioeng, 2009. **103**(3): p. 631-8.
367. Nasser, M.I., *et al.*, *Current situation and future of stem cells in cardiovascular medicine.* Biomedicine & Pharmacotherapy, 2020. **132**: p. 110813.
368. Lewis, K., *Riddle of Biofilm Resistance.* Antimicrobial Agents and Chemotherapy, 2001. **45**(4): p. 999-1007.
369. Høiby, N., *et al.*, *Antibiotic resistance of bacterial biofilms.* Int J Antimicrob Agents, 2010. **35**(4): p. 322-32.
370. Van Houdt, R. and C.W. Michiels, *Biofilm formation and the food industry, a focus on the bacterial outer surface.* Journal of Applied Microbiology, 2010. **109**(4): p. 1117-1131.
371. Lu, Y., *et al.*, *Vibration loading promotes osteogenic differentiation of bone marrow-derived mesenchymal stem cells via p38 MAPK signaling pathway.* J Biomech, 2018. **71**: p. 67-75.

372. Baskan, O., *et al.*, *Frequency-specific sensitivity of 3T3-L1 preadipocytes to low-intensity vibratory stimulus during adipogenesis.* In Vitro Cellular & Developmental Biology - Animal, 2022. **58**(6): p. 452-461.
373. Li, Y.H., *et al.*, *Primary cilia respond to intermittent low-magnitude, high-frequency vibration and mediate vibration-induced effects in osteoblasts.* Am J Physiol Cell Physiol, 2020. **318**(1): p. C73-c82.
374. Cho, H., H.J. Park, and Y.K. Seo, *Induction of PLXNA4 Gene during Neural Differentiation in Human Umbilical-Cord-Derived Mesenchymal Stem Cells by Low-Intensity Sub-Sonic Vibration.* Int J Mol Sci, 2022. **23**(3).
375. Zhang, C., *et al.*, *Influence of different intensities of vibration on proliferation and differentiation of human periodontal ligament stem cells.* Arch Med Sci, 2015. **11**(3): p. 638-46.
376. Benjakul, S., C. Leethanakul, and S. Jitpukdeebodintra, *Low magnitude high frequency vibration induces RANKL via cyclooxygenase pathway in human periodontal ligament cells in vitro.* J Oral Biol Craniofac Res, 2019. **9**(3): p. 251-255.
377. Ye, M., *et al.*, *Vibration Induces BAFF Overexpression and Aberrant O-Glycosylation of IgA1 in Cultured Human Tonsillar Mononuclear Cells in IgA Nephropathy.* Biomed Res Int, 2016. **2016**: p. 9125960.
378. Lu, F., *et al.*, *NeuroD1 promotes neuroblastoma cell growth by inducing the expression of ALK.* Cancer Sci, 2015. **106**(4): p. 390-6.
379. Tondreau, T., *et al.*, *Bone marrow–derived mesenchymal stem cells already express specific neural proteins before any differentiation.* Differentiation, 2004. **72**(7): p. 319-326.
380. Tao, H., R. Rao, and D.D.F. Ma, *Cytokine-induced stable neuronal differentiation of human bone marrow mesenchymal stem cells in a serum/feeder cell-free condition.* Development, Growth & Differentiation, 2005. **47**(6): p. 423-433.